Study of Mycobacterium tuberculosis N-acetyl-glucosamine-1-phosphate uridyltransferase (GlmU)

THESIS

Submitted in partial fulfilment
of the requirements for the degree of

DOCTOR OF PHILOSOPHY
By

VIJAY SONI

ID No. 2011PHXF423H

Under the supervision of

Prof. D. Sriram

And

Under the co-supervision of

Dr. Vinay K Nandicoori

(National Institute of Immunology, New Delhi)

BITS Pilani
Pilani | Dubai | Goa | Hyderabad

BIRLA INSTITUTE OF TECHNOLOGY AND SCIENCE, PILANI

2015

Acknowledgment

At first I would like to thank the greatest architect of the universe and my parents. Any attempt to list the people and opportunities with which my life has been richly blessed would be like trying to count the stars in the heaven.

It's a great pleasure and immense satisfaction to express my deep gratitude towards my research supervisor, ***Prof. D. Sriram****, Professor, Department of Pharmacy, BITS, Pilani-Hyderabad campus, and co- supervisor* ***Dr. Vinay K. Nandicoori,*** *Scientist VI, National Institute of Immunology, New Delhi for their regular guidance, suggestions and support which they bestowed to me. Mere acknowledgement with words is inadequate to express my gratitude to them. The work environment given to me under them, the experiences gained from them and their creative working culture are treasured and will be remembered throughout my life. Dr. Vinay motivated me constantly and supported me at many odd conditions. He is excellent person and scientist. His guidance for science and life will always guide me throughout my career. Thanks a ton Sir!!*

I deeply acknowledge and extend heartfelt thanks to ***Prof. P. Yogeeswari****, Professor, Department of Pharmacy, BITS, Pilani-Hyderabad campus, for her valuable suggestions, guidance and precious time which she offered me throughout my research.*

I am thankful to my DAC members ***Prof. P. Yogeeswari*** *and* ***Prof.Sajeli Begum*** *for their guidance and encouragement during this period. I am grateful to* ***Prof. Bijendra Nath Jain****, Vice-Chancellor (BITS) and Director* ***Prof. V.S.Rao*** *(Hyderabad campus), for allowing me to carry out my doctoral research work in the institute.*

I am thankful to ***Prof. M. M. S. Anand,*** *Registrar and* ***Prof. S.K.Verma,*** *Dean, Academic Research (Ph.D. Programme), BITS Pilani for their support to do my research work. I would like to express my sincere thanks to* ***Prof. M.B.Srinivas,*** *Dean, Administration and* ***Dr. Vidya Rajesh,*** *Associate Dean, Academic Research (Ph.D. Programme), BITS-Pilani, Hyderabad campus for their continuous support and encouragement during my research work. I would like to express my gratitude to* ***Dr. Shrikanth Y. Charde****, Head of the Department, Pharmacy, for providing me with all the necessary laboratory facilities and for helping me at various stages of my research work. I sincerely acknowledge the help rendered by* ***Dr. V.V.Vamsi Krishna, Dr.Punna Rao Ravi****,* ***Dr.Balram Ghosh****,* ***Dr. Swati Biswas****,* ***Dr.Onkar Kulkherni****, and* ***Dr.Arti Dhar*** *faculty at the BITS-Pilani, Hyderabad campus. I take this opportunity to sincerely acknowledge the Open source Drug Discovery and Development (OSDD)-CSIR, Government of India, New Delhi, for providing me financial assistance.*

I am grateful to ***Dr. Rajmani*** *and Tuberculosis Aerosol Challenge Facility (TACF) of ICGEB and very much thankful for their support in all animal experiments. I would like to thank the Central Confocal Microscopy, Scanning Electron Microscopy facility, Biocontainment facility at the National Institute of Immunology, New Delhi, Scanning Electron Microscopy facility at the Advance Instrumentation Research Facility (AIRF) of Jawaharlal Nehru University and Transimission Electron Microscopy Facility at CSIR-Institute of Genomic & Integrative Biology. I am thankful to* ***Dr. Kalpana Rajanala*** *for her help in confocal imaging. I am thankful thank* ***Ms. Rekha Rani*** *and* ***Mr. Mahendra Pratap*** *Singh for their support in SEM/TEM imaging.*

I am very much grateful to all my BITS-Pilani Hyderabad campus friends ***Ganesh S, Manoj, Ganesh P, Jean, Sridhar, Parameshwar, Sridevi, Mallika, Shalini, Reshma A, Reshma S, Madhu, Saketh Sriram, Priyanka P, Priyanka S, Hasitha, Patrisha, Ram, Brahmam, Radhika, Gangadhar, Srikanth, Shubam, Praveen, Suman, Mahibalan, Rukaiyya, Shailendar, Poorna, Santosh, Preethi, Omkar, Anup, Shubmita, Vishnu and Nikhila*** *for the time they had spent for me and making my stay at campus a memorable one. My special thanks to* ***Bobesh, Renuka, Kaoushik and Brindha*** *who helped me at every moment. I take this opportunity to thank one and all for their help directly or indirectly. I express my thanks to our BITS laboratory assistants,* ***Mrs. Saritha, Mr. Rajesh, Mr. Ramu, Mr.Seenu*** *and* ***Mrs. Rekha.***

I sincerely thank ***Mahesh ji*** *and* ***Babu Bhaiya*** *at Nii, without them, not even a single day of work in the lab would have been possible. I am thankful to them for being very supportive and helpful. I would like to thank* ***Radhey Shyam ji, Yam Bhaiya, Nitin*** *from STL-II lab for constant support and* ***Radhey Shyam ji*** *for constant encouraging words. I am thankful to* ***Dr. Amit*** *who initiated the GlmU project. I would like to thank my current and past lab members at Nii* ***Kalpana, Shazia, Sandeep, Yogesh, Sathya, Divya, Prabhjot, Preeti, Manisha, Pankaj, Baasanti, Divya Arora, Mehak, Saba, Dr. Savita, Aditya Sharma, Dr. Gagan*** *and other wonderful lab members who stood by me in thick and thin of the things and for making my journey wonderful. I am also thankful to* ***Rohini, Sharad*** *and* ***Nihalji*** *who supported me regularly for many experiments and instruments assessment. Further, I would like to thank* ***Dr. Sagar Sen Gupta*** *and STL-2 lab members* ***Suhas, Jyoti, Dr. Vivek, Dr. Pervin, Mansoor, Arun, Himanshi and Raina*** *for being supportive for everything. I am also thankful to my best friends* ***Mumtaz, Sunder ji, Aparna, Ananya, Leena, Naeem, Bahadur, Raghvender, Sushil, Ajay*** *and to my all* ***Freemasonary*** *friends and brethrens to be with me always to boost me up every time.*

I am grateful to ***Prabhjot*** *for being my constant support and best buddy in Nii and lab for last three years of my PhD. Her counseling and guidance in my odd times really brought a lot of confidence and boost for research and this made my decisions perfect and improved. I am also thankful to her for correcting my thesis and paper. Thanks* ***Prabhu****!!*

I am very much fortunate to have wonderful Bhai in lab; ***Yogiii****!! He has been dear friend right from my first year in lab. I am thankful for his steady support, motivation and help during whole time of my PhD. We have enjoyed at our best. Thanks* ***Bhai****!!*

I would like to thank to our collaborators ***Prof. Balaji Prakash*** *and his students* ***Pravin Jagtap*** *and* ***Vaibhav Singh Bais*** *for their help in solving crystal structure and regular support in work. I owe a great deal of appreciation and gratitude to* ***Dr. Satyajit Rath (Nii), Dr. V. Nagaraja (IISc), Dr. T. S. Balganesh (OSDD), Dr. Ayub Qadri (Nii), Dr. Geetha Vani (OSDD) and Dr. Avinash Bajaj (RCB)*** *for scientific discussions and critical inputs.*

I would like to begin by dedicating this piece of work to my parents ***Mr. Babulal Soni and Mrs. Jashoda Soni****, whose dreams have come to life with me getting the highest degree in education. I owe my doctorate degree to my parents who; with their continuous care, support and encouragement kept my morale high. Thanks are due if I don't dedicate this thesis to my sisters Mrs.* ***Asha Soni, Dr. Nitu Soni, my Jijaji Mr. Vinod Soni and my nephew Devansh Soni*** *whose constant and motivating support, love and affection made me reach this height.*

Date:

Vijay Soni

Abstract

Mycobacterium tuberculosis (*Mtb*), the causative agent of tuberculosis is the most successful and dynamic human pathogen. It can also persist in immunologically educated host for long time in latent form and cause active disease at any stage. Regularly arising and difficult to treat strains (MDR/ XDR) are alarming us to investigate new drug targets and anti-TB molecules. Cell wall of *Mtb* is key bacterial organelle to develop new sets of inhibitors. *M. tuberculosis* N-acetyl-glucosamine-1-phosphate uridyltransferase ($GlmU_{Mtb}$) is a bi-functional enzyme engaged in the synthesis of two metabolic intermediates N-acetylglucosamine-1-phosphate (GlcNAc-1-P) and UDP-GlcNAc, catalyzed by the C- and N-terminal domains respectively. UDP-GlcNAc is a key metabolite essential for the synthesis of peptidoglycan, disaccharide linker, lipoarabinomannan, arabinogalactan and mycothiols. In this study we have done structural and biochemical characterization of $GlmU_{Mtb}$, it's biological and genetic validation as a drug target at *in vitro*, *ex vivo* and *in vivo* level and finally designing and development of new anti-$GlmU_{Mtb}$ inhibitor and checked its site of binding, specificity and *in vivo* efficacy.

Here we have present the crystal structures of $GlmU_{Mtb}$ in complex with substrates/products bound at the acetyltransferase active site. Analysis of these and mutational data, allow us to infer a catalytic mechanism operative in $GlmU_{Mtb}$. In this SN2 reaction, His-374 and Asn-397 act as catalytic residues by enhancing the nucleophilicity of the attacking amino group of glucosamine 1-phosphate. Ser-416 and Trp-460 provide important interactions for substrate binding. A short helix at the C-terminal extension uniquely found in mycobacterial GlmU provides the highly conserved Trp-460 for substrate binding. Importantly, the structures reveal an uncommon mode of acetyl-CoA binding in $GlmU_{Mtb}$; we term this the U conformation, which is distinct from the L conformation seen in the available non-mycobacterial GlmU structures. Residues, likely determining U/L conformation, were identified, and their importance was evaluated. In addition, we identified that the primary site for PknB-mediated phosphorylation is Thr-418, near the acetyltransferase active site. Down-regulation of acetyltransferase activity upon Thr-418 phosphorylation is rationalized by the structures presented here.

While *glmU*$_{Mtb}$ was predicted to be an essential gene, till date the role of GlmU$_{Mtb}$ in modulating the *in vitro* growth of *Mtb* or its role in survival of pathogen *ex vivo* / *in vivo* have not been deciphered. Here we present the results of a comprehensive study dissecting the role of GlmU$_{Mtb}$ in arbitrating the survival of the pathogen both *in vitro* and *in vivo.* We find that absence of GlmU$_{Mtb}$ leads to extensive perturbation of bacterial morphology and substantial reduction in cell wall thickness under normoxic as well as hypoxic conditions. Complementation studies show that the acetyl- and uridyltransferase activities of GlmU$_{Mtb}$ are independently essential for bacterial survival *in vitro* and also support that there are no alternative pathways for the production of GlcNAc-1-P and UDP-GlcNAc. GlmU$_{Mtb}$ is also found to be essential for mycobacterial survival in THP-1 cells as well as in guinea pigs. Remarkably, depletion of GlmU$_{Mtb}$ at any stage of bacterial growth *in vitro*, *ex vivo* or from infected murine lungs, four weeks post infection, led to radical reduction in the bacillary load.

Next both structure and shape based drug designing were employed to develop new inhibitors against UTP, GlcNAc-1-P and allosteric locus of uridyltransferase active site of GlmU$_{Mtb}$. Compound 4, UTP competitive inhibitor was showing IC$_{50}$ of 42 µM and better affinity than UTP in isothermal titration calorimetry. *In silico* molecular dynamics (MD) simulation studies, for compound 4, carried out for 10 ns showed the protein-compound complex to be stable throughout the simulation with relative RMSD in acceptable range. Further shape based inhibitors' designing resulted in two subsequent generations of inhibitors; Asinex and oxazolidine derivatives. One oxazolidine inhibitor, Oxa33, was found to be active at IC$_{50}$ of ~10 µM and specifically bind at allosteric site. Finally the administration of Oxa33 to infected mice resulted in significant decrease in the bacillary load.

Taken together, this study provides an insight into substrate recognition, catalytic mechanism for acetyl transfer, features unique to GlmU$_{Mtb}$, genetic and biological validation of GlmU$_{Mtb}$ as a potential drug target. Oxa33 can be pursued as a lead molecule, which needs to be developed further to improve its efficacy.

Table of Contents

List of Figures

List of Tables

List of abbreviations

μM	:	Micromolar
δ	:	Chemical shift
^{13}C NMR	:	Carbon Nuclear Magnetic Resonance
^{1}H NMR	:	Proton Nuclear Magnetic Resonance
ATP	:	Adenosine Triphosphate
CFU	:	Colony Forming Unit
CoA	:	Coenzyme A
DMSO	:	Dimethyl Sulphoxide
DOTS	:	Directly Observed Treatment, Short course
DSF	:	Differential Scanning Flourimetry
FBS	:	Fetal Bovine Serum
bp	:	Base pairs
GLIDE	:	Grid based Ligand Docking and Energetics
HEPES	:	4-(2-Hydroxyethyl)piperazine-1-ethanesulfonic acid
HPLC	:	High Pressure Liquid Chromatography
IC_{50}	:	Half maximal Inhibitory Concentration
IPTG	:	Isopropyl β-D-1-thiogalactopyranoside
J	:	Coupling constant
kDa	:	Kilo Daltons
K_m	:	Kinetic constant
ml	:	millilitre
LCMS	:	Liquid Chromatography-Mass Spectrometer
LAM	:	Lipoarabinomannan
LM	:	Lipomannan
LTBI	:	Latent Tuberculosis Infection
M.P	:	Melting point
MABA	:	Microplate Alamar Blue Assay
MCS	:	Multiple Cloning Site
MDR TB	:	Multidrug Resistant Tuberculosis

$MgCl_2$	:	Magnesium chloride
$MgSO_4$	:	Magnesium sulphate
MIC	:	Minimum Inhibitory Concentration
ml	:	Milliliter
mmol	:	Millimole
Mtb	:	*Mycobacterium tuberculosis*
h		Hours
Ni-NTA	:	Nickel-nitroloacetic acid
nM	:	Nanomolar
nm	:	Nanometre
NRP	:	Non-Replicating Persistant
OADC	:	Oleic acid, Albumin, Dextrose, Catalase
ADC	:	Albumin, Dextrose, Catalase
ORF	:	Open Reading Frame
PAGE	:	Polyacrylamide Gel Electrophoresis
PCR	:	Polymerase Chain Reaction
PDB	:	Protein Data Bank
pfu	:	*Pyrococcus furiosus*
M	:	Molar
PIM	:	Phosphatidyl-myo-inositol mannoside
pM	:	Picomolar
PMP	:	Pyridoxal monophosphate
PMSF	:	Phenylmethyl sulfonyl fluoride
R	:	Aromatic ring
RFU	:	Relative Fluorescence Units
RMSD	:	Root Mean Square Deviation
rpm	:	Rotation per minute
rt	:	Room Temperature
RT-PCR	:	Real time Polymerase Chain Reaction
SAR	:	Structure-Activity Relationship
SDS	:	Sodium Dodecyl Sulphate
SP	:	Standard Precision

TB	:	Tuberculosis
TLC	:	Thin Layer Chromatography
T_m	:	Melting temperature
V_{max}	:	Maximum velocity
XDR TB	:	Extensively Drug Resistant Tuberculosis
XP	:	Extra Precision
A_{600}	:	Absorbance at 600 nm
BSA	:	Bovine serum albumin
DNA	:	Deoxyribonucleic acid
EDTA	:	Ethylenediaminetetraacetic acid
ELISA	:	Enzyme linked immunosorbent assay
mM	:	Millimolar
OD	:	Optical density
PBS	:	Phosphate buffered saline
TAE	:	Tris-acetate-EDTA
TE	:	Tris-EDTA
UV	:	Ultraviolet
WT	:	Wild type
GlcNAc	:	N-acetylglucosamine
GlcN-1P	:	Glcusamine-1Phosphate
GlcNAc-1P	:	N-acetylglucosamine-1Phosaphate
UDP-GlcNAc	:	Uridine diphosphate N-acetylglucosamine
$GlmU_{Mtb}$	:	GlmU from *M. tuberculosis*
$GlmU_{SP}$	:	GlmU from *S. pneumoniae*
$GlmU_{CG}$	:	GlmU from *C. glutamicum*
$GlmU_{EC}$	:	GlmU from *E.coli*
$GlmU_{MS}$	:	GlmU from *M. smegmatis*
UTP	:	Uridine triphosphate
UMP	:	Uridine diphosphate
CD	:	Circular dichroism

Chapter 1.

Introduction

Chapter 1.

Introduction

1.1 Tuberculosis: A killer within.

Tuberculosis (also called as phthisis or consumption) is caused by *Mycobacterium tuberculosis* (*M.tb.*), a bacteria that has evolved both as a symbiont and pathogen ever since humans have spread out of Africa almost 40,000 years ago [1, 2]. The co-evolution of *M.tb.* with humans for such long periods has resulted in extensive evolutionary adaptation, which facilitated *M.tb.* survival inside the lungs and established it as a potent pathogen. *M.tb.* hijacks different host metabolic and signalling pathways and bypasses the immune response in order to survive inside host. *M.tb.* can remain in lungs in asymptomatic latent form for a very long time, which can get activated at any opportune time. Stringent & lipid rich cell envelope, slow metabolic rate and precise regulation of pathogenic factors make it a dreadful pathogen.

WHO reports suggest that one third of the world population is suffering with latent TB, which has ~10 % lifetime chance to convert into active TB. It is second most deadly disease after AIDS as 9 million cases were reported in 2014 with 16.67% mortality and 3.5% MDR-TB cases (WHO report 2014). Out of these, 24% and 11% cases are from India and China, respectively. New cases are arising at a rate of ~1% world population per year and 90-95% of them remain asymptotic.

Initial mild symptoms, slow detection technology, limited treatment, genetic homogeneity and spread through air present strong challenges to the society in their fight against TB. WHO has approved a resolution "*2015 Global TB Strategy*" to reduce the death toll by 90-95% from the endemic regions by 2035. Policy Implementation Package (PIP) has been initiated to develop a roadmap for new TB drugs/ regimens to support various countries (PIP 2013, The END TB Strategy). Main emphasis of new policies against TB include better drug supply, tracking system, case management, pharmacovigiliance, national implementation plan, drug resistance surveillance and research for effective diagnostic and treatment strategies.

1.2 Mycobacterium tuberculosis: The sleeping fiend.

Classification

Domain: *Bacteria*
Phylum: *Actinobacteria*
Class: *Actinobacteria*
Order: *Actinomycetales*
Family: *Mycobacteriaceae*
Genus: *Mycobacterium*
Species: *Mycobacterium tuberculosis* complex (**MTC**: *M. africanum, M. bovis, M. canettii, M. microti, M. tuberculosis*)

M.tb. as the causative agent of tuberculosis (pulmonary and extra pulmonary, Fig 1.1) was first revealed by Robert Koch in 1883. This finding by Robert Koch brought him the honour of Nobel Prize in 1905. *M.tb.* is a rod shaped non-motile pathogenic bacteria with highly lipid rich cell wall. Generally it is categorized as acid fast and gram positive due to absence of true outer membrane and thick peptidoglycan. *M.tb.* divides in 18-20 h and resides in the human alveolar macrophages with the dimensions ranging from 0.2-0.4 & 2-10 μm. *M.tb.* can be stained by Ziehl – Neelsen stain, Kynioun stain, Auramin O and Rhodamine B [5]. *M.tb.* can be killed at 60 °C in 20 min or 2 h in sunlight and is sensitive to formaldehyde and gluteraldehyde. While it remains viable for 8-10 days in droplet nuclei, in culture it stays alive for 6-8 months at room temperature. Its colonies are dry, elevated, and uneven, with crumpled surface and are creamy white in colour.

M.tb. is an opportunistic pathogen and has a dynamic nature of infection. TB infection can occur either by new bacilli or through activation of already existing but latent bacilli. Generally a type of equilibrium exists between active and latent bacilli and disruption of this equilibrium causes acute infection. The acute infection may be due to decreased immunity and/or increased endogenous re-infection rates. According to dynamic re-infection hypothesis non-replicating bacteria will drain constantly towards the bronchial tree and spread infection, which is once again followed by generation of granuloma [6].

The major challenges in controlling TB are the phenotypic adaptations and resistance of dormant and persistent *M.tb.* against existing therapies. Numbers of bacterial factors have been reported to play important roles in maintaining and resuscitating the dormant bacteria. These include *M.tb.* sigma factors (RpoV, SigA, SigF and SigB), isocitrate lyase, DevR/ DevS and DosR, lysine amino transferase, PcaA, α-crystallin, RelA, PE-PGRS family, NarX, NarK and NarG, MprAB etc [7-12]. Host immune system also plays a crucial role in latency, mainly $CD4^+$ cells,

$CD8^+$ cells, tumour necrosis factor-α and interferon-γ [13, 14]. *M.tb* found in two physiological forms with distinct characteristics.

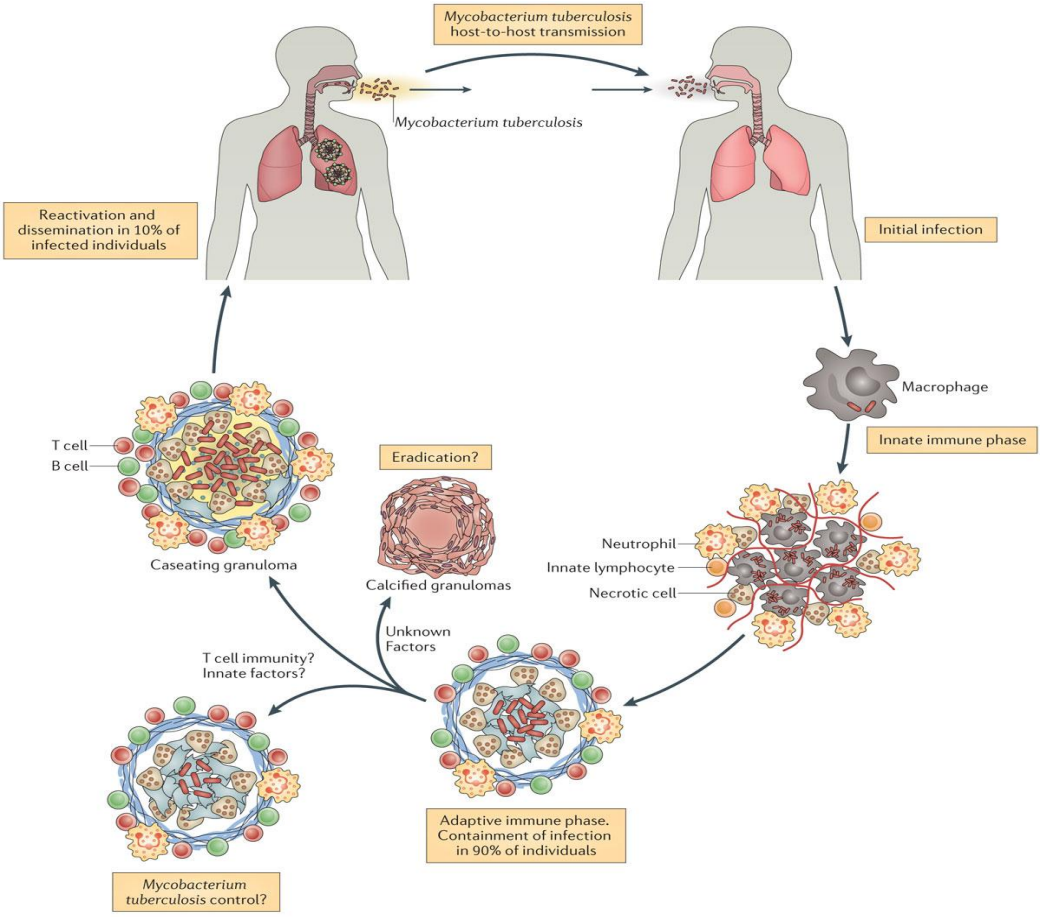

Figure. 1.1. Tuberculosis pathogenesis: TB infection starts by inhalation of *M.tb.* containing aerosol droplets. In response to the infection, innate immune system starts recruiting inflammatory cells at the site of infection. Bacteria starts propagating to lymph nodes and bacterial antigen presentation by dendritic cells leads to priming of T cells, which results in increase in number of antigen-specific T cells. Activated macrophages, B cells, T cells, and various leukocytes start to form granuloma. TB infection can remain in the latent form without any clinical symptoms. While a small percentage of human can develop active TB, which discharges *M.tb.* from granuloma. The disease can be transmitted by coughing through infectious droplets. [15]

1.3 Extra pulmonary tuberculosis (EPTB).

M.tb. infection is not only limited to lungs, but can spread to other organs and such an infection is known as Extra Pulmonary Tuberculosis (EPTB). EBTB occurs as a result of massive uncontrolled dissemination of *M.tb.* into the blood stream and all over the body due to active primary infection or reactivation of latent TB. Any

site of the body may be affected and it is very common among elderly, immunocompromised and children below 4 year of age. Lymph nodes**,** liver, bones and joints**,** abdominal**,** peritoneal area**,** gastrointestinal organs, pericardial zone, genitourinary organs**,** cutaenous parts**,** ocular region and brain have been reported to be the major organs and tissues affected with EPTB. Infection of lymph nodes through plural effusion is the most common form of EPTB. Fever, weakness, malaise, chills and often progressive dyspnea are common symptoms of EPTB. In case of bone marrow involvement in EPTB; anaemia, leukemoid reaction and thrombocytopenia can also be symptoms. Meningitis TB can cause stroke and focal neurologic symptoms leading to coma and death of the infected person. As compared with the conventional methods, detection of EPTB is easier with CT-scan, MRI and endoscopy. At times biopsy and /or surgery are required for final confirmation of EPTB [16]

1.4 Origin of MDR, XDR and TDR: Challenges in the battle.

Drug resistance in *M.tb.* is an acquired survival phenomenon that results in the evolution of multi drug resistance (MDR) and extensively drug resistance (XDR) or totally drug resistance (TDR) strains of *M.tb.* Resistance to two most important and effective drugs rifampicin (RIF) and isoniazid (INH) among the four drug regimen is described as MDR TB. Treatment of MDR-TB involves second line of drugs for ~2 years. The second lines of drugs are harmful, expensive and cause serious side effects. Thus combating MDR-TB has become a challenge to governments across the world.

Table 1.1: Genes involved in drug resistance in *M.tb* [17].

Drug	**Gene(s) implicated in resistance**
Rifampicin	*rpoB*; β -subunit of RNA polymerase
Isoniazid	*katG*: catalase-peroxidase
	oxyR-ahpC: alkylhydrokinase reductase
	inhA: enoyl-ACP reductase
	kasA: β -ketoacyl acyl carrier protein synthase
Ethionamide	*inhA*: enoyl-ACP reductase
Streptomycin	*rpsl*: ribosomal protein S12 involved in rrs:16S RNA
Fluoroquinolones	*gyrA*: DNA gyrase
Pyrazinamide	*pncA*: pyrazinamidase
Ethambutol	*embCAB*: Arabinosyl transferase

XDR-TB arises due to mismanagement of MDR-TB patients and it represents *M.tb.* strains that are resistant to any fluroquinolone and to one of the three injectable second lines of drugs (capreomycin, kanamycin, and amikacin). Therefore treatment of XDR-TB is extremely difficult. According to the reports 70% of XDR-TB patients die within one or two months of diagnosis. Totally drug resistance (TDR-TB) was first reported in Italy in 2003 and also has also been found in India and Iran but it is not as widely reported.

Drug resistance arises due to spontaneous and random mutations in the *M.tb.* genome, resulting in reduced sensitivity to one or more drugs [18]. Recent information on genetics of reported drug resistance is compiled in table 1.1. Deletion or mutations in *katG* gene resulted in INH resistance in clinical isolates [19]. Later three more genes (*inhA, kasA and ahpC*) were also reported to result in INH resistance [20-22]. Rifampicin resistance is mostly due to deletions or insertions (single polymorphism in 95% isolates) in the 81 bp long region of *rpoB* gene [23]. Mutation rate of INH resistance is $2–3 \times 10^{-8}$ mutations/ bacterium/ generation (i.e. one mutation may arise in 10^6 bacilli) while for the rifampicin the mutation rate is 2.25×10^{-10} mutations/ bacterium/ generation (one mutation may arise in 10^8 bacilli), which is slower than the mutation rate of INH [18].

1.5 Vaccine development: Fight against M. tuberculosis.

The only known vaccine for tuberculosis is Bacillus Calmette–Guérin (BCG) which is prepared from attenuated *M. bovis* strain. The efficacy of BCG significantly varied in different clinical trials. Recent results show that BCG reduces infection by 19-27% and the progression of TB by ~71% [24]. BCG vaccination is more effective

Table 1.2: Subunit candidates for TB vaccine.

Location	Name	Comments
Secreted	ESAT-6, CFP-10	Highly immunogenic T cell antigens, secreted via the ESX1 system, encoded at RD1 locus
	TB10.4	Highly immunogenic, unknown function
	Ag85, Ag85B	Mycolyl transferase enzymes, Highly immunogenic and abundant
Intracellular	KatG	Catalase
	PPE18	Member of PPE family
	M.TB.32C	Serine proteinase
	HSP65	Heat shock protein
Surface	HBHA	Heparin-binding heamagglutinin, involved in adhesion and spreading

Table 1.3: Tuberculosis vaccines in or on their way to the clinic [25, 26].

Vaccine	Comments	Reference
Live mycobacterial vaccines: modified BCG		
rBCG30	Live, recombinant BCG, overexpressing Ag85B from *M.tb.*. Currently in Phase I clinical trials.	[27]
rBCG::Δ*ureC-llo*$^{+}$	Live, recombinant BCG, urease-deficient mutant that expresses the *lysteriolysin-O* gene from *L. monocytogenes*. Currently in Phase I clinical trials.	[28, 29]
rBCG-Aeras 403	BCG Danish with endosome escape and overexpression of several proteins including Ag85A, Ag85B and TB10.4, Currently in Phase I clinical trials.	[26]
BCG::RDI	BCG Pasteur with reintroduction of RD-1 locus which contains protective Ags, Currently in Phase I clinical trials	[26]
Pro-apoptotic BCG	BCG Tice with diminished superoxide dismutase activity, Currently in Phase I clinical trials	[26]
Live mycobacterial vaccines: modified Mycobacterium tuberculosis		
M. tuberculosis PhoP	Deletion of virulence associated gene *phoP* from *M.tb.* MT103 strain, Phase I clinical trials	[26]
M. tuberculosis mc^{2}6030	*M.tb.* H37Rv with deletion of *panCD* and RD-1 locus, Phase I clinical trials.	[26]
M. tuberculosis mc^{2}6020	*M.tb.* H37Rv with deletion of the *lysA* and the *panCD* locus, Phase I clinical trials.	[26]
Subunit vaccines		
*M.tb.*72f	Recombinant protein composed of a fusion of Rv1196 and Rv0125 from *M.tb.*. Delivered in an oil-in-water emulsion, containing the immunostimulant 3-deacylated-monophosphoryl lipid A and a purified fraction of *Quillaja saponaria* (Quil A). Currently in Phase I clinical trials.	[30, 31]
Ag85B-ESAT-6	Recombinant protein, composed of a fusion of ESAT-6 and Ag85B from *M.tb.*. Delivered in the IC31 adjuvant or in cationic liposomes. Clinical trials planned in 2005.	[32-34]
Naked DNA and viral-vectored vaccines		
MVA-Ag85A	Live, recombinant, replication-deficient vaccinia virus, expressing Ag85A from *M.tb.*. Currently in clinical trials.	[35, 36]
Hsp65 (GroEL) DNA	Conserved antigen from *Mycobacterium leprae* for immunotherapy, Currently in clinical trials.	[26]
Aeras 402 (Ad35.TB-S)	Non-replicating Ad35 expressing multiple TB proteins including Ag85A, Ag85B and TB10.4, Ongoing pre-clinical studies.	[26]
Double-stranded RNA capsids		
Double-stranded RNA capsids	Double-stranded RNA capsids encoding TB antigens for oral delivery, Ongoing pre-clinical studies.	[26]

-in protecting against milliary tuberculosis (extra pulmonary tuberculosis) compared with the pulmonary tuberculosis [37]. Vaccine candidates can be divided into different categories (a) live mycobacterial vaccine: attenuated bacteria or genetically modified bacteria (b) subunit vaccine: different immunogenic proteins as immune activator and (c) DNA vaccine (Table 1.3).

Currently many anti-tuberculosis vaccines are either in the pre clinical trials or in the Phase I trials (Table 1.3). Modified version of BCG strains which can either expresses one or more *M.tb.* proteins (such as Ag85B) or *M.tb*. RD1 region are currently under different stages of consideration as possible live vaccines (Table 1.3). In addition, modified *M.tb.* strains wherein virulence associated genes like *phoP*, *panCD* along with *RD1* region or *panCD* with *lysA* have been deleted are also being tested as vaccine candidates. Besides these various subunits (Table 1.2) such as Ag85, ESAT-6, *Rv1196* and *Rv0125* are used mostly due to their ability to generate robust immune response. A recent advancement in vaccine is to introduce DNA, which can overexpress various immunogenic proteins either directly or through different carrier virus (e.g. Vaccinia virus).

1.6 Recent developments in drugs and success in the therapeutics.

Development of anti-tuberculosis drugs started from 1944 after the discovery of Streptomycin (Fig 1.2). Most of the anti-tuberculosis drugs were discovered from 1940 to 1965. In the past 50 years only one new drug, namely Bedaqulin has been approved by FDA (2012). Increasing threat and evolution of MDR, XDR and TDR tuberculosis makes it necessary to urgently develop new sets of drugs to treat TB. Table 1.4 lists the first line and second line of drugs that are used in the current regimen and their targets.

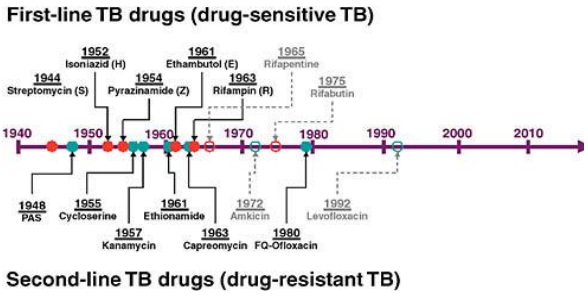

Figure. 1.2. Timeline representing anti-TB drug discovery. The dotted lines indicate that these drugs are not first in class. (http://www.nap.edu/openbook.php?record_id=12570&page=83)

These drugs are effective against active tuberculosis and a treatment of 6 to 7 months is required to eradicate TB from the infected patients. In case of latent TB

infection, a long duration of INH or INH with EMB or INH with PZA has been used to clear the dormant bacteria. (Table 1.4)

Table 1.4: First and Second line of anti-tuberculosis drugs [38].

Drug name and short name (year of discovery)	**Target**	**Effect**
First line drugs		
Isoniazid ***(H)*** (1952)	Enoyl-[acyl-carrier-protein] reductase	Inhibits mycolic acid synthesis
Rifampicin ***(R)*** (1963)	RNA polymerase, beta subunit	Inhibits transcription
Pyrazinamide ***(Z)*** (1954)	S1 component of 30S ribosomal subunit	Inhibits translation and trans-translation, acidifies cytoplasm
Ethambutol ***(E)*** (1961)	Arabinosyl transferases	Inhibits arabinogalactan biosynthesis
Second line drugs		
Para-amino salicylic acid ***(Pas)*** (1948)	Dihydropteroate synthase	Inhibits folate biosynthesis
Streptomycin ***(S)*** (1944)	S12 and 16S rRNA components of 30S ribosomal subunit	Inhibits protein synthesis
Ethionamide ***(Eto)*** (1961)	Enoyl-[acyl-carrier-protein] reductase	Inhibits mycolic acid biosynthesis
Ofloxacin ***(Ofx)*** (1980)	DNA gyrase and DNA topoisomerase	Inhibits DNA supercoiling
Capreomycin ***(Cm)*** (1963)	Interbridge B2a between 30S and 50S ribosomal subunits	Inhibits protein synthesis
Kanamycin ***(Km)*** (1957)	30S ribosomal subunit	Inhibits protein synthesis
Amikacin ***(Amk)*** (1972)	30S ribosomal subunit	Inhibits protein synthesis
Cycloserine ***(Dcs)*** (1955)	d-alanine racemase and ligase	Inhibits peptidoglycan synthesis

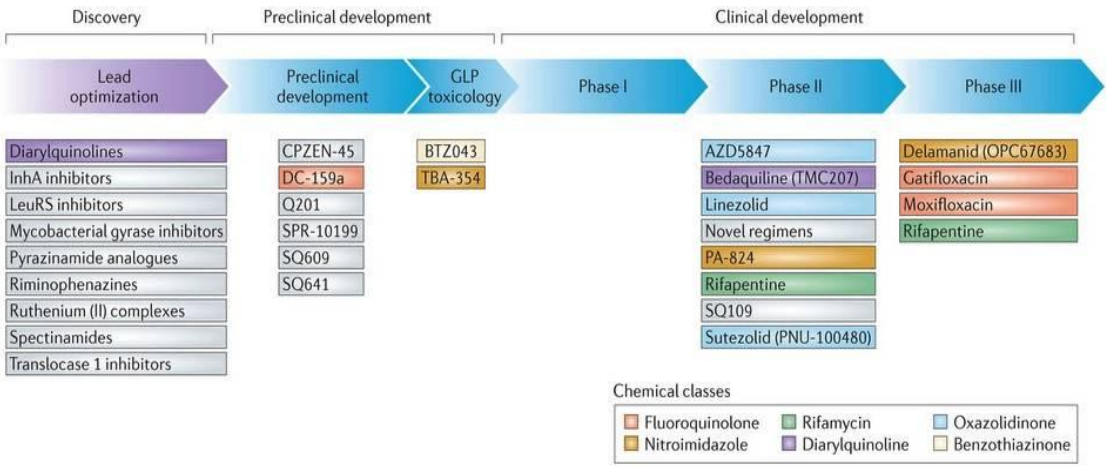

Figure. 1.3. Development of novel anti-tuberculosis drugs and treatment. Inhibitors which are under development and validation are shown here [38].

Treatment of TB requires effective administration of drugs through Directly Observed Therapy (DOT) and follow up program. WHO has started many new strategies including PIP, The END TB Strategy and STOP TB etc towards new drug discovery and development. These efforts resulted in discovery of new drugs such as Delamanid (OPC67683) and Bedaquiline (TMC207), which can be used in combination with current therapy to treat MDR-TB. Challenges in the new target discovery include drug toxicity, intolerance, expensive trials, limited animal models and off target effects. An ideal TB drug should be more potent, effective against latent bacilli, *M.tb.* in different physiological states, compatible with HIV drugs (for co-infection patients) and existing TB drugs, and should reduce the time of treatment [39-41]. Figure 1.3 depicts promising new TB drugs that are in pipeline. Various new molecules have been investigated and new treatment regimens are under clinical phase of the trial (Fig 1.4). Many of the drugs (rifampicin, fluoroquinolones, riminophenazines and oxazolidinones) are repurposed (from other regimen of different disease) against TB.

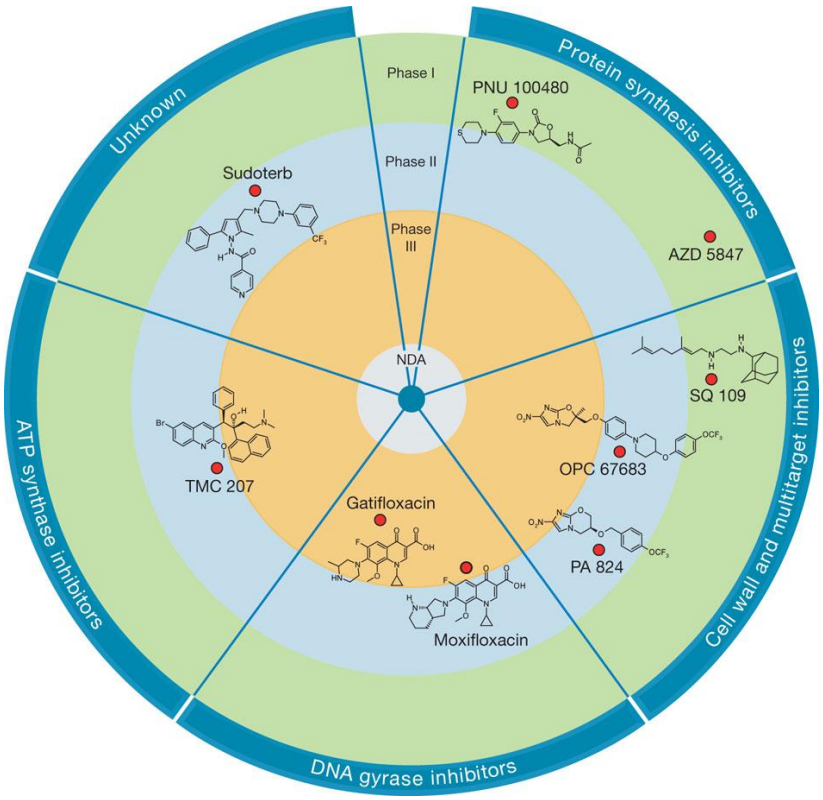

Figure. 1.4. Important anti-tuberculosis drugs which are in clinical trial. Every drug candidate is presented with the target family and its clinical phase. TMC 207 has been approved by FDA in 2012 [40].

Next generation of therapeutics requires bidirectional development that targets bacteria and also reduce the host facilities upon entering inside the body. Since *M.tb.* is an intracellular bacterium that exploits the host system to infect and spread; suppressing the host pathways (i.e. apoptosis, various *M.tb.* driven host signalling pathways) and enhancing the immune response may circumvent the tuberculosis infection. Beside these, proper understanding of the biology of *M.tb.* and its important genes would pave new path for further development of next generation of inhibitors to cure TB.

1.7 Genetics and evolution of M. tuberculosis: Codes and secrets behind the door.

M.tb. genome contains ~4000 genes (4.411 Mb, 65.6% G + C content), of which 40% are characterized, 44% have probable functions, while the remaining 16% are uncharacterized [43]. Among the 61 possible tRNA genes, Cole et al., identified 43 tRNA coding genes and none of them have 'A' in the first position of the anticodon, suggesting extensive wobble base pairing during translation. Almost 10% of total genes are related to PE and PPE family (glycine and acidic residues rich protein family) from PGRS (polymorphic GC rich-sequence) loci. Almost 200 genes belong to oxidoreductases, oxygenases and dehydrogenases, >100 genes are thought to be involved in regulation and signal transduction (including 11 pairs of sensor histidine kinase and response regulator and two component regulatory and 11 eukaryotic-like serine/ threonine protein kinases, etc), ~200 genes code for enzymes--related to lipid metabolism and ~36 genes code for fatty acid degradation [43]. All

Table 1.5: General classifications of *M. tuberculosis* genes [42].

Function	**No. of genes**	**% of total**	**% of Total coding capacity**
Lipid metabolism	225	5.7	9.3
Information pathways	207	5.2	6.1
Cell wall and cell processes	517	13.0	15.5
Stable RNAs	50	1.3	0.2
IS elements and bacteriophages	137	3.4	2.5
PE and PPE proteins	167	4.2	7.1
Intermediary metabolism and respiration	877	22.0	24.6
Regulatory proteins	188	4.7	4.0
Virulence, detoxification and adaptation	91	2.3	2.4
Conserved hypothetical function	911	22.9	18.4
Proteins of unknown function	607	15.3	9.9

the genes corresponding to different functional categories genes are shown in table 1.5.

MTC contains number of mycobacteria (all are clonal in their spread) which have evolved at the horn of Africa (Fig 1.5) [44, 45]. Extensive point mutation, InDels, insertions (IS*6110*, IS*1081*, gene duplication, replication errors), deletions (RecA, IS-mediated, replication errors) and translocations are responsible for the origin of pathogenic *M.tb.* strains. Studies revealed that almost 10,000 years ago an abrupt increase in human population (during Neolithic demographic transition) was critical and string selective force for the successful spread of *M.tb.* [46]. The main human infecting species can be categorized into seven different types as shown in the table 1.6. Types 2 & 3, type 5 & 6 are closely related lineages.

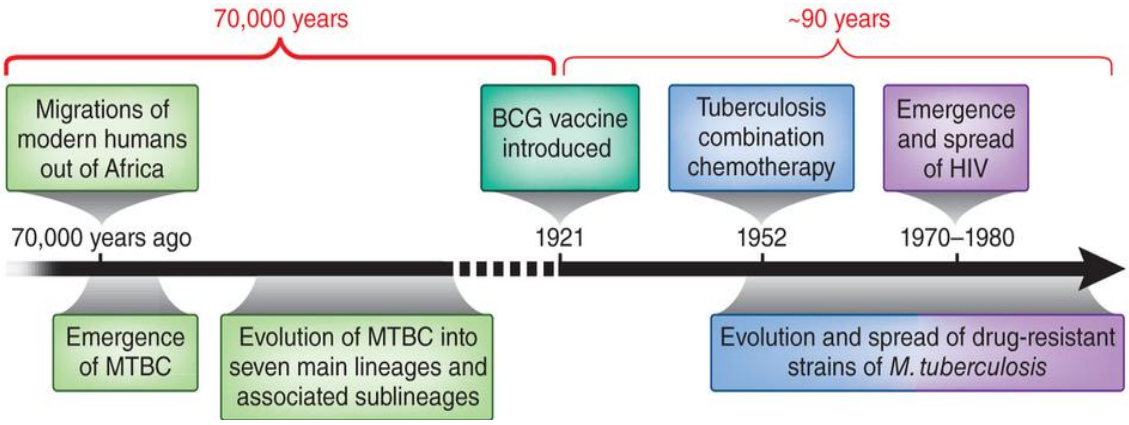

Figure. 1.5. Timescale depicting the progression of *M.tb.* with human and the evolution of drug resistance strains. [46]

Table 1.6: Various bacterial types of *M. tuberculosis* [47].	
Types	**Description**
Type 1	East- African-Indian (EAI) & some Manu (Indian) strains
Type 2	Beijing group
Type 3	Central Asian (CAS) strains
Type 4	Ghana and Haarlem (H/T), Latin America-Mediterranean (LAM) and X strains.
Type 5	*Mycobacterium africanum* and found mainly and at high frequency in West Africa.
Type 6	
Type 7	Isolated from the Horn of Africa

1.8 Immunology of M. tuberculosis: Protective strategies of M.tb.

After entering the body, *M.tb.* faces the host immune system of the body. From the clinical and experimental animal data it was evident that $CD4^+$ T cells [48-50], IFN-γ, IL-12, [48, 49, 51, 52], and TNFα [53, 54] play an important role in tuberculosis infection (Fig 1.6).

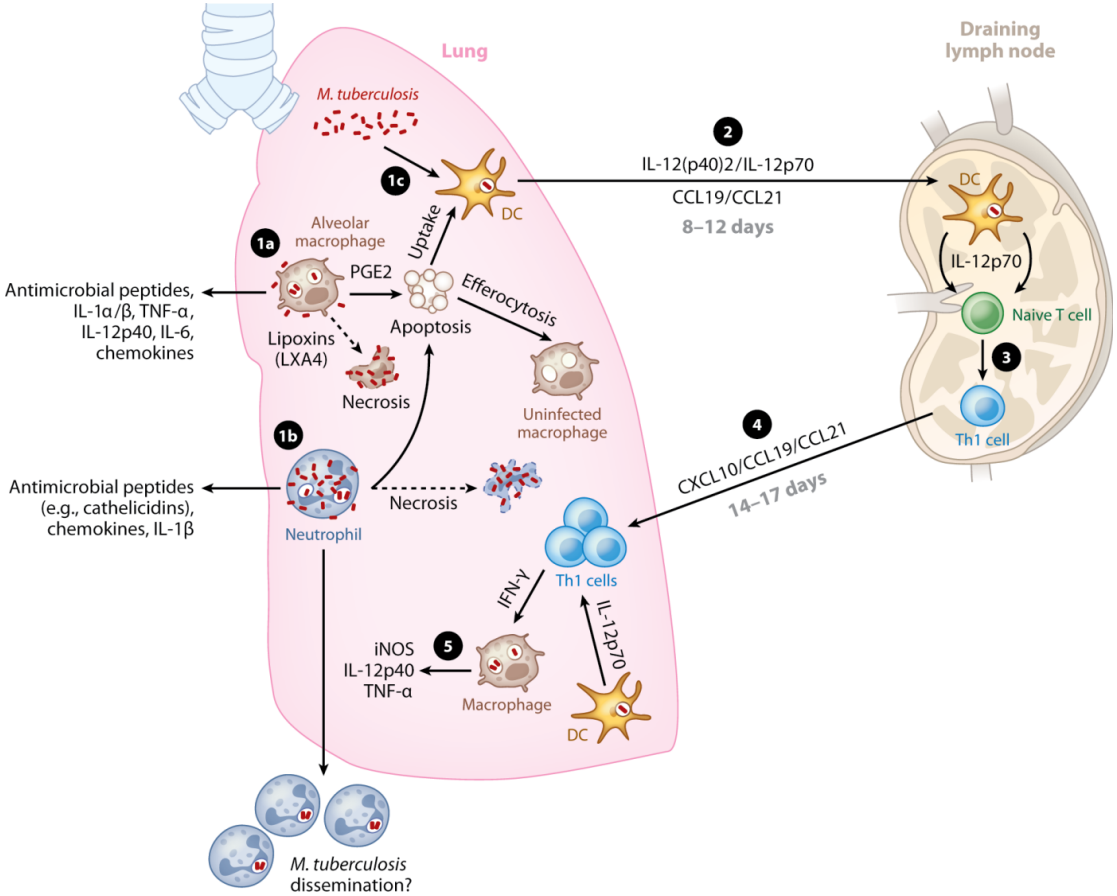

Figure. 1.6. Cellular immune response against *M.tb.* After infection with *M.tb.*, they are taken up by the native lung alveolar macrophages (1a), neutrophils (1b) and lung DCs (1c). This is followed by generation and secretion of cytokines, chemokines and antimicrobial peptides. Further induction of apoptosis or necrosis of infected macrophages will be determined by balance of lipid mediators like lipoxin (LX) A4 (pronecrotic) or prostaglandin E2 (proapoptotic). Infected apoptotic cells either can be engulfed by resident dendritic cells (DCs) or by uninfected lung macrophages through efferocytosis (1c). In next 8-12 days after infection, *M.tb.* infected DCs migrate to the lymph nodes under the influence of IL-12 (p40)2 and IL-12p70 and CCL19 and CCL21 chemokines (2) and drive naive T cell differentiation toward Th1 cells (3). 14–17 days post infection antigen-specific Th1 cells migrate back to lungs in chemokine-dependent manner (4) followed by production of IFN-γ which activate macrophages, cytokine production and generation of anti-microbial factors such as iNOS (5). (Adapted from O'Garra et al. [55])

Symptoms of active pulmonary tuberculosis (weight loss, fever, night sweats, regular cough, haemoptysis, lungs cavities and thoracic lymphadenopathy) are indicating of TB infection in host. (Fig 1.6) [56, 57]. While latent TB has no direct sign of detection and this quiescent form is maintained by strong host immune response (Fig 1.6).

After the infection bacilli are phagocytosed by alveolar macrophages [58] or neutophils [59, 60] or by dendritic cells [61] (Fig 1.6). Cell to cell spread is facilitated by either necrotic or apoptotic cell death through lipoxin A4 (LXA4; pronecrotic) and prostaglandin E2 (PGE2; proapoptotic) mediated pathways (Fig 1.6). [62-65]. These infected macrophages can be engulfed by uninfected macrophage (process called efferocytosis) followed by killing of *M.tb.* [66]. Further bacilli can be delivered to dendritic cells (DCs), which activate $CD4^+$ T-cells and generate profound anti-tuberculosis immune response (Fig 1.6) [67].

1.9 Cell wall of M. tuberculosis: Protective armour of foe.

Cell wall of *M.tb.* consists of an inner layer and outer layer (contains lipids and protein) which is orthogonal to the bacterial surface [68]. Outer cell wall consisting of lipomannan, lipoarabinomannan (LAM), phthiocerol-containing lipids like dimycolyl trehalose or cord factor, phthiocerol dimycocerosate, *M.tb.* specific sulfolipids and phosphatidyl-inositol mannosides. In *M.tb.* LAM are terminally capped with mannose containing β-Ara residue (ManLAMs) [69, 70]. The inner part is made up of peptidoglycan (PG), arabinogalactan (AG) and mycolic acid (MA) covalently linked and forming MA-AG-PG complex (Fig 1.7).

Peptidoglycan (PG) of *M.tb.* is versatile in composition and sturdy, which is responsible for the rod shape of the bacteria. PG is composed of both peptide and glycan. Glycan part is mainly made of long and covalently connected repeating units of *N*-acetylglucosamine (NAG) and *N*-acetylmuramic acid (NAM). Peptide: l-alanyl-d-*iso*-glutaminyl-*meso*-DAP-d-alanine is linked to the NAM through the lactyl group [71]. Cell wall of *M.tb.* is categorized as chemotype IV, consisting peptidoglycan with arabinogalactan and *meso*-DAP [72]. Interestingly muramic acid of *M.tb.* cell wall has an either N-acetyl or N-glycolyl group [73-75]. Cross linking in PG is between DAP-DAP (75%) or DAP-alanine (25%). DAP-DAP linkages and presence

of N-glycolyl group on muramic acid are the reasons behind the rigidity of *M.tb.* PG [76].

Synthesis of the PG includes various steps and enzymes, which are analogous to other bacterial cell wall synthesis pathways (as depicted in fig 1.7). These include the production of UDP-GlcNAc from fructose-6-phosphate through series of reactions catalyzed by enzymes GlmS, GlmM and GlmU. Next enoyl pyruvate is added to 3rd position of UDP-GlcNAc by MurA followed by its reduction into UDP-NAM by MurB [77]. Next set of reactions add 1-alanine (by MurC), d-glutamine (by MurD), DAP (by MurE) and d-alanyl-d-alanine (by MurF) to generate UDP-NAM-pentapeptide called as Park's nucleotide (Fig 1.7). Subsequent transfer of UDP-NAM-pentapeptide to decapreny-l-phosphate by MurX generates Lipid I [75].

At this stage NAM part of Lipid I can be glycolated by NamH to *N*-glycolylmuramic acid (Fig 1.7) [78]. Transfer of GlcNAc moiety from UDP-GlcNAc by MurG produces Lipid II (Fig 1.7), which is subsequently transferred to the plasma membrane through bactoprenol. Cell membrane proteins FtsW and/or RodA work as translocase/flippase for the translocation of these precursors from inside to the outside of the membrane (Fig 1.7) [79-81]. Next sets of reactions happen in the 'pseudoperiplasmic' space. Here transglycosylase links all peptidoglycan monomers to the existing PG strands [82] and strengthen the PG. Also DAP-DPA linkage, which provides resistance against β-lactams, is carried out by transpeptidase [83, 84]. Since there is no ATP in periplasmic space, cleavage of d-alanyl-d-alanine is thought to furnish the required energy.

Arabinogalactan (AG) is most abundantly present in the *M.tb.* cell wall and provides integrity. Arabinogalactan forms phosphodiester linkage with muramic acid and is required for anchoring mycolic acid layer with the PG layer (Lederer *et al.*, 1975, [85]. In the arabinogalactan, both arabinose and galactan are --present in the furanose form [86]. Arabinan chains are made up of 1→5 linked α-d-Ara*furanose* with the linkage generated by *3,5*-α-d-Ara*f* residues. Arabinan chain is attached to the 5th position (by 1→5 linkage) of galactan. All galactan (containing arabinan) are connected by alternating 1→5 and 1→6 linkage of almost 30 residues [87].

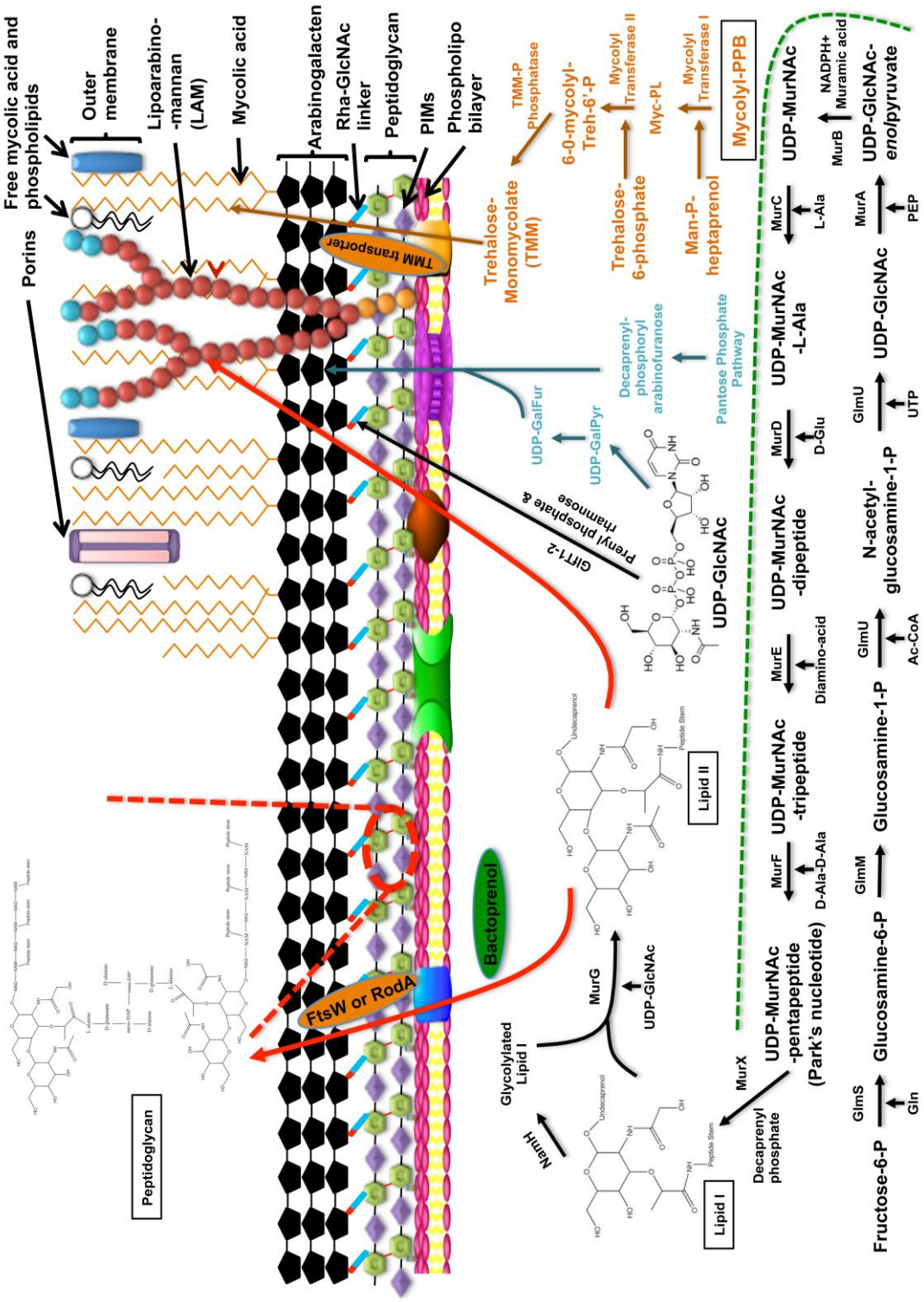

Figure. 1.7. Cell wall biosynthesis pathways in *M. tuberculosis.* Peptidoglycan synthesis is depicted in black. Arabinogalactan biosynthesis is presented in blue and Mycolic acid synthesis is depicted in orange.

Phosphoryl-N-acetylglucosaminosyl-rhamnosyl linkage {α-l-Rha*p*-(1→3)-α-d--GlcNAc-(1→P)} provides attachment of AG to muramic acid of PG [88, 89]. It was also found that some of the galactan are not arabinosylated and make unbranched galactan polymer. Clusters of mycolic acids are attached with ester linkage to all four available position of 2/3 of the terminal arabinose moiety.

Synthesis of AG happens in combination with the synthesis of Rha-GlcNAc linker. This linker is produced by the transfer of UDP-NAG to prenyl phosphate and rhamnose [90]. Remaining two steps occurs separately for the AG biosynthesis. These include synthesis of UDP-galactofuranose (UDP-GalFur) from UDP-galactopyranose (UDP-GalPyr) [91] and decaprenylphosphoryl- arabinofuranose from the pentose phosphate pathway (Fig 1.7) [92, 93]. Further galactofuranose polymerizes and forms long linear chain on which arabinofuranose moieties are added [94, 95]. Finally this AG complex is ligated to peptidoglycan with the release of decaprenyl phosphate with the help of some unknown enzymes (Fig 1.7).

Mycolic acids (MA), made up of short α-alkyl- and long β-hydroxyl-fatty acids (60-90 carbon per chain), are majorly responsible for the permeability of the cell wall [96]. Most of the MA exists as tetramycolyl-pentaarabinofuranosyl clusters that linked to AG with ester linkage [88, 97]. The biosynthesis of MA, catalyzed by mycolyltransferase I, involves the transfer of mycolyl-S-PPB (thioester linked mycolic acid to PPB domain of Pks13) to Man-P-heptaprenol to generate Myc-PL (6-*O*-mycolyl- β -D-mannopyranosyl-1-phosphoheptaprenol) (Fig 1.7). In the next step Myc-PL reacts with trehalose-6-P (catalyzed by mycolyltransferase II) to generate 6-*O*-mycolyl-Treh-6'-P (TMM-P), which is subsequently dephosphorylated by TMM-P phosphatase to generate TMM (Trehalose Mono Mycolate). TMM thus generated is transported out of the cell in an ATP energy dependent reaction catalyzed by TMM transporter (ABC transporters), wherein it participates in the synthesis of trehalose di-mycolate (TDM) and arabinogalacten-mycolate (Fig 1.7) [98].

Involvements of eukaryotic like serine/ threonine protein kinases (STPKs) were found to be important in the cell wall synthesis. Out of all 11 STPKs of *M.tb.* PknA and PknB were shown to play important role in regulating cell wall synthesis.

Both PknA and PknB phosphorylate GlmU [99], PcaA, PapA5 and *Rv1422* [100-102]. Apart from this many cell division protein including FtsZ, FipA and Wag31 have been shown to be phosphorylated by PknA or PknB [103, 104]. In addition, enzymes involved in mycolic acid synthesis such as β-ketoacyl ACP synthase (KasA), KasB, β-ketoacyl-ACP reductase (MabA), hydroxyacyl-ACP dehydratases (HadAB and HadBC) and enoyl-ACP reductase (InhA) have been identified to be targets of PknA and PknB mediated phosphorylation [105-110].

Chapter 2.

Review of literature

Chapter 2.

Review of literature

In addition to providing strong interphase, cell wall of *M.tb.* also plays critical role during cell division and in the establishment of infection. Therefore perturbing the bacterial cell wall with the help of inhibitors would have significant impact both on bacterial survival and virulence. Due to the emergence of MDR, XDR strains of *M.tb.* we require newer targets and strategies to combat the infection. Remedial approaches that would involve development of newer inhibitors should take into consideration drug resistance strains and latent bacteria. *M.tb.* cell wall composition changes during latency, suggesting that cell wall could be one of the reasons for prolonged survival. *M.tb.* cell wall synthesis is a complex process that requires coordination between various enzymes and substrates (Chapter 1, Fig 1.7). Targeting enzymes that are required for the production of key metabolites in the pathway would result in perturbation of cell wall synthesis, which eventually may lead to cell death. In this study we have worked on $GlmU_{Mtb}$, an enzyme with dual activity required for the synthesis of UDP-GlcNAc.

2.1 Cell wall metabolism and catabolism.

Cell wall metabolism includes synthesis and assimilation of various components of the cell wall. *M.tb.* cell wall contains many glycoproteins and glycolipids, thus providing strong and less permeable armour around it. As discussed in Fig 1.7, *M.tb.* cell wall metabolism can be divided into four different events.

(i) Biosynthesis of peptidoglycan.

(ii) Biosynthesis of mycolic acid.

(iii) Generation of Arabinogalactan.

(iv) Synthesis of lipoarabinomannan and other lipoproteins.

Table 2.1 represent potential target enzymes involved in the cell wall synthesis that have been investigated as possible candidates for therapeutic intervention. Most of the established drugs against TB such as D-Cycloserine, Ethambutol, and INH act on the enzymes that are involved in cell wall synthesis.

Table 2.1: Validated cell wall synthesis enzymes of *M.tb.* as drug target.

		Validation					
Metabolic pathway	**Protein**	**Gene replace-ment mutant survival *in vitro***	**Gene replace-ment mutant survival *in vivo***	**Crystal structure PDB**	**Co-crystal structure**	**Inhibitors**	**Reference**
Peptidoglycan biosynthesis	Alanine-racemase	Unable to survive	NA	1XFC	D-cycloserine	D-cycloserine	[111]
	D-Ala-D-Ala ligase	Unable to survive	NA	2i87	NA	D-cycloserine	[111, 112]
	GlmM	Unable to survive	NA	NA	NA		[113, 114]
	GlmU	Unable to survive	NA	3SPT, 4G3S, 3D98	NA		[3, 4, 115]
Arabinogalactan biosynthesis	EmbA–C	Unable to survive	NA		Co-factor (PLP)	Ethambutol	[95, 116]
	AftA	Unable to survive	NA	NA	NA	NA	[117]
	Phospho-ribosyltransferase	Unable to survive	NA	NA	NA	NA	[118]
	Galactofura-osyl - transferase	Unable to survive	NA	NA	NA	NA	[119]
	dTDP-deoxy-hexulose reductase	Unable to survive	NA	NA	NA	NA	[120]
	RmlA–D	Unable to survive	NA	NA	NA	NA	[120]
Mycolic acid biosynthesis	ENR (InhA)	Unable to survive	NA	NA	NA	Isoniazid	[20, 121, 122]
	AcpM	Unable to survive	NA	NA	NA	NA	[123]
	FabD	Unable to survive	NA	NA	NA	NA	[123]
	FabH	Unable to survive	NA	1U6E, 1U6S	NA	NA	[124, 125]
	MabA	Unable to survive	NA	1I01	NA	NA	[126, 127]
	KasA	Unable to survive	NA	NA	NA	Thiolactom-ycin	*[128]*
	KasB	Unable to survive	NA	NA	NA	Thiolactom-ycin	*[128]*
	MmaA4		Attenuate-d	NA	NA	NA	*[129]*
	Pks13	Unable to survive	NA	NA	NA	NA	*[130]*
	Acyl-AMP ligase	Unable to survive	NA	NA	NA	NA	*[131]*
	FadD32	Unable to survive	NA	NA	NA	NA	*[131]*
	AccD4	Unable to survive	NA	NA	NA	NA	*[131]*
	AccA3	Unable to survive	NA	NA	NA	NA	*[132]*
	AccD5	Unable to survive	NA	NA	NA	NA	*[132]*
	AccE5	Unable to survive	NA	NA	NA	NA	*[132]*

Peptidoglycan and arabinogalactan are capaciously altered with amide, succinyl, glycolyl and galactosamine residues [133-135]. *M.tb.* also has unusual 3-3 peptide cross linking instead of traditional 4-3 peptide cross linking in PG [133]. Mycolic acid is synthesized in three different forms namely; methoxy-meroacids, α-meroacids and keto-meroacids, with varied length of acyl chains, saturations and cyclopropanations [98]. Mycolic acid contents of the cell wall composition have been reported to vary during infection and latency [136, 137]. Further the transcription levels of the enzymes involved in lipid and mycolic acid synthesis also vary during the infection [138]; suggesting these changes could be a part of adaptive response of the bacteria to generate a heterogeneous population. Such adaptations in bacterial population diversity would allow the pathogen to survive in adverse dynamic stress encountered in the host, such as antibiotics and immune response.

In general cell wall of bacteria contributes more than 20% of dry mass. Therefore, cell wall breakdown process in every generation would be a huge energy and nutrients consuming process for the microorganism specially for a bacteria like *M.tb.*, which resides inside the host cells in both active and dormant forms. Therefore, cell wall contents need to be reutilized either as carbon source or as a precursor through salvage pathways. Many other bacteria such as *E. coli* and *B. subtilis* recycle the cell wall catabolic intermediates. *M.tb.* has β-lactamases protein which monitors the cell wall synthesis and remodelling [139-142]). In *M.tb.*, number of proteins such as transporters and hydrolases are involved in the cell wall remodelling but the recycling have not yet been characterized.

2.2 UDP-GlcNAc synthesis and its role in prokaryotes and eukaryotes.

The synthesis of UDP-GlcNAc, a critical metabolic intermediate occurs in the cytosol (Fig 1.4). The *de novo* synthesis involves conversion of fructose-6-phosphate, a metabolic intermediate of glycolysis, to UDP-GlcNAc through isomerisation, acetyl and uridyltransferase activities of different enzymes. While the enzymes of the pathway leading to UDP-GlcNAc synthesis from fructose-6-phosphate are conserved in prokaryotes, they are distinct from the corresponding enzymes in the eukaryotic pathway (Fig. 2.1).

In addition to the *de novo* pathways both prokaryotes and eukaryotes can employ salvage pathway, which utilizes the GlcNAc from the extracellular milieu.

Salvage pathway in the eukaryotes involves GlcNAc transporters (GLUTs) to import GlcNAc from the surroundings and a sugar kinase to phosphorylate it at the 6th position to form GlcNAc-6-P, which can be utilised by the *de novo* biosynthetic pathway [143]. Salvage pathway in prokaryotes involves N-acetylglucosamine transporters (NGTs) to transport GlcNAc followed by phosphorylation to generate GlcNAc-6-P. GlcNAc-6-P can either undergo deacetylation or isomerisation followed by deacetylation to generate intermediates of de novo biosynthetic pathway (Fig 2.1). However till date the presence of salvage pathways has not been reported in mycobacteria. While in prokaryotes UDP-GlcNAc is mostly used as metabolic precursor for the synthesis of cell wall components, in eukaryotes the major function is that of GlcNAcylation of proteins [144].

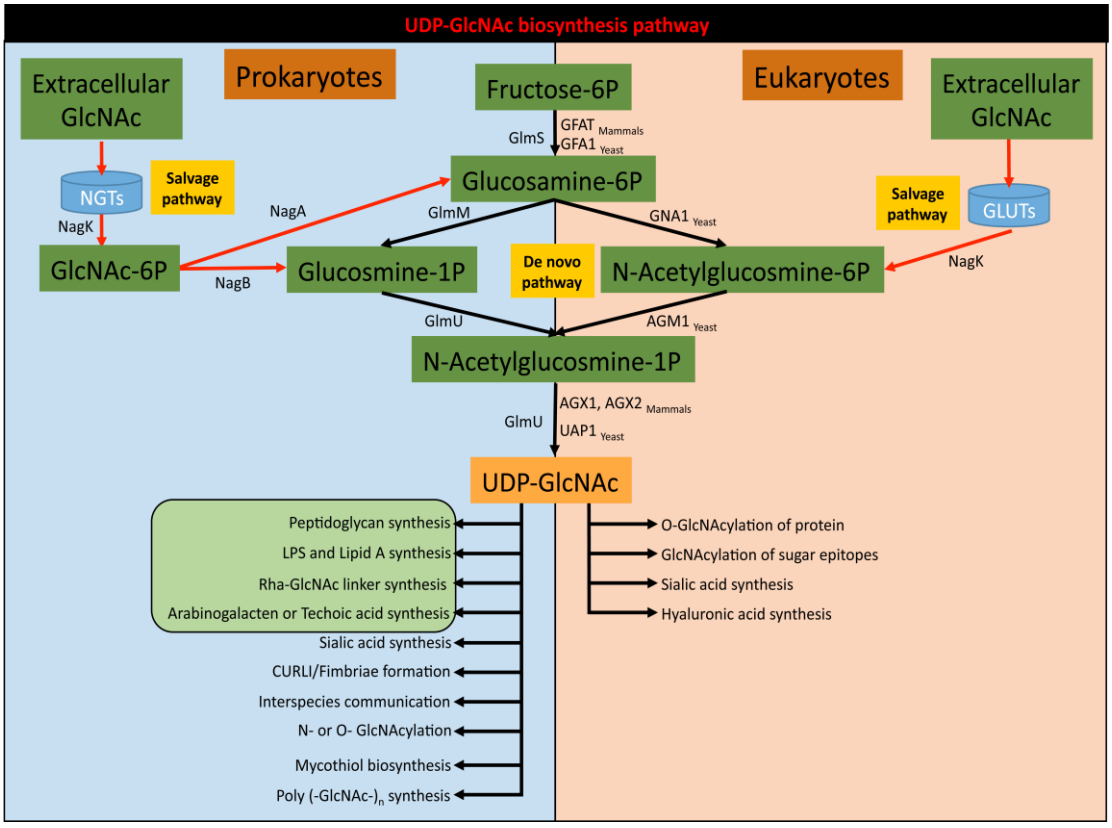

Figure. 2.1. UDP-GlcNAc synthesis pathways in prokaryotes and eukaryotes.

```
HumanUAP        MASEQDVRARLQRAGQEHLLRFWAELAPEPRAALLAELALLEPEALREHCRRAAEACARP 60
HumanGNA1       ---------------------------MKPDETPMFDPSLLKEVDWSQNTATFSPAISPT 33
MtbGlmU         MTFPGDTAVLVLAAGPGTRMRSDTPKVLHTLAGRSMLSHVLHAIAKLAPQR-LIVVLGHD 59
                                         ..         :*.             . .

HumanUAP        HGPPPDLAARLRPLPPERVGRASRSDPETRRRWEEEGFRQISLNKVAVLLLAGGQGTRLG 120
HumanGNA1       H---PGEGLVLRPLCTADLNRG-------------------------FFKVLGQLTETG 64
MtbGlmU         HQRIAPLVGELADTLGRTIDVALQDRPLGTGHAVLCGLSALPDDYAGNVVVTSGDTPLLD 119
                *   .     *       :. .                          .. . *: .  .

HumanUAP        VTYPKGMYRVGLPSRKTLYQLQAERIRRVEQLAGERHGTRCTVPWYVMTSEFTLGPTAEF 180
HumanGNA1       VVSPE------------------------QFMKSFEHMKKSGDYYVTVVEDVTLG----- 95
MtbGlmU         ADTLADLIATHRAVSAAVTVLTTT----LDDPFGYGRILRTQDHEVMAIVEQTDATPSQR 175
                .                              :   .  :  :          : * .

HumanUAP        FREHNFFHLDPANVVMFEQRLLPAVTFDGKVILERKDKVAMAPDGNGGLYCALEDHKILE 240
HumanGNA1       -------QIVATATLIIEHKFIHSCAKRG-----RVEDVVVSDECRG------------- 130
MtbGlmU         EIREVNAGVYAFDIAALRSALSRLSSNNAQQELYLTDVIAILRSDGQTVHASHVDDSALV 235
                        : .     :.  :    :  .       : :.:  .

HumanUAP        DMERRGVEFVHVYCVDNILVRLADPVFIGFCVLQGADCGAKVVEKAYPEEPVGVVCQVDG 300
HumanGNA1       -------------------KQLGKLLLSTLTLLSKKLNCYKITLECLPQN-VGFYKKFG- 169
MtbGlmU         AGVNNRVQLAELASELN-RRVVAAHQLAGVTVVDPATTWIDVDVTIGRDTVIHPGTQLLG 294
                                  :.   :  . ::.      .:      :  :    :.

HumanUAP        VPQVVEYSEISPETAQLRASDGSLLYNAGNICNHFFTRGFLKAVTREFEPLLKPHVAVKK 360
HumanGNA1       -------------------------YTVS--EENYMCRRFLK------------------ 184
MtbGlmU         RTQIGGRCVVGPDTTLTDVAVG---DGASVVRTHGSSSSIGDGAAVGPFTYLRPGTALGA 351
                                        ..    :     : .

HumanUAP        VPYVDEEGNLVKPLKPNGIKMEKFVFDVFRFAKNFAALEVLREEEFSPLKNAEPADRDSP 420
HumanGNA1       ------------------------------------------------------------
MtbGlmU         DGKLGAFVEVKNSTIGTGTKVPHLTYVGDADIGEYSNIG--ASSVFVNYDGTSKRRTTVG 409

HumanUAP        RTARQALLTQHYRWALRAGARFLDAHGAWLPELPSLPPNGDPPAICEISPLVSYSGEGLE 480
HumanGNA1       ------------------------------------------------------------
MtbGlmU         SHVRTGSDTMFVAPVTIGDGAYTGAGTVVREDVPPGALAVSAGPQRNIENWVQRKRPGSP 469

HumanUAP        VYLQGREFQSPLILDEDQAREPQLQES 507
HumanGNA1       ---------------------------
MtbGlmU         AAQASKRASEMACQQPTQPPDADQTP- 495
```

Figure. 2.2. Protein alignment of $GlmU_{Mtb}$ with human Glucosamine-6-phosphate N-acetyltransferase (GNA1 or GNPNAT1) and human UDP-N-acetylhexosamine pyrophosphorylase-like protein 1 (UAP or UAP1L1) enzymes.

Additionally, in eukaryotes UDP-GlcNAc can also be utilised for the sialic acid biosynthesis, GlcNAcylation of sugar epitopes and hyaluronic acid biosynthesis [145-150]. While in prokaryotes it has been reported to be involved in many pathways such as peptidoglycan, Lipid A subunit of lipopolysaccharide of gram negative bacteria, Rha-GlcNAc linker, arabinogalactan, teichioc acid in gram positive bacteria, sialic acid in selected bacteria, poly (-GlcNAc-)$_n$ in som bacteria and *N*- GlcNAcylation in few prokaryotes [94, 135, 151-153]. While in mycobacteria UDP-GlcNAc was known to be utilized in peptidoglycan, arabinogalactan, Rha-GlcNAc linker, lipid I and in mycothiol biosynthesis [90, 94, 154-156].

2.3 N-acetyl-glucosamine-1-phosphate uridyltransferase (GlmU).

GlmU, present exclusively in the prokaryotes, is a bi-functional enzyme, with acetyltransferase and uridyltransferase activities catalyzed by the C- and N- terminal domains respectively. The carboxyl-terminal domain of GlmU transfers the acetyl moiety from acetyl CoA onto glucosamine-1-phosphate to generate N-acetylglucosamine-1-phosphate (GlcNAc-1-P). The N-terminal uridyltransferase domain of GlmU then catalyzes the transfer of UMP (from UTP) to GlcNAc-1-P to form UDP-GlcNAc (Fig 2.4). Interestingly, eukaryotic and prokaryotic acetyltransferase and uridyltransferase enzymes are quite distinct with little or no similarity (Fig 2.2).

Acetyltransferase reaction (C-terminal domain)

GlcN-1-P + Acetyl CoA ⟶ GlcNAc-1-P + CoA (1)

Uridyltransferase reaction (N-terminal domain)

GlcNAc-1-P + UTP ⟶ UDP-GlcNAc + PPi (2)

GlmU is an evolutionary conserved protein, which is present both in gram-positive and negative bacteria (Fig 2.3). GlmU has been extensively studied earlier in number of bacteria such as *E. coli, H. influenzae, S. pneumoniae, and X. oryzae*. Importantly, UDP-GlcNAc synthesis is not present in some of the bacteria of bacteroidetes phylum. Such bacteria utilize host resources such as sugar containing food material in the gut or other GlcNAcylated secretary proteins from the surroundings to synthesize their cell wall [157-159].

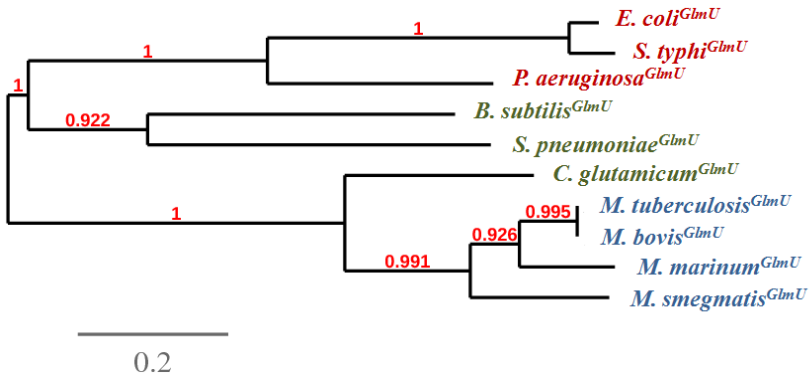

Figure. 2.3. Phylogenetic tree showing evolution of $GlmU_{Mtb}$ and very little differences among GlmU from various bacteria.

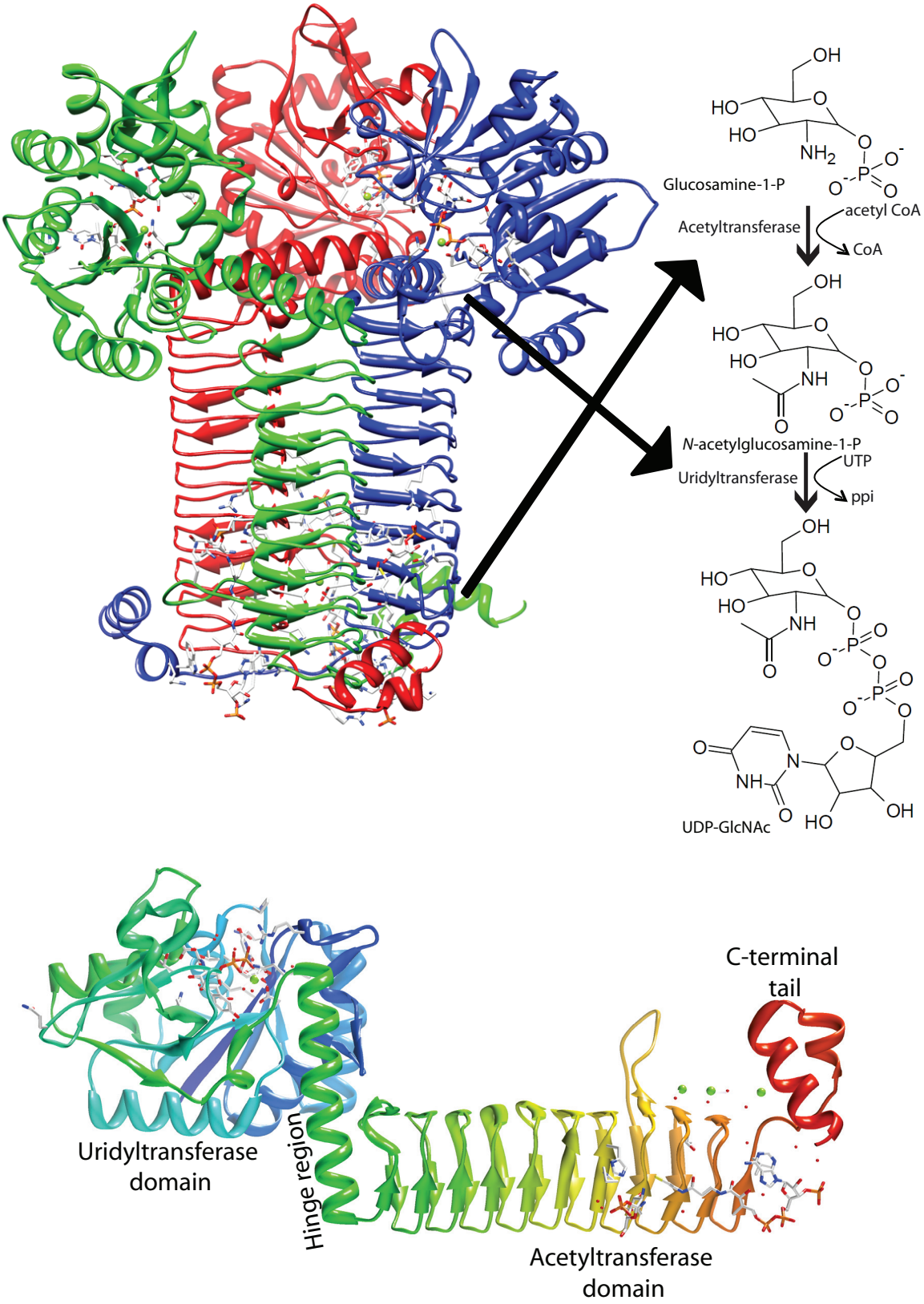

Figure. 2.4. ***M. tuberculosis*** **GlmU structure: (A)** Trimeric structure of $GlmU_{Mtb}$, each monomer is in different colour. Arrows showing $GlmU_{Mtb}$ catalysed reactions (shown beside the structure): acetyltransferase reaction at C-terminal and uridyltransferase reaction at N-terminal domain. **(B)** Monomer of $GlmU_{Mtb}$ representing various domains and regions of $GlmU_{Mtb}$.

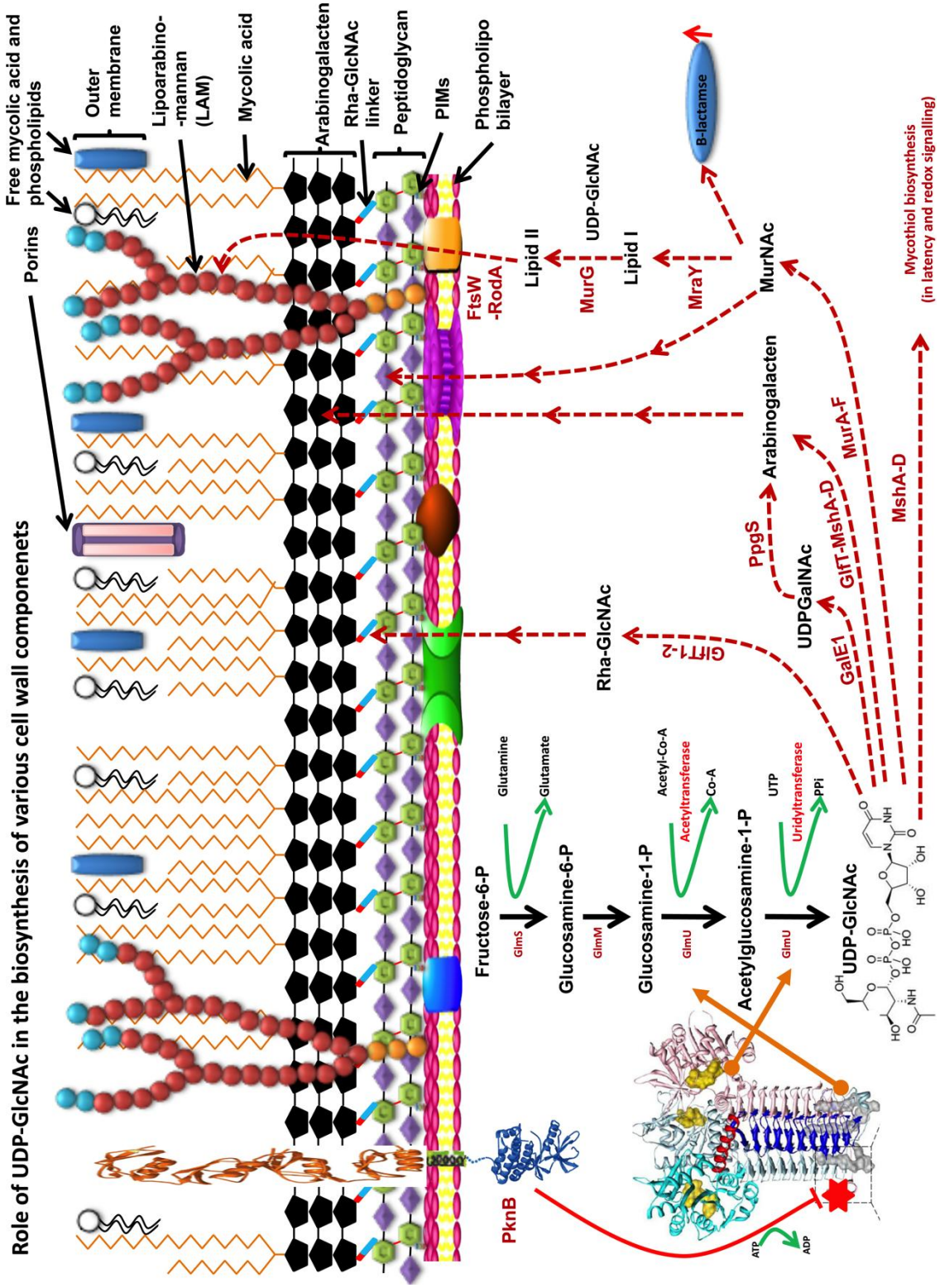

Figure. 2.5. Role and regulation of $GlmU_{Mtb}$ and UDP-GlcNAc in *M.tb.*

Table 2.2: Crystal structures information of GlmU from different bacteria.

Bacteria	Ligand for co-crystal	Domain	PDB-ID	Ref/year
Yersinia pestis	Apo	Both	3FWW	2012
Yersinia pestis	GlcN-1-P	Acetyltransferase	4FCE	2012
M. tuberculosis	Apo	Both	3DK5	[99]
M. tuberculosis	UDP-GlcNAc	Uridyltransferase	3DJ4	[99]
M. tuberculosis	ATP	Uridyltransferase	4K6R	[160]
M. tuberculosis	CoA, GlcN-1-P and UDP-GlcNAc	Both	3ST8	[3]
M. tuberculosis	Ac CoA and UDP-GlcNAc	Both	3SPT	[3]
M. tuberculosis	UDP-GlcNAc, PPi	Uridyltransferase	4G3S	[161]
M. tuberculosis	GlcN-1-P	Acetyltransferase	4HCQ	[161]
H. influenzae	Allosteric inhibitor	Uridyltransferase	2VD4	[162]
H. influenzae	Quinazoline Compound	Uridyltransferase	2W0V	[162]
H. influenzae	Aminoquinazoline Compound	Uridyltransferase	4E1K	[163]
S.pneumoniae	Arylsulfonamide compound	Acetyltransferase	4AAW 4AC3,	[164]
S.pneumoniae	Ac CoA	Acetyltransferase	1HM0, 1HM8	[165]
S.pneumoniae	Apo	Both	1G95	[166]
S.pneumoniae	UDP-GlcNAc and Mg^{2+}	Uridyltransferase	1G97	[166]
E. coli	UDP-GlcNAc	Uridyltransferase	1FWY	[167]
E. coli	Ac CoA and UDP-GlcNAc	Both	1HV9	[168]
E. coli	UDP-GlcNAc, desulpho-CoA and GlcNAc-1-P	Both	2OI7	[169]
E. coli	UDP-GlcNAc, CoA and GlcN-1-P	Both	2OI6	[169]
E. coli	UDP-GlcNAc and Acetyl-CoA	Both	2OI5	[169]
E. coli	Arylsulfonamide compound	Acetyltransferase	4AA7	[164]
E. coli	Sulfonamide inhibitors	Acetyltransferase	3TWD	[170]

Crystal structures of GlmU in either Apo or in complex with the substrates/inhibitors have been solved from different organisms. These structures provided insights into the active site residues, the mechanism of acetyl and uridyltransferase activities and binding mode of different class of inhibitors. The first structure to be solved was that of *E. coli* GlmU, which provided structure of the N-

terminal domain that contains uridyltransferase active site and its kinetics [167]. Crystal structure of *S. pneumoniae* GlmU, solved in 2001 described the acetyltransferase activity and its mechanism [165]. Over the next few years, structures of GlmU with various substrates in from *E. coli*, *S. pneumoniae***,** *H. influenzae***,** *M. tuberculosis* and *Yersinia pestis* have helped in delineating the mode of substrate interaction and provided insights into the kinetic mechanism of the reactions (Table 2.2). Interestingly none of these structures were either in complex with UTP or GlcNAc-1-P. Recently Dr. Prakash's group obtained crystal structure snapshots of GlmU at different time points after soaking the GlmU crystals with the substrates of uridyltransferase activity (GlcNAc-1-P and UTP). These snapshots allowed modelling of the products- pyrophosphate (PPi) and UDP-GlcNAc at the active site. Co-crystal of GlmU with ATP has shown that, while uridyltransferase active site can accommodate other nucleotides, it has very low biochemical efficiency [160]. Structures with acetyltransferase substrates could only be solved when the N-terminal domain of GlmU was also occupied with the final product UDP-GlcNAc [3].

M. tuberculosis GlmU ($GlmU_{Mtb}$) is a trimeric and bi-functional enzyme of 495 amino acids. The N-terminal uridyltransferase domain (1-249 aa; globular domain made up of α-helix and β-strands) and the C-terminal acetyltransferase domain (271-495 aa made up of and LβH-sheets) are separated by a hinge region (250-270 aa; α-helix only). First reaction (acetyltransferase) of $GlmU_{Mtb}$ is catalyzed by the C- terminal domain, in which the acetyl group from acetyl-CoA is transferred to the glucosamine-1-P sugar (SN_2 reaction mechanism) to generate *N*-acetylglucosamine-1-P (GlcNAc-1-P). Next GlcNAc-1-P diffuses to the N-terminal uridyltransferase domain, wherein the UMP from UTP is transferred to GlcNAc-1-P to generate UDP-GlcNAc [3]. $GlmU_{Mtb}$ has a unique C-terminal tail (437-495 aa; α-helix only), which is absent in orthologs GlmU protein sequences from other organisms. Hinge region interacts with uridyltransferase active site and substrates glucosamine-1-P and acetyl-CoA. Unique C-terminal tail was shown to have important role in the acetyltransferase activity [99]. The loop region in the vicinity of the both the active sites play important roles in catalysis. Loop region in the C-terminal from Asn397 to Thr406 interacts with acetyl-CoA and stabilizes it during

the acetyltransferase reaction. It helps in transferring the acetyl group. Second (Ser98-Asn107) and third (Ser197-Leu208) loop regions at the uridyltransferase active site hold the active site confirmation and provide required interactions with the substrates UTP and GlcNAc-1-P. Hinge region fixes the location and the movement of the N-terminal lobe and thus provides appropriate volume and area for the substrates to enter.

Kinetic modelling studies predicted higher affinity for the product UDP-GlcNAc towards uridyltransferase active site domain compared with the substrates UTP and GlcNAc-1-P [171]. Two Mg^{+2} ions also play a critical role in stabilizing the interaction of the substrate (UTP) and the product (UDP-GlcNAc) at the active site [161]. Cysteine residues (Cys307 & Cys324) at acetyltransferase domain have also been found to be essential for the acetyltransferase activity of *E. coli* GlmU [172] although, there are no such Cys residues are present in $GlmU_{Mtb}$ (Fig 2.6).

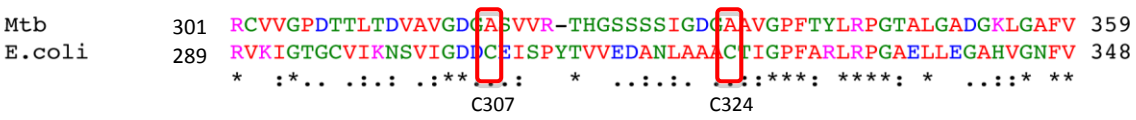

Figure. 2.6. Sequence alignment of *M.tb.*-GlmU with *E. coli*-GlmU: Representing the important Cys residues (Cys307 & Cys 324) at acetyltransferase domain of *E. coli* GlmU and presence of Ala residues in *M.tb.*-GlmU at that place.

MenginLecreulx D *et al*. (in 1993) determined the biochemical parameters and elucidated its role of GlmU in the cell wall biosynthesis by deleting *glmU* gene from *E.coli* [173]. Next the regulation of *glmUS* operon was determined, which shows that NagC protein acts in a co-ordinated way to activate and repress the transcription of *glmUS* operon [174]. While the initial studies clearly showed that GlmU is a bi-functional and trimeric protein, its importance for the survival of the bacilli was not determined. Gehring *et al*. shows first time that both the activities could be separated in *E. coli* GlmU and the individual domains are biochemically active [175]. Pompeo F *et al.* found that trimerization of *E. coli* GlmU is essential for the bacterial survival by complementing both domains individually in *glmU* mutant bacteria [176]. Earlier reports of high throughput screening in *M.tb.* predicted $GlmU_{Mtb}$ as an essential gene [177]. Zang W *et al.* demonstrated the essentiality of GlmU in *M. smegmatis* by generating a temperature sensitive gene knock down

strain. This report also standardized a microtiter plate assay to study both the activities of $GlmU_{MS}$ reactions [115]. Parikh A *et al.* identified $GlmU_{Mtb}$ to be a substrate of $PknA_{Mtb}$ & $PknB_{Mtb}$ and showed that the phosphorylation of $GlmU_{Mtb}$ at the acetyltransferase domain results in reduced acetyltransferase activity [99] (Fig 2.5).

2.4 GlmU: Inhibitors development.

Work on *E. coli* and *M. smegmatis* GlmU suggested that *glmU* is an essential gene and its removal would result in bacterial death. Extensive structural and biochemical data have enabled design and development of inhibitors targeting GlmU in pathogenic bacteria. These include aminoquinazolines, quinazolines, sulfonamide, arylsulfonamide and many other derivatives. Arylsulfonamide containing competitive (to acetyl-CoA) inhibitors were developed against acetyltransferase active site of *E. coli* GlmU and the co-crystal structure was determined [164]. With the help of *in silico* approach, Mehra R *et al.* have identified and optimized inhibitors against *E. coli* GlmU. Structure, ligand, pharmacophore and QSAR based approach followed by *in silico* and *in vitro* screening was used to identify eight potential inhibitors against acetyltransferase active site of *E. coli* GlmU [178]. In a high throughput screening by Pereira MP *et al.* identified 37 new competitive inhibitors against acetyl-CoA [179]. However till date no inhibitors have been developed against the uridyltransferase site of *E. coli* GlmU. Series of competitive (to UTP and GlcNAc-1-P) and un-competitive inhibitors were identified against GlmU of *X. oryzae*, with their IC_{50} values ranging from 0.8 to 23.2 μM [178, 180]. GlmU of *H. influenzae* is very well studied compared with its orthologs from other bacteria. Numbers of aminoquinazolines and sulfonamide compounds were found to be effective inhibitors of uridyltransferase and acetyltransferase activities of *H. influenzae* GlmU [163, 170, 181]. Larsen NA *et al.* determined the co-crystal structure of aminoquinazolines inhibitors with the *H. influenzae* GlmU and showed that it occupies UTP binding site and locks the GlmU in Apo enzyme like form [163]. Mochalkin I *et al.* discovered an allosteric site inhibitor (with 3-aminopiperidine core; IC_{50} 18 μM) for *H. influenzae* GlmU and determined its co-crystal structure with GlmU at 1.9 Å resolution. This inhibitor bind to allosteric site near to GlcNAc-1-P binding site and prevents the structural rearrangement that are

critical for the enzymatic activity, thus paving way for the structure based drug design with new mode of action [162].

Green OM *et al.* developed series of arylsulfonamide containing inhibitors targeting the acetyltransferase activity of *S. pneumoniae* GlmU. Co-crystal structure with inhibitor revealed that it occupies the acetyl-CoA binding site, thus competitively inhibiting the activity [164]. Aminoquinazolines inhibitors were discovered against the uridyltransferase activity of *M.tb.* GlmU with the lead inhibitor having an IC_{50} value of 74 μM [113]. In another study sugar substrate analogs of acetyltransferase were used as inhibitors against *M.tb.* GlmU and some of them were found to be competitive and un-competitive to GlcN-1-P [182]

Different prediction analysis also suggests series of molecules and methodologies to design and develop new inhibitors against GlmU. Singla D *et al.* developed a new web server to predict inhibitors against GlmU protein. In this study QSAR and docking based models were developed based on 84 different compounds from PubChem BioAssay (AID 1376) and 40 molecules were predicted to be potential GlmU inhibitors [183]. Taken together it can be said that GlmU is an essential gene and it could be a potential target for therapeutic intervention. Structure functional analysis of *M.tb.* GlmU and knowledge from already known co-crystals of other bacterial GlmU can be used to generate next generation of inhibitors against $GlmU_{Mtb}$.

Table 2.3: GlmU from different bacteria targetted for inhibitors designing.					
Organism	**Site targeted**	**Mechanism**	**Analogs of**	**PDB ID**	**Reference**
E. coli	Acetyl-transferase	Competitive	Acetyl-CoA (arylsulfonamide)	4AA7	[164]
		Competitive uncompetitive	Acetyl-CoA GlcN-1-P		[179]
		Not evaluated	Acetyl-CoA GlcN-1-P		[184]
X. oryzae	Uridyl-transferase	Competitive, non-competitive, and un-competitive	GlcNAc-1-p and UTP		[180]
		Competitive and un-competitive	GlcNAc-1-p And UTP		[178]
H. influenzae	Acetyl-transferase	Competitive	Scetyl-CoA (sulfonamide inhibitors)		[170]
		Competitive	Acetyl-CoA (sulfonamide inhibitors)		[181]
	Uridyl-transferase	Competitive	UTP (aminoquinazolines)	4E1K	[163]
		Allosteric	Small molecule inhibitor	2VD4	[162]
S. pneumoniae	Acetyl-transferase	Competitive	Acetyl-CoA (arylsulfonamide)	4AC3 4AAW	[164]
M. tuberculosis	Acetyl-transferase	Competitive and un-competitive	GlcN-1-P		[113]
	Uridyl-transferase	Not evaluated	UTP (aminoquinazolines)		[182]

Chapter 3.

Objectives and plan of work

Chapter 3.

Objectives and plan of work

3.1 Defining the problem and purpose of the study.

Mycobacterium tuberculosis (M.tb.) is a very old, dynamic, deadly, widespread and challenging pathogen to human. The co-evolution of *M.tb.* with humans for long period has resulted in extensive evolutionary adaptation, which facilitated *Mtb* survival inside the lungs and established it as a potent pathogen. [1, 2] and such a long association of this pathogen with human race has resulted in evolution of various offensive and defensive tactics in the bacterium to sabotage the host immune system [185]. In 2013 almost 9.0 million cases were reported with 16.67% mortality rate. Amongst the reported cases in 2013, 3.5% cases were of MDR-TB (WHO report 2014). Increasing death rate is alarming that attempts to combat TB must speed up with new sets of therapeutic targets and therapy not only against active bacilli but also against latent *M.tb*. A variety of signalling and metabolic pathways participate to sustain the pathogenic nature of *M.tb*. These include nutrient metabolism and catabolism, synthesis of cell wall, secretion of different bio-molecules, DNA and RNA synthesis etc. Most of these pathways are very crucial to sustain *M.tb.* inside the host and hence facilitate its success as a pathogen.

Cell wall of *M.tb.* gives essential flexibility to bacteria to adjust during division, growth and infection. *M.tb.* cell envelop includes three defined cell layers made up of plasma membrane, a cell wall made up of peptidoglycan that contains meso-DAP, and an external layer of myco-capsule which contains mycolic acid, unique arabinogalactan and lipoarabinomannan [186-188]. Synthesis of cell wall requires various enzymes from cytoplasm and inner or outer side of cell membrane. Many of these enzymes have been used or are proposed as therapeutic targets; hence, understanding of the key pathways for the synthesis of these outer layers would pave a way ahead for new drug targets.

Synthesis of UDP-GlcNAc is central for the cell wall synthesis and the process remained essentially conserved in prokaryotes during the course of evolution. N-acetyl-glucosamine-1-phosphate uridyltransferase (GlmU) is a homotrimer, bi-functional and essential bacterial enzyme which holds a key role in *de novo* production of the essential metabolite UDP-GlcNAc in *M.tb.* [175, 189]. Carboxy terminal domain of GlmU (LβH structure) catalyzes acetyltransferase activity in which acetyl moiety, from acetyl CoA, transfers onto glucosamine-1-P thus generating GlcNAc-1-P (reaction 1). GlcNAc-1-P further diffuses to the N-terminal uridyltransferase domain (rossmann folded) of the GlmU, where UMP from UTP transfers onto GlcNAc-1-P and finally producing UDP-GlcNAc (reaction 2) [189].

Acetyltransferase reaction (C-terminal domain)

GlcN-1-P + Acetyl CoA ⟶ GlcNAc-1-P + CoA **(1)**

Uridyltransferase reaction (N-terminal domain)

GlcNAc-1-P + UTP ⟶ UDP-GlcNAc + PPi **(2)**

This UDP-GlcNAc is further metabolized in multiple pathways to generate peptidoglycan, lipid A, arabinogalactan, Rha-GlcNAc linkers, lipoarabinomannan and mycothiol in *Mtb* [88, 155, 190-194]. As there is no comparable enzyme in human, therefore, targeting *glmU* would be valuable for new therapeutic intervention against TB [171, 195, 196].

Despite many studies, there are no starting point molecules which target $GlmU_{Mtb}$ specifically. Also further insights in to the functional significance of $GlmU_{Mtb}$ during active TB infection and latency were still absent. GlcNAc can be resupplied, to form UDP-GlcNAc, from alternative connecting pathways of cell wall reutilization [68] or from GlcNAcylated proteins of host (bacteroidetes phylum) [197, 198]. Therefore, in order to establish $GlmU_{Mtb}$ as a new potential drug target, it is important to understand that how UDP-GlcNAc synthesis by $GlmU_{Mtb}$ gets regulated during various stages of growth and infection inside the host.

In this study, following major questions were aimed to investigate the role of $GlmU_{Mtb}$ in bacterial survival, infection and new inhibitor development.

3.2 Objectives and plan of work

3.2.1 Structural and biochemical characterization of $GlmU_{Mtb}$.

3.2.2 Dissecting the role of $GlmU_{Mtb}$ in arbitrating the survival of the pathogen.

3.2.3 Design and development of new anti-$GlmU_{Mtb}$ inhibitors.

(3.2.1.) Structural and biochemical characterization of $GlmU_{Mtb}$.

Crystal structure was determined in collaboration with Dr. Balaji Prakash (IIT-Kanpur) and biochemical aspects of $GlmU_{Mtb}$ were performed by us. Followings are the main objectives of this research.

- **i.** Characterizing the active site of acetyltransferase activity at the C-terminal domain.
- **ii.** Determining the unique features (short C-terminal α-helix tail, uncommon mode of binding pattern of acetyl-CoA) of the C-terminal domain of $GlmU_{Mtb}$.
- **iii.** Identifying the $PknB_{Mtb}$ mediated phosphorylation site on $GlmU_{Mtb}$.
- **iv.** Characterization of the uridyltransferase active site of $GlmU_{Mtb}$.

***Results*.**

Important residues (H374A, N397A and S416A) were mutated and checked for their biochemical activities and kinetics using malachite green assay. Both H374 and N397 were found to play central role in acetyltransferase reaction. Additionally, the conformation of bound acetyl-CoA in $GlmU_{Mtb}$ displayed unique 'U' shaped pattern in compared with the 'L' shaped conformation in $GlmU_{E.coli}$. The importance of U shaped conformation was confirmed by generating mutations at the interacting residues R439T, A451R and their double mutant (R439T+A451R) or tetra mutant (R439T+A451R+I457K+R455T). Further, we found that a short helix present at the C-terminal extension provides a key tryptophan, which appears to be critical for acetyl-CoA binding and acetyltransferase activity as well. This was validated by generating different truncation mutants (Δ15, Δ25, Δ30 and Δ37) and W460A point mutant or by chimeric $GlmU_{Mtb}$ proteins consisting of C-terminal tail of $GlmU_{E.coli}$ or vice-versa. With the help mass spectrometry, we identified T418 and T156 to be the major and minor PknB target sites on $GlmU_{Mtb}$. We have generated phohoablative (T418A) and phosphomimatic (T418E) and T418S mutant, which retain the hydroxyl group, and deciphered how T418 phosphorylation down regulates the

acetyltransferase activity. Characterization of uridyltransferase active site was carried out by mutating important residues (based on the crystal structures) like R19A, K26A, D114A/E and N239A, which play a role in stabilizing the Mg^{+2} ion and the substrates, decreased the uridyltransferase activity. Thus characterization of both active sites provides a base towards developing new sets of inhibitors targeting $GlmU_{Mtb}$.

(3.2.2.) Dissecting the role of $GlmU_{Mtb}$ in arbitrating the survival of the pathogen.

Based on the transposon mutagenesis studies *$glmU_{Mtb}$* was predicted to be an essential gene. The present study was undertaken to see the effects of depleting $GlmU_{Mtb}$ on pathogen survival in the host animal. Objectives of this study were:

Further there are no studies investigating the question of whether both the activities of $GlmU_{Mtb}$ are independently essential for the growth or survival of the bacterium.

- **i.** Generation and validation of conditional gene replacement mutant in *H37Rv* and *mc^2155*.
- **ii.** Investigating the role of $GlmU_{Mtb}$ in modulating the *in vitro* growth of *M.tb.* (in normaxic or hypoxic conditions).
- **iii.** Determining the impact of $GlmU_{Mtb}$ depletion on c bacterial cell morphology in normoxic and hypoxic conditions.
- **iv.** To investigate if both uridyltransferase and acetyltransferase activities of $GlmU_{Mtb}$ are essential for pathogen survival.
- **v.** Investigating the role of $GlmU_{Mtb}$ in survival of pathogen in THP-1 (*ex vivo*) or in mice/guinea pig (*in vivo*) infection model.

Results.

We present the results of a comprehensive study dissecting the role of $GlmU_{Mtb}$ in arbitrating the survival of the pathogen both *in vitro* and *in vivo.* We have generated a conditional gene replacement mutant of *$glmU_{Mtb}$* and find that depletion of $GlmU_{Mtb}$ at any stage of bacterial growth (normoxia or hypoxia) results in irreversible bacterial death due to perturbation of cell wall synthesis. SEM analysis revealed severe morphological perturbations in the absence of $GlmU_{Mtb}$, with the bacilli showing wrinkled surface and fused cells. TEM analysis showed that whereas in *Rv* and *RvΔglmU* cell wall structure and thickness are comparable, there was a

marked decrease in cell wall thickness in *RvΔglmU* cells where $GlmU_{Mtb}$ was not expressed. Complementation studies show that both uridyltransferase and acetyltransferase activities of $GlmU_{Mtb}$ are essential for pathogen survival, and imply that the only source of the metabolities GlcNAc-1-P and UDP-GlcNAc is through the $GlmU_{Mtb}$ mediated synthesis pathway. $GlmU_{Mtb}$ is also found to be essential for mycobacterial survival in THP-1 cells as well as in guinea pigs. We investigated the effect of $GlmU_{Mtb}$ depletion from a fully-infected lung using murine infection model. Interstingly, depletion of $GlmU_{Mtb}$ from infected murine lungs led to radical reduction in the bacillary load.

(3.2.3.) Design and development of new anti-$GlmU_{Mtb}$ inhibitors.

$GlmU_{Mtb}$ and the acetyltransferase and uridyltransferase enzymes found in eukaryotes share very little sequence similarity. Although efforts have been made by different groups to target bacterial GlmU proteins, the specificity of these inhibitors for GlmU *in vivo* have not been established. Therefore the main focus of this study was the development and assessment of new anti-$GlmU_{Mtb}$ molecules based on our structural, biochemical and biological knowledge. The objectives of the study were:

- **i.** Design and development of various inhibitors (Asinex inhibitors) against the $GlmU_{Mtb}$ uridyltransferase allosteric site based on earlier reported crystal structure.
- **ii.** Determination of various biochemical and biophysical parameters of the final lead molecules.
- **iii.** MD simulation study of the lead molecule to predict the binding site on $GlmU_{Mtb}$.
- **iv.** Cloning and purification of various mutants of binding site and determine their IC_{50} values.
- **v.** Generation of $GlmU_{Mtb}$ over expressing *Rv* strain to determine the specificity.
- **vi.** Efficacy and toxicity check of the lead compound.
- **vii.** Development and screening of inhibitors against the uridyltransferase catalytic site.
- **viii.** Computational analysis and biophysical experimentation of the lead molecule.

Results.

In addition to the acetyltransferase and uridyltransferase active site pockets, $GlmU_{Mtb}$ also contains an allosteric site. Binding of any suitable molecule/inhibitor to the allosteric site would prevent the conformational change essential for $GlmU_{Mtb}$ uridyltransferase catalytic activity. To target the allosteric site on $GlmU_{Mtb}$ we drew on crystal structure data of *H. influenza* GlmU ($GlmU_{HI}$) bound to its allosteric small molecule inhibitor. The Asinex database was screened against shape as described and the resulting 43 hits were biochemically characterized for their ability to inhibit $GlmU_{Mtb}$ uridyltransferase activity. One of the promising molecules was used for further structural optimization. Of the 53 structurally optimized compounds one molecule, namely (4*Z*)-4-(4-benzyloxybenzylidene)-2-(naphthalen-2-yl)-1,3-oxazol-5(4*H*)-one (Oxa33), was found to be an efficient inhibitor of $GlmU_{Mtb}$ activity with an IC_{50} of 9.96±1.1 μM. Docking and MD simulation studies revealed polar, non-polar and hydrophobic interactions between Oxa33 and the allosteric site residues. Oxa33 inhibited the *in vitro* growth of *M.tb. H37Rv* with a minimum inhibitory concentration (MIC) of ~75 μM (~30 μg / ml). To ascertain if this inhibitory effect was due to inhibition of $GlmU_{Mtb}$ activity we overexpressed $GlmU_{Mtb}$ in the cells prior to drug treatment and determined the effect of this on the MIC value. In concurrence with the *in vitro* growth data, overexpression of $GlmU_{Mtb}$ alleviated Oxa33-mediated clearance of *M.tb.* from THP-1 cells. Finally, we analysed the efficacy of Oxa33 in clearing bacilli from infected lungs using a murine infection model. The administration of Oxa33, a novel oxazolidine derivative that specifically inhibits $GlmU_{Mtb}$, to infected mice resulted in significant decrease in the bacillary load.

Inhibitors were also developed based on the substrates of uridyltransferase activity of $GlmU_{Mtb}$. Crystal structure information was used to design 9 compounds against UTP and GlcNAc-1-P. Extensive computational analysis and docking were performed to determine the various parameters of these compounds. Out of these 9 inhibitors, compound no 4 was showing IC_{50} of 42.02 μM with a better K_a value (1.34×10^7). Compound no. 4 can be pursued as a lead molecule which needs to be developed further to improve its efficacy.

Chapter 4.

Material and methods

Chapter 4.

Material and methods

4.1 Chemicals and reagents.

Restriction enzymes and *pfu* DNA polymerase were purchased from New England Biolabs. pENTR/ directional TOPO cloning kit (Invitrogen), pQE2 (Qiagen), were procured from the respective sources. Analytical grade chemicals and oligonucleotide primers were procured from Sigma. Malachite green phosphate assay kit (POMG-25H) was purchased from BioAssay System (Gentaur). Electron microscopy reagents were purchased from Electron Microscopy Sciences. Media components were purchased from BD Biosciences. Doxycycline hydrochloride was purchased from Biochem pharmaceutical. [γ-^{32}P]ATP (6000 Ci/mmol) was purchased from Perkin Elmer.

4.2 Cloning, mutagenesis and purification of $GlmU_{WT/\ mutants}$.

glmU from different organisms (*M.tb H37Rv, E.coli DH10B, S. pneumoniae, C. glutamicum,* and *M. smegmatis*) were PCR amplified from respective genomic DNA using appropriate primers (appendix table for primers). Site directed mutations, truncations and chimeras of $glmU_{Mtb}$ and $glmU_{EC}$ were generated with the help of overlapping PCR or with normal PCR and the amplicons were cloned into *NdeI-HindIII* sites of pQE-2, pNIT (Kan^R or Chl^R) and pST-KT vectors. Nucleotide sequences of the recombinants were verified by DNA sequencing. Recombinants generated (appendix table for constructs) were used for expression and purification in *E. coli* or[99] expression in mycobacteria (*M.tb.* or *MS*).

For protein purification pQE-2 clones were transformed into *E. coli* BL21 (DE3) CODON PLUS cells. Over expression and solubility were determined after running on SDS-PAGE. Primary culture was grown overnight at 37°C. Secondary culture was grown with aeration at 37°C to mid-logarithmic phase (0.6 OD_{600}). This secondary culture was induced with 0.2 mM IPTG (isopropyl -D-thiogalacto-pyranoside) at 18°C for 12 h. Cells were centrifuged at 4°C, 5000 rpm, re-suspended in PBSG buffer at 1:10 ratio (1 g pellet in 10 ml lysis buffer; 1X PBS containing 5% glycerol, 1 mM DTT and protease inhibitors) and sonicated (40 power, 45 sec pulse/

halt, 20 cycles) to lyse the bacteria. Lysates hence generated, were subjected to centrifugation at 8,000 rpm for 30 min followed by 1 h centriguation at 10,000 rpm at 4°C to obtain the clear supernatant. Hexa His tagged-$GlmU_{WT/mutants}$ proteins were trapped on pre-equilibrated Ni-NTA agarose (Sigma) column by incubating for 3.5 h at 4°C on a twirler. Bound protein was washed with 10X column volume with the buffer (PBSG + 500 mM NaCl, 1 mM DTT and protease inhibitors) and with 2X column volumes of the elution buffer (25 mM Tris-Cl pH 8.0, 5% Glycerol, 140 mM NaCl, 1 mM DTT and protease inhibitors) containing 10 mM and 25 mM imidazole. Finally His tagged proteins were eluted with the elution buffer containing 200 mM of imidazole followed by dialysis against the storage buffer (25 mM Tris-Cl pH 7.4, 140 mM NaCl in, 15% Glycerol; buffer is changed 3 times at 6, 9 and 12 h during the dialysis). Purified proteins were aliquoted, estimated with the help of Bradford method and stored at -80°C till further usage.

4.3 Molecular dynamics simulations for $GlmU_{Mtb}$: Δ30 and Δ35.

The crystal structure of $GlmU_{Mtb}$ in complex with acetyl-CoA (PDB ID: 3SPT) was used to get the initial coordinates of unleganded $GlmU_{Mtb}$. To cope with the CPU time required for the simulations, the enzyme was truncated to include only the C-terminal acetyltransferase domain. Since the two domains that catalyze the two reactions in $GlmU_{Mtb}$ are independent, this premise was convincing. The three LβH domains of the monomers that form the trimer were included, as the acetyltransferase active site has contributions from all the three. Last 30/35 amino acids were deleted at the C-terminal tail to generate model for $GlmU_{Mtb}$: Δ30/Δ35 constructs. The protein structure was solvated with box of dimensions 70.504 Å x 88.108 Å x 96.459 Å having TIP3P water molecules. The system was neutralized by the addition of 7 Cl^- counter ions. The whole protein was treated with Parm99 version of the force field. Preliminary minimization of the water shell was followed by the minimization for the entire system. Each MD simulation was carried out for 1 ns, using constant pressure at 1 bar (NPT simulation) to equilibrate the density. This was followed by a 2 ns simulation at constant temperature (300 K) and constant volume (NVT simulation). The simulation was carried out using a 12 Å cut-off for non-bonded interaction. A time step of 1 fs was used and SHAKE algorithm was used to constrain the bond lengths between hydrogens and heavy atoms [199]. In this way,

MD simulations were carried out for $GlmU_{Mtb}$: Δ30 and Δ35 constructs using AMBER09.

4.4 Acetyl and uridyltransferase assays.

Uridyltransferase assays were performed in an 8 or 30 µl reaction volume containing 25 mM HEPES buffer (pH 7.6), 10 mM $MgCl_2$, 1 mM DTT with 0.5 mM GlcNAc-1-P and 1 mM UTP, 0.04 U thermostable inorganic pyrophosphatase (TIPP) and varying concentrations of $GlmU_{Mtb}$ or $GlmU_{Mtb}$ mutants for 30 min at 30°C. Reactions were terminated by incubating at 65^0C for 30 min and the product formed was estimated by malachite green phosphate assay kit according to the manufacturer's recommendation. In the malachite green assay, thermostable inorganic pyrophosphatase (TIPP) hydrolyses inorganic pyrophosphate PPi (one of the products of uridyltransferase reaction) into two inorganic phosphates (Pi). This Pi thus released reacts with the ammonium molybdate to generate phospho-molybdate which reacts with malachite green in the reaction mix to give a blue green coloured product that can be estimated at 620 nm.

The acetyltransferase activity of GlmU was monitored in a coupled assay, wherein the end product of second reaction, PPi was detected with the help of malachite green assay. Briefly, the 8 or 30 µl reaction acetyltransferase assay mix contained 25 mM HEPES buffer (pH 7.6), 10 mM $MgCl_2$, 1 mM DTT with 1 mM GlcN-1-P and 1 mM acetyl-CoA. Subsequent to 30 min incubation at 30°C, reactions were terminated at 65°C for 30 min. The product, GlcNAc-1-P, was estimated by performing coupled uridyltransferase assay in a reaction containing 0.04 U thermostable inorganic pyrophosphatase, 1 mM UTP and 20 pmoles of $GlmU_{Mtb}$:1-352 deletion mutant [99], which was estimated with the help malachite green phosphate assay kit.

4.5 Determining the kinetic parameters (K_m and V_{max}) for the acetyltransferase activity.

In order to determine the kinetic parameters of the acetyltransferase active site, either acetyl-CoA or GlcN-1-P was varied while keeping the other substrate at 1 mM. Concentration of the enzyme, $GlmU_{Mtb}$ or the acetyltransferase active site mutants or $GlmU_{EC}$, used for the reaction, was determined by performing range finding experiments. The reactions were performed for 30 min at 30°C followed by

termination by heating it at 65°C for 30 min. The product GlcNAc-1-P formed was measured by coupling this reaction with uridyltransferase assay as described above. Unit activity of the enzyme was defined as the nM of product formed/min/pmole of the enzyme. GraphPad prism software was used for non-linear regression analysis to compute the K_m and V_{max} values.

4.6 Generation of glmU conditional gene mutant in M. tuberculosis.

Conditional gene mutant of $glmU_{Mtb}$ was generated by providing additional copy of $glmU_{Mtb}$ under externally regulated Tet-off promoter at *attP* site. As the tetracycline-inducible system is an effective means to regulate gene expression, we introduced the integration-proficient pST-KirT-*glmU* construct (wherein $glmU_{Mtb}$ gene was cloned under a promoter that shuts down upon ATc addition) into *M.tb. H37Rv*. For this the hexa-His tag in the pST-KiT construct [200] was replaced with an N-terminal FLAG tag, and the tetracycline repressor gene (*tetR*) was replaced with a reverse *tetR* (*rtetR*) from pTC28S15-OX (Addgene # 20316) [201] to create plasmid pST-KirT (see vector map in appendix).

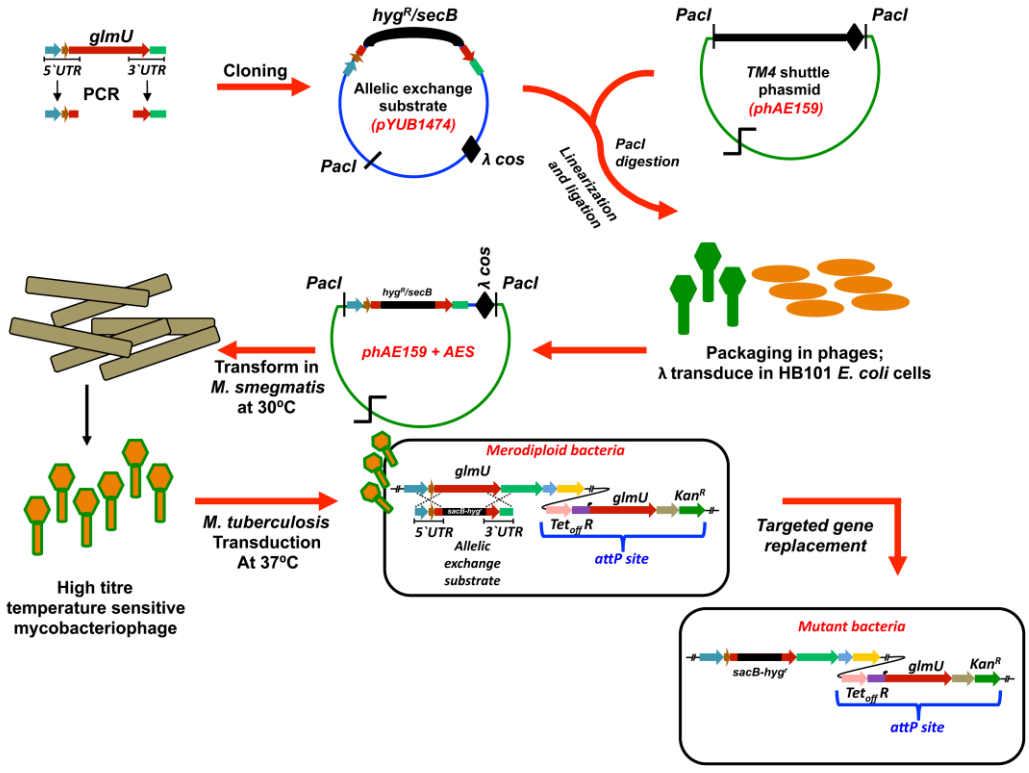

Figure. 4.1. ***Schematic diagram of glmU gene deletion mutant generation.***

To generate the integrating shuttle plasmid, pST-KirT-*glmU*$_{Mtb}$, the *glmU*$_{Mtb}$ gene was excised from pQE2-*glmU*$_{Mtb}$ using *NdeI-HindIII* digestion and was sub-cloned into the corresponding sites on pST-KirT. The integration-proficient plasmid containing the inducible *glmU*$_{Mtb}$ gene was electroporated into mycobacterial cells to create the merodiploid strain *Rv::glmU*$_{Mtb}$.

Whereas the expression of GlmU$_{Mtb}$ from its native locus remained unaltered, the expression of FLAG-GlmU$_{Mtb}$ in *Rv::glmU* strain was drastically compromised in the presence of ATc (Western blot inset, Fig 6.2A). For allelic exchange substrate preparation 5' and 3' genomic flank sequences of *glmU*$_{Mtb}$ (approximately 1 kb on either side) were amplified, the amplicons digested with *PflMI,* and ligated with the antibiotic resistance cassette (*sacB/hyg*^{R}, ~3.60 kb) and the *oriE* fragment containing *λ cos* sites (~1.6 kb) from obtained by digesting pYUB1474 construct with *PflMI* (appendix vector map), to generate the allelic exchange substrate (AES). The AES was linearized using the unique *PacI* site and cloned into the corresponding site in temperature sensitive shuttle phagemid phAE159. Phagemid phAE159 (51 kb) is derived from Mycobacteriophage *TM4*. This phage was customized by removing non-essential genes and incorporating *oriE* and *amp*^{R} genes and a single *λ cos* site between *PacI* sites. *λ cos* site (12 bp conserved sequence) can be identified by the terminase enzyme which is present at the junction of the phage head, and nicks the phage DNA at *λ cos* site. This event warrants the packaging of the single DNA molecule inside the phage head. Ligation product (phAE159-*glmU*-AES) were transduced into *E.coli* HB101 cells and phagemids were isolated using mini prep kit (Qiagen). Positive recombinant phagemids were electroporated in *mc*^{2}*155* strain. Electroporated phagmids were mixed with the actively growing culture of mc^{2}155 and incubated at 30^{o}C for 3 days. Generated phages were checked for the temperature sensitivity by replica plating and incubating the plates at 30^{o}C or 37^{o}C (Fig 4.1). High titre phages were prepared by repeated extractions from multiple plates. Phage titres (PFU; Plaque Forming Units) were calculated by following formula.

PFU/ml = 10 x (number of plaques) x dilutions factor

Merodiploid strain of *Rv::glmU* was transduced with the temperature sensitive phages [202, 203]and selected at non-permissive temperature 37^{o}C to drive

the recombination. Colonies obtained 35 days post plating were screened by patching on 7H11 plates with and without anhydrotetracycline (ATc, 1.5 µg/ml). The fidelity of homologous recombination at the native locus was confirmed by amplification across the replacement junctions using appropriate primers.

4.7 Analysis of growth patterns and western blotting.

M. tuberculosis was cultured and maintain at BSL-3 facility following the rules and regulations approved by the institutional bio-safety committee (NII, New Delhi). H37Rv (*Rv*), *RvΔglmU* or *RvΔglmU::glmU*$_{WT/mutants}$ cultures were grown in Middlebrook 7H9 medium supplemented with 10% ADC (albumin, dextrose and catalase) or on 7H11 agar medium supplemented with 10% OADC (oleic acid, ADC). To analyze bacterial growth *in vitro*, *Rv* and *RvΔglmU* bacterial cultures were inoculated at A_{600} of 0.1, in the presence or absence of anhydrotetracycline (ATc), and A_{600} was measured every 24 h for 6 or 8 days. For spotting analysis, cells were harvested by centrifugation, washed twice with PBST (0.05% Tween 80) to remove ATc, re-suspended in 7H9 medium, and serially diluted in the same medium, followed by spotting 10 µl aliquots of the various cell dilutions on 7H11 agar plates to assess cell viability after 21 days. In order to determine the role of $GlmU_{Mtb}$ at different growth stages of *M.tb.*, $GlmU_{Mtb}$ was depleted on different days post inoculation by the addition of ATc and A_{600} was measured every day (cultures were diluted 10 times with media when the A_{600} was beyond the detection range). All experiments were performed in triplicate and the average A_{600} readings were plotted as the function of time. To investigate the ability of *glmU* wild type, truncation and point mutants to rescue growth upon depletion, *Rv or RvΔglmU::glmU*$_{wt/mutants}$ strains were cultured in the presence or absence of ATc for 5 days followed by A_{600} measurement (n=3).

For the western blot analysis 50 or 100 ml of 7H9 + 10% ADC were inoculated with *Rv*, *RvΔglmU* or *RvΔglmU::glmU*$_{WT/mutants}$ at A_{600} of 0.1 and the cultures were allowed to grow for 5 days in presence or absence of ATc. Bacteria were pelleted down and re-suspended in 0.8 ml 1x PBS with protease inhibitors. Whole cell lysates (WCL) were prepared using mini bead beater (Biospec products) with 0.1 mm Zirconia/ Silica (equal to the volume of bacterial suspension) beads followed by centrifugation at 13,000 rpm for 1 h at 4^{o}C. WCLs were resolved on

10% SDS-PAGE, transferred to nitrocellulose membrane, and probed with anti-$GlmU_{Mtb}$ and anti-GroEL1 antibodies as described earlier.

4.8 Hypoxia experiments.

To determine the impact of $GlmU_{Mtb}$ depletion during hypoxia in *Rv* and *RvΔglmU* strains, hypoxia was established in 1.5 ml HPLC tubes or 500 ml flasks with penetrable caps, following modified Wayne model [104, 204]. Cultures were seeded at A_{600} 0.1 in 7H9 media containing 10% ADC and 1.5 µg/ml of methylene blue and left at 37°C with intermittent manual mixing. ATc (1.5 µg/ml) or isoniazid (INH; 50 ng/ml) were injected into the cultures at different time points and the number of CFUs were enumerated on day 0, 20 and 42.

4.9 Scanning electron microscopy (SEM) and transmission electron microscopy (TEM).

For SEM and TEM, imaging, bacteria were fixed with 4% paraformaldehyde and 2.5% gluteraldehyde in 0.1 M Sodium cacodylate buffer (pH 7.3). Residual fixative was removed by washing them twice with 0.1 M cacodylate buffer. For SEM, samples were further treated with 1% Osmium tetraoxide for 2 h in the dark. Dehydration was performed with gradually increasing concentrations of ethanol. The samples were completely dried by final re-suspension in hexamethyldisilazane (HMDS). 10 µl of the sample was mounted on autoclaved coverslip which was fixed with carbon tap on metallic stubs and coated with gold followed by imaging using Carl Zeiss Evo LS scanning electron microscope.

For TEM fixed bacteria were embedded in 2% agar blocks before proceeding further. Samples were subsequently treated with 2% osmium tetraoxide for 1 h followed by dehydration in graded series of ethanol (30%, 50%, 70%, and 100%) washes and infiltrated in Epon 812 resin and polymerised at 60°C for 72 h. Ultrathin sections (70 nm – 90nm) cut using an Ultramicrotome, were placed on copper grids and stained with 5% uranyl acetate and 0.2% lead citrate. Sections were examined on Tecnai G2 20 twin (FEI) transmission electron microscope.

4.10 THP1 infection.

THP1 cells were maintained in RPMI 1640 (Gibco) supplemented with 10% FBS, L-glutamine (2 mM), HEPES (10 mM) and PEN-STREP (1%). 5 x 10^5/well cells were seeded in a 24 well plate or on cover slips in a six well plate. Cells were

treated with 10 ng/ml phorbol 12-myristate 13-acetate (PMA) in serum free media for 24 h followed by 12 h recovery in complete media. Cells were infected with either unlabelled or FITC labelled *Rv*, *RvΔglmU* or *Rv::glmU*$_{tet\text{-}on}$ strains at a multiplicity of infection (MOI) of 1:10 for 4 h followed by two washes with 1X PBS and 2 h gentamicin (100 ug/ml) treatment to remove any extracellular bacteria. Cells were washed twice with 1X PBS and re-suspended in complete media in presence and absence of ATc (400 ng/ ml)/ Oxa33/ INH or 2.5% DMSO vehicle. For examination of cells under a fluorescence microscope, infected cells (48 h post-infection) were labelled with Lyso Tracker red DND 99 dye (50 nM) followed by washing and, fixing (in 4% paraformaldehyde). Cells were mounted with the antifade (Invitrogen) mounting agent and the slides were observed under confocal microscope and the percentage co-localization was estimated. In order to enumerate CFU counts, cells were lysed at different time points post infection with PBS containing 0.1% TritonX100 at 37°C (15 min) and different dilutions were plated on 7H11 agar containing 10% OADC plates. CFUs were determined after 21 days and plotted with standard error of mean on GraphPad Prism 5.0.

4.11 Guinea pigs and mice infections.

25 ml cultures of *Rv* and *RvΔglmU* strains grown till A_{600} of 0.6-0.8 were spun down, washed twice with 1X PBS and re-suspended in 15 ml of 1X PBS. In order to make single cell suspension, cultures were passed 10 times through 27½ gauge needle and 20 ml syringe. Approximately 4 week old guinea pigs or 2 month old mice of either sex were kept for one week in individually ventilated cages at TACF, ICGEB, New Delhi for acclimatization. Each group (n=6 for guinea pigs and n=6-12 for mice) were infected through aerosol route (with 10^8 CFU for guinea pigs or with $2x10^8$ CFUs for mice) using Madison Aerosol Chamber (University of Wisconsin, Madison, WI). To determine the implantation dosage, the bacillary load in the lungs of 2 guinea pigs or 2 mice was determined 24 h post-infection. Lungs were dissected out and homogenated in saline followed by plating on 7H11 containing 10% OADC and PANTA (namely Polymixin B, Aziocillin, Nalidaxic acid, Trimethoprim and Amphotericin B from BD Biosciences). Both guinea pigs and mice were properly fed and maintained at 25°C with regular light cycles.

To investigate the impact of $glmU_{Mtb}$ depletion on survival of the pathogen, doxycycline hydrochloride (Dox, 1 mg/ kg with 5% dextrose in drinking water) was provided on every third day to *Rv* and *RvΔglmU* infected animals, either from the time of the infection up to 28 days (guinea pig experiment), or 4 weeks post-infection up to 56 days (mice infection experiments, with equal CFUs in lungs). To assess the impact of INH or Oxa33 treatment on pathogen survival, *Rv*-infected mice (4 weeks post-infection) were supplied with INH (25 mg/ kg body weight, with 5% dextrose in drinking water) or Oxa33 (50 mg/ kg body weight, with 2.5% Tween-80, injected intra peritoneal) every third day for 8 weeks. Separate groups of uninfected or infected mice with or without Oxa33 treatment were also maintained as necessary controls. Bacillary loads in the lungs and spleens of infected guinea pigs and mice were determined 4 weeks and 12 weeks post-infection. Experimental procedures for mice and guinea pigs were approved by the Institutional Animal Ethics Committee of National Institute of Immunology, New Delhi, India.

4.12 Histopathology.

During the dissection a section of lungs and spleen was separated and fixed in 10% neutral buffered formalin and stored at room temperature (RT). Organs were set in paraffin wax and sections of five microns were cut using microtome. These sections were fixed and double staining was performed with haematoxylin and eosin (H&E). Coded samples were analysed by an experienced pathologist having no prior knowledge of experiment. Evaluation of granuloma was performed both at 40X and 400X magnifications. Granuloma score was tabulated based on the presence of granuloma with or without necrosis or fibrosis [205].

4.13 Determination of percentage inhibition, IC_{50} and MIC.

To determine the percent inhibition by different compounds (Asinex molecules or oxazolidine derivatives) the enzyme ($GlmU_{Mtb}$; 0.75 pmoles) was pre-incubated with either 5% DMSO or 100/ 20 μM final concentration of compounds for 30 min prior to performing uridyltransferase activity assays. In order to determine the IC_{50} values, $GlmU_{wt/mutant}$ proteins (0.75 pmoles) were pre-incubated in a 30 μl reaction volume (with 20 μM of GlcNAc-1-P and 20 μM of UTP) with different concentrations of Oxa33 compound for 30 min followed by the uridyltransferase assay as described earlier. Colour change was estimated at 620 nm on ELISA plate

reader (Labexim) using ScanPlus software. Further calculations were performed using Microsoft Excel and plotted using standard error of mean on GraphPad Prism 5.0 software.

To determine minimum inhibitory concentration (MIC), $5x10^5$ bacteria of *Rv* or *Rv::glmU*$_{tet\text{-}on}$ (overexpressing $GlmU_{Mtb}$) cultures (grown in the presence or absence of 2 µg/ml ATc) were mixed with 100 µl of 2.5% DMSO or different concentrations of Oxa33/ INH in 96-well plates, and incubated at 37ºC for 6 days. After 6 days, 40 µl of resazurin dye (0.02% in 5% Tween-80) was added to each well and the colour change was observed after 12-24 h. The MIC was determined as the lowest concentration of compound that completely inhibited cell growth (blue colour).

4.14 In vitro kinase assays and phosphopeptide mapping.

In vitro kinase assays were performed by incubating 5 pmoles of $PknB_{1\text{-}330}$ and 25 pmoles of $GlmU_{Mtb}$ or $GlmU_{T418A}$ in a 30 µl reaction in 1x kinase buffer (25 mM HEPES (pH 7.6), 10 mM $MnCl_2$, 1 mM DTT) and 10 µCi [γ-^{32}P] ATP for 30 min at 30ºC. Reactions were terminated by addition of 10 µl of 4× SDS sample buffer. Samples were resolved on 10% SDS-PAGE and transferred to the nitrocellulose membranes and subjected to autoradiography.

Peptide mapping was executed as described by Boyle [206] using Hunter's apparatus (CBS Scientific). Radio labelled bands corresponding to the phosphorylated $GlmU_{Mtb}$ were excised and digested with trypsin at 37ºC. These tryptic peptides were resolved on two dimensional thin layer cellulose chromatography plates (2D-TLC) [206]. Peptides were electrophoretically resolved, in the first dimension, based on their charges in pH 1.9 buffer (25 ml formic acid, 78 ml glacial acetic acid and 897 ml deionized water). Further dried 2D-TLC plates resolved in the second dimension based on their R_f values in phosphor-chromatography buffer (375 ml n-butanol, 250 ml pyridine, 75 ml glacial acetic acid and 300 ml deionized water) and dried plates were subjected to autoradiography to visualize the phosphopeptides as spots. For identification of phosphorylation site using mass spectrometry, *in vitro* kinase assays were carried out using 50 pmoles of $PknB_{1\text{-}330}$ and 50 pmoles of $GlmU_{Mtb}$ in a 200 µl reaction in 1X kinase buffer containing 1 mM ATP for 1 h at 30ºC.

4.15 Identification of PknB targeted phosphorylation site.

In vitro phosphorylated $GlmU_{Mtb}$ was resolved on SDS-PAGE and commassie stained $GlmU_{Mtb}$ bands were excised for in-gel digestion. Gel pieces were treated three times with de-staining solution (25 mM ammonium bicarbonate in 50% acetonitrile) at 37°C for 30 minutes. Protein samples were reduced with 5 mM TCEP followed by alkylation with 50 mM iodoacetamide for 1 h. Gel pieces were digested overnight with 1 µg of trypsin gold (Promega) followed by clean up using zip tip (Millipore). The dried peptides were dissolved in 5% acetonitrile containing 0.1% formic acid. The tryptic peptide samples (~500 ng) were separated for each experiment via Thermo Scientific Proxeon nano LC using a C18 analytical column (Newobjective, USA), at a flow rate of 300 nl/min for 90 minutes. Running method consists of acetonitrile gradient of 5 - 40% for 60 min, 80% for 10 min and finally 90% for 20 min using acetonitrile containing 0.1% formic acid. The LTQ Orbitrap velos performed a full MS scan (RP 60,000) followed by nineteen Data-Dependent MS/MS scans with detection of the fragment ions in the linear ion trap. Target values were 1e6 for full FTMS scans and 1e4 for ion trap MS*n* scans. Supplemental activation was used for all ETD MSn scans. Data analysis was performed using Proteome Discoverer 1.3 software suite. For search engines SEQUEST, the peptide precursor mass tolerance was set to 10 ppm and fragment ion mass tolerance to 0.8 Da. Carbamidomethylation on cysteine residues was used as fixed modification and oxidation of methionine, deamidation of asparagine as well as phosphorylation of serine, threonine and tyrosine was used as variable modifications. Spectra were searched against *Mycobacterium tuberculosis* Uniprot database. The spectra were also search against decoy database using a target false discovery rate (FDR) of 1% for strict and 5% for relaxed conditions.

4.16 Shape based screening and molecular docking studies.

ROCS (Rapid Overlay of Chemical Structures), a shape based technique for rapid similarity analysis through overlapping was used to assess the compounds. This method considers both shape and a colour force field for the optimization of overlaps. Gaussian and shape tanimoto scoring were used to assess the volume and shape overlaps of the compounds, respectively. As the chemical functionality is critical, the chemical feature based similarity was also considered using ROCS

colour score whose force field was composed of SMARTS patterns of the chemical functions [207, 208]. The shape tanimoto score and scaled colour score were considered during the selection of the compounds for further virtual screening. The compounds selected were subjected to molecular docking studies using Glide *v*5.8 of Schrödinger molecular modelling suite 2012 (Glide *v*5.8, Schrödinger, LLC, New York, NY, 2012). The compounds were subjected to a series of docking protocols high throughput virtual screening (HTVS), standard precision (SP) and extra precision (XP) docking. As the docking progresses from HTVS to XP, the algorithm differs, which starts from a simple docking of compounds and ends with docking protocol with high precision and parameterization while cutting off the number of compounds.

4.17 Synthesis of 4-(4-(benzyloxy)benzylidene)-2-(naphthalen-1-yl)oxazol-5(4H)-one.

To the glycine solution (3.0 g, 39.89 mmol) in water under constant stirring at 0°C, NaOH (3.19 g, 79.78 mmol) was added. This was followed few minutes later by the addition of 1-naphthoyl chloride (7.20 mL, 47.86 mmol) in 1, 4-Dioxane (20 ml) and the contents were stirred at room temperature for 6 h. The reaction mixture was concentrated to half the volume and 60 ml EtOAc was added. The EtOAc layer was washed with sat $NaHCO_3$ (2 × 30 mL) followed by H_2O (2 × 20 mL). The separated organic layer was dried and concentrated over anhydro Na_2SO_4 to obtain solid compound, which was washed with hexanes to get 2-(1-naphthamido) acetic acid (8.30 g, 90%) as a white solid (M.P. 152°C[1]). 2-(1-naphthamido)acetic acid (2.0 g, 8.73 mmol), NaOAc (0.21 g, 2.62 mmol) and 4-benzyloxybenzaldehyde (1.85 g, 8.73 mmol) were taken in acetic anhydride and heated at 106°C for 3 h. The solid formed was filtered and washed with water to remove traces of acetic anhydride, and ethanol to remove unreacted aldehyde and other organic impurities. Final compound 4-(4-(benzyloxy)benzylidene)-2-(naphthalen-1-yl)oxazol-5(4H)-one (Oxa33; 3.14 g, 88%), purified as a yellow solid, was confirmed with nuclear magnetic resonance (NMR) [209].

4.18 Isothermal titration calorimetry.

To investigate the binding of various ligands (such as inhibitors, GlcN-1P, Acetyl-CoA, UTP, GlcNAc-1P or UDP-GlcNAc) to $GlmU_{Mtb}$, Isothermal Titration

Calorimetry (ITC) was performed (MicroCal 2000 VP-ITC, GE Healthcare) [170]. $GlmU_{Mtb}$ was purified and dialyzed into buffer containing 15% Glycerol, 140 mM NaCl, 100 mM $MgCl_2$ in 25 mM Tris-Cl (pH 7.4) and 2% DMSO. Different concentrations of ligands (625 µM of Oxa33/ 500 µM of compound 4 from second set of Asinex inhibitors or 500 µM of GlcN-1P/ acetyl-CoA/ UTP/ GlcNAc-1P or UDP-GlcNAc) were diluted in identical dialysis buffer. Ligands were injected for titrations with syringe (rotating at 307 rpm) into ITC cell containing 25 µM of $GlmU_{Mtb}$ or blank buffer at 25°C. Each injection lasted for 20 sec with 300 s interval between every step. The quantity of heat associated with every injection was calculated by combining the area beneath every heat burst curve (microcalories/second vs. seconds). Data was corrected for the buffer signal and fitting was done by one-site or two site binding model. Origin software (version 7.0) was used to obtain different thermodynamic binding parameters.

4.19 In vitro cytotoxicity.

Oxa33 was evaluated for its cytotoxic activity in THP1 cells with the help of alamar blue assay. Serially diluted inhibitors (in 2.5% DMSO) were incubated with 5 × 10^3 differentiated THP-1 cells in 96 well plates for 3 days. After 3 days cells were incubated for 5 h with 10 µl of alamar blue and colour development was measured using micro-plate reader at 570 nm.

4.20 Differential Scanning Fluorimetry.

10 µl of purified $GlmU_{Mtb}$ (2 µg) was incubated with 500 µM of Oxa33 or other inhibitors or 5% DMSO or various concentrations of substrates or products (1000, 500, 250, 125 and 62.5 µM) of the reactions catalyzed by $GlmU_{Mtb}$, in a buffer containing 25 mM HEPES buffer (pH 7.6) and 10 mM $MgCl_2$ for 20 min at room temp. 10X Sypro Orange in equal volume was added to the above mix and incubated in BioRad CFX Connect™ real time PCR system for temperature scan from 20°C to 95°C at 0.5°C/min with FRET filter settings. Sypro Orange dye binds to the hydrophobic residues while protein is unfolding which gives fluorescence (RFU). Results were analysed in BioRad CFX manager 2.1 software.

4.21 Docking and molecular dynamics simulations studies of $GlmU_{Mtb}$ with Oxa33.

Molecular dynamics (MD) simulation for the protein-ligand complex was carried out for a time scale of 20 ns so as to analyze the stability of molecular

interactions between the ligand and protein employing Newton's Laws of Motions. Desmond molecular dynamics system *v*3.1 was used for carrying out the simulations employing OPLS-AA force field [210]. The protein-ligand complex was solvated using TIP3P water model which was setup as an orthorhombic solvent box, keeping a cut-off of 10 Å from any solute atom in all directions [211]. Na^+ counter ions were added in order to neutralize the system. A cut-off of 14 Å was maintained for calculating the solvent-solvent and solute-solvent non-bonded interactions. Initially, the system was minimized keeping the convergence threshold criteria of 1.0 $kcal.mol^{-1}.Å^{-1}$ so as to allow the adjustment of atoms to the system environment. A simulation for each system was performed using isothermal-isobaric ensemble (NPT) including a relaxation process. Under NPT, the system was simulated for 12 ps using a Berendsen thermostat with temperature of 10K and a pressure of 1 atm. The later step of relaxation protocol included the simulation of the system for 24 ps with a temperature of 300 K and 1 atm pressure with and without restraints on solute heavy atoms. M-SHAKE algorithm was used with an integration time step of 2 fs for rearranging the hydrogen bonds in the simulation [212]. The temperature and pressure of the system were maintained at 300 K and 1.013 atm respectively. The molecular dynamics simulation was run for 20 ns recording the trajectory frames at an interval of every 4.8 ps and the trajectory analysis was carried out using the Simulation Event Analysis of Desmond.

4.22 Protein Preparation and Grid generation.

The crystal structure of $GlmU_{Mtb}$ containing substrates, N-acetyl Glucosamine-1-Phosphate (GlcNAc-1-P) and uridine triphosphate (UTP) (from IIT-Kanpur) was processed using Protein Preparation Wizard module of Schrodinger 9.3 [3, 161]. This involved some parameters such as assigning bond orders as the protein is large and contain two substrates, addition of hydrogens as pdb file does not contain hydrogens, adjusting bond orders and formal charges for any cofactors if needed, correcting mislabelled elements, adjusting the ionization and tautomerization states of both protein and substrates etc. The crystallographic water molecules at distance above 5 Å were removed. However, the water molecules interacting with the active sites were retained. Further, protein was optimized by an iterative process for the hydrogen-bonding network by re-orienting the hydroxyl groups and amide groups of

Asn and Gln, and choosing appropriate states and orientation of the imidazole ring of Histidine residues using PROPKA [213]. In the next approach of protein preparation, minimization of the protein was performed using OPLS_2005 force field up to maximum deviation of 0.8 Å before it was processed for generating grid (Schrödinger Suite 2012 Protein Preparation Wizard). To soften the potential for non-polar parts of the receptor, all atoms were scaled for van der Waal radii of 1.0 Å with partial atomic charges less than the cut-off value of 0.25 electron unit. The binding region (grid) was defined with 14.32 Å,-13.30 Å, 43.25 Å and 9.9 Å,-11.5 Å,-36.6 Å boxes, corresponding to X, Y and Z coordinates, over the co-crystallized ligands GlcNAc-1-P and UTP present in the active site respectively.

4.23 Dataset Preparation.

Asinex database, containing 500,000 compounds downloaded from http://www.asinex.com, was prepared using LigPrep module of Schrödinger 9.3 so as to produce high quality structures with various ionization states, tautomers, stereo chemistries and ring conformations (Schrödinger Suite 2012 Protein Preparation Wizard). Epik was used to adjust the tautomerization and ionization states of molecules at pH 7.0 ± 2.0. Generation of ligand conformers was done for all the database molecules using ConfGen. All the molecules were minimized and energy filtered using the OPLS_2005 force field, using a distance dependent dielectric constant with a prefactor of 4. A maximum of 32 conformations for every ligand were generated which were further used for screening.

4.24 Virtual Screening.

$GlmU_{Mtb}$ protein with GlcNAc-1-P and UTP was prepared in order to proceed towards the docking studies. Initial filtering of molecules was performed in accordance with the Lipinski rule of five for drug likeliness upon which virtual screening workflow was applied. The virtual screening workflow, performed by employing the Glide module of Schrödinger 9.3 (Schrödinger Suite 2012 Protein Preparation Wizard), included the high throughput virtual screening (HTVS) of Asinex molecules; followed by Standard Precision mode of docking (SP) thereby retaining the top 10% hits. The retrieved molecules were further refined to exclude false positives using the Extra Precision (XP) mode of docking.

4.25 Docking using AutoDock Vina (ADVINA) and GOLD.

Compounds with better interactions and docking score selected from XP protocol were preceded to docking with $GlmU_{Mtb}$ protein using AutoDock Vina (ADV_{INA}) [214] and GOLD [215] so as to better classify the compounds based on the binding affinity and GOLD score. ADV_{INA}, non-commercial software available for academic purpose, is highly preferred for providing protein flexibility by side-chain movements of some predefined residues at the active site. The docking scores obtained from ADV_{INA} represent the free energy of binding *(ΔG)* of the compounds with which they can bind to the protein. Another docking program considered in the present study was Genetic Optimization for Ligand *Docking* (GOLD) suite 5.2.

4.26 IFD and QPLD.

The docking studies, performed earlier, were carried out using a rigid receptor type where the protein remains rigid and several conformations of ligand molecules were docked to the protein active site. But in reality, considering the solution state of a protein, it undergoes some conformational changes while accommodating ligand at the active site either by side chain movements or backbone movements. Therefore, in order to consider the flexibility of receptor and to obtain far better realistic results from docking calculations, Induced fit docking (IFD) was performed. Molecules that show good docking scores as conferred from the XP mode of docking and having better interaction profile were considered in our IFD studies. The steps involved in IFD protocol are: (a) Docking of molecules and retaining poses (20 poses per ligand) having Coulomb-vdW score less than 100 and H-bond score, less than –0.05; (b) Side chain prediction of the ligand-protein complex using Prime, for residues present around 5 Å of ligand pose and their minimization; (c) Re-docking each protein-ligand complex within a specified energy of the lowest-energy structure (30 kcal/mol).

Generally, ligands, in free-state, have partial charges over individual atoms which will be varied during docking calculations owing to the presence of receptor field. This polarization of charges on the ligand molecules by virtue of receptor flexibility can be calculated by quantum mechanical (QM) calculations. The same was applied for the selected molecules from XP docking studies and were subjected to Quantum polarized ligand docking (QPLD). The QM/MM docking involves a set

of steps such as: (a) Glide docking of the selected ligands to the protein; (b) Charge calculation on the ligands induced by protein using QSite; (c) Redocking of the best ligand poses with the protein.

4.27 Binding Free Energy Calculations.

All the free energy bindings were calculated using Prime-MMGB/SA methods. The approach is well known for predicting the theoretical free energy of binding for ligand molecules with protein receptor [216]. For calculation, docked poses were energy minimized and energies were calculated using same OPLS_2005 force field employing the generalized-Born (GB)/surface area (SA) continuum model for water as solvent. Equation 1 was used for computing the free energy of binding ($\Delta G_{Binding}$) as

$$\Delta G_{Binding} = \Delta E + \Delta G_{Solv} + \Delta G_{SA} \quad \text{Equation 1}$$

$$\text{Where, } \Delta E = E_{Complex} - (E_{Protein} + E_{Ligand}) \quad \text{Equation 2}$$

$$\Delta G_{Solv} = \Delta G_{Solv\ Complex} - (\Delta G_{Solv\ Protein} + \Delta G_{Solv\ Ligand}) \quad \text{Equation 3}$$

$$\Delta G_{SA} = \Delta G_{SA\ Complex} - (\Delta G_{SA\ Protein} + \Delta G_{SA\ Ligand}) \quad \text{Equation 4}$$

As for description of above terms used in the equations, **E** represents the energy minimized states used in the calculations, **Solv** and **SA** represents the solvation model and surface area associated energy respectively. Calculation of entropy was ignored in the determination of ΔG. The requisite simulations using GB/SA continuum model were carried out in Prime*v*3.1. It should be noteworthy to mention that for the computation carried out employing GB model, we have used Gaussian surface instead of van der Waals surface scaling. The reason of above being is that Gaussian surface represents better for solvent-accessible surface area compared to that using van der Waals scaling [217].

4.28 Molecular Dynamics Simulations.

Binding estimates for ligand with the $GlmU_{Mtb}$ have been estimated from our initial docking studies. To analyze and estimate the deviation in binding pose, employing the receptor flexibility and using the quantum parameters, we have re-exercised the docking studies using IFD and QPLD approach respectively. In order to seek the depth of molecular interaction between ligand and receptor, we have performed molecular dynamics simulation employing Newton's Laws of Motions. One lead inhibitor (compound 4) showing good inhibition was used in complex with

$GlmU_{Mtb}$ in MD simulation for a time scale of 10 ns. Our main objective in this regard is to explore the macroscopic properties in presence of solvent system (such as temperature, pressure number of interacting atom pairs) which should be based on its microscopic properties like bonded (distance, angle, dihedrals, improper) and non-bonded properties (van der Waal and couloumbic). In a way to analyze the simulation of compound 4 bound receptor complex, we have also run a 10 ns molecular dynamics simulations for the $GlmU_{Mtb}$ crystal structure containing both the substrates (GlcNAc-1-P and UTP). All the MD calculations were based on OPLS-AA force field using Desmond [210]. The complex was solvated using TIP3P water models in orthorhombic solvent box, with a boundary cut-off of 10 Å from any solute atom in all directions [211]. Appropriate numbers of counter ions were added to neutralize the system. Prior to the production run, an initial minimization of the system was performed with convergence threshold criteria of 1 $Kcal.mol^{-1}.Å^{-1}$. Next to this step, minimization of the system was performed with and without restraints on solute atoms for 12 ps time at 10 K temperature employing Berendsen thermostat (isothermal-isobaric ensemble). Further the temperature of the system was raised up to 300 K at 1atm pressure for 24 ps time. A cut-off of 14 Å was used for calculating the non-bonded interactions. M-SHAKE algorithm was used for reordering the hydrogen bonds in the simulation with integration time step of 2 fs [212]. The trajectory frames were recorded at an interval of 4.8 ps and total time scale of MD simulation was continued for 10 ns.

4.29 Survival curve and maximum dose tolerance.

Different groups of BALB/c mice (n=4 mice per group) were treated with a range of Oxa33 inhibitor (25 mg/kg, 50 mg/kg, 100 mg/kg and 200 mg/kg in 2.5% Tween-80) by intra peritoneal route for 30 days on every alternate day. Observations were taken as relative change in body weight and survival of mice and plotted as function of time in GraphPad Prism 5.0.

4.30 Estimation of Oxa33 from treated mice lungs.

Tetrahydrofuran (THF) was found to be best solvent after checking the solubility of Oxa33 in various organic solvents. UV spectrophotometric based wave scan analysis confirmed the λ_{max} of Oxa33 at 401 nm in THF. A standard curve (ranging from 2.5 µg/ ml to 40 µg/ ml of Oxa33) was prepared by taking absorbance

at 401 nm. Further BALB/c mice were treated with Oxa33 (50 mg/kg in 2.5% Tween-80) by intra peritoneal route for 3 weeks and 56 weeks on every alternate day and lungs were isolated. Lungs were macerate in THF with Dounce homogenizer followed by collection of isolated Oxa33 and estimation with Oxa33 standard curve

4.31 Statistical analysis.

Student's *t*-test (two tailed non parametric) was used to analyze the significance of cell wall thickness, THP1 and animal infection experimental results. SigmaPlot version 10.0 and GraphPad Prism version 5.0 was used for the statistical analysis and for plotting the results.

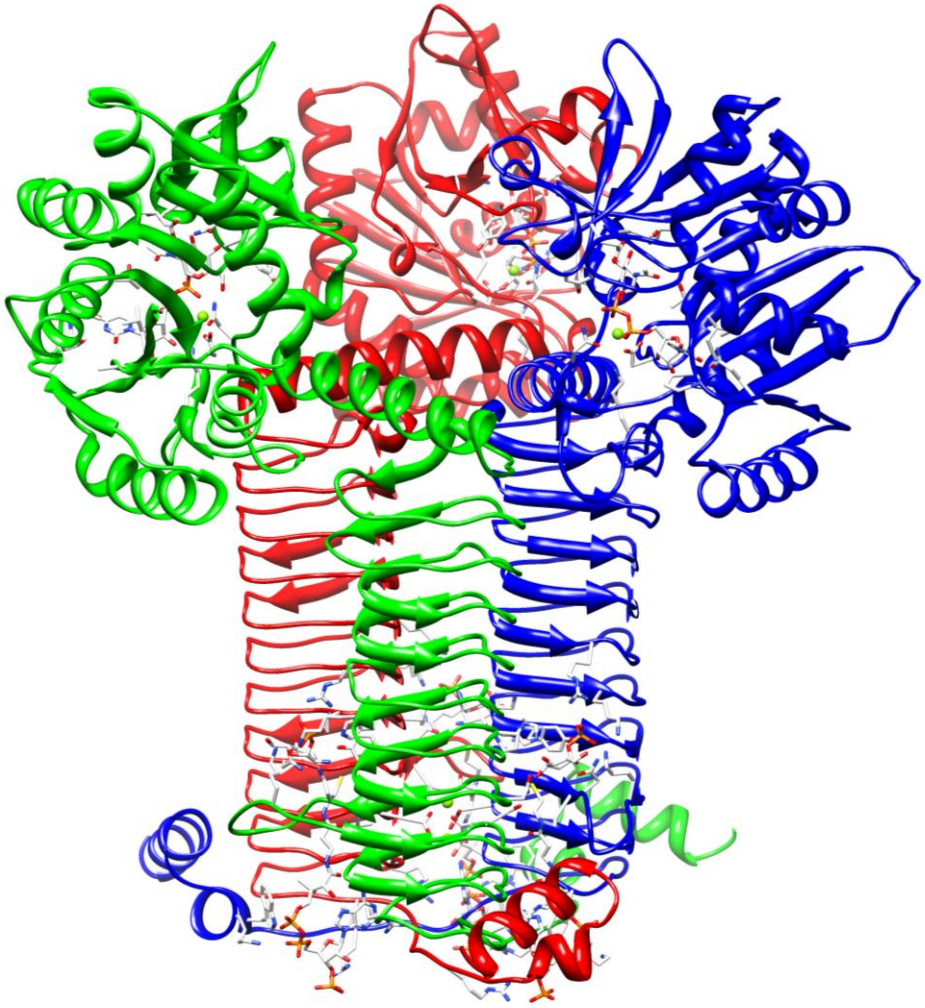

Chapter 5.

Structural characteristics and biochemical characterization of $GlmU_{Mtb}$

Chapter 5.

Structural characteristics and biochemical characterization of $GlmU_{Mtb}$

5.1 Introduction

Tuberculosis is a major threat to human health. The mycobacterial cell wall consists mainly of lipopolysaccharides and mycolic acid. It's complex and specialized nature makes the enzymes involved in its formation ideal for therapeutic intervention. GlmU, a prokaryotic enzyme conserved both in Gram positive and Gram negative bacteria, is involved in the biosynthesis of UDP-N-acetylglucosamine-1-phosphate (UDP-GlcNAc) [218]. It is a bifunctional protein with two independent active sites catalyzing acetyl transfer and uridyl transfer reactions on glucosamine-1-phosphate (GlcN-1-P). It synthesizes two key intermediates of cell wall biosynthesis pathways, N-acetylglucosamine-1-phosphate (GlcNAc-1-P) and UDP-GlcNAc. The carboxy terminal acetyltransferase domain catalyzes the transfer of the acetyl group from acetyl-CoA to the amine group of GlcN-1-P to produce GlcNAc-1-P [189]. GlcNAc-1-P then diffuses to the N-terminal domain of the protein, where it is activated to form UDP-GlcNAc by the transfer of UMP from UTP. UDP-GlcNAc, the end product, is utilized for synthesizing lipopolysaccharide and peptidoglycan components of the cell wall. Given this important role for GlmU, it is not surprising that it is essential for the growth of *M. tuberculosis* and *M. smegmatis* [115, 177]. Hence, understanding the catalytic mechanisms employed by $GlmU_{Mtb}$ would be valuable towards the discovery of inhibitors targeting cell wall biosynthesis in mycobacteria. Elucidating the acetyl transfer reaction catalyzed by the C-terminal domain is the focus of the work presented here.

Several structures of GlmU and their homologues were determined to understand the reactions catalyzed by this enzyme. The structure of GlmU from *Escherichia coli* ($GlmU_{Ec}$) [168, 169] and *Streptococcus pneumoniae* ($GlmU_{Sp}$)

[165] bound to acetyl-CoA at the C-terminal acetyltransferase active site are available. Determining the structures of $GlmU_{Mtb}$ bound to substrates of the acetyl transfer reaction was important. Attempts to obtain acetyl-CoA bound crystals of $GlmU_{Mtb}$ by co-crystallization or by soaking acetyl-CoA with the apo crystals were unsuccessful [4, 219] until UDP-GlcNAc was provided. In collaboration with Prof. Balaji Prakash group at IIT Kanpur, we determined structures of $GlmU_{Mtb}$, in complex with acetyl-CoA or CoA or GlcN-1-P. These allowed identifying likely catalytic residues and together with mutational data, we infered a reaction mechanism for the acetyl transfer reaction. Additionally, features unique and highly conserved in the *Mycobacteriaceae* family could be noted from these studies. Of these, a short helix present at the C-terminal extension provides a key tryptophan, which appears critical for acetyl-CoA binding. Besides, an uncommon mode of binding of the substrate acetyl-CoA was identified to be a feature unique to $GlmU_{Mtb}$. The unique features reported here, would aid elucidating structure-function relationships in the enzyme, which may be gainfully employed towards drug design against $GlmU_{Mtb}$.

In addition we identified the major PknB target site on $GlmU_{Mtb}$ and deciphered how T418 phosphoryltion regulates the acetyltransferase activity. Based on the previous structures of $GlmU_{Mtb}$ in complex with GlcNAc-1-P or UDP-GlcNAc we have performed mutational and biophysical studies to understand the mechanism of uridyltransferase reaction. Further we deterimend the role of Mg^{+2} ions in uridyltransferase activity and the binding parameters of different substrates and final product of $GlmU_{Mtb}$.

5.2 Results

5.2.1 Structure of $GlmU_{Mtb}$[AcCoA] complex.

In a previous study, a unique C-terminal extension in $GlmU_{Mtb}$ was identified, whose deletion led to abrogation of its acetyltransferase activity [99]. Previous attempts to obtain acetyl-CoA bound crystals by co-crystallization or by soaking apo crystals with acetyl-CoA have been unsuccessful [4, 219]. The structures of $GlmU_{Ec}$ and $GlmU_{Sp}$ bound to acetyl-CoA (at the acetyltransferase active site) revealed that the uridyltransferase active site was simultaneously occupied by UDP-GlcNAc – the product of the uridyltransfer reaction. It is likely that UDP-GlcNAc stabilizes the N-

terminal domain while acetyl-CoA binds the C-terminal active site. Therefore anticipating such stabilization, attempts were made to crystallize $GlmU_{Mtb}$ with acetyl-CoA, in the presence of UDP-GlcNAc (P.K.A.Jagtap M.tech thesis, Dr. Balaji Prakash's group, IIT-Kanpur). Structure of $GlmU_{Mtb}$ bound to acetyl-CoA, referred as $GlmU_{Mtb}$[AcCoA], was determined to a resolution of 2.33 Å. A careful analysis of the structure of $GlmU_{Mtb}$[AcCoA] revealed that hydrogen bonds stabilize the polar groups of acetyl-CoA and hydrophobic interactions stabilize its large carbon chain. A structural superposition of $GlmU_{Mtb}$ structures in the presence and absence of acetyl-CoA clearly reveals that a loop disordered in the apo structure becomes ordered upon acetyl-CoA binding. This conformational change appears significant as it contributes Tyr398 to stabilize acetyl-CoA. The backbone oxygen of Tyr398 interacts with the oxygen atom of the acetyl and amino group of acetyl-CoA. This interaction stabilizes the loop and leads to its ordering.

5.2.2 Ground state structure bound to both of the substrates allows identifying residues likely catalyzing the acetyltransferase reaction.

In order to obtain the structure bound to both the substrates of the acetyltransferase reaction, $GlmU_{Mtb}$[AcCoA] crystals were soaked with the second substrate GlcN-1-P and the structure was determined to a resolution of 1.98 Å. The objective of these attempts was to understand acetyl group transfer from acetyl-CoA to GlcN-1-P, which leads to the formation of the product GlcNAc-1-P. Therefore, we anticipated that the active site would contain either the substrates or the product. Surprisingly, the electron density present at the active site did not reveal the presence of the acetyl moiety and it depicted the presence of only CoA and GlcN-1-P. However, this structure closely mimics the ground state and is referred $GlmU_{Mtb}$[CoA:GlcN-1-P]. This structure lacks the acetyl group of acetyl-CoA and allows identification of residues likely to be important for catalysis. His374, Asn397, Ala391 and Ser416 were identified as probable candidate residues, as these were within 3.5 Å to the reacting groups, i.e. the amine of GlcN-1-P and thiol group of CoA (Fig 5.1A). As the backbone amine, and not the side chain atom(s) of Ala391 is involved in the interaction, it could not be mutated. The rest were individually mutated to alanines, the mutations were confirmed by DNA sequencing and mutant proteins were expressed, purified and analyzed on SDS-PAGE to assess their purity

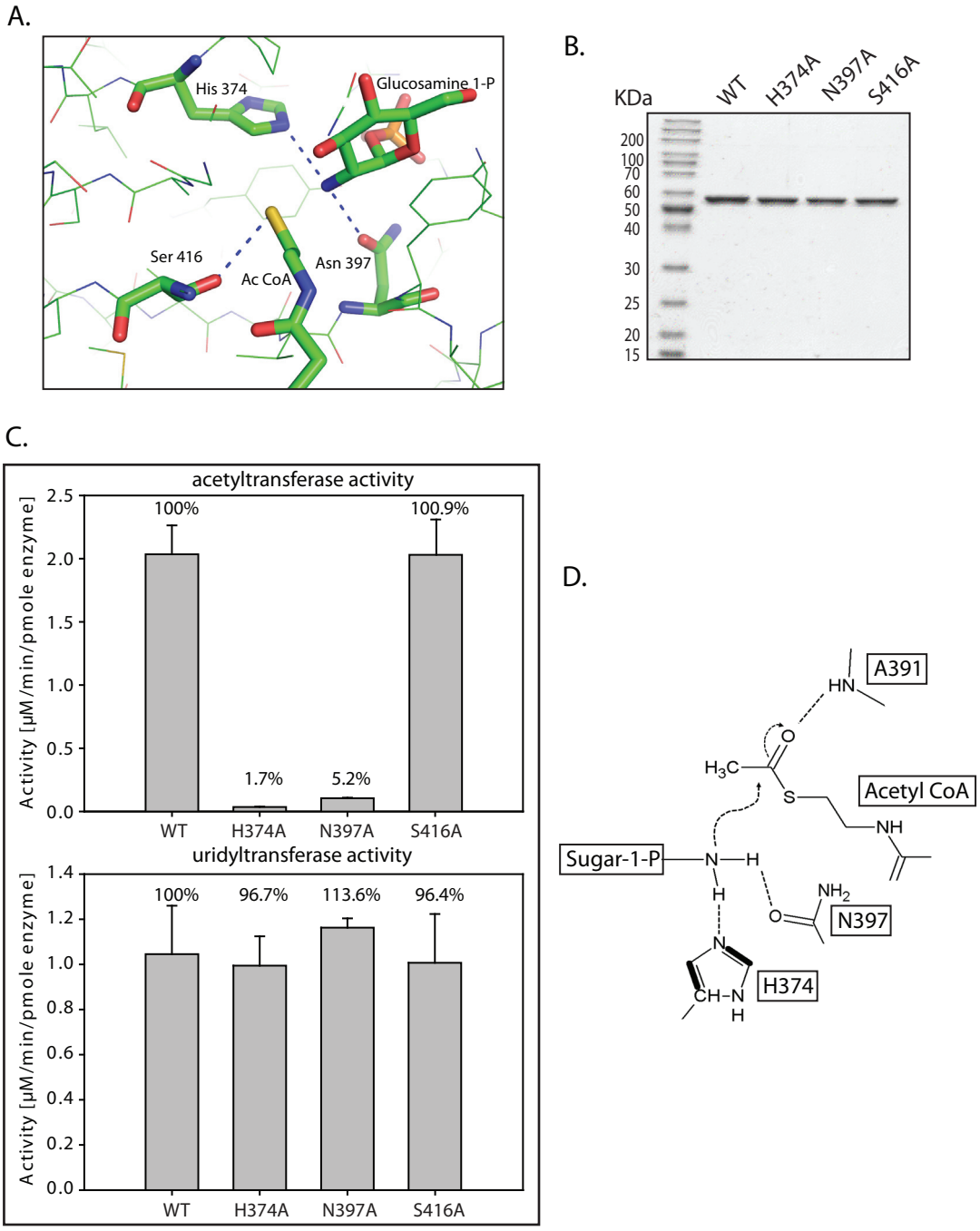

Figure 5.1. Residues participating in the acetyltransfer reaction: (A) The acetyltransferase active site of $GlmU_{Mtb}$ reveals probable catalytic residues H374, N397 and S416, which are highly conserved. Backbone amide of A418 that interacts with the acetylgroup is not shown. **(B)** SDS-PAGE gel showing the purity of His_6 tagged mutants and wild type $GlmU_{Mtb}$ proteins employed in the study. **(C)** Active site mutants were generated and their acetyltransferase activities were assayed. The activities of H374A and N397A are almost abolished. On the other hand, the activity of S416A is not affected significantly. Uridyltransferase activities of the proteins were used as a control. **(D)** A schematic of the proposed acetyltransferase reaction mechanism in $GlmU_{Mtb}$ (see text). The amino group activated by His374 and Asn397 launches a nucleophilic attack on the carbonyl carbon of acetyl-CoA. Simultaneously, the resultant negative charge on the carbonyl oxygen (oxyanion) is stabilized by the amide backbone of Ala391.

(Fig 5.1B). Since the mutations were in the active site of the acetyltransferase domain, one would expect uridyltransferase activity to be unaffected (Fig 5.1C, lower panel). This was used as an internal positive control. In agreement, the uridyltransferase activity of $GlmU_{Mtb}$ wild type (called $GlmU_{Mtb}$-WT henceforth) and the mutants was found to be comparable (Fig 5.1C). On the other hand, the acetyltransferase activity by mutants H374A and N397A was almost abolished and that by S416A was unchanged (Fig 5.1C, upper panel). In order to further understand the effect of these mutations, we have determined the kinetic parameters of both the substrates (Table 5.1). Indeed, K_m and V_{max} values obtained for S416A mutant were comparable to those obtained for $GlmU_{Mtb}$-WT, indicating that S416 neither plays a role in catalysis nor in substrate binding. For the mutants N397A and H374, K_m values were similar to that observed for $GlmU_{Mtb}$-WT, whereas the V_{max} values were greatly compromised. We speculate that both N397 and H374 are required for catalysis. Based on these and the prevailing mechanistic inferences on $GlmU_{Sp}$ and $GlmU_{Ec}$ studies, we believe that the catalytic mechanism, would involve His374, Asn397 and Ala391 (Fig 5.1D).

Table 5.1: Kinetic parameters (K_m and V_{max}) for the acetyltransferase activity of $GlmU_{Mtb}$ and active site mutants. Kinetic parameters were determined as described under "materials and methods." Standard deviation (S.D.) values were calculated using the data obtained from three independent experiments.

Protein	K_m (μM)	V_{max} (nM/min/pmole enzyme)	Relative(%) V_{max}/K_m
Acetyl CoA			
$GlmU_{Mtb}$	355.0±45.9	5.9±0.8	100
GlmU-H374A	300.0±0.05	0.05±0.01	0.96
GlmU-N397A	355.1±38.9	0.13±0.04	2.18
GlmU-S416A	360.1±20.5	5.6±2.2	92.39
Glucosamine-1-P			
$GlmU_{Mtb}$	353.3±64.6	7.5±1.3	100
GlmU-H374A	300.0±0.6	0.05±0.02	0.8
GlmU-N397A	282.5±20.7	0.08±0.03	1.4
GlmU-S416A	370.0±44.3	6.8±2.0	86.7

5.2.3 Acetyl-CoA adopts different conformations when bound to $GlmU_{Mtb}$ and $GlmU_{Ec}$.

Structural superposition of $GlmU_{Mtb}$[AcCoA] and $GlmU_{Ec}$[AcCoA] (PDB ID: 3SPT and 2OI5 respectively) revealed a significant difference in the conformation of the adenine ring of acetyl-CoA (Fig 5.2A-C). For ease of presentation, we termed the conformations of acetyl-CoA bound to $GlmU_{Ec}$ as 'L' conformation, whereas that bound to $GlmU_{Mtb}$ as 'U' conformation based on the shape adopted by it (Fig 5.2A, B respectively). Careful analysis of both structures revealed that two key residues that interact with acetyl-CoA are interchanged in the two enzymes. How may these substitutions give rise to the observed differences i.e. the 'L' and 'U' conformations, in acetyl-CoA conformation? It may be reasoned as follows. One of these residues, Arg440 in $GlmU_{Ec}$ interacts with the backbone oxygen atoms of acetyl-CoA, which appears to hinder the adenine ring from bending onto the carbon backbone of acetyl-CoA, and restricts it to the 'L' conformation. In $GlmU_{Mtb}$ this arginine is replaced by an alanine. Ala, unlike Arg, cannot restrict the adenine ring similarly and therefore allows it to adopt a 'U' conformation (Fig 5.2D). Also, in $GlmU_{Mtb}$, the 'U' conformation appears to be further stabilized due to cation-π interactions from Arg439, which in $GlmU_{Ec}$ is substituted by Thr428, whose shorter side chain cannot provide a similar stabilization (Fig 5.2E).

To inquire whether the substitutions presumed to provide a different binding conformation to acetyl-CoA in $GlmU_{Mtb}$ are uniquely conserved in *Mycobacteriaceae* family, the sequences of GlmU homologs were aligned. Indeed, the substitutions responsible for the 'U' conformation are restricted to *Mycobacterium* genus and some members of Actinobacteria phyla, whereas those responsible for the 'L' conformation, as in $GlmU_{Ec}$, are conserved in all the other homologues (Fig 5.4A-C). The structures of acetyl-CoA, bound to different protein structures present in PDB, were analyzed using ValiGurl server. From this, it was apparent that the 'U' conformation is atypical; as out of all the observed conformations, only 8 had RMSD $\leq$ 2 Å (Fig 5.3C). In order to ascertain the importance of the aforesaid residues in acetyltransferase activity, mutations A451R and R439T were created in $GlmU_{Mtb}$, both independently and simultaneously, to

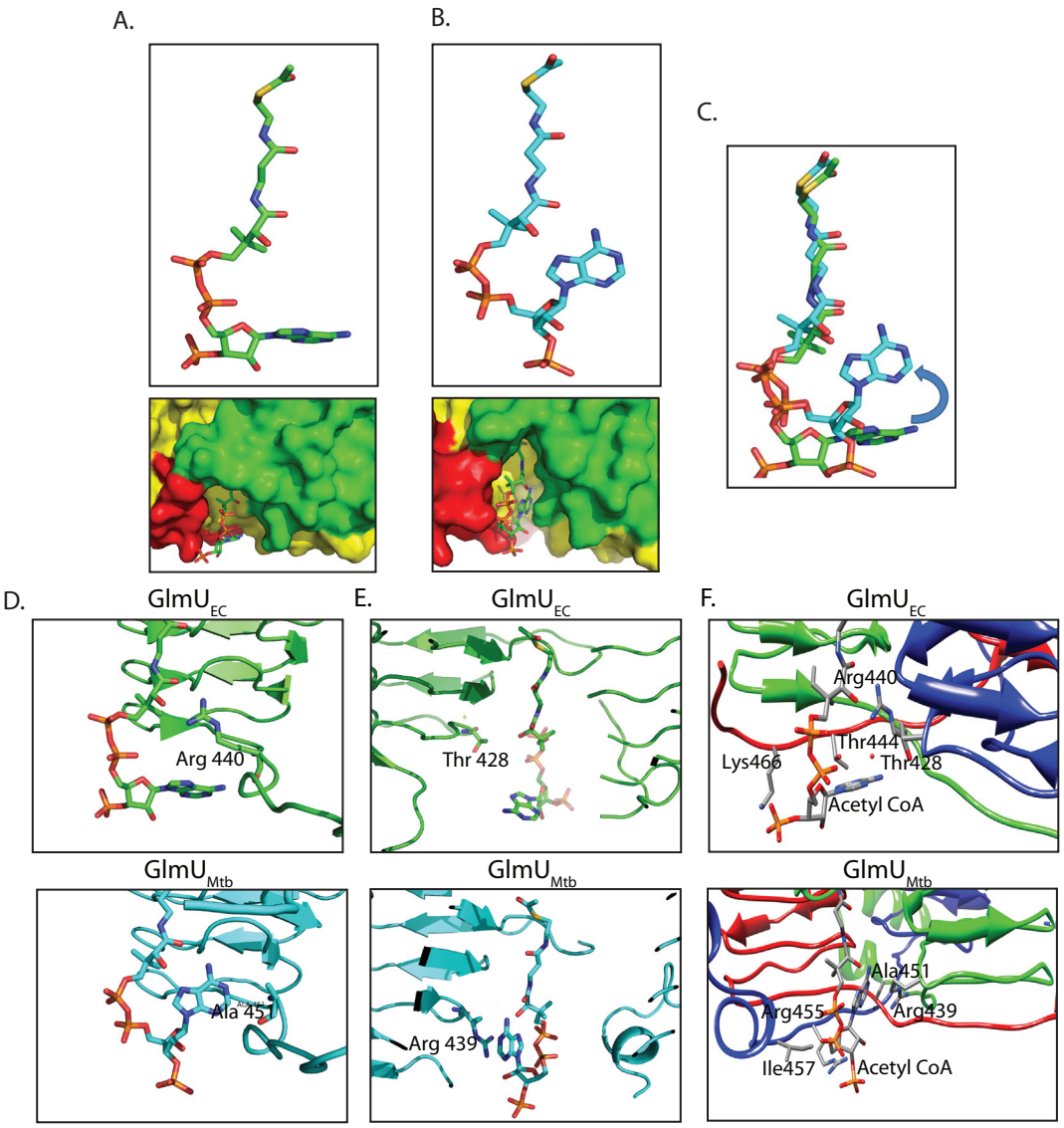

Figure 5.2. Different conformations of acetyl-CoA bound to GlmU$_{Ec}$ and GlmU$_{Mtb}$: **(A)** GlmU$_{Ec}$ displays an 'L' confirmation of acetyl-CoA with the adenine base laying flat. A surface representation (below) shows the adenine base and backbone phosphates of acetyl-CoA bound to GlmU$_{Ec}$ are exposed to the solvent and the backbone phosphates interacts with the water molecules. **(B)** Acetyl-CoA bound to GlmU$_{Mtb}$ displays a 'U' conformation with a bent adenine base, whose amine groups interact with the oxygens of the backbone. A surface representation (below) is shown with the three monomers colored green red and yellow. The adenine base of acetyl-CoA bound to GlmU$_{Mtb}$ is buried at the interface of two monomers of the trimer. The backbone phosphates interact with W460 and K454 contributed by the tail of the third monomer of the trimer [see fig 10 C]. **(C)** Superposition of the 'U' and 'L' conformations of acetyl-CoA. It shows a ~90° bend at the adenine base on the backbone carbon chain in the 'U' conformation. **(D)** Comparing the two conformations, Arg440 in GlmU$_{Ec}$ interacts with the backbone oxygens of acetyl-CoA, which prevents the adenine base from bending onto itself. On the other hand, Ala451 at an analogous position in GlmU$_{Mtb}$ is less bulky, and hence would not hinder the base from bending. (E) The 'U' conformation of acetyl-CoA in GlmU$_{Mtb}$ is further stabilized by Arg439, which provides cation-π interaction to the adenine base. No such stabilizing interaction is seen in GlmU$_{Ec}$, as Thr428Ec substitutes Arg439Mtb here. (F) Comparing the structures of GlmU$_{Mtb}$ and GlmU$_{Ec}$ two other substitutions viz. Ile457 to Lys and Arg455 to Thr, were also noted. Together all of these were believed to reverse the 'U' conformation to an 'L' conformation.

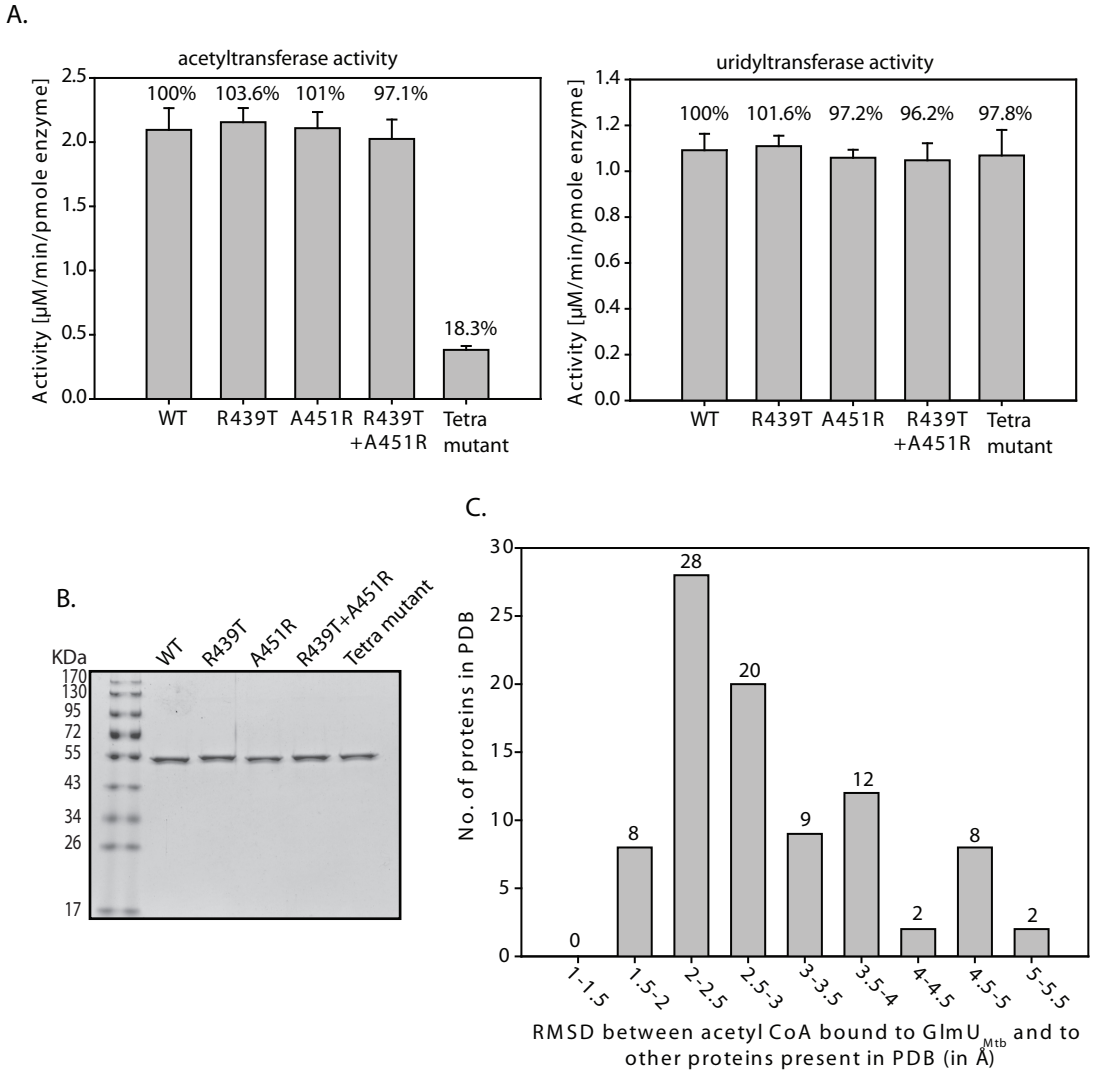

Figure 5.3. Activity of mutants for acetyl CoA confirmation: (A) Acetyltransferase activities for mutants R439T, A451R, double mutant (R439T+ A451R) and a tetra mutant (A451R, R439T, I457K and R455T) are shown. Uridyltransferase assays were used as internal controls. **(B)** SDS-PAGE gel depicting single bands of purified WT and mutant His_6 tag $GlmU_{Mtb}$. **(C)** Comparison of the conformation of the bound acetyl-CoA in $GlmU_{Mtb}$ and the proteins present in PDB. RMSD between the acetyl-CoA moieties bound to GlmUMtb and those bound to other proteins present in the PDB is shown. This data is presented in the histogram above. Numbers within the bars represent the number of proteins in PDB, wherein the conformation of acetyl-CoA superposes with the 'U' conformation seen in $GlmU_{Mtb}$ with an RMSD in the range mentioned below the bars. Only 8 proteins have RMSD less than or equal to 2Å.Visual inspection further confirmed that these adopt an almost U-like conformation.

A.

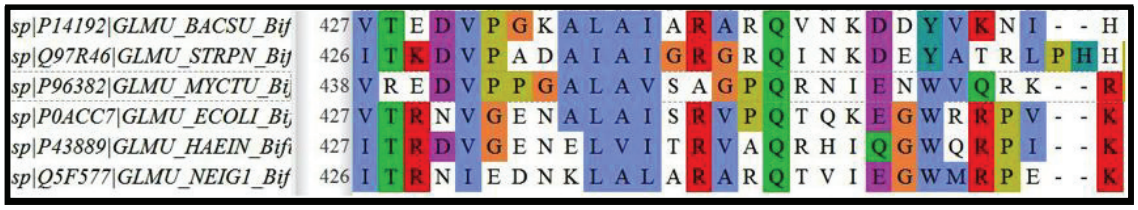

B.

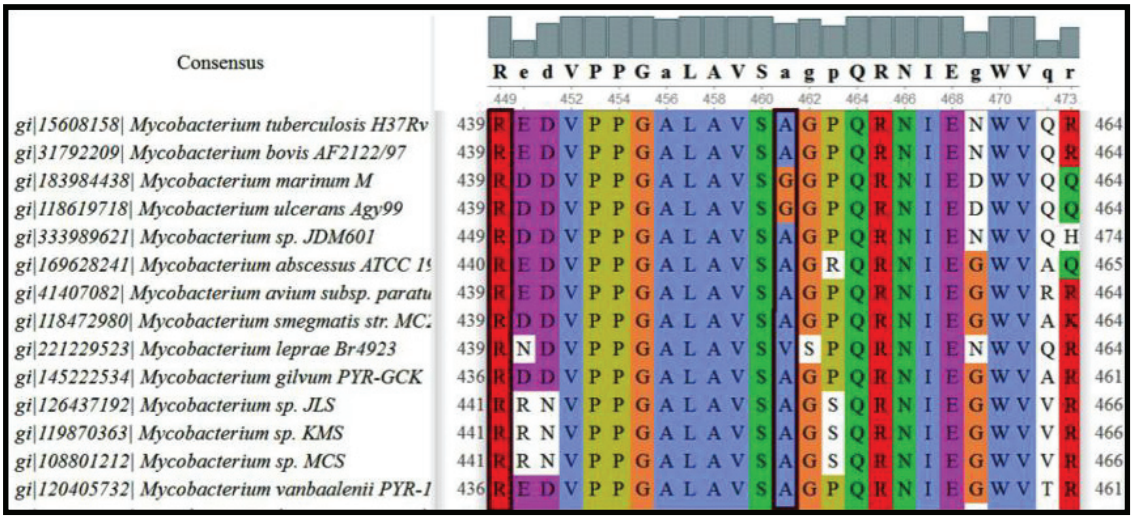

C.

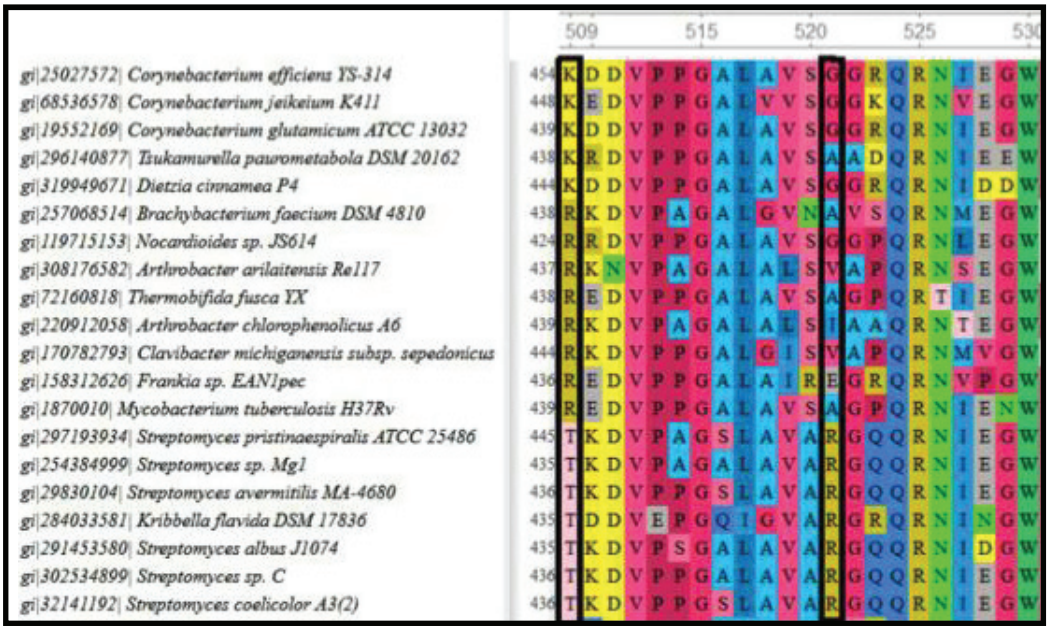

Figure 5.4. Sequence alignment showing the conservation of the two conformations of acetyl-CoA in the GlmU from different organisms: (A) Sequence alignment of the structures of GlmU present in Protein Data Bank reveals that the point amino acids which confer U shaped conformation to the acetyl-CoA bound to the $GlmU_{Mtb}$ is present only in *M. tuberculosis*. **(B)** Sequence alignment of GlmU from the genus Mycobacterium depicts that the amino acids conferring the 'U' shaped conformation are highly conserved in this species. **(C)** Analysis of GlmU in the phylum Actinobacteria, which Mycobacterium genus belongs to, reveals two groups; one having residues, responsible for the 'U' conformation and another having those responsible for the 'L' conformation of the bound acetyl-CoA.

mimic the corresponding residues in $GlmU_{Ec}$. From the structures, it appeared that- --the different nature of these substitutions would possibly result in an altered conformation of the adenine base of acetyl-CoA moiety. However, neither the single mutants A451R and R439T nor the double mutant (A451R + R439T) affected the acetyltransferase activity significantly (Fig 5.3A). A careful analysis of the structures brought out two more substitutions that were suspected to be important for the U/L conformation of acetyl-CoA. These are I457K and R455T (Fig 5.2F). When these mutations were included to create a tetra mutant (A451R, R439T, I457K and R455T), a marked reduction in acetyltransferase activity was noted (Fig 5.3A). Perhaps all of these residues collectively provide the unique 'U' or 'L' conformations to acetyl-CoA. Crystal structures of these mutants would evaluate the possible reversal of acetyl-CoA conformation at the active site, but attempts to crystallize these mutants were unfortunately not successful. Interestingly, the difference between $GlmU_{Mtb}$ and $GlmU_{Ec}$ in the C-terminal tail lies only in these four residues A451, R439, I457 and R455. Overall, the tail region of $GlmU_{Mtb}$ appears to play a significant role, perhaps in providing the 'U' conformation to acetyl-CoA. The absence of activity in the tetra mutant likely indicates an importance of the 'U' conformation for $GlmU_{Mtb}$.

5.2.4 A short helix governs the interaction of W460 with acetyl-CoA.

Previously, it was reported that a 30-residue extension at the C-terminus of $GlmU_{Mtb}$ is crucial for its activity [99]. Upon revisiting the data, the mutant based on which this inference was drawn, actually had a 37, and not 30, amino acid deletion in the C-terminus. In order to comprehensively investigate the importance of these 37 amino acids to the acetyltransferase reaction, we generated four truncation mutants, where the C-terminal 15, 20, 25, 30 and 37 amino acids were deleted. These are called $GlmU_{Mtb}\Delta15$, $\Delta25$, $\Delta30$ and $\Delta37$, respectively (Fig 5.5A). The control experiments suggested that the uridyltransferase activities of all the mutants were comparable to $GlmU_{Mtb}$-WT (Fig 5.5B). Interestingly, deleting up to 30 residues at the C-terminal region had little impact on the acetyltransferase activity, whereas a further deletion of seven residues, i.e. $\Delta37$, significantly affects the activity (Fig 5.5B). The mutant $\Delta37$ is devoid of the region (458 to 464) that forms a short helix at the C-terminus and this region appears important for the acetyltransferase activity.

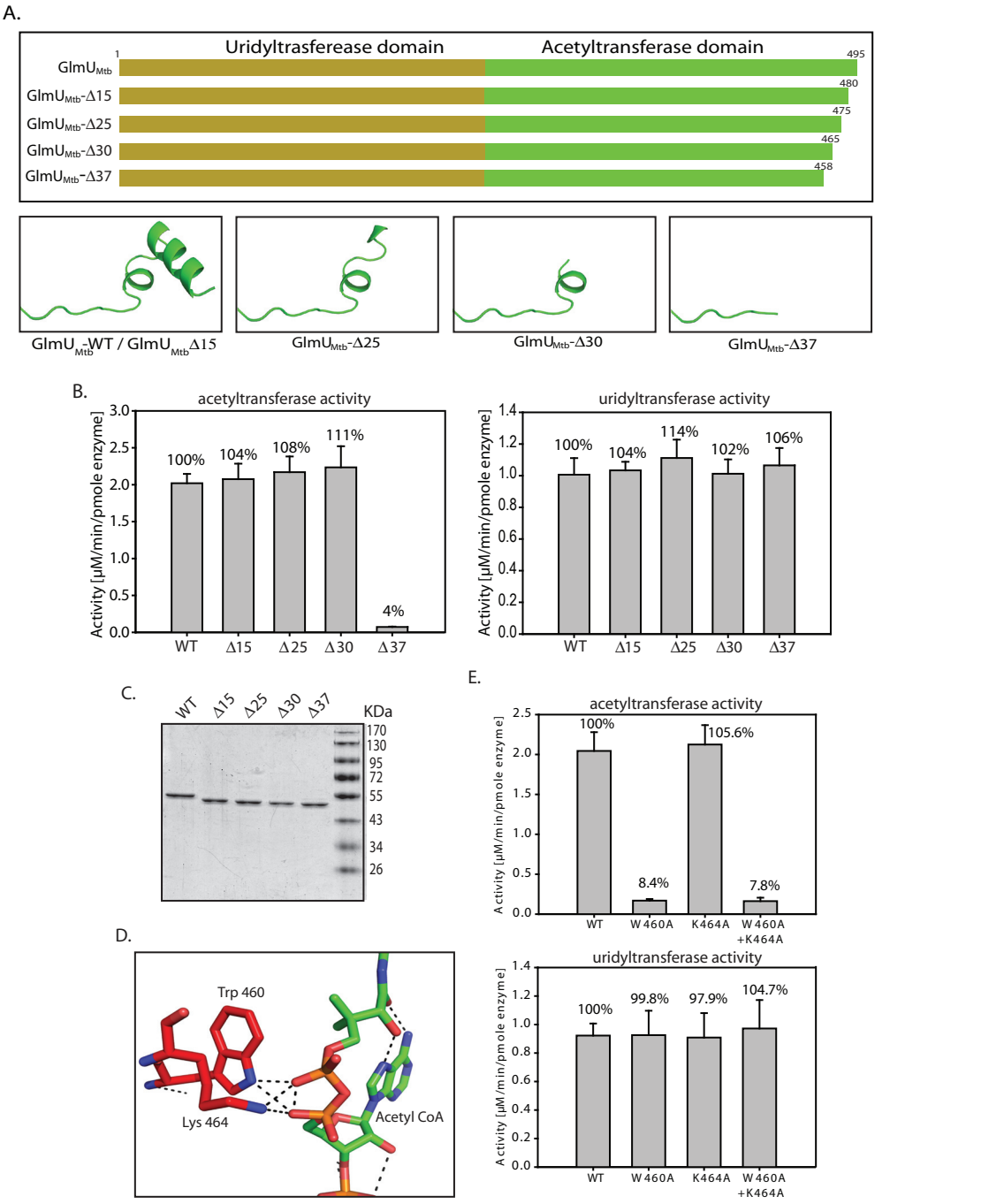

Figure 5.5. Tail truncation experiments identify residues important for acetyltransferase activity: (A) Residues were mutated sequentially from the C-terminal tail of $GlmU_{Mtb}$ to create Δ15, Δ25, Δ30 and Δ37 truncation mutants. Secondary structures present in this region are shown in the lower panels for each of these constructs. A short helix (one and half turns) and a longer one of three turns are present in WT, and Δ15, while in Δ30 and Δ25 only the short helix is present. Δ37 lacks both of these. **(B)** Acetyltransferase assays show that a complete loss in activity is seen only for Δ37, whereas the others show an activity comparable to the wild type protein. **(C)** SDS-PAGE gel showing the purity of the purified His_6 truncated $GlmU_{Mtb}$ protein. **(D)** Structure analysis of $GlmU_{Mtb}$[AcCoA] structure revealed that W460 and K464 lie in this region and provide important interactions with the backbone phosphate of acetyl-CoA. **(E)** W460A mutant displays complete loss in acetyltransferase activity, while K464A does not. The loss in activity of the double mutant (W460A + K464A) reinforces the importance of W460. The control uridyltransferase assays are shown on the right.

Delving further, we find that Trp460 and Lys464 are provided by this region, which interact with the backbone phosphate oxygens of the acetyl-CoA in $GlmU_{Mtb}$[AcCoA] structure (Fig 5.5D). To address the role of these residues in acetyltransferase activity, we mutated W460 and K464 to alanines; both independently and simultaneously. It is apparent from the assays that while K464A is as active as $GlmU_{Mtb}$-WT, for W460A and the double mutant (K464A+W460A) acetyltransferase activity is significantly compromised (Fig 5.5E). These studies implicate W460 contributed by the single turn helix, to be an important element in stabilizing acetyl-CoA binding.

In order to further confirm whether the single turn helix governs the interaction of W460 in $GlmU_{Mtb}$, we generated chimeras of $GlmU_{Mtb}$ and $GlmU_{Ec}$ as depicted in Fig 5.6A. The uridyltransferase activities for Mt-Ec and Ec-Mt chimeras were similar to those observed for $GlmU_{Mtb}$ and $GlmU_{Ec}$, which is anticipated since the uridyltransferase domains are unaltered in these chimeras (Fig 5.6B, right panel). The acetyltransferase activity of Ec-Mt chimera was also similar to the activity of $GlmU_{Ec}$, indicating that the *E. coli* protein tolerates the exchanged C-terminal region from $GlmU_{Mtb}$ (Fig 5.6B, left panel). In stark contrast, the activity of Mt-Ec chimera is significantly compromised, indicating that the C-terminal region of $GlmU_{Ec}$ cannot satisfactorily replace the role played by the analogous region of $GlmU_{Mtb}$ (Fig 5.6B, left panel). So as to develop deeper insights, we determined the kinetic parameters of acetyltransferease activity for $GlmU_{Mtb}$, $GlmU_{Ec}$, Mt-Ec and Ec-Mt chimeras (Table 5.2). It is apparent from the relative V_{max}/K_m values obtained that $GlmU_{Ec}$ is ~6-8 fold more efficient compared to $GlmU_{Mtb}$ enzyme. The difference is only due to higher V_{max} values for $GlmU_{Ec}$ compared with $GlmU_{Mtb}$. Compromised activity of Mt-Ec chimera is due to both very low V_{max} and high K_m values. While $GlmU_{Ec}$ tolerates presence of $GlmU_{Mtb}$ carboxy terminal region (Ec-Mt), swapping compromises the efficiency by ~50%.

This striking difference appears to be due to the short helix at the C-terminal region of $GlmU_{Mtb}$. Abolishing its interaction with acetyl-CoA by either mutating W460 or by disrupting the helix severely compromises the activity of $GlmU_{Mtb}$. Unexpectedly, in the structure of $GlmU_{Ec}$, neither does this region form a short helix nor does the analogous tryptophan W449 interact with acetyl-CoA. An examination

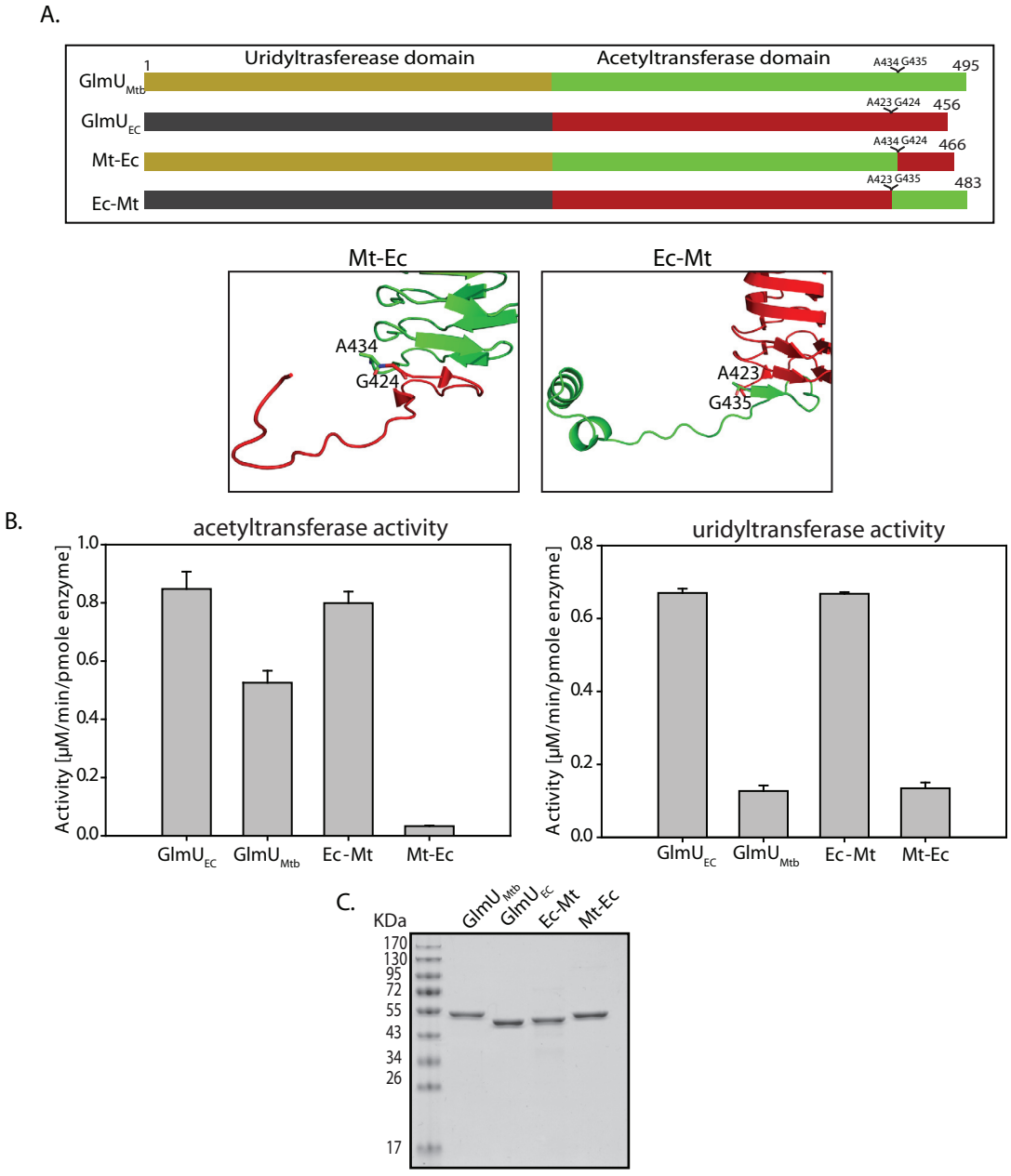

Figure 5.6. A short helix at the C-terminal extension in $GlmU_{Mtb}$ modulates acetyltransferase activity: (A) The $GlmU_{Ec}$-$GlmU_{Mtb}$ (Ec-Mt) and $GlmU_{Mtb}$-$GlmU_{Ec}$ (Mt-Ec) chimeras were made as depicted. $GlmU_{Ec}$ – red; $GlmU_{Mtb}$ – green. **(B)** The activities of $GlmU_{Ec}$-WT and $GlmU_{Mtb}$-WT are shown along with the chimeras Ec-Mt and Mt-Ec. The activity of Ec-Mt chimera is comparable to that of $GlmU_{Ec}$-WT. On the other hand, the activity Mt-Ec chimera is severely diminished. Uridyltransferase activities for the mutants were used as a control. **(C)** SDS-PAGE representing single bands of purified His_6 tagged WT or chimera GlmU proteins.

of $GlmU_{Ec}$ and $GlmU_{Mtb}$ structures show that the distance between W449 and phosphate oxygen of acetyl-CoA is ~4 Å.

Table 5.2*:* Kinetic parameters (K_m and V_{max}) for the acetyltransferase activity of $GlmU_{Mtb}$ and C-terminal chimeras of $GlmU_{Mtb}$ and $GlmU_{Ec}$. Kinetic parameters were determined as described in Table 5.1 legend. Standard deviation values were calculated using the data obtained from three independent experiments.

Protein	K_m (μM)	V_{max} (nM/min/pmole enzyme)	Relative(%) V_{max} /K_m
Acetyl CoA			
$GlmU_{Mt}$	420.9±40.6	4.4±0.3	100
$GlmU_{Ec}$	554.4±75.2	36.0±3.7	621.0
Mt-Ec	1227.7±149.8	0.08±0.005	0.6
Ec-Mt	442.6±24.2	14.0±0.1	302.5
Glucosamine-1-P			
$GlmU_{Mt}$	414.5±13.1	5.1±0.1	100
$GlmU_{Ec}$	279.6±39.7	30.3±1.1	877.8
Mt-Ec	968.3±62.3	0.08±0.007	0.64
Ec-Mt	722.1±93.7	13.9±0.9	156.0

However, it is likely that this difference is due to the 'L' conformation of acetyl-CoA in $GlmU_{Ec}$, and minor alterations in their positions or the 'U' conformation would possibly bring these two within interacting distance (Fig 5.7A). However, its mutation to alanine (W449A) in $GlmU_{Ec}$ also displays a strong reduction in acetyltransferase activity (Fig 5.7B). While this is not surprising considering the strong conservation of a tryptophan at this position across GlmU homologues, it is contrary to the observation that W449 does not interact with acetyl-CoA in $GlmU_{Ec}$. Perhaps, on the energy landscape, the structures of $GlmU_{Ec}$ and $GlmU_{Mtb}$ represent two distinct minima (with almost similar energies) with distinct conformations of the C-terminal region: Molecular Dynamics (MD) simulations could further clarify if it is possible to shuttle between these states with ease. Nevertheless, these results bring out an important contribution of W460/W449 in stabilizing acetyl-CoA at the active site.

In comparison to $GlmU_{Mtb}$, $GlmU_{Ec}$ lacks the short helix, but the residues analogous to K464 and W460 are conserved. Therefore, to gauge the importance of W460 and the short helix, we resorted to Molecular Dynamics simulations, using the acetyltransferase domain of $GlmU_{Mtb}$ (as described in Experimental Procedures). The

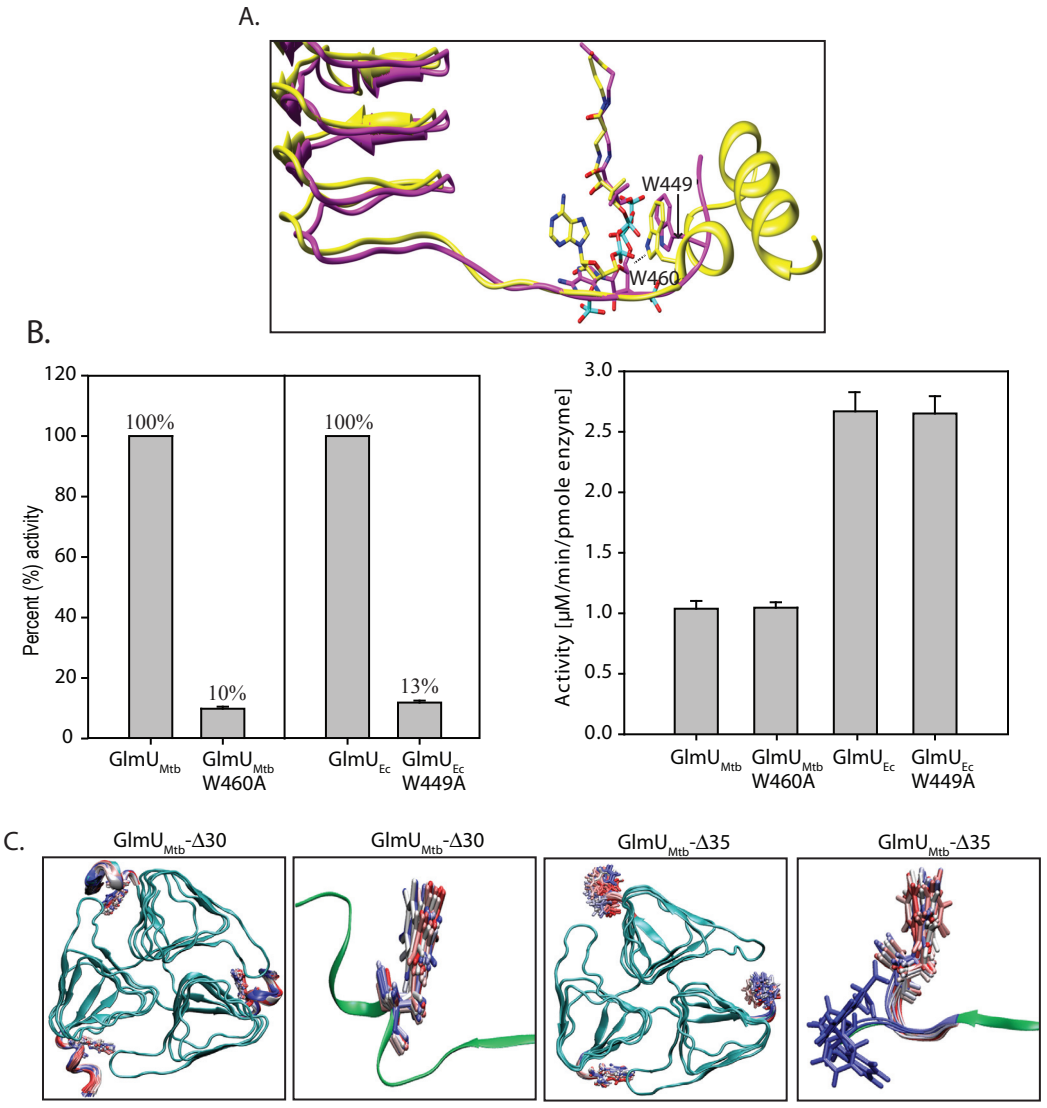

Figure 5.7. Comparative analysis of the C-terminal tail from *Mtb* and *E.coli* GlmU:(A) Structural comparison of the C-terminal tails in $GlmU_{Mtb}$ and $GlmU_{Ec}$. Structural superposition of $GlmU_{Mtb}$ (yellow) and $GlmU_{Ec}$ (pink) shows that W460 in $GlmU_{Mtb}$ makes a hydrogen bonding interaction to the phosphate oxygen of acetyl-CoA, while in $GlmU_{Ec}$ the same oxygen is at a distance > 4 Å from the analogous W449. **(B)** $GlmU_{Mtb}$-W460 and $GlmU_{Ec}$-W449 were mutated in the respective wild type proteins. Relative acetyltransferase activities measured for these are shown in the left panel, while the corresponding uridyltransferase activities are depicted in the panel on the right. Activities are compared for the pairs $GlmU_{Ec}$-WT and $GlmU_{Ec}$W449A; $GlmU_{Mtb}$-WT and $GlmU_{Mtb}$W460A. **(C)** The trajectories of W460 during MD simulation runs for 2 ns, for $GlmU_{Mtb}$-Δ30 and $GlmU_{Mtb}$-Δ35 show a very high fluctuation in the position of W460.

simulations were run for 2 ns at constant volume and constant temperature, which was followed by a run for 0.9 ns at constant pressure and temperature. They show that throughout the simulation, the short helix and the tryptophan side chain remains stable for the constructs with intact C-terminal tail and also for the Δ30 construct. However, for an *in silico* generated Δ35 construct, where the C-terminal part following W460 was deleted, a very high mobility for W460 was noted in the simulations. This inference is based on a high RMSD for W460 side chain. The RMSD values were 0.614 for constructs with intact C-terminal tail, 0.661 for Δ30 construct and 4.693 for Δ35 construct (Fig 5.7C). This indicates that the region following W460 is important in maintaining an orientation of W460 appropriate for substrate binding.

5.2.5 Thr418 in $GlmU_{Mtb}$ is a major phosphorylation site.

$GlmU_{Mtb}$ is phosphorylated by protein kinase B (PknB). This phosphorylation down-regulates the acetyltransferase activity of $GlmU_{Mtb}$ leaving the uridyltransferase activity unaffected. In order to identify the $PknB_{Mtb}$ target sites on $GlmU_{Mtb}$, we resorted to high-resolution mass spectrometry analysis of *in vitro* phosphorylated protein. LC-MS analysis showed presence of two phosphopeptides with precursor m/z 906.76 and 880.40 corresponding to phosphorylated mass of triply charged semi-tryptic peptide from residues 153-175 and tryptic peptide from residues 413-439, respectively. MS/MS analysis of these two precursors unambiguously identified T156 and T418 to be the target phosphorylation sites (Fig 5.8A & B). Analysis of peptide spectrum matches of all the identified $GlmU_{Mtb}$ phosphopeptides in multiple LC-MS runs indicated that phosphorylation on T418 is ~5 times more abundant as compared to T156. Peptide map analysis of *in vitro* phosphorylated PknB showed two major spots, which disappear when T418 residue is mutated to alanine (Fig 5.9A). However, minor spots could be detected both in wild type and the mutant, which may correspond to T156 phosphorylation. Comparison of intensities of various spots also suggests T418 to be the most abundant phosphorylation site on $GlmU_{Mtb}$ (Fig 5.9A).

The acetyltransferase activity of T418E that mimics a phosphorylated Thr, was severely compromised as compared to $GlmU_{Mtb}$-WT protein (Fig 5.9B, upper panel). Surprisingly, the activity of T418A mutant was also severely compromised

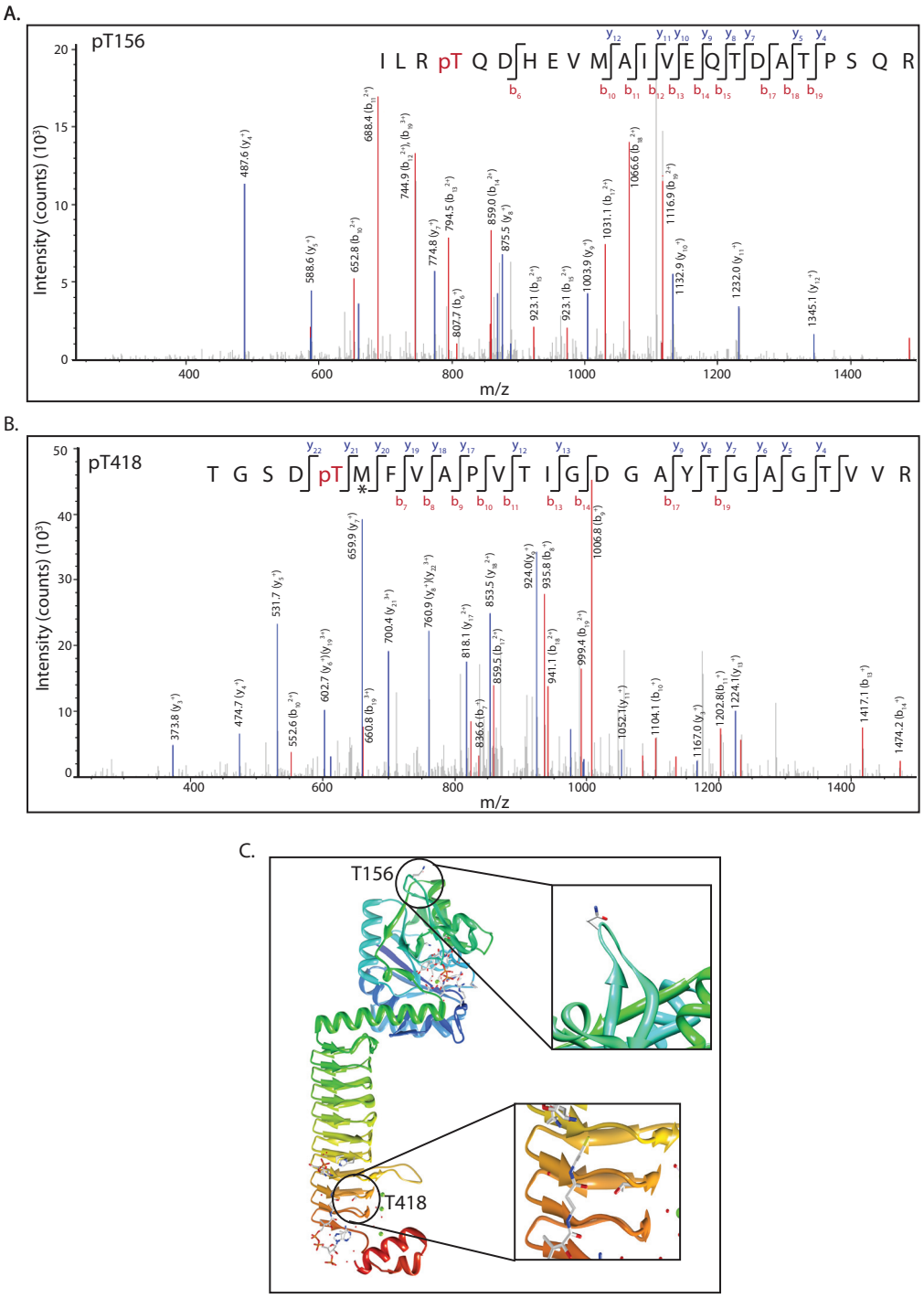

Figure 5.8. Identification of phosphorylation site. LC-MS/MS data showing collision-induced fragmentation mass spectra identifying two phosphopeptides in $GlmU_{Mtb}$ protein. pT indicates the site of phosphorylation. * indicates methionine oxidation: (A) MS/MS spectrum of precursor m/z 906.76 (+3) and MH+: 2718.29111 Da, of semi-tryptic phosphopeptide ILR(pT)QDHEVMAIVEQTDATPSQR. Unambiguous location of the intact phosphate group on Thr-156 was evident by the observation of the "b" ion series containing b6, b10, b11, b12, b13, b14, b15, b17, b18 and b19. **(B)** MS/MS spectrum of precursor m/z 880.40 (+3) and MH+: 2639.20804 Da of phosphopeptide TGSD(pT)MFVAPVTIGDGAYTGAGTVVR. Unambiguous location of the intact phosphate group on Thr-418 was apparent by the observation of the "y" series ion y22 and "b" ion series containing b7, b8, b9, b10, b11, b13, b14, b17 and b19. **(C)** $GlmU_{Mtb}$ ribbon structure swhows 'pT' residues; T156 at uridyltransferase domain and T418 at acetyltransferase domain respectively.

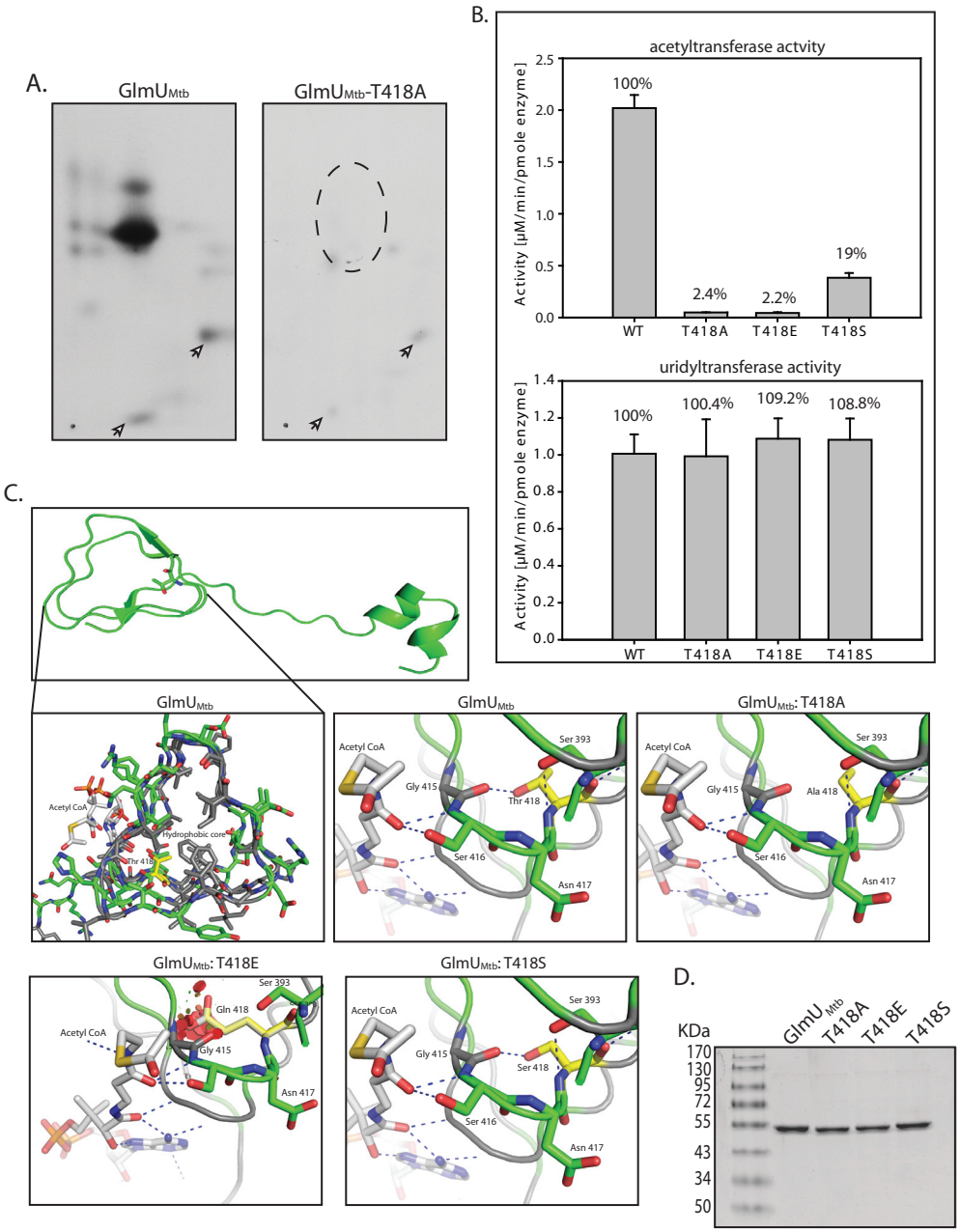

Figure 5.9. The effect of phosphorylation of $GlmU_{Mtb}$ by $PknB_{Mtb}$: (A) *In vitro* phosphorylated $GlmU_{Mtb}$ or mutants were digested with trypsin and the resulting phosphopeptides were mapped by two-dimensional resolution on thin layer chromatography. **(B)** Thr418 was mutated to glutamate (phospho-Thr mimic) and to alanine (phosphoryltation negative). Acetyltransferase activities of $GlmU_{Mtb}$-WT and the phospohomutants are shown in the left panel. Corresponding uridyltransferase activities are shown in the right panel. **(C)** The acetyltransferase domain, which consists of the β-helix has a highly hydrophobic core (grey colored residues) and a few polar residues. Thr418 is shown in yellow. Hydroxyl group of T418 makes a hydrogen bond with the backbone oxygen of Gly415. Mutation of T418 to alanine (T418A) would disrupt this interaction (black arrow) whereas mutation to a glutamate (T418E) would introduce steric clashes in the region as shown by red patches. However, mutation to serine (T418S) would preserve the polar interaction with the backbone of Gly415. The hydroxyl and backbone amine group of Ser416 interacts with the backbone oxygen of the acetyl-CoA. It is expected that perturbing these interactions would affect the positioning of the acetyl group for catalysis. **(D)** SDS-PAGE gel showing single bands of purified His_6 tagged WT and phosphomutants of $GlmU_{Mtb}$.

suggesting an essential role for the side chain oxygen (Fig 5.9B, upper panel). Mutating T418 to serine preserved some activity. Analysis of the structures of $GlmU_{Mtb}$ reveals that the region near T418 lies in a hydrophobic core of the LβH of the acetyltransferase domain and forms a hydrogen bond with the backbone carbonyl oxygen of Gly415 (Fig 5.9C). As the region is highly hydrophobic, an imbalance in charge would destabilize the region. The mutation T418A will not satisfy the interaction with Gly415. The introduction of a bulky negatively charged phosphate group due to phosphorylation of T418 will cause a steric clash and disturb the stabilizing interactions (Fig 5.9C). This would further destabilize the interactions between the adjacent stacks of the β helix. As these stacks provide stabilizing interactions to acetyl-CoA, their destabilization will result in loss of acetyltransferase activity.

5.2.6 Uridyltransferase active site of $GlmU_{Mtb}$.

Next we sought to understand the functional importance of critical $GlmU_{Mtb}$ amino acids in the uridyltransferase active site. In earlier studies $GlmU_{Mtb}$ was crystallized either in apo form or with UDP-GlcNAc or as various substrates pairs (ref). Based on these studies, amino acid residues R19, K26, D114 and N239 were considered critical either for interactions with Mg^{+2} ion or the product UDP-GlcNAc (Fig 5.10A). While D114 and N239 directly interact with Mg^{+2} ions, R19 and K26 interact with oxygens of UDP-GlcNAc. To determine their role in uridyltransferase activity, we have mutated R19, K26 and N239 residues to alanine and D114 to arganine residue. The R19A, K26A, D114A and N239A mutants were found to be inactive for the uridyltransferase activity, signifying that these residues are catalytically important (Fig 5.10B). The mutant D114E exhibited 50% reduced activity, demonstrating the significance of D114 in precisely coordinating Mg^{+2} (Fig 5.10B). Since the mutations were in the uridyltransferase domain, acetyltransferase activity was performed as the internal control, which as expected remained unchanged (Fig 5.10C). We have measured the acetyl and uridyltransferase activities at different concentrations of Mg^{+2}. While the uridyltransferase activity seems to follow Michaelis-Menten kinetic pattern, the acetyltransferase activity was marginally altered with increasing concentration of Mg^{+2} (Fig 5.10E), suggesting a critical role for Mg^{+2} in modulating uridyltransferase activity.

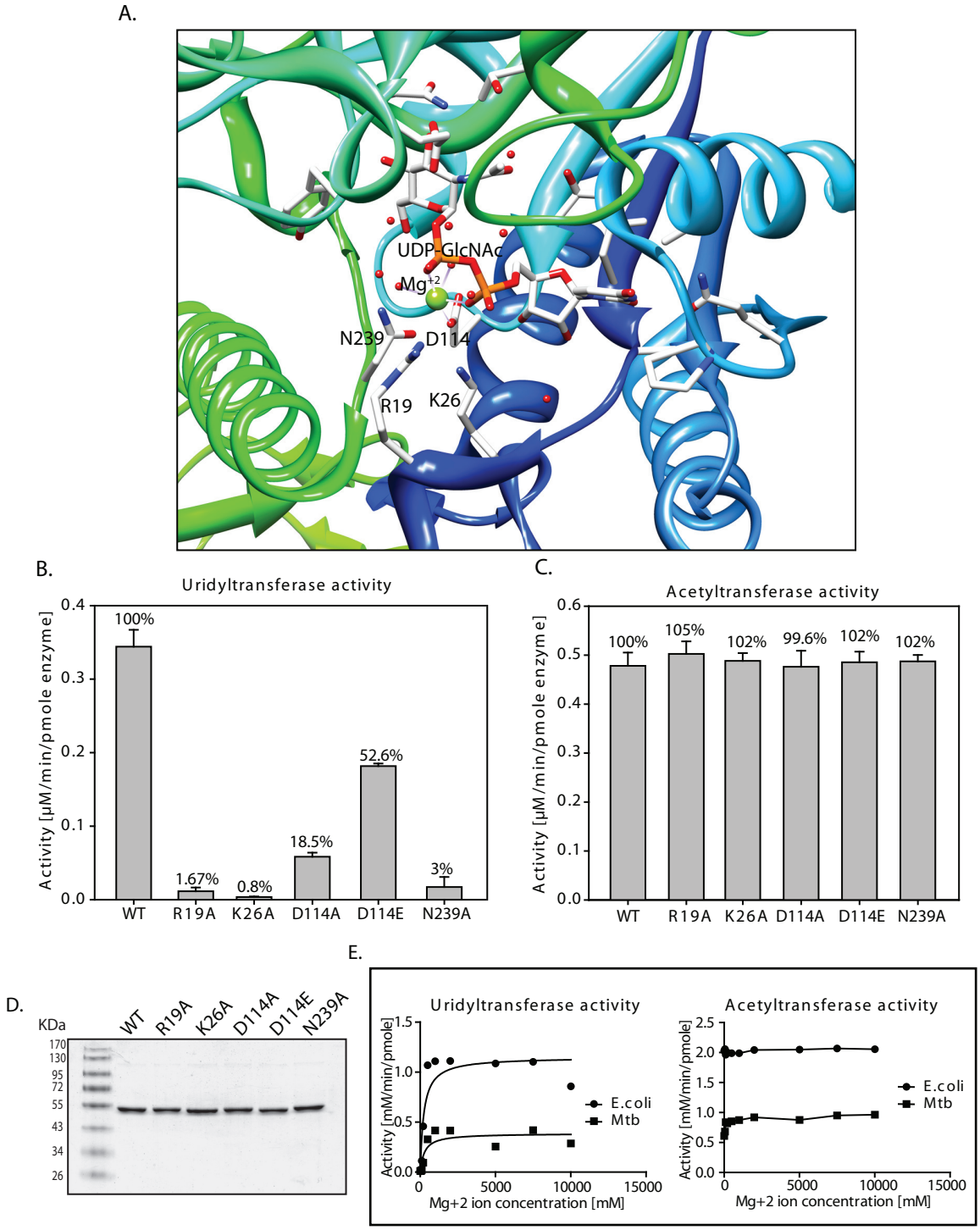

Figure 5.10. Uridyltransferase active site and active site mutants of $GlmU_{Mtb}$: (A) Cartoon representing the uridyltransferase active site bound with Mg^{+2} and UDP-GlcNAc **(B)** The mutants R19A, K26A, D114A and N239A show a drastic decrease in the uridyltransferase activity as compared to the wild type protein signifying an important role for these residues in catalysis. D114E mutant shows half the activity as compared to the wild type, indicating that proper positioning of Mg^{2+}A is necessary for the reaction. **(C)** Acetyltransferase activity was used as control; for, these residues are present in the uridyltransferase domain and should not alter the acetyltransferase activity. **(D)** The protein gel (SDS-PAGE) to assess the purity of the mutant proteins is shown. **(E)** Kinetic analysis of Mg^{+2} ion with $GlmU_{Mtb}$ and $GlmU_{Ec}$. Uridyltransferase activity follow regular kinetic pattern while no effect was observed on acetyltransferase activity.

5.2.7 Binding studies of substrates and product.

Energetics of ligands binding with any protein is important to ascertain the affinity and the strength of the interaction. In order to study the binding parameters we have performed isothermal titration calorimetry and differential scanning fluorimetry (DSF). DSF results signify that acetyl-CoA, GlcN-1-P or both in combination do not show strong interaction (marginal changes in T_m values) with $GlmU_{Mtb}$. UTP or GlcNAc-1-P show minor positive shift in T_m values with increasing concentrations (Table 5.3). In contrast, a drastic shift in T_m (8-10° C) was observed when a combination of UTP and GlcNAc-1-P (equimolar) was used. Similar T_m shift (8- 12° C) was also observed when the enzyme was titrated with UDP-GlcNAc, suggesting that the drastic T_m shift observed when a combination of both UTP and GlcNAc-1-P were used, was may be due to the formation of product UDP-GlcNAc.

We next performed ITC experiments to investigate the binding parameters. While both of the sugar substrates (GlcN-1-P and GlcNAc-1-P) did not give any significant binding pattern in the study, we obtained proper binding isotherms with the other substrates- acetyl CoA and UTP and the final product UDP-GlcNAc (Fig 5.11 & 5.12). Parameters suggest that UTP binding follows two site binding pattern while Ac-CoA and UDP-GlcNAc follow one site binding pattern. UTP binds with greater affinity with K_a value of 1.7×10^6 and the binding stoichiometry of 1.22. This binding was majorly entropy driven with ΔG = -8504.8 cal/mol and exothermic enthalpy change ΔH = -2.4 kcal/mol (Table 5.4). The acetyl-CoA binds with relatively lesser affinity (compared with UTP) with the K_a value of 5.05×10^4 and binding stoichiometry of n = 0.5. Total entropy change was ΔG = -6416.25 cal/ mol with lesser enthalpy change ΔH = -6.6 kcal/mol as compared with UTP (Table 5.4). Interestingly the final product, UDP-GlcNAc, shows very good isotherm of binding pattern with K_a value of 7.43×10^5, the binding stoichiometry of n ≈1.2 and entropy of -8009.46 (Table 5.4). We have also checked the effect of binding of each substrate on either domain when the other domain is occupied. Towards this we have pre-incubated $GlmU_{Mtb}$ with one of the substrates (acetyl-CoA or UTP) for 15 min prior to the injection of other substrate in the cell. We observed only marginal changes in

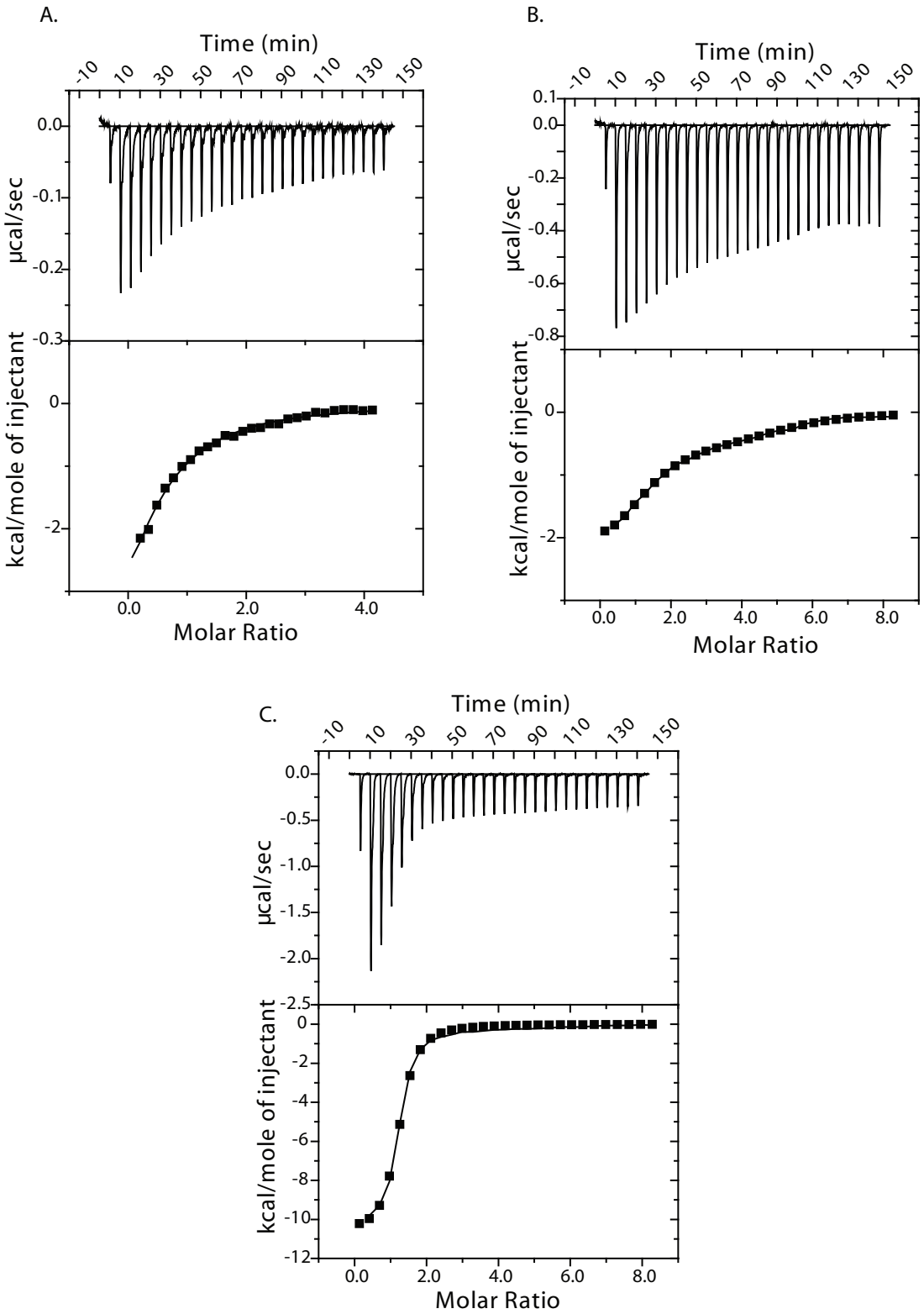

Figure 5.11. Isothermal titration calorimetry results of different substrates and products with $GlmU_{Mtb}$: 500 µM of various ligands were injected in 25 µM of $GlmU_{Mtb}$ and released heat increased over the period of time (µcal/sec) is presented in upper panel while corresponding binding isotherm presented in lower panel. **(A)** With acetyl CoA, fitted for one site binding **(B)** With UTP, fitted for two site binding **(C)** With final product UDP-GlcNAc, fitted for one site binding

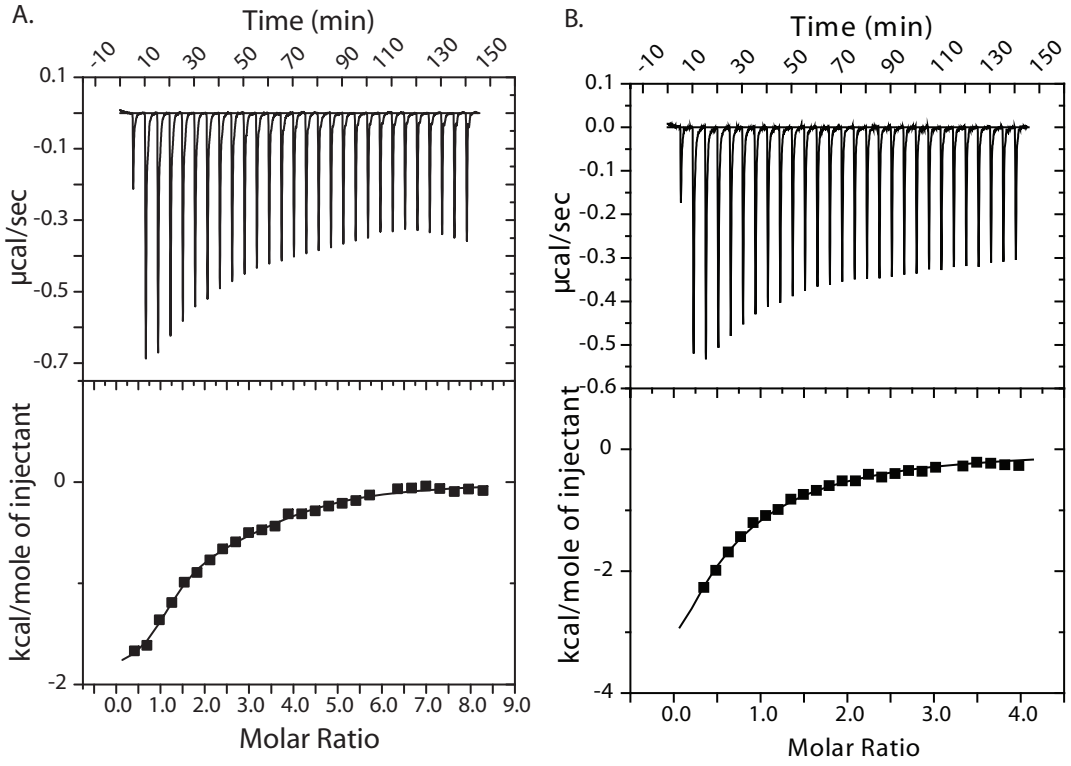

Figure 5.12. Isothermal titration calorimetry results of different combinations of substrates with $GlmU_{Mtb}$: 500 µM of either acetyl CoA or UTP were injected in 25 µM of $GlmU_{Mtb}$which was pre-incubated with either UTP or acetyl CoA and released heat increased over the period of time (µcal/sec) is presented in upper panel while corresponding binding isotherm presented in lower panel. **(A)** Pre incubation of $GlmU_{Mtb}$with acetyl CoA, followed by injection of 500 µM UTP, fitted for two site binding **(B)** Pre incubation of $GlmU_{Mtb}$with UTP, followed by injection of 500 µM acetyl CoA, fitted for one site binding.

the binding parameters of acetyl-CoA or UTP even when the other domain is occupied (Table 5.4).

Table 5.3: Change in T_m (°C) with various concentrations of substrates and product of $GlmU_{Mtb}$.

Substrates	62.5 µM	125 µM	250 µM	500 µM	1000 µM
Acetyl CoA	-0.33	-0.33	0.5	1.17	4.17
GlcN-1-P	0.5	0.5	-0.33	-0.33	-0.33
Ac Co A + GlcN-1-P	-0.5	-0.83	-0.83	-0.83	0.33
UTP	0.83	1.17	1.33	2.17	3.33
GlcNAc-1-P	0.33	0.5	0.33	0.33	0.33
UTP+ GlcNAc-1-P	6.83	7.83	9.0	9.67	10.0
UDP-GlcNAc	8.17	9.33	10.33	10.83	11.67

Table 5.4: Binding parameters for $GlmU_{Mtb}$ from ITC experiments.

Parameters	Acetyl-CoA	UTP	UDP-GlcNAc	UTP pre-incubation followed by Acetyl-Coa	Acetyl-Coa pre-incubation followed by UTP
Model	*One site*	*Two site*	*One site*	*One site*	*Two site*
Chi^2	1712	335.3	2.706E4	1540	835.5
N1	0.499±0.0787	1.22±0.047	1.15±0.0154	0.42±0.12	1.0±0.09
K_a1	5.05E4±5.54E3	1.7E6±3.6E5	7.43E5±8.93E4	4.06E4±4.7E3	1.3E6±5.3E5
ΔH1 (cal/mol)	-6573±1178	-2366±161	-1.08E4±209.7	-1.02E4±3172	-1947±150
ΔS1 (kcal/mol)	-0.526	20.6	-9.23	-13.2	21.4
ΔG1 (cal/mol)	-6416.25	-8504.8	-8009.46	-6286.4	-8324.2
N2		3.98±0.2			2.7±0.36
K_a2		1.51E5±3.5E4			6.77E4±1.97E4
ΔH2 (cal/mol)		-517.0±78.3			-858.3±236
ΔS2 (kcal/mol)		22.0			19.2
ΔG2 (cal/mol)		-7073			-6579.6

5.3 Discussion

As seen from the structures of $GlmU_{Mtb}$, the substrate acetyl-CoA binds at the trimeric interface. Its stabilization by interactions from all three monomers implicates the importance of trimerization for the acetyltransferase activity. Acetyl-CoA is similarly stabilized in $GlmU_{Ec}$ and $GlmU_{Sp}$ [165, 169]. In an attempt to obtain the crystals of $GlmU_{Mtb}$ in the product bound form of acetyltransferase reaction, (1) $GlmU_{Mtb}$[AcCoA] crystals were soaked in GlcN-1-P; and (2) $GlmU_{Mtb}$ was co-crystallized with GlcNAc-1-P and CoA. Although both revealed the presence of GlcN-1-P at the active site, they yielded incomplete information in not depicting electron density for the acetyl group. This can be due to the presence of catalytically active pairs of the acetyltransferase reaction in the reaction mixture, as the reverse reaction will lead to the presence of the reactants and products of the reaction, both, at any given time. If CoA and GlcN-1-P have more affinity for the active site as compared with acetyl-CoA and GlcNAc-1-P, then due to the presence of all the four components in the reaction mixture, CoA and GlcN-1-P would preferentially bind the active site.

Although the acetyl group could not be positioned in the active site, the $GlmU_{Mtb}$[CoA:GlcN-1-P] structure enabled the identification of His-374, Asn-397, Ala-391, and Ser-416 as potential catalytic residues (Fig 5.2A). Acetyltransferase assays using H374A, N397A, and S416A mutants revealed that mutating His374 and Asn397, but not Ser416, affects catalytic activity. For the $GlmU_{Mtb}$-WT and the mutants, kinetic constants were determined separately for the two substrates acetyl-CoA and GlcN-1-P (Table 5.1). The V_{max} for H374A and N397A is drastically reduced as compared with $GlmU_{Mtb}$-WT. Furthermore, the K_m values remain unchanged for both acetyl- CoA and GlcN-1-P, signifying that the mutants do not affect binding of the substrates. In the structure, the amine group of GlcN-1-P is only 3.14 Å away from the thioester group of CoA. Based on enzyme kinetics for $GlmU_{Mtb}$-WT and the mutants, we propose a catalytic mechanism where, the amine group of GlcN-1-P is activated for nucleophilic attack onto the carbonyl carbon of acetyl-CoA to form the products GlcNAc-1-P and CoA, as shown in a schematic (Fig 5.1C). We also infer that a conserved histidine (His-374 in $GlmU_{Mtb}$) deprotonates the amine group. Besides, the nucleophilicity of the nitrogen (of the amine group) is

further enhanced due to an H-bond interaction with the side chain oxygen of Asn-397 (Fig 5.1C). The activated amino group then makes a nucleophilic attack on the carbonyl carbon of acetyl-CoA, which is electrophilic. Simultaneously, this leads to the generation of an oxyanion on the carbonyl oxygen. The additional negative charge on the carbonyl oxygen is stabilized by an H-bond with the backbone amide of a conserved alanine Ala391, as shown in (Fig 5.1). This mechanism is in line with that proposed for $GlmU_{Ec}$ and $GlmU_{Sp}$ [165, 169]. Furthermore, it was suggested that the acetyltransferase reaction follows an SN_2 mechanism [169]. In this mechanism, the amino group of the GlcN-1-P is believed to be activated by a conserved histidine (His374 in case of $GlmU_{Mtb}$). Although a role for histidine in catalysis was clearly suggested, the role of Asn-397 has not been addressed satisfactorily. Olsen *et al.* [169] only suggest that this Asn makes an interaction with the amine group (of GlcN-1-P) and do not mention its involvement in the catalysis. However, for $GlmU_{Sp}$, the role of this Asn has been interpreted in providing a stable binding of acetyl-CoA [165]. This view is negated by the kinetics data (Table 5.1) and the analysis of the crystal structures presented here. Apart from this, in the case of $GlmU_{Ec}$, a conserved serine was also believed to orient itself to stabilize the oxyanion group. However, upon mutating the analogous Ser-416 of $GlmU_{Mtb}$, a significant difference (in activity) was not observed (Fig 5.1B, Table 5.1). In agreement with our data, mutational analysis carried out on the basis of amino acid residue conservation in the carboxyl terminal region of $GlmU_{Mtb}$ also showed importance for His374 and Trp460 in catalysis [220].

Another intriguingly different aspect is the conformation of acetyl-CoA/CoA bound to $GlmU_{Mtb}$ and that bound to $GlmU_{Ec}$/$GlmU_{Sp}$. An analysis of the conformations of the acetyl-CoA present in the Protein Data Bank revealed that only eight entries have an acetyl-CoA conformation as that found in $GlmU_{Mtb}$, suggesting this conformation is atypical in nature (root mean square deviation < 2 Å, Fig. 4B). However, it is not uncommon for small molecules/ ligands to adopt a wide range of conformations by varying only a few rotatable bonds. These changes in binding conformation may have a biological significance, including differences in reaction kinetics by homologous enzymes. Usually, catalytic mechanisms adopted by homologous enzymes from different species are conserved and the conformation

adopted by substrates may not be identical. In these active sites, the residues near the reaction centre are conserved to preserve the nature of the reaction mechanism. However, some that are away from the reaction centre contribute to substrate binding. Differences in these, (among homologues) may manifest as differences in substrate binding [221]. The residues interacting with the acetyl group of acetyl-CoA in $GlmU_{Mtb}$ are largely conserved among GlmU homologues, except for Arg439, Ala451, Arg455, and Ile457 near the adenine base of acetyl-CoA. As indicated in Fig 5.2, *D–F*, in $GlmU_{Ec}$, residues analogous to these are Thr428, Arg440, Thr444, and Lys446, respectively. Analysis of crystal structures suggested that the nature of these substitutions might significantly alter the conformation of the adenine base of acetyl-CoA moiety. We reasoned that these are likely responsible for the U or L conformations of acetyl-CoA seen in $GlmU_{Mtb}$ and $GlmU_{Ec}$. However, upon mutating Ala451 to Arg and Arg439 to Thr, either independently in single mutants or simultaneously in a double mutant, did not affect the acetyltransferase activity (Fig 5.3A). Interestingly, when additional mutations Ile457 to Lys and Arg455 to Thr were also included to create a tetra mutant, acetyltransferase activity were significantly affected (Fig 5.3A). However, these experiments do not clarify whether the conformation of acetyl-CoA is altered from U to L in the tetra mutant. $GlmU_{Ec}$ and $GlmU_{Mtb}$ exhibit a large difference in their basal activities, with $GlmU_{Ec}$ being 6–8 fold more efficient compared with its $GlmU_{Mtb}$ counterpart. This study raises a possibility that the observed difference in activity may be associated with the distinct U/L conformations of acetyl-CoA. However, further investigations are required to evaluate the same.

Besides these differences, differential regulation operates in $GlmU_{Mtb}$. In an earlier report [99], we showed that $PknB_{Mtb}$ phosphorylates a threonine residue in the C-terminal domain of $GlmU_{Mtb}$, which in turn down-regulates the acetyltransferase activity. Here, with the help of mass spectrometry, we identified Thr156 and Thr418 to be the target sites on $GlmU_{Mtb}$. Peptide mapping analysis and peptide spectrum matches from multiple LC-MS runs suggested Thr418 to be the most abundant phosphorylation site (Fig 5.9A & B). An analysis of the structure of $GlmU_{Mtb}$ revealed Thr156 to be present in a surface- exposed loop and away from the uridyltransferase active site (Fig 5.10C). This is in line with the observation that the

uridyltransferase activity is unaffected upon $PknB_{Mtb}$-mediated phosphorylation. However, Thr418 is important in providing stability to the left-handed helix: the T418A mutant, whose acetyltransferase activity is completely abolished, reflects this importance (Fig 5.9 B & C). Based on the structure of $GlmU_{Mtb}$[AcCoA], it is possible to explain the effect of phosphorylation at Thr418 on the acetyltransferase activity. It is evident that the introduction of a highly charged and bulky phosphate group on Thr418 would destabilize the hydrophobic region immediately surrounding it (Fig 5.9C). A T418E mutant generated to mimic the phosphorylated threonine corroborates this as it shows a complete abolishment of acetyltransferase activity (Fig 5.9B). Thr418 lies in an important region that is directly involved in making polar contacts with the backbone oxygen of acetyl-CoA via the backbone amine group of Gly415. By affecting the precise positioning of the acetyl group, phosphorylation appears to regulate acetyl transfer.

Another regulation of the acetyltransferase activity is due to the unique C-terminal extension in $GlmU_{Mtb}$. It contributes a short helix, which presents an important residue Trp460 for acetyl-CoA binding (Fig 5.5A). Crystal structure analysis and biochemical studies reiterate its importance. Zhang *et al. [219]*, by modelling acetyl-CoA into the apo structure of $GlmU_{Mtb}$, suggested an interaction of Trp-460 and the substrate. Crystal structures of $GlmU_{Hi}$ (from *Haemophilus influenzae*) bound with acetyltransferase inhibitors were reported recently [170]. These depict an important contribution by the equivalent Trp449 in inhibitor binding. Interestingly, drug resistant strains of *H. influenza* carry a mutation at Trp449, which results in the loss of this stacking interaction with the inhibitors.

Uridyltransferase activity also holds vital role in $GlmU_{Mtb}$ catalyzed reaction. Mutational studies of the uridyltransferase active site residues suggest a role for R19, K26, D114 and N239 in stabilizing Mg^{+2} ions and UDP-GlcNAc (Fig. 11). Mg^{+2} is required for the uridyltransferase activity, in agreement with this we found that the uridyltransferase activity of $GlmU_{Mtb}$ follows Michaelis-Menten kinetic pattern with increasing concentration of Mg^{+2}, while the activity of acetyltransferase reaction seems to be independent of Mg^{+2} ion concentration (Fig 5.10 E). Biophysical experiments' results (DSF and ITC) indicate that both of the sugar substrates (GlcN-1-P and GlcNAc-1-P) do not have good affinity for $GlmU_{Mtb}$. UTP has best affinity

for $GlmU_{Mtb}$ as compared with all the other substrates (Fig 5.11 & 5.12, Table 5.3 & 4). Also binding of one substrate in one domain does not impact the affinity for the other substrates in the other domain. Besides the substrates, $GlmU_{Mtb}$ seems to have affinity for the final product UDP-GlcNAc suggesting possible feedback inhibition of the uridyltransferase activity, a likely additional mode of regulation of $GlmU_{Mtb}$ activity (Fig 5.12, Table 5.3).

Overall, $GlmU_{Mtb}$ forms an ideal drug target to develop antitubercular drugs. The synthesis of UDP-GlcNAc takes place via a different route in eukaryotes than that in prokaryotes. In eukaryotes, acetyl transfer occurs on GlcN-6-P instead of GlcN-1-P. Also, the acetyltransferase and uridyltransferase reactions are catalyzed by two different enzymes, which show little homology to $GlmU_{Mtb}$ [195, 222, 223]. Identifying structural differences is necessary for the design of selective inhibitors against $GlmU_{Mtb}$. The U conformation of acetyl-CoA found in $GlmU_{Mtb}$ and the active site residues that make this possible can be a target site. Besides, we also identify that a small, one-and-a-half-turn helix in the C-terminal extension, a feature unique to $GlmU_{Mtb}$, and a conserved tryptophan (Trp460) are important contributors to the acetyl transfer reaction. Altering these interactions or the conformation of the short helix could be a viable strategy. Moreover characterization of uridyltransferase active site and the presence of feedback inhibition provide alternative scheme to develop next generation of anti-TB inhibitors specific to $GlmU_{Mtb}$. Perhaps, all of these are suggestive that targeting the uridyl and acetyltransferase domains to inhibit the action of $GlmU_{Mtb}$ may be a reasonable strategy.

5.4 Conclusion

Important residues (H374A, N397A and S416A) were mutated and checked for their biochemical activities and kinetics using malachite green assay. Both H374 and N397 were found to play central role in acetyltransferase reaction. Additionally, the conformation of bound acetyl-CoA in $GlmU_{Mtb}$ displayed unique 'U' shaped pattern in compared with the 'L' shaped conformation in $GlmU_{E.coli}$. The importance of U shaped conformation was confirmed by generating mutations at the interacting residues R439T, A451R and their double mutant (R439T+A451R) or tetra mutant (R439T+A451R+I457K+R455T). Further, we found that a short helix present at the C-terminal extension provides a key tryptophan, which appears to be critical for

acetyl-CoA binding and acetyltransferase activity as well. This was validated by generating different truncation mutants (Δ15, Δ25, Δ30 and Δ37) and W460A point mutant or by chimeric $GlmU_{Mtb}$ proteins consisting of C-terminal tail of $GlmU_{E.coli}$ or vice-versa. With the help mass spectrometry, we identified T418 and T156 to be the major and minor PknB target sites on $GlmU_{Mtb}$. We have generated phohoablative (T418A) and phosphomimatic (T418E) and T418S mutant, which retain the hydroxyl group, and deciphered how T418 phosphorylation down regulates the acetyltransferase activity. Characterization of uridyltransferase active site was carried out by mutating important residues (based on the crystal structures) like R19A, K26A, D114A/E and N239A, which play a role in stabilizing the Mg^{+2} ion and the substrates, decreased the uridyltransferase activity. Thus characterization of both active sites provides a base towards developing new sets of inhibitors targeting $GlmU_{Mtb}$.

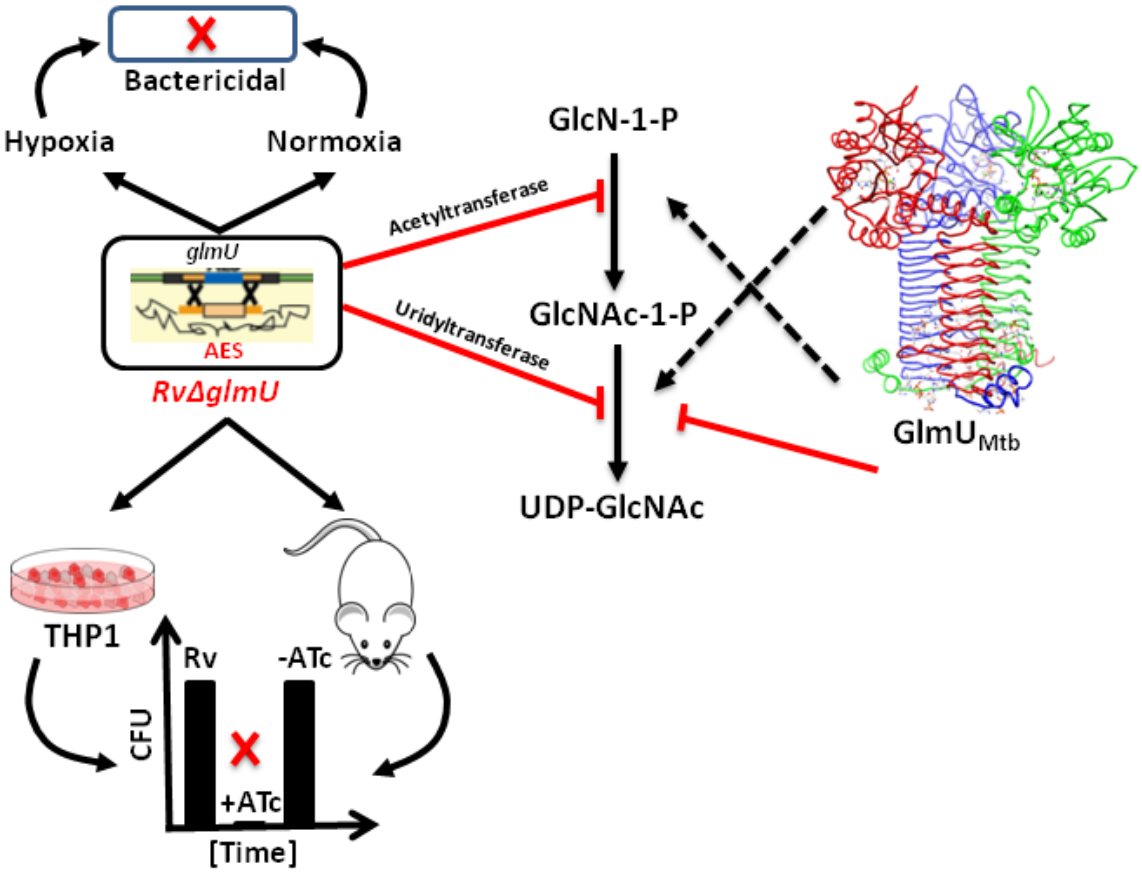

Chapter 6.

Bio-pathological significance of $GlmU_{Mtb}$

Chapter 6.

Dissecting the role of $GlmU_{Mtb}$ in arbitrating the survival of the pathogen.

6.1 Introduction

The cell wall, which contains a number of virulence determinants, is the first line of defence for survival of the pathogen in the hostile host environment [42]. The mycobacterial cell envelope includes three layers of cell membrane and a cell wall made up of peptidoglycan, mycolic acid, arabinogalactan and lipoarabinomannan (LAM) [186-188]. Mostly existing first line and second line drugs used to treat TB such as isoniazid, ethambutol, ethionamide and cycloserine, act on enzymes engaged in the synthesis of different cell wall components[38]. The current high mortality rates of infected individuals as well as increasing incidence of multidrug-resistant (MDR) and extensively drug-resistant (XDR) tuberculosis (TB) among patients underscore the importance of finding new targets for therapeutic intervention.

$GlmU_{Mtb}$ is a bi-functional enzyme, with acetyltransferase and uridyltransferase activities catalyzed by the C- and N- terminal domains respectively (Fig 2.4)[175, 189]. The carboxy-terminal domain of $GlmU_{Mtb}$ transfers the acetyl moiety from acetyl CoA onto glucosamine-1-phosphate to generate N-acetylglucosamine-1-phosphate (GlcNAc-1-P). The N-terminal uridyltransferase domain of $GlmU_{Mtb}$ then catalyzes the transfer of UMP (from UTP) to GlcNAc-1-P to form UDP-GlcNAc (Fig 2.4)[189]. The UDP-GlcNAc thus produced is among the central metabolites that is required for the synthesis of peptidoglycan, lipid A, arabinogalactan, Rha-GlcNAc linkers, poly $(\text{-GlcNAc-})_n$, mycothiol (required for maintaining redox homeostasis), and N- or O- GlcNAcylation[88, 155, 190-194]. The crystal structure of *M.tuberculosis* GlmU ($GlmU_{Mtb}$) displays two-domain architecture with a N-terminal α/β- like fold and a C-terminal left-handed parallel-β-helix structure [4, 224]. Unlike its orthologs, $GlmU_{Mtb}$ has a long carboxy-terminal tail which displays little secondary structure [3]. Results from transposon

mutagenesis experiments have indicated *glmU$_{Mtb}$* to be an essential gene, supported by the fact that *M. smegmatis* is unable to grow in the absence of *glmU$_{smeg}$* [115, 177, 225]. However, no studies have addressed the question of whether both the activities of GlmU$_{Mtb}$ are independently essential for the growth or survival of the bacterium.

While the enzymes required for the synthesis of UDP-GlcNAc are well conserved among prokaryotes, they are very different from those found in eukaryotes, making GlmU$_{Mtb}$ an attractive putative drug target [196, 226]. Furthermore, the importance of GlmU$_{Mtb}$ for growth under hypoxic conditions and in an *in vivo* infection model is yet to be investigated. In the present study we have generated a conditional gene replacement mutant of *glmU$_{Mtb}$* and used this mutant to investigate any role GlmU$_{Mtb}$ may play in modulating the growth of the bacterium *in vitro*, *ex vivo* and *in vivo*. The data presented here demonstrate that GlmU$_{Mtb}$ is a viable and promising target for therapeutic intervention against tuberculosis.

6.2 Results

6.2.1 GlmU$_{Mtb}$ depletion perturbs cell wall structure and affects the bacterial survival in normoxia.

As the tetracycline-inducible system is an effective means to regulate gene expression [201], we introduced the integration-proficient pST-KirT-*glmU* construct (wherein *glmU$_{Mtb}$* gene was cloned under a promoter that shuts down upon ATc addition) into *M.tb. H37Rv* (*Rv*) and *M. smegmatis* (*MS*) (Fig 6.1A, 6.2A & 6.3A). Whereas the expression of GlmU$_{Mtb}$ from its native locus remained unaltered, the expression of FLAG-GlmU$_{Mtb}$ in *Rv::glmU* strain was drastically compromised in the presence of ATc (Western blot inset, Fig 6.2A). These merodiploid strains were transduced with temperature sensitive phage, and the fidelity of homologous recombination at the native locus was confirmed by amplification across the replacement junctions using appropriate primers (Fig 6.2B & 6.3B). A comparison of GlmU$_{Mtb}$ expression in the presence and absence of ATc revealed that the protein was not detectable by western blot analysis after 6 days of growth in the presence of ATc (Fig 6.2E). In *M. smegmatis*, GlmU starts depleting after 6 h of ATc addition (Fig 6.3D). While the growth of *Rv*Δ*glmU* or *MS*Δ*glmU* in the absence of ATc was similar to *Rv or MS,* in the presence of ATc the growth was drastically compromised (Fig 6.2C & 6.3E). A comparative analysis of growth by spotting of serially diluted cultures of *Rv* and *Rv*Δ*glmU* or radial striking (for *MS* and *MS*Δ*glmU*) grown in the

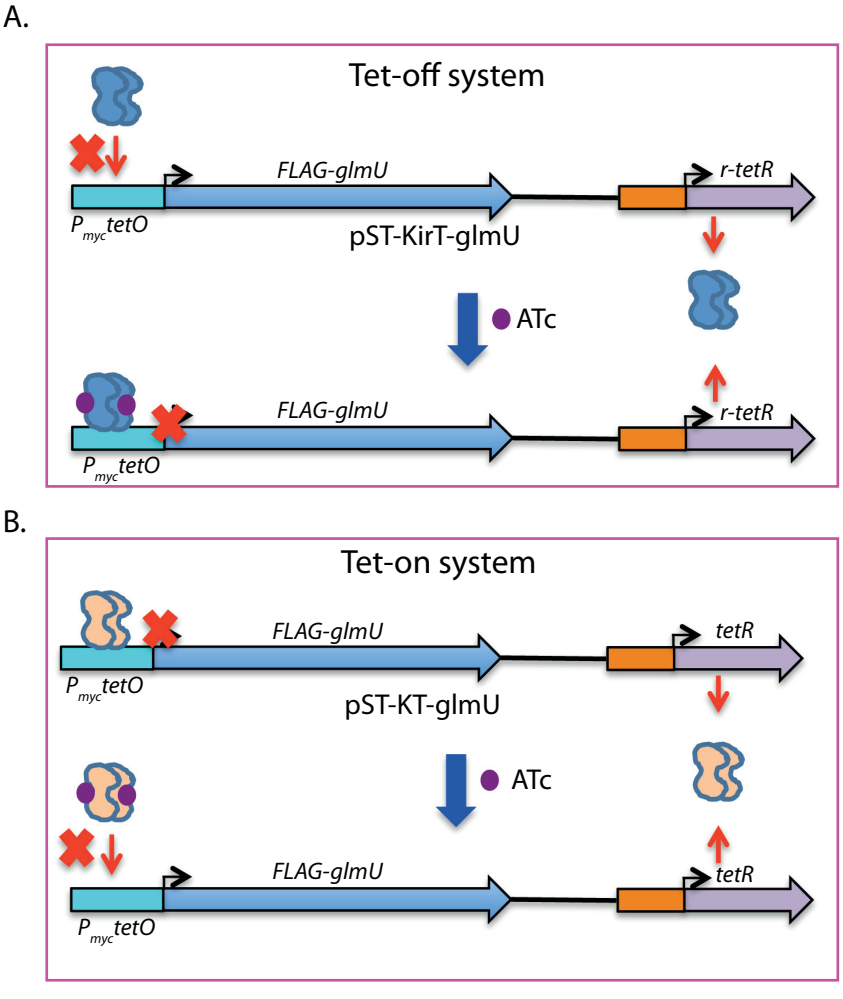

Figure 6.1. Tet Off and Tet On schematic diagram: (A) pST-KirT-*glmU* vector (integrated at *attP* site) showing repressor, operator and FLAG-*glmU* cloned in it. Association of ATc with repressor stimulate it's binding to operator sequence, thus stops transcription. **(B)** pST-KT-*glmU* vector (non-integrated) showing repressor, operator and FLAG-*glmU* cloned in it. Association of ATc with repressor hinder it's binding to operator sequence, thus stops transcription.

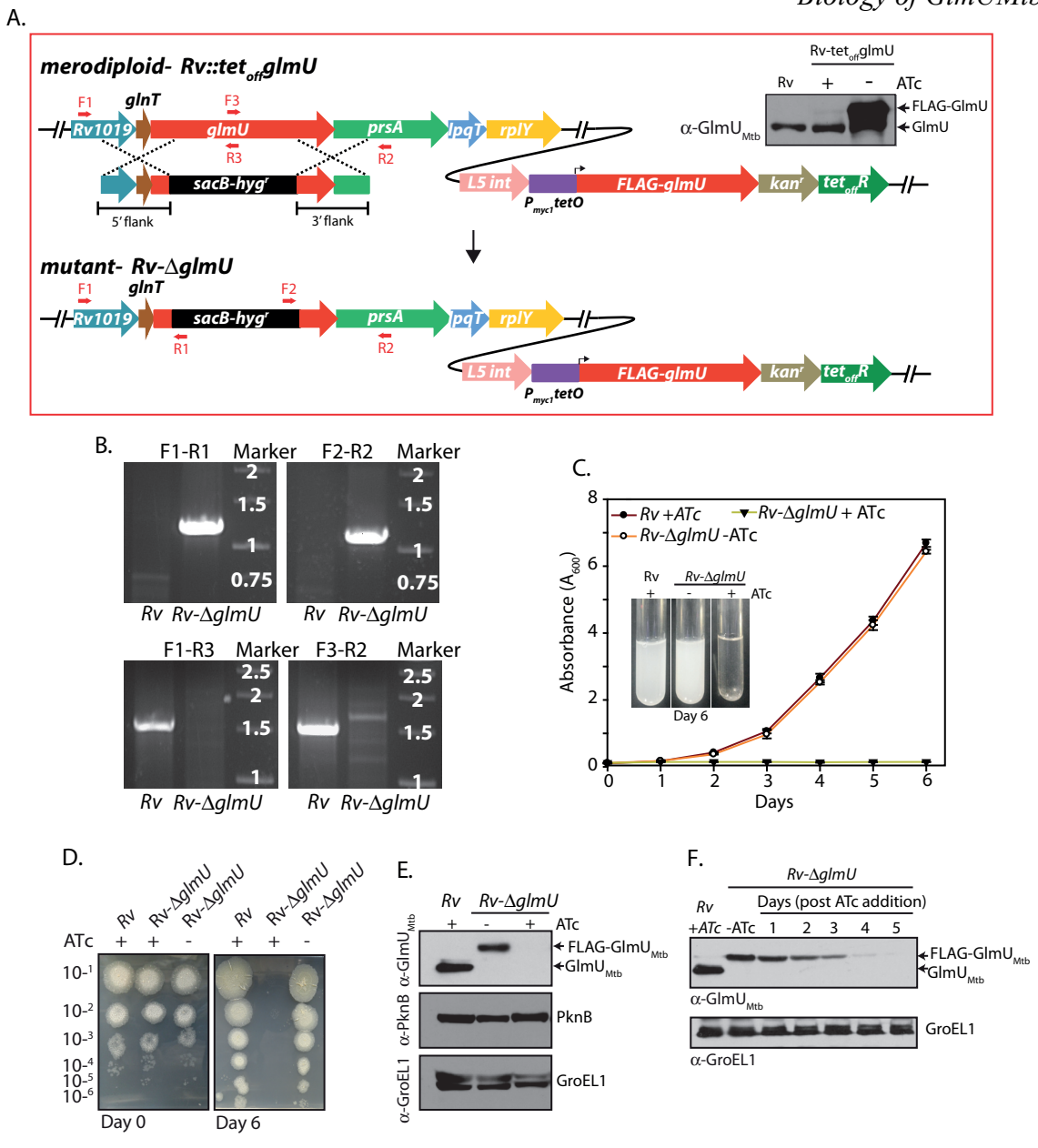

Figure 6.2. GlmU$_{Mtb}$ is essential for *Mtb* survival: (A) Schematic diagram representing the genomic location of *glmU$_{Mtb}$* (*Rv1018c*) and homologous recombination between flanking sequence in the phagemid and the genomic locus. Primers used for the PCR amplification are depicted. Upper right panel shows the immunoblot. WCLs from *Rv* or *Rv::glmU* grown in the presence or absence of ATc were resolved and probed with anti-GlmU antibodies. Bands corresponding to the endogenous GlmU and ectopic FLAG-GlmU are indicated. **(B)** Agarose gel showing the PCR amplification of the *Rv* & putative *RvΔglmU* mutant using specific primers. Primers F1 and R2 are beyond the flanks, R1 and F2 belongs to resolvase sites in *sacB/hygR* cassette and F3 and R3 binds to the native *glmU$_{Mtb}$*. Amplification with F1-R1 or F2-R2 primers results in 1.23 kb or 1.17 kb size products with *RvΔglmU* strain but none with the Rv. Whereas PCRs with F1-R3 or F3-R2 primers amplifies 1.5 kb band with the *Rv* and none with the *RvΔglmU* mutant. **(C)** *Rv* and *RvΔglmU* cultures grown to an A_{600} of 0.8 were used to seed fresh cultures at an initial A_{600} of 0.1 in the presence or absence of ATc as indicated and the day wise growth was monitored for six days. Inset shows the growth in the culture tubes after six days, mean, s.e.m, n=3. **(D)** Day 0 and Day 6 cultures grown in the presence or absence of ATc were serially diluted and spotted on 7H11 agar plates. **(E)** Whole cell lysates (WCL) were prepared from the large scale cultures of *Rv* and *RvΔglmU* grown in the absence and presence of ATc for five days. 20 µg of WCLs were resolved and probed with anti-GlmU$_{Mtb}$, anti-PknB and anti-GroEL1 antibodies. Band corresponding to endogenous GlmU$_{Mtb}$ and FLAG-GlmU$_{Mtb}$ are indicated. **(F)** Large scale cultures were inoculated at A600 of 0.1 in the presence or absence of ATc and the WCLs were prepared on different days post ATc addition (as indicated). WCLs were resolved and probed with anti-GlmU$_{Mtb}$ and anti-GroEL1 antibodies.

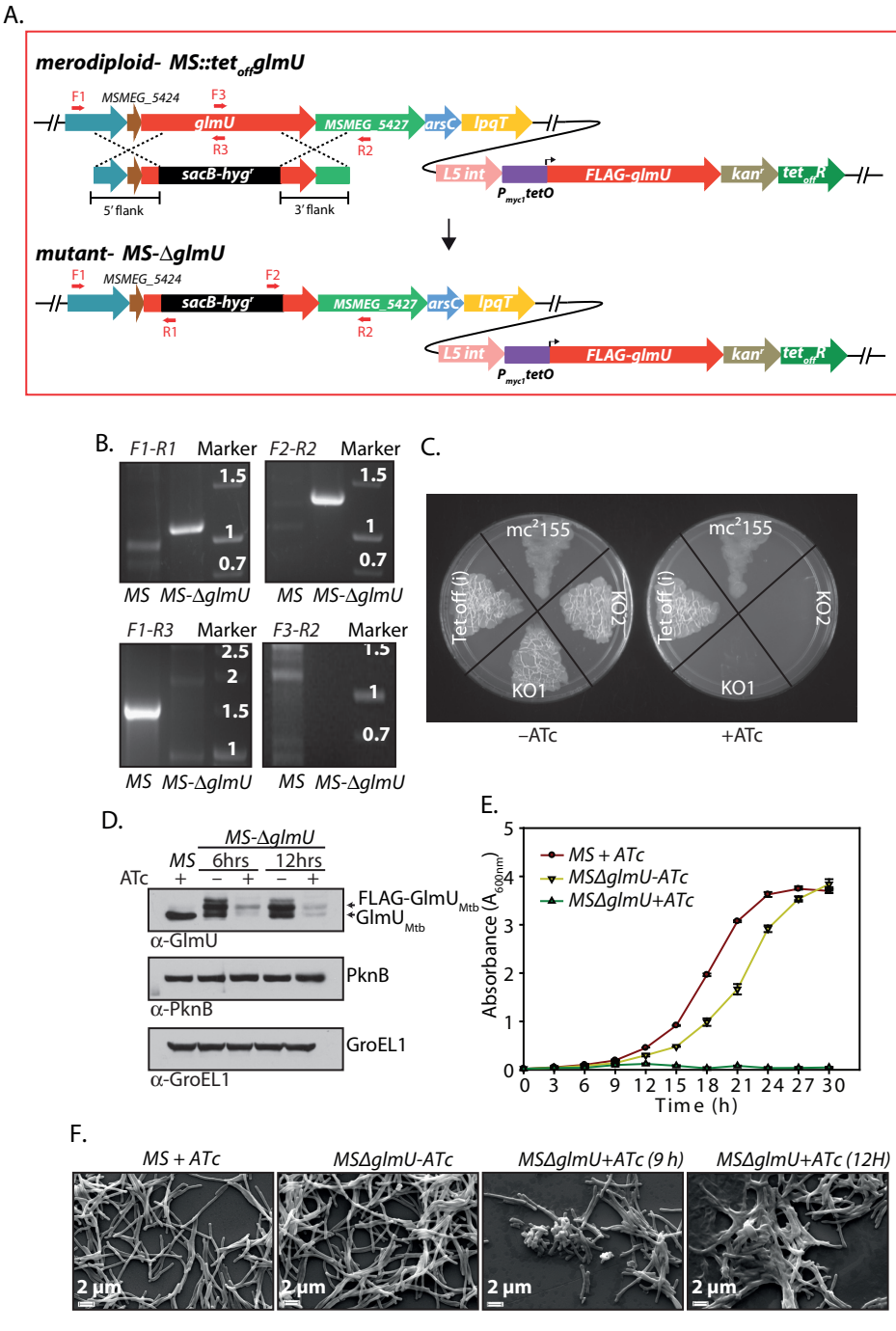

Figure 6.3. GlmU$_{MS}$ is essential for *M. smegmatis* survival: (A) Schematic diagram representing the genomic location of *glmU$_{MS}$* (*MSMEG_5426*) and homologous recombination between flanking sequence in the phagemid and the genomic locus. **(B)** Agarose gel showing the PCR amplification of the *MS* & putative *MSΔglmU* mutant using specific primers. Primers F1 and R2 are beyond the flanks, R1 and F2 belong to resolvase sites in *sacB/hygR* cassette and F3 and R3 bind to the native *glmU$_{MS}$*. Amplification with F1-R1 or F2-R2 primers results in 1.08 kb or 1.29 kb size products with *MSΔglmU* strain but none with the *MS*. Whereas PCRs with F1-R3 or F3-R2 primers amplifies 1.6 kb or 1.26 kb band with the *MS* and none with the *MSΔglmU* mutant. **(C)** *MS, MS::glmU* and *MSΔglmU* cultures grown to an A_{600} of 0.8 and streaked on 7H11 agar plates with or without ATc **(D)** Western blott showing endogenous GlmU and FLAG-GlmU at 6 h & 12 h post ATc addition. For loading control PknB and GroEL1 were probed. **(E)** Growth curve analysis of *MS* and *MSΔglmU* in presence or absence of ATc up to 30 h, mean, s.e.m, n=3. **(F)** SEM images of *MS* and *MSΔglmU* at 6 h & 12 h of GlmU$_{MS}$ depletion. Scale bars showing 2 µm.

presence versus absence of ATc showed that $GlmU_{Mtb}$ depletion by addition of ATc led to complete inhibition of growth, with no growth detected after 6 days (for *M.tb.*) or 30 h for *MS* (Fig 6.2D & 6.3E). Interestingly, analysis of $GlmU_{Mtb}$ expression every 24 hours post-ATc addition uncovered significant reduction in $GlmU_{Mtb}$ expression by the third day itself (Fig 6.2F). These results indicate that $GlmU_{Mtb}$ is required for the bacterial survival. To determine the impact of $GlmU_{Mtb}$ depletion on cellular morphology we carried out SEM and TEM imaging analysis of *Rv* or *MS and Rv*Δ*glmU* or *MS*Δ*glmU* cells grown for three days (for *Rv*)or 30 h (for *MS*) in the absence or presence of ATc. SEM analysis revealed severe morphological perturbations in the absence of $GlmU_{Mtb}$, with the bacilli showing wrinkled surface and fused cells (Fig 6.4A and 6.3F). TEM analysis showed that whereas in *Rv* and *Rv*Δ*glmU* cell wall structure and thickness are comparable, there was a marked decrease in cell wall thickness in *Rv*Δ*glmU* cells where $GlmU_{Mtb}$ was not expressed (cells grown in the presence of ATc; Fig 6.4B & 6.4C).

6.2.2 Impact of $GlmU_{Mtb}$ depletion on dormant bacteria.

Subjecting *M.tb.* cultures *in vitro* to hypoxic stress (gradual decrease of oxygen) results in reprogramming of metabolic pathways and upregulation of stress response genes, and is considered to be an *in vitro* model for the dormancy [204, 227]. We used the Wayne model to investigate the consequence of $GlmU_{Mtb}$ depletion on the dormant bacteria under hypoxic conditions [204]. Accordingly, hypoxia was established and maintained for 42 days with depletion of $GlmU_{Mtb}$ or addition of INH for either 22 days, or for 2 days (Fig 6.5A, line diagram). In agreement with previous reports, we observed that bacteria were tolerant to INH under hypoxic conditions [228] (Fig 6.5B), with a thicker cell wall being observed under hypoxic conditions compared with the normoxic cultures (Fig 6.5C & 6.5D). Depletion of $GlmU_{Mtb}$ for 22 days resulted in complete clearance of growth, which was also reflected in severe morphological perturbations and drastic reduction in cell wall thickness (Fig 6.5C & 6.5D). Significantly, $GlmU_{Mtb}$ depletion for as less as 2 days decreased cell viability by three orders of magnitude (Fig 6.5A) and decrease in cell wall thickness (~18%; Fig 6.5C & 6.5D). Taken together, the data suggests that the absence of $GlmU_{Mtb}$ in hypoxic condition leads to aberrant cell wall thickness and morphology, eventually leading to the death of the cell.

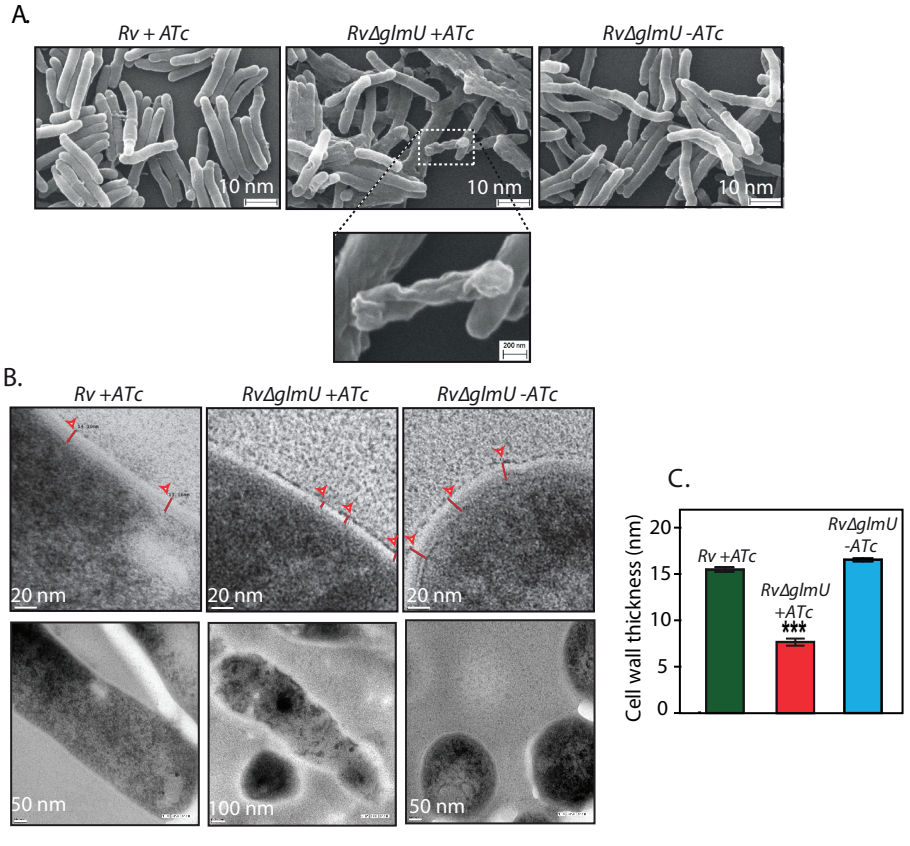

Figure 6.4. **$GlmU_{Mtb}$ depletion perturbs morphology and cell wall structure: (A)** Scanning electron microscopy of *Rv* and *RvΔglmU* grown for 72 h with or without ATc as indicated. Scale bars in upper panel were 10 nm and for the inset was 200 nm. **(B)** Transmission electron micrographs results at 50,000X of *Rv* and *RvΔglmU* cultures grown with or without ATc. Red lines depict the cell wall thickness. Scale bar: 20 to 100 nm. **(C)** Cell wall thickness was measured in nm for 15 to 22 cells for each sample. ***p<0.0001, two tailed non parametric t-test, mean, s.e.m.

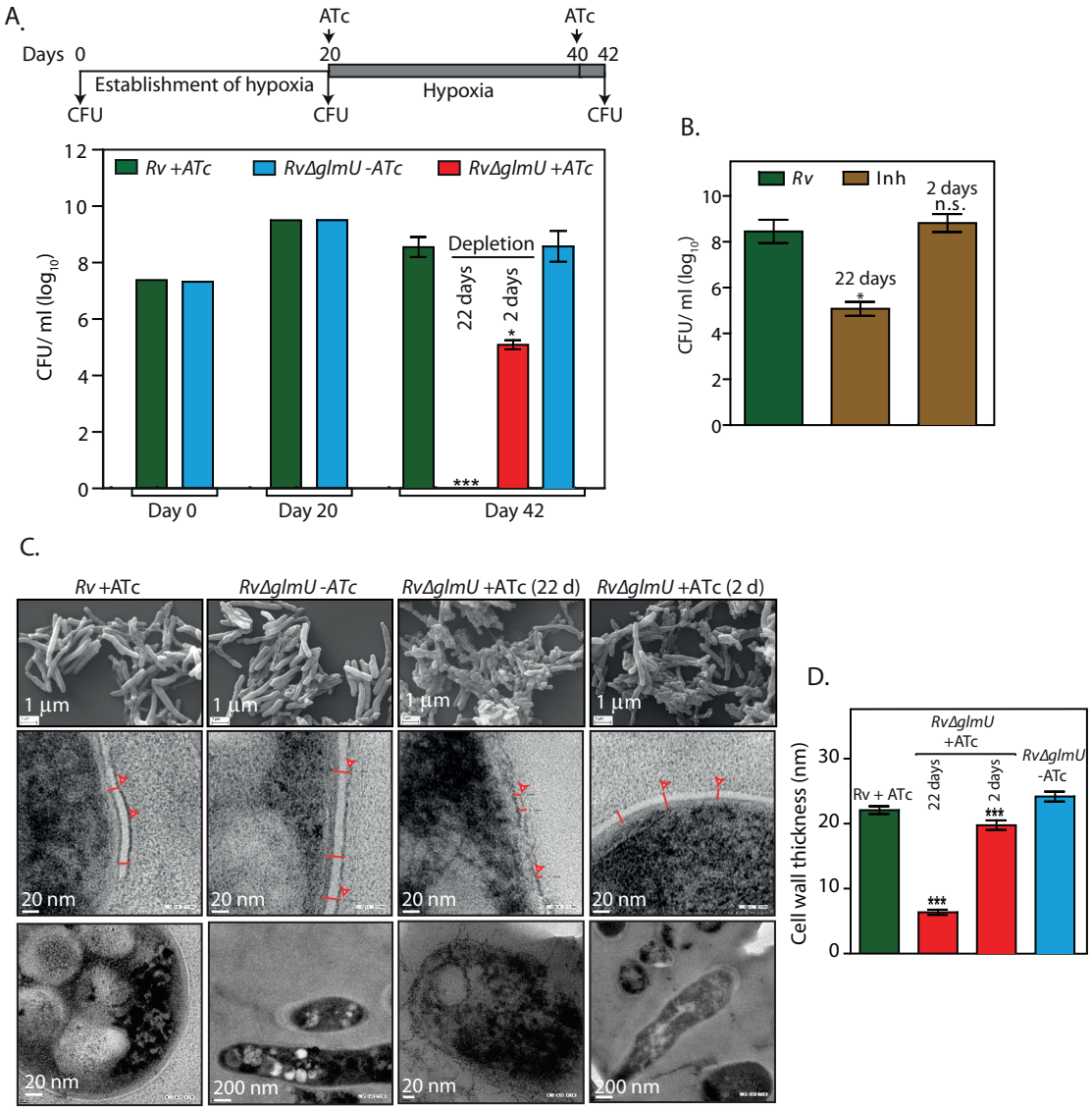

Figure. 6.5 $GlmU_{Mtb}$ is essential during dormancy: (A) *Rv* and *RvΔglmU* cultures were seeded at an initial A_{600} of 0.1 in 1.5 HPLC tubes or in 500 ml flasks containing penetrable caps. Establishment of hypoxia was monitored with the help of methylene blue color change (blue to colorless). ATc was added to *Rv* on 20th day and to *RvΔglmU* for 22 and 40th day. CFUs were enumerated on day 0, day 20 and day 42, mean, s.e.m, n=3. **(B)** CFU results of INH treatment on hypoxic *Rv* or *RvΔglmU* cultures. INH (50 ng/ml) was added to the hypoxic *Rv* cultures on 20th and 40th day. CFUs were enumerated on day 42. *p<0.05 or NS: non-significant, two tailed non parametric t-test, mean, s.e.m., n=3. **(C)** Large scale hypoxic cultures were pelleted down on day 42 and processed for scanning electron microscopy (upper panel) or transmission electron microscopy (lower panel) imaging. (SEM: scale bars: 1 µm; TEM scale bar: 20 nm). Cell wall thickness is indicated by red lines. **(D)** Cell wall thickness was measured in nm for 20 to 54 cells from the TEM images of different samples. ***p< 0.0001 and 0.0005, two tailed non parametric t-test, mean, s.e.m.

6.2.3 Acetyl and uridyltransferase activities of GlmU are independently essential.

Biochemical investigations have shown that the N-terminal fragment (1-352 amino acids) and C-terminal fragment (150-495 amino acids) of $GlmU_{Mtb}$ can independently undertake uridyltransferase and acetyltransferase activities respectively (Fig 6.6A- D) [3, 224]. The active site residues that are necessary for these activities have also been identified (Fig 6.5A & D) [3]. To investigate if both activities are essential to cell survival, we have generated previously reported truncation mutants GlmU-N and GlmU-C [99]. We also generated $GlmU_{K26A}$ and $GlmU_{H374A,}$ the uridyltransferase and acetyltransferase active site mutants, and $GlmU_{DM}$ wherein both the active site residues were concomitantly mutated. $GlmU_{Mtb}$ wild type and mutant proteins were purified (Fig 6.6C) and their uridyltransferase and acetyltransferase activities were assayed. While GlmU-C and $GlmU_{K26A}$ mutants showed acetyltransferase activity, as expected they did not show any uridyltransfease activity (Fig 6.6D). On the other hand GlmU-N and GlmUH374A had uridyltransferase activity but not the acetyltransferase activity (Fig 6.6D). As expected the double mutant did not have either uridyl or acetyltransferase activity (Fig 6.6D). Next, complementation assays using one or other truncations / active site mutants were carried out. The FLAG-$GlmU_{Mtb}$ and the complemented untagged wt-$GlmU_{Mtb}$ proteins were found to be expressed at similar levels (Fig 6.6E). The episomally expressed wt-$GlmU_{Mtb}$ could rescue the *Rv*Δ*glmU* phenotype in the presence of ATc (Fig 6.6F). Contrastingly, while the various $GlmU_{Mtb}$ mutant proteins were expressed at levels comparable to that of FLAG-$GlmU_{Mtb}$ (Fig 6.6E), none of them rescued the growth defects of the *Rv*Δ*glmU* strain in the presence of ATc (Fig 6.6F). These results indicate that both uridyltransferase and acetyltransferase activities of $GlmU_{Mtb}$ are essential for pathogen survival and imply that the only source of the metabolites GlcNAc-1-P and UDP-GlcNAc is through the $GlmU_{Mtb}$ mediated synthesis pathway.

6.2.4 Role of different mutants of GlmU in bacterial survival.

Previously (Chapter 5), we have identified residues that are critical for uridyl and acetyltransferase activities. We have also determined the criticality of carboxy terminal tail in modulating the acetyltransferase activity. Here, we sought to determine the impact of these mutants in complementing the *Rv*Δ*glmU* or *Ms*Δ*glmU*

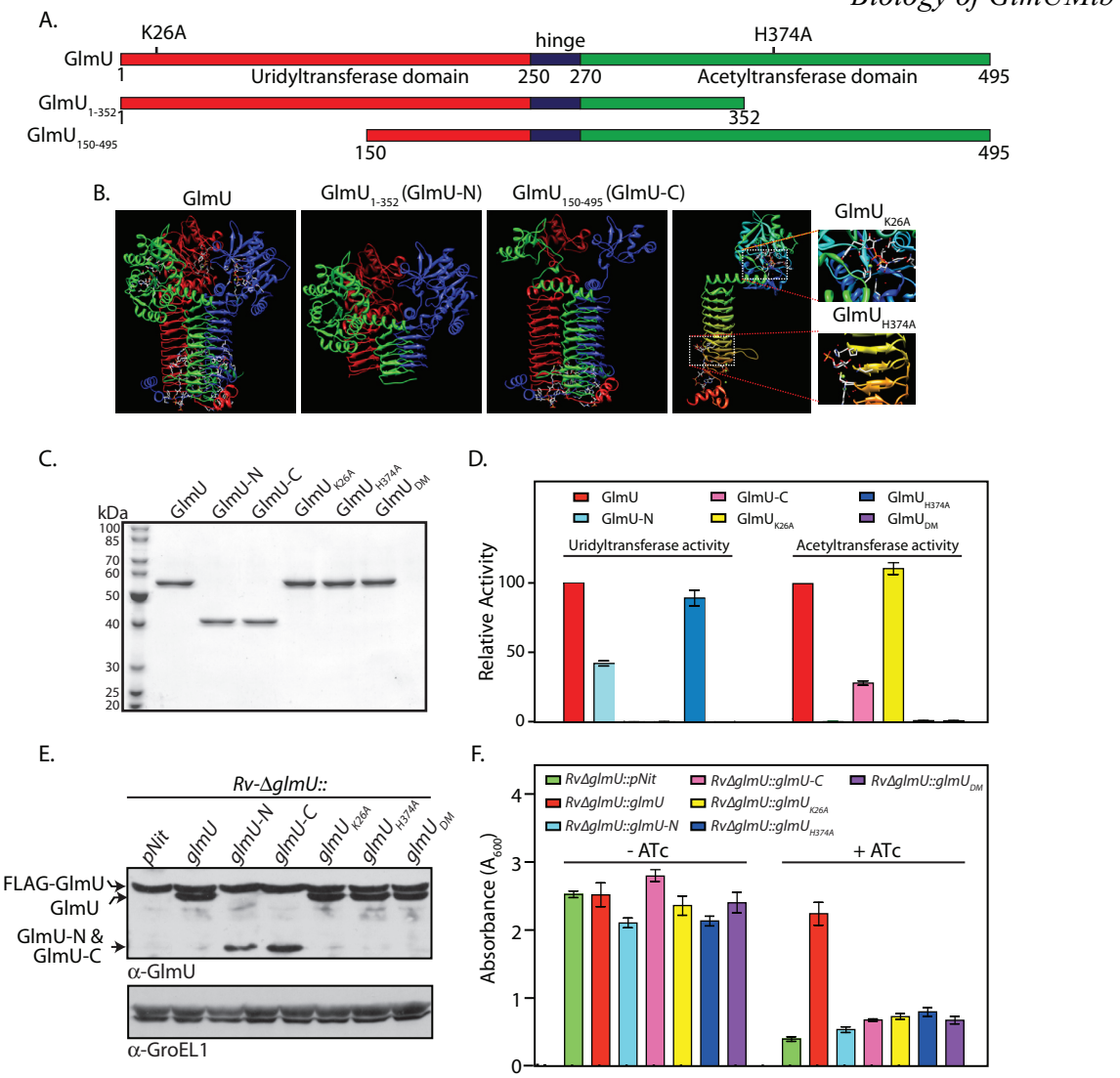

Figure 6.6. Acetyl and uridyltransferase activities are independently essential: (A) Schematic representation of $GlmU_{Mtb}$ depicting different domains, active site residues and the deletion mutants. **(B)** Cartoon of different domains and full length $GlmU_{Mtb}$. Right most pictures depicted the location of active site mutants at N- terminal and C- terminal domains. **(C)** $GlmU_{Mtb}$ and $GlmU_{Mtb}$-mutants were purified as described earlier and the 1 µg of the purified proteins were resolved on 10% SDS-PAGE and stained with coomassie. **(D)** Uridyltransferase (left panel) and acetyltransferase (right panel) activities were carried out as describe in Methods using 0.5 to 20 pmoles of wild type or mutant $GlmU_{Mtb}$ proteins. Activity was defined as µM product formed / min / pmole of enzyme. Relative activity of the mutants were calculated with respect to the activity of $GlmU_{Mtb}$, which was normalized to 100%. The experiment was repeated three times and the error bars indicate s.e.m. **(E)** Wild type and mutated $GlmU_{Mtb}$ genes were cloned into pNit vector without any N- or C- terminal tag. *pNit-glmU*$_{wt}$ or *pNit-glmU*$_{mutant}$ constructs were electroporated into *RvΔglmU*, and the WCLs prepared from *RvΔglmU* and *RvΔglmU::glmU*$_{mutant}$ cultures were resolved and probed with anti-GlmU and anti-GroEL1 antibodies. Bands corresponding to FLAG-$GlmU_{Mtb}$, complemented $GlmU_{wt/mutant}$ and the deletion fragments of $GlmU_{Mtb}$ are indicated. **(F)** *RvΔglmU* and *RvΔglmU::glmU*$_{mutant}$ cultures were seeded at an initial A_{600} of 0.1 and grown for five days in the absence or presence of ATc, mean, s.e.m, n=3.

mutants upon depletion of GlmU. Further we wanted to investigate the ability of GlmU orthologs from *E. coli, C. glutamicum* and *S. pneumonia* to complement the functionality of $GlmU_{Mtb}$ or $GlmU_{Ms}$. Towards this; GlmU deletion mutants, point mutants and orthologs were cloned into either into the pNIT vector (episomal) or pMAL1357 vector (integrating). The *Rv*Δ*glmU* mutant was electroporated with pMAL1357-$GlmU_{constructs}$, the *Ms*Δ*glmU* mutant was electroporated with pNIT-$GlmU_{constructs}$. Although we used integrating pMAL1357 constructs for the complementation, the results with the wild type and active site mutants (WT, K26A, H374A and DM) were similar to those observed in figure 6.6. While the wild type GlmU complemented efficiently, mutants and N and C-terminal truncations failed to complement the *Rv*Δ*glmU* or *Ms*Δ*glmU* mutants (Fig 6.7A & 6.8A). Next we sought to determine the impact of carboxy terminal deletions on their ability to complement GlmU functionality. With the exception of wild type GlmU and $GlmU_{\Delta 15}$, none of the other carboxy terminal deletion mutants or $GlmU_{W460A}$ could complement the functionality of GlmU in *Rv*Δ*glmU* or *Ms*Δ*glmU* mutants upon depletion (Fig 6.7B & 6.8B). We investigated the ability of GlmU orthologs from other organisms to complement its functionality in *Rv*Δ*glmU* or *Ms*Δ*glmU* mutants. In case of *Rv*Δ*glmU* mutant, expression of $GlmU_{MS}$ and $GlmU_{CG}$ resulted in partial rescue, however $GlmU_{SP}$ and $GlmU_{EC}$ failed to complement the phenotype (Fig 6.7C). On the other hand in case of *Ms*Δ*glmU* mutant, with the exception of $GlmU_{CG}$ mutant remaining orthologs effectively supported the growth (Fig 6.8C). Although these results are quite intriguing, we do not know the reasons for the differential ability of orthologs to complement *Rv*Δ*glmU* and *Ms*Δ*glmU* mutants. We would have to investigate these findings further by determining the expression levels of the orthologs and precisely quantify the differences in their ability to rescue the phenotype by performing CFU analysis. Finally, we analyzed the ability of GlmU phosphorylation site mutants (T418A, T418E and T418S) to complement the functionality. While both $GlmU_{T418A}$ and $GlmU_{T418E}$ failed to functionally rescue the glmU depletion phenotype, $GlmU_{T418S}$ seems to be able to rescue the growth partially (Fig 6.7D & 6.8D). The ability of T418S to partially rescue the phenotype supports our suggestion (in Chapter 5) that the hydroxyl group of T418 plays an important role in catalysis.

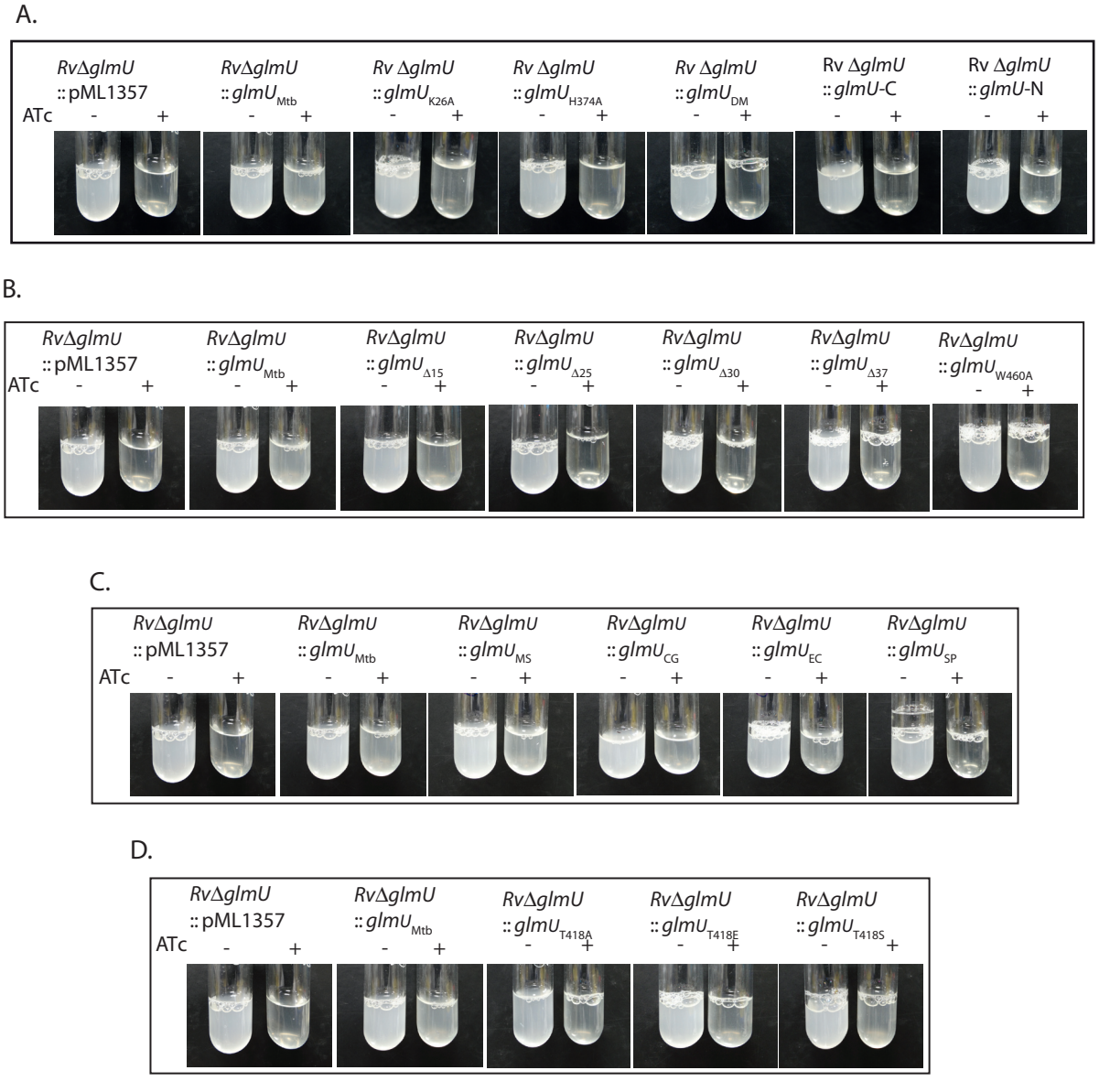

Figure 6.7. Complementation of $GlmU_{Mtb}$ mutants, truncations and orthologs: In all expreiments *glmU* mutant strains of *Rv* were complemented with constutively expressing promoter of pML1357 and checked for survival in cultures. **(A)** Active site mutants (K26A, H374A and their double mutant) and individual domains (N-terminal domail or C-terminal domain) **(B)** Truncations of $GlmU_{Mtb}$ lacking 15, 25, 30 or 37 amino acids from C-terminal. **(C)** Orthologs of $GlmU_{Mtb}$ from different bacteria. *MS: M. smegmatis, CG: C. glutamicum, EC: E. coli, SP: S. pneumoniae* **(D)** Phosphomutans of $GlmU_{Mtb}$: T418A, T418E, T418S.

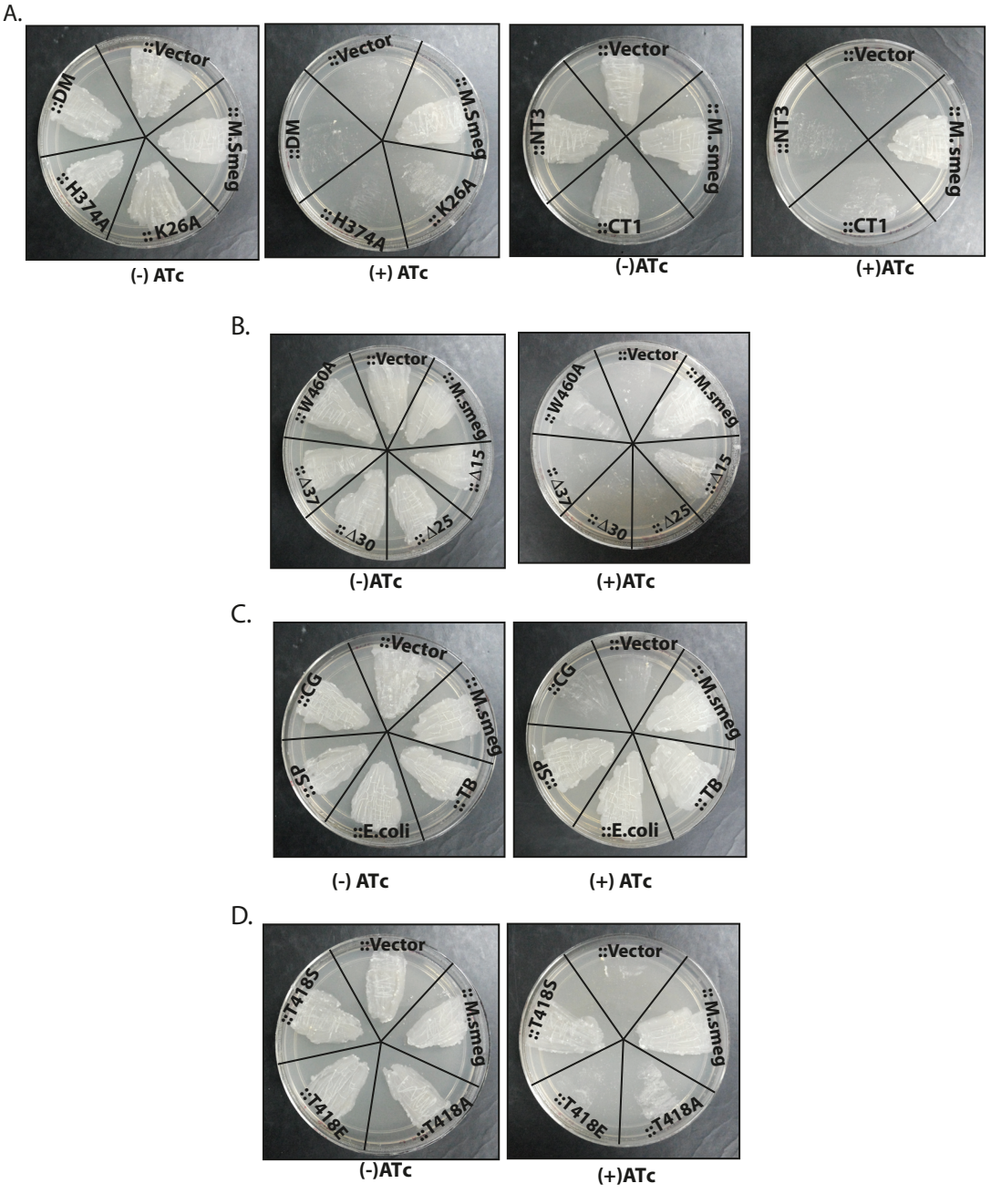

Figure 6.8. Complementation of $GlmU_{MS}$ mutants, truncations and orthologs: In all expreiments *glmU* mutant strains of *MS*were complemented with constutively expressing inducer of pNIT and checked for survival in cultures. **(A)** Active site mutants (K26A, H374A and their double mutant) and individual domains (N-terminal domail or C-terminal domain) **(B)** Truncations of $GlmU_{Mtb}$ lacking 15, 25, 30 or 37 amino acids from C-terminal. **(C)** Orthologs of $GlmU_{Mtb}$ from different bacteria. *MS: M. smegmatis, CG: C. glutamicum, EC: E. coli, SP: S. pneumoniae* **(D)** Phosphomutans of $GlmU_{Mtb}$: T418A, T418E, T418S.

6.2.5 Presence of $GlmU_{Mtb}$ is obligatory for the survival of M.tb. in the host.

M.tb. cells devoid of an intact cell wall have been found to be capable of surviving inside the host [229, 230]. Some pathogens have been reported to resort to cell wall "recycling" for the synthesis of UDP-GlcNAc, and others have been known to utilize GlcNAc from the host for this purpose [157, 197, 198, 231]. However, such mechanisms have not yet been reported in *M.tb*. To investigate these possibilities we examined the impact of $GlmU_{Mtb}$ depletion on survival of the pathogen in the host. Using an *ex vivo* THP-1 infection model we observed ~80% phagolysosome fusion in the absence of $GlmU_{Mtb}$ (Fig 6.9A & B; compare *Rv*Δ*glmU* with *Rv*Δ*glmU* +ATc). This was also reflected in the survival pattern of the pathogen upon depletion of $GlmU_{Mtb}$ (Fig 6.9C), with survival being strongly compromised in absence of $GlmU_{Mtb}$. The impact of $GlmU_{Mtb}$ depletion was evident as early as 24 h post-infection, with a dramatic drop in survival by 48 hours post-infection (Fig 6.9C). The consequences of $GlmU_{Mtb}$ depletion on survival of the pathogen *in vivo* were evaluated using guinea pig infection model. CFUs obtained 24 h after infection suggested efficient and equivalent implantation of both wild type and mutant bacilli in the lungs of guinea pigs (Fig 6.9D). Discrete bacilli were observed in the lungs of guinea pigs infected with *Rv* and *Rv*Δ*glmU* 28 days post-infection (Fig 6.9E). In contrast, the lungs of the guinea pigs infected with *Rv*Δ*glmU* in the presence of doxycycline were clear (Fig 6.8E). In addition splenomegaly was significantly-reduced upon depletion of $GlmU_{Mtb}$ (*Rv*Δ*glmU* + Dox; Fig 6.9F & G). Whereas the bacillary load in the lungs and spleen of guinea pigs infected with *Rv* and *Rv*Δ*glmU* were comparable, we did not detect any bacilli when the *Rv*Δ*glmU* infected guinea pigs were administered Dox (Fig 6.9D). In accordance with these observations, while the gross pathology of lungs infected with *Rv* and *Rv*Δ*glmU* displayed considerable granulomatous architecture, normal lung parenchyma was observed upon $GlmU_{Mtb}$

Table 6.1: Granuloma scores of the infected guinea pig lungs.

Group (guinea pigs)	Bacterial strains/ treatment	Organs	No. of granulomas with necrosis, Score : 5	Total granulomas score
4th week	*Rv* (+Dox)	Lungs	6	30
	*Rv*Δ*glmU* (-Dox)	Lungs	6	30
	*Rv*Δ*glmU* (+Dox)	Lungs	0	0

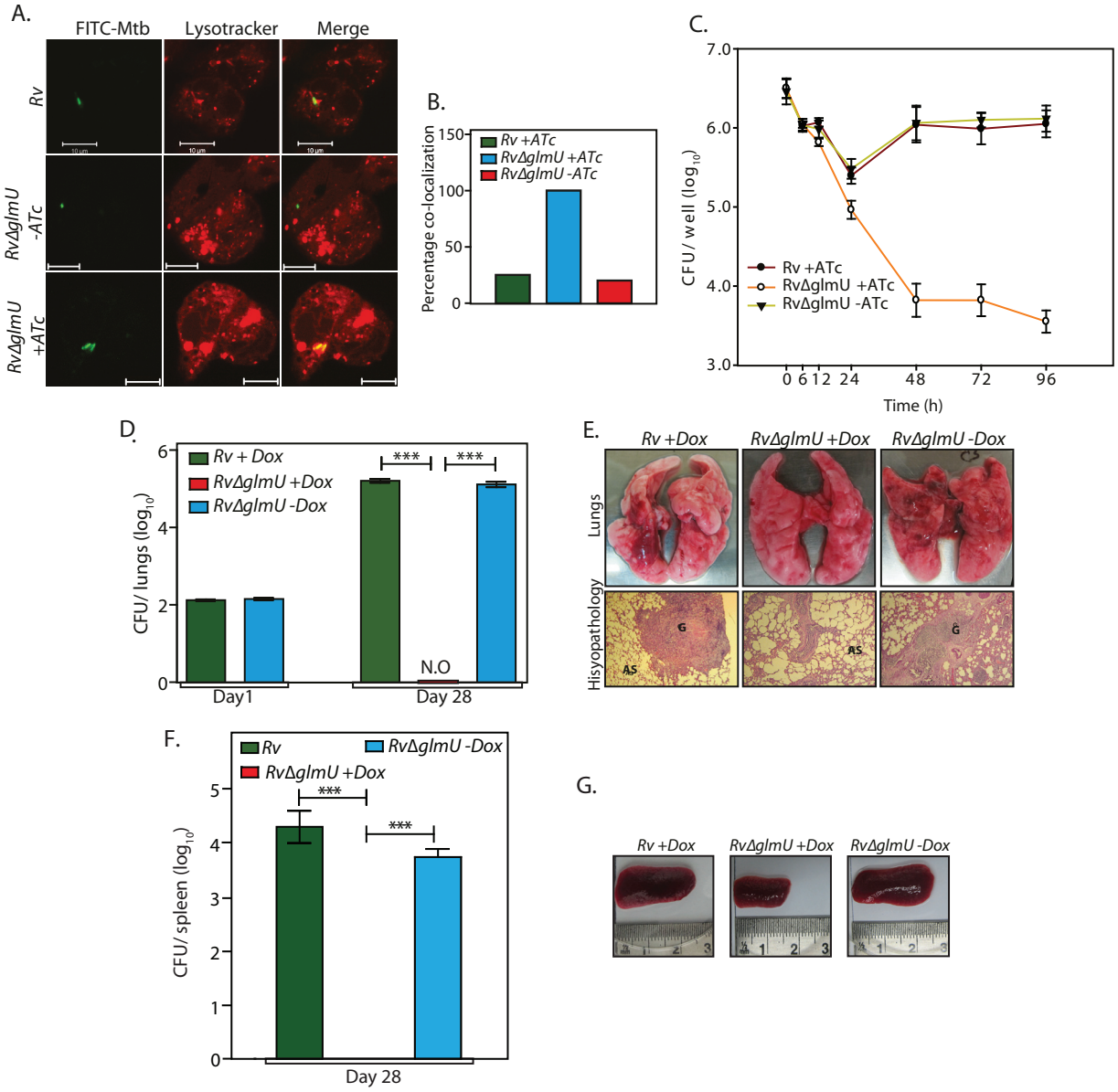

Figure 6.9. Presence of $GlmU_{Mtb}$ is obligatory for the survival of *Mtb* in the host: (A) Confocal microscopy images of THP1 cells infected with *Rv* and *RvΔglmU* in the presence or absence of ATc as indicated were taken 48 h post infection. Scale bars, 10 µm. **(B)** Quantification of percentage co-localization of bacterium and lysosomes in Fig 5A. n=10 to 15. **(C)** PMA differentiated THP1 cells were infected with *Rv* and *RvΔglmU* and either ATc (1.5 µg) or the vehicle were added at 0 h. CFUs were enumerated at different time points post infection, mean, s.e.m, n=3. **(D)** Guinea pigs were infected with 150-200 bacilli CFUs of *Rv* or *RvΔglmU* and Dox was provided in the water as indicated. Guinea pigs (n=2) were sacrificed on day 1 and homogenates from the lungs were plated in triplicates to determine the implantation. Guinea pigs (n=6) were sacrificed four weeks post infection and CFUs were determined in the lung homogenates and results were plotted with log10 /lung on the Y-axis and samples on the X-axis. At four weeks post infection mean CFUs for *Rv +Dox* or *RvΔglmU* +Dox and *RvΔglmU* –Dox were 5.2, 0 and 5.11 on $\log_{10}$ scale.***p<0.0001, two tailed non parametric t-test, mean, s.e.m., n=6. **(E)** Overall pathology (upper panel) and histopathology (lower panel, HE, 40X) of the infected guinea pig lungs four weeks post infection. Both *Rv* +Dox and *RvΔglmU* -Dox were having prominent granuloma and necrotic lesions in the central and epithelioid cells and lymphocytes around it. Guinea pigs infected with *RvΔglmU* +Dox were showing normal lung parenchyma with clear alveolar spaces. G = Granuloma, AS = Alveolar Space. **(F)** CFU data from guinea pig spleens. ***p<0.0001 or, two tailed non parametric t-test, mean, s.e.m., n=6. **(G)** Overall pathology of the infected spleens from the guinea pigs 4 weeks post infection.

depletion (Fig 6.9E, Table 6.1). These results suggest that the presence of $GlmU_{Mtb}$ is obligatory for mycobacteria to survive in the host.

6.2.6 Depletion of GlmU from infected lungs leads to clearance of pathogen.

It was apparent from the data presented above that the addition of ATc or Dox at the time of inoculation or at the time of infection does not allow mycobacterial cell growth or survival in the host. In the ideal candidate for therapeutic intervention, inhibiting the activity of depleting the enzyme at any stage of the infection should result in pathogen clearance. We assessed this parameter of $GlmU_{Mtb}$ by providing ATc at different stages of bacterial growth (early, log and stationary phases) and investigating its influence on cell survival in liquid cultures. Addition of ATc to *Rv*Δ*glmU* cultures on the 2nd, 4th or 6th day after inoculation significantly thwarted growth (Fig 6.10A). A similar analysis of bacterial growth by serial dilution of cultures followed by spotting on solid medium also revealed that viability was compromised by ~2 log fold 48 h after the addition of ATc, indicating that $GlmU_{Mtb}$ depletion negatively impacted cell survival regardless of which stage of cell growth it was depleted at (Fig 6.10C).

The influence of $GlmU_{Mtb}$ depletion on an established *ex vivo* infection was estimated by providing ATc 24 h post-infection in a THP-1 infection model. As expected the bacillary load in THP-1 cells infected with *Rv* and *Rv*Δ*glmU* were similar at 0 and 24 h after infection (Fig 6.10B). In contrast, while at 96 h post-infection the bacillary load for *Rv*- and *Rv*Δ*glmU*- infected THP-1 cells remained the same, the addition of ATc to *Rv*Δ*glmU*- infected THP-1 cells 24 h after infection decreased the pathogen load by ~2.5 log fold, indicating that the reduction of $GlmU_{Mtb}$ levels impacts pathogen survival even in an established *ex vivo* infection

Table 6.2: Granuloma scores of the infected mice lungs.

Group (mice)	**Bacterial strains/ treatment**	**Organs**	**No. of granulomas without necrosis, Score : 2.5**	**Total granulomas score**
4th week	*Rv*	Lungs	4	10
	*Rv*Δ*glmU* (-Dox*)	Lungs	4	10
12th week	*Rv* (+Dox)	Lungs	3	7.5
	*Rv*Δ*glmU* (-Dox)	Lungs	6	15
	*Rv*Δ*glmU* (+Dox)	Lungs	0	0

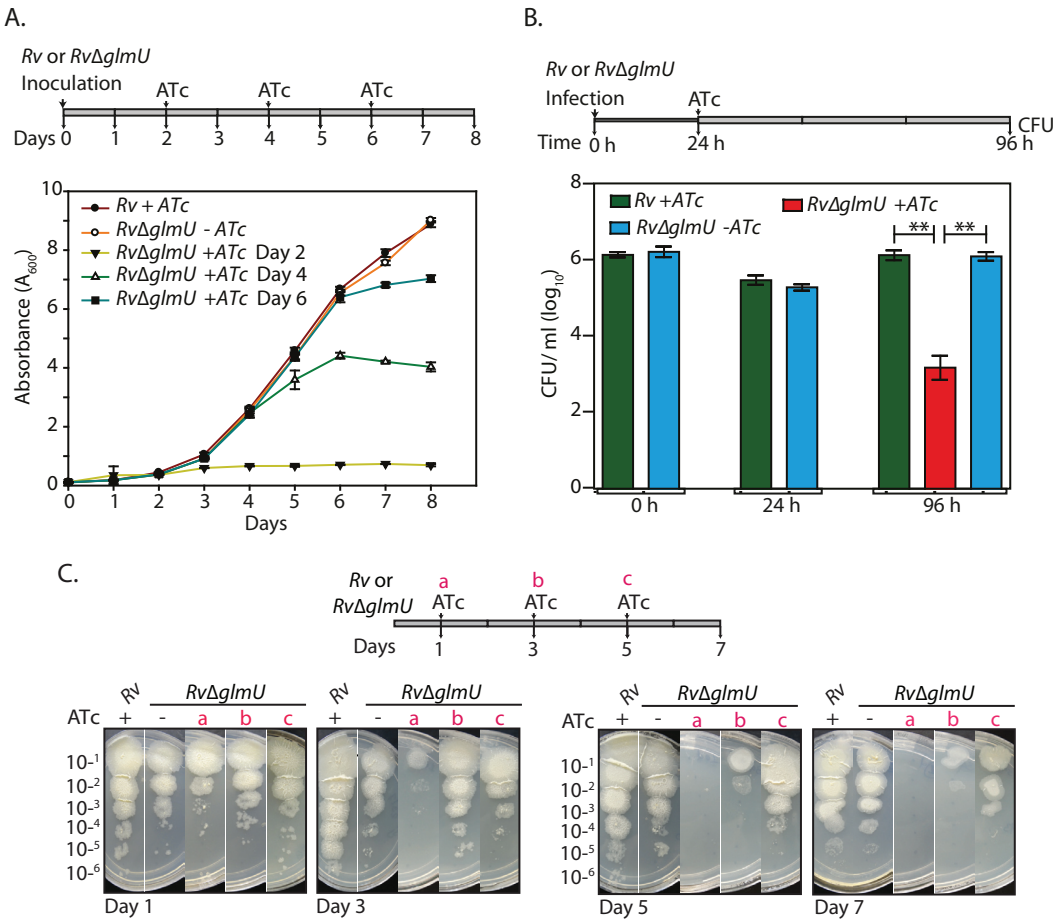

Figure 6.10. Depletion of $GlmU_{Mtb}$ at any stage of growth is deleterious for *Mtb*: (A). *Rv* and *RvΔglmU* cultures were inoculated at an initial A_{600} of 0.1 and the growth was monitored every day for eight days. ATc was added to the *Rv* culture on day 2 and *RvΔglmU* cultures were either grown in the absence of ATc or was supplemented with ATc in the growth media on 2nd, 4th or 6th day, mean, s.e.m., n=3 **(B)** Differentiated THP-1 cells were infected *Rv* or *RvΔglmU* cultures and the infection was allowed to be established for 24 h. 24 h post infection ATc was supplemented in the media for *Rv* and *RvΔglmU* infected cultures. As a control THP1 cells infected with *RvΔglmU* were grown without ATc. CFUs were enumerated at 0, 24 and 96 h post infection. **p<0.005, two tailed non parametric t-test, mean, s.e.m., n=3. **(C)** *Rv* and *RvΔglmU* cultures were inoculated at an initial A_{600} of 0.1. ATc was added to the *Rv* culture on day 1 (a) and *RvΔglmU* cultures were either grown in the absence of ATc or was supplemented with ATc in the growth media on 1st (a), 3rd (b) or 5th (c) day. Serially diluted cultures were spotted on 7H11 agar plates after day 1, 3, 5 and 7.

(Fig 6.10B). We extended this investigation to analyze the effect of $GlmU_{Mtb}$ depletion from a fully-infected lung using murine infection model. As anticipated, the bacillary load in the lungs of mice infected with *Rv* and *RvΔglmU* were comparable both on Day 1 and on Day 28. Administration of Dox to *RvΔglmU* infected mice for the next 56 days (Day 28 to Day 84) drastically decreased the CFUs in the lungs (Fig 6.11A) and the pathogen was completely cleared from the spleen (Fig 6.11C). Unlike the lungs of mice infected with *Rv* and *RvΔglmU*, mice infected with *RvΔglmU* to whom Dox was administered displayed a total absence of lesions and granuloma in the lungs (Fig 6.11B & Table 6.2). Collectively, these data suggest a fundamental role for UDP-GlcNAc, the end product of the $GlmU_{Mtb}$ mediated enzymatic reaction, in modulating the persistence of *M.tb.* infection.

6.3 Discussion.

Cell wall provides the structural rigidity and protects bacteria from various environmental and physiological insults. Biosynthesis of the cell wall of bacteria is a complex process requiring enzymes localized to different cellular compartments [232]. Due to the essentiality of the enzymes involved in there, they are considered attractive targets for anti-microbial therapies. The majority of the first line and second line anti-tuberculosis drugs from the existing regimen target enzymes involved in cell wall synthesis [38]. These include Isoniazid and Ethionamide targeting enoyl-[acyl-carrier-protein] reductase and inhibiting mycolic acid synthesis, Ethambutol targeting arabinosyl transferase and inhibiting arabinogalactan biosynthesis, and Cycloserine targeting D-alanine racemase and ligase, which inhibits peptidoglycan synthesis[38]. However most of these drugs are not very effective against dormant/ latent *M.tb*. $GlmU_{Mtb,}$ an enzyme with dual activity, synthesizes a core metabolite necessary for the synthesis of cell wall peptidoglycan, UDP-GlcNAc [175]. UDP-GlcNAc may also be essential during persistence because (i) a static number of CFU mask significant replication balanced by death [233] and new envelope is required for this replication or because (ii) new envelope is required even in the absence of bacterial replication. Interestingly, we found that depleting $GlmU_{Mtb}$ during both normoxic and hypoxic growth resulted in substantial decrease in cell viability (Fig. 6.5). This is most likely due to the requirement of UDP-GlcNAc, which in addition to participating in cell wall synthesis is also required for

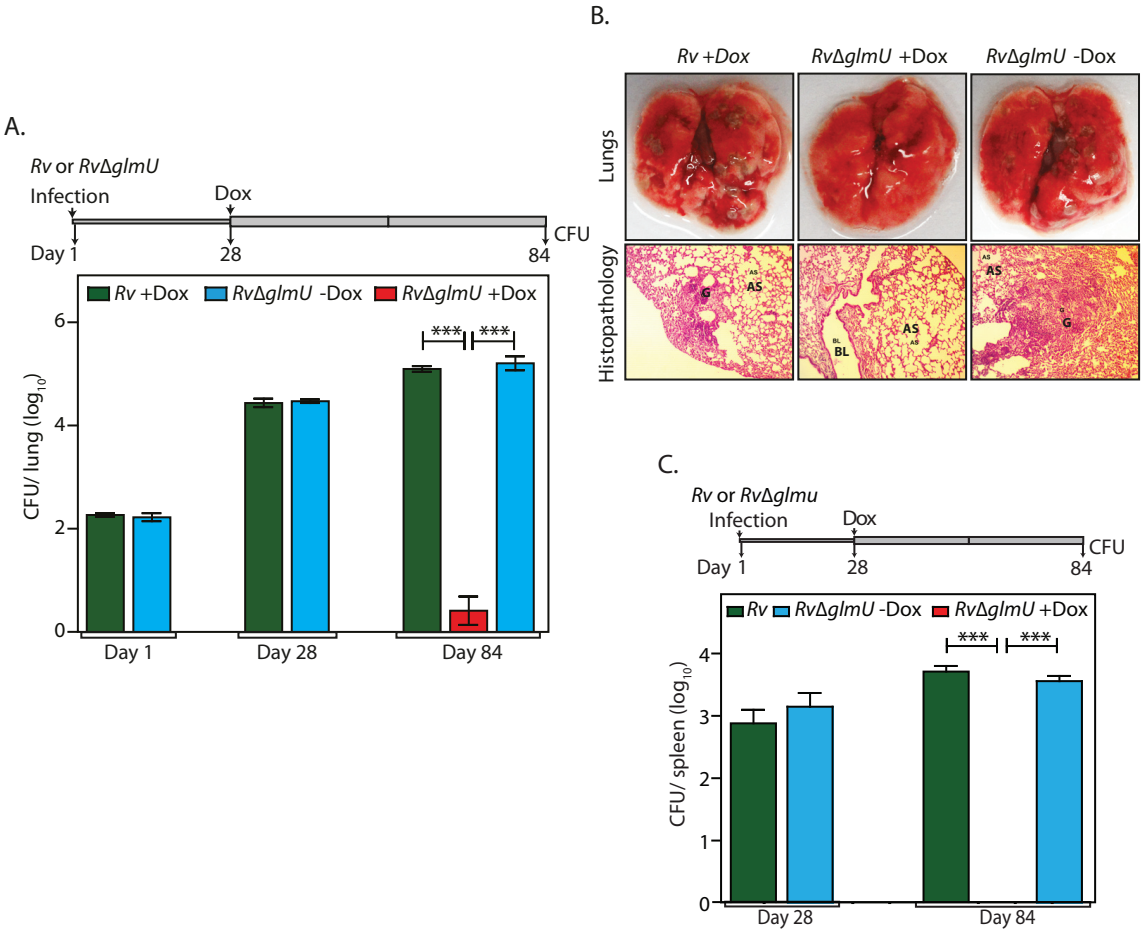

Figure 6.11. Depletion of $GlmU_{Mtb}$ from infected lungs leads to clearance of pathogen: **(A)** BALB/c mice were infected with *Rv* and *RvΔglmU* strains and the infection was established for next 28 days. Subsequently, Dox was provided (with 5% dextrose on every alternate day) in the drinking water for *Rv* infected mice. One group of *RvΔglmU* infected mice were administered with Dox and other with vehicle control for the next 56 days. CFUs were enumerated on day 1, day 28 and day 84 post infection. At 28th days post infection mean CFUs for *Rv* and *RvΔglmU* infected mice were 4.43 and 4.47 on log10 scale and 84th days post infection mean CFUs for *Rv* +Dox or *RvΔglmU* +Dox and *RvΔglmU* –Dox were 5.1, 0.42 and 5.2 on log10 scale. ***p<0.0005, two tailed non parametric t-test, mean, s.e.m., n=6 to 9. **(B)** Overall pathology and histopathology of infected BALB/c mice lungs. Infected lungs dissected on 84th day after infection from *Rv* (+Dox) and *RvΔglmU* (-Dox) infected mice shows clear lesions (upper panel) and granuloma with lymphocytes and foamy histiocytes (lower panel, HE stain, 100x) while *RvΔglmU* (+Dox) was showing normal lung parenchyma and no granuloma. G = Granuloma, BL = Bronchial Lumen, AS = Alveolar Space. **(C)** CFUs of spleen of infected mice on day 28 and day 84 post infection in above mentioned (Fig 7A) experiment. At 28 days post infection mean CFUs for the spleens of *Rv* and *RvΔglmU* infected mice were 2.9 and 3.15 on log10 scale and 84 days post infection mean CFUs for ***Rv*** +Dox or *RvΔglmU* +Dox and *RvΔglmU* –Dox infected spleens were 3.67, 0 and 3.5 on log10 scale. ***p<0.0005, two tailed non parametric t-test, mean, s.e.m., n=6 to 9.

other cellular processes such as myothiol biosynthesis (to maintain redox homeostasis), sialic acid biosynthesis and N- or O- GlcNAcylation [88, 155, 190, 192-194].

While UDP-GlcNAc is a critical metabolite for both prokaryotes and eukaryotes, the enzymes involved in its *de novo* synthesis are significantly different [191]. In addition, both prokaryotes and eukaryotes can utilize GlcNAc from different sources to synthesize UDP-GlcNAc through salvage pathways [234-236]. *Capnocytophaga canimorsus,* a member bacteria from Bacteroidetes phylum lacks endogenous GlmM and GlmU required for the synthesis of GlcNAc and it instead relies on GlcNAc obtained from forages glycans from the host mucin and N-linked glycoproteins [197]. Depending on the enzymes of the salvage pathways present in the bacterial system, it would require either both the activities or only the uridyltransferase activity of GlmU$_{Mtb}$ for UDP-GlcNAc synthesis. Till date the presence of alternate salvage pathway in *M.tb.* has not been demonstrated. However, even with an operating salvage pathway GlmU$_{Mtb}$ is essential for the utilization of host GlcNAc to form UDP-GlcNAc. In line with this, we find that depletion of GlmU$_{Mtb}$ during *ex vivo* or *in vivo* infection either at the start or after infection has been definitively established leads to clearance of pathogen. Taken together, our results suggest that GlmU$_{Mtb}$ is required for bacterial survival, even during dormancy. Also depleting GlmU$_{Mtb}$ at any stage of growth is bactericidal. Both *ex vivo* and *in vivo* infection experiments suggest that depletion of GlmU$_{Mtb}$ in completely infected condition will clear out *M.tb.* from lungs and spleen. Hence GlmU$_{Mtb}$ can be targeted for next generation of inhibitors development.

6.4 Conclusion.

We present the results of a comprehensive study dissecting the role of GlmU$_{Mtb}$ in arbitrating the survival of the pathogen both *in vitro* and *in vivo.* We have generated a conditional gene replacement mutant of *glmU$_{Mtb}$* and find that depletion of GlmU$_{Mtb}$ at any stage of bacterial growth (normoxia or hypoxia) results in irreversible bacterial death due to perturbation of cell wall synthesis. SEM analysis revealed severe morphological perturbations in the absence of GlmU$_{Mtb}$, with the bacilli showing wrinkled surface and fused cells. TEM analysis showed that whereas in *Rv* and *RvΔglmU* cell wall structure and thickness are comparable, there was a

marked decrease in cell wall thickness in *Rv*Δ*glmU* cells where GlmU$_{Mtb}$ was not expressed. Complementation studies show that both uridyltransferase and acetyltransferase activities of GlmU$_{Mtb}$ are essential for pathogen survival, and imply that the only source of the metabolities GlcNAc-1-P and UDP-GlcNAc is through the GlmU$_{Mtb}$ mediated synthesis pathway. GlmU$_{Mtb}$ is also found to be essential for mycobacterial survival in THP-1 cells as well as in guinea pigs. We investigated the effect of GlmU$_{Mtb}$ depletion from a fully-infected lung using murine infection model. Interstingly, depletion of GlmU$_{Mtb}$ from infected murine lungs led to radical reduction in the bacillary load.

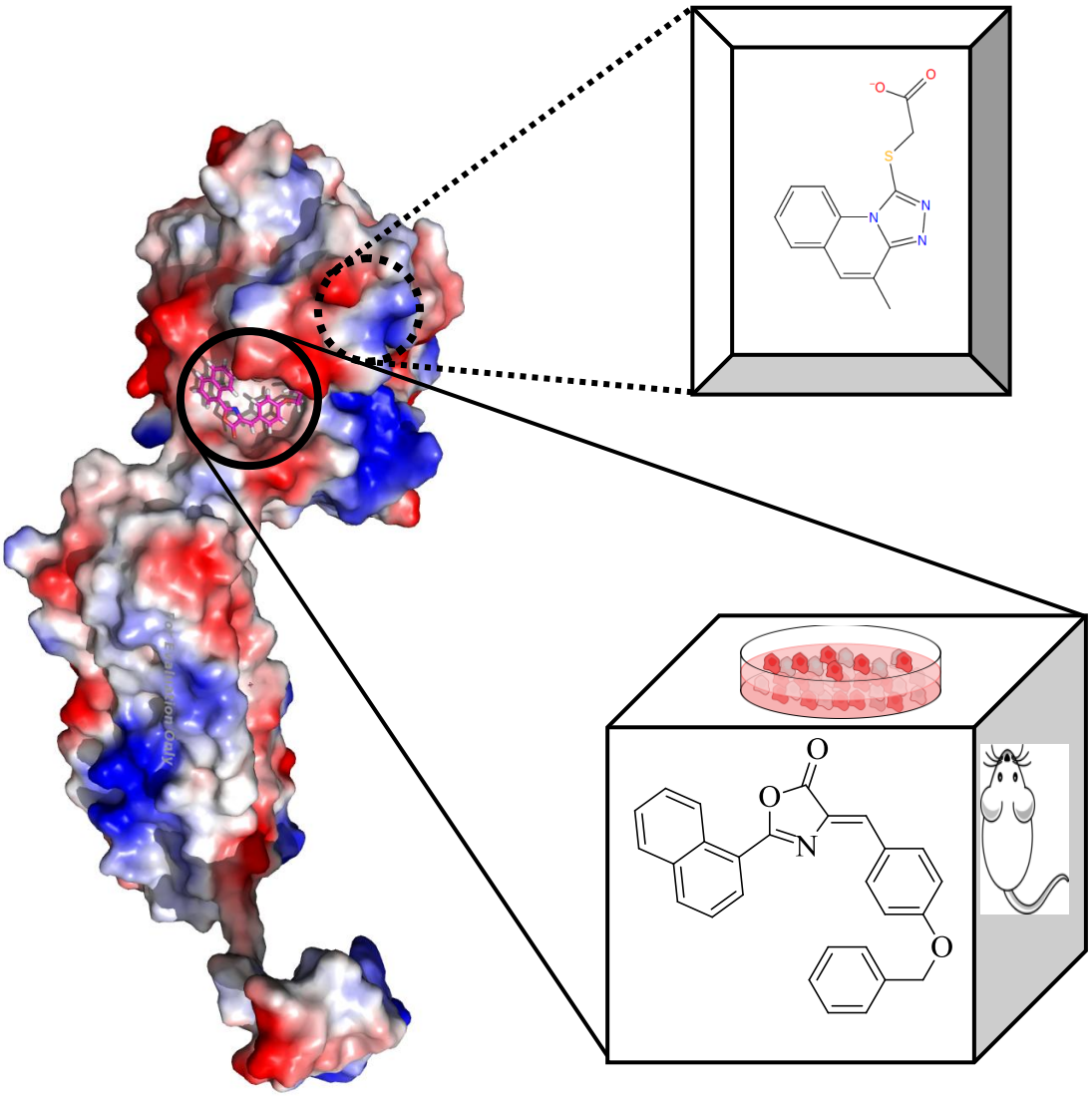

Chapter 7.

Designing and development of anti-GlmU$_{Mtb}$ inhibitors

Chapter. 7

Design and development of anti-GlmU$_{Mtb}$ inhibitors

7.1 Introduction

M. tuberculosis (*M.tb.*), was found to develop mutations for many of the marketed drugs such as mutations in *katG* gene against isoniazid, *rpoB* gene against rifampicin, which made them ineffective for treating multi drug resistant TB (MDR-TB) [237]. The available marketed first line drugs are capable of achieving more than 90% of efficacy, yet their benefit is cut short because of bacterial resistance. The resistance among the pathogenic strains, which prevents treatment by both first line and second line drugs, manifests as a more dreadful condition known as extensively drug resistant TB (XDR-TB). Among many factors contributing to the drug resistance against *M.tb.*, one of the major concerns is the high lipophilic content of its cell wall. This architecture of cell wall involves an outer highly lipophilic mycolic acid deposit and inner peptidoglycan layer, which are being covalently connected by a polysaccharide known as arabinogalactan [115]. This molecular makeup of mycobacterial cell wall makes the entry of several drugs difficult, thus reducing the effectiveness.

N-acetylglucosamine-1-phosphate uridyltransferase (GlmU$_{Mtb}$) is one of the vital enzymes, necessary for formation of the building blocks of mycobacterial cell wall. UDP-GlcNAc, the final product of GlmU$_{Mtb}$ biosynthetic pathway, has a significant role in mycobacterial physiology, by acting as a substrate for peptidoglycan biosynthesis [219]. Moreover, GlcNAc is a crucial component of a disaccharide α-L-rhamnosyl-(1,3)-α-D-GlcNAc-phosphate, which acts as a linker between the peptidoglycan layer and arabinogalactan. Interestingly, in eukaryotes such bi-functional enzymes capable of performing both steps are absent and synthesis of UDP-GlcNAc is carried out by two independent enzymes, UDP-N-

acetylglucosaminePPase (Uaplp) and glucosamine-6-phosphate acetyltransferase (GNA1) [195, 238].

Researchers have developed compounds that inhibit the activities of the orthologs of $GlmU_{Mtb}$ (GlmU from *T. brucei*, *P. aeruginosa*, *E. coli*, *H. influenza* and *X. oryzae) in vitro* [162, 163, 170, 179, 180, 239-241]. Bioinformatics analysis and kinetic modeling data advocate $GlmU_{Mtb}$ to be a potential target for the development of suitable inhibitors [171]. In concurrence with these predictions, effective inhibitors have been developed against, the acetyltransferase and uridyltransferase domains of $GlmU_{Mtb}$ [113, 182]. However, the precise sites of inhibitor-protein interactions and the efficacy of the inhibitors *ex vivo* or *in vivo* have not been investigated.

Earlier studies in *M. smegmatis* showed that gene replacement mutant of GlmU could only be generated in the presence of ectopic copy, suggesting essentiality of GlmU for maintenance of its cell wall integrity and survival of mycobacterium [115]. Our results presented in Chapter 6 demonstrated that depletion of $GlmU_{Mtb}$ both *in vitro* and *in vivo* results in clearance of *M.tb*. These observations make $GlmU_{Mtb}$ an attractive target for development of newer potent anti-tubercular drugs. In the similar context, it is important to determine, which among the available sites on $GlmU_{Mtb}$ would be appropriate for the effective inhibition. Computational kinetic modelling study on $GlmU_{Mtb}$ has shown uridyltransferase reaction to be the rate limiting step and offers more flexibility [171]. Previously, it was revealed that UTP binds first at the uridyl site, inducing the conformational changes, which subsequently accommodates GlcNAc-1-P, thus allowing the uridyltransferase reaction to proceed [162]. The uridyl site accommodates two functionally important magnesium ions as cofactors, involved in the catalysis process [161]. Studies have suggested that the formation of UDP-GlcNAc is a two metal ion dependent process, which are involved in the substrate stabilization, nucleophile activation and transition-state stabilization [161]. Our study also supports the presence of feedback inhibition by the final product, UDP-GlcNAc (chapter 5, Fig 12 & Table 7.3), which makes the uridyltransferase active site an attractive target for the development of new inhibitors.

In the present study, we aimed at identifying potential inhibitors against the uridyltransferase site of $GlmU_{Mtb}$ employing various computational, biological and

biochemical tools. We have performed two studies targeting the uridyltransferase activity of $GlmU_{Mtb.}$ In one study we targeted the allosteric site and in the other we targeted the active site (competitive inhibitor). Already known allosteric site and inhibitor of *H. influenzae* GlmU was used to develop a shape based designing followed by chemical derivatization to get final compound Oxa33. This compound was checked against *M.tb.* at *in vitro, ex vivo* and *in vivo* infection level. Also the specificity was confirmed against $GlmU_{Mtb}$ using MD simulations and mutational studies.

Second set of inhibitors were developed against the uridyltransferase active site using the published crystal structure information. The *in silico* studies were cross correlated using various docking methodologies like induced fit docking (IFD), quantum polarized ligand docking (QPLD), taking into account the flexibility of the active site residues and their partial charges. Our theoretical binding energies based on molecular mechanics and molecular dynamics studies correlated well according to our findings. We also investigated the nature of small molecule effect over $GlmU_{Mtb}$ by means of *in vitro* enzyme inhibition studies followed by biophysical studies such as isothermal titration calorimetry (ITC) to determine the experimental binding affinity of selected compounds. The thermodynamic parameters elucidated via theoretical and experimental methodologies, described in this study for $GlmU_{Mtb}$ is thus believed to be helpful in designing of novel anti-mycobacterial compounds.

7.2 Results

7.2.1 Allosteric site inhibitors.

7.2.1.1 Design and development of allosteric site inhibitors against $GlmU_{Mtb}$.

In addition to the acetyltransferase and uridyltransferase active site pockets, $GlmU_{Mtb}$ also contains an allosteric site. Binding of any suitable molecule/inhibitor to the allosteric site would prevent the conformational change essential for $GlmU_{Mtb}$ uridyltransferase catalytic activity. In the present study, we aimed at the design and synthesis of $GlmU_{Mtb}$ allosteric site inhibitors and their efficacy and specificity towards the protein. For this purpose the crystal structure of $GlmU_{HI}$ complexes with a small-molecule inhibitor (PDB code 2VD4) at its allosteric site was considered as the starting point. The design methodology and the workflow are shown in figure 7.2. The $GlmU_{HI}$ inhibitor, 4-chloro-N-(3-methoxypropyl)-N-[(3s)-1-(2-

A.

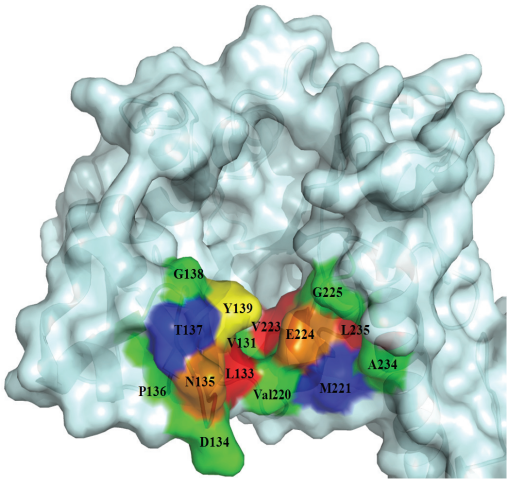

B.

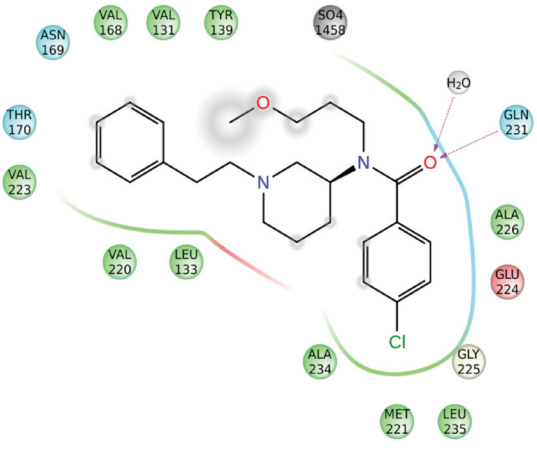

C.

```
QAAPFFKDN--ENIVVLYGDAPLITKETLEKLIEAK--PENGIALITVNL
CGLSALPDDYAGNVVVTSGDTPLLDADTLADLIATHRAVSAAVTVITTTL
 . . : *:   *:**  **:**:  :** .** ::   . .:::**..*

DNPTGYGRIIR-ENGNVVAIVEQKDANAEQLNIKEVNTGVMVSDGASFKK
DDPFGYGRILRTQDHEVMAIVEQTDATPSQREIREVNAGVYAFDIAALRS
*:* *****:* :: :*:*****.**...* :*:***:** . * *:::.

WLARVGNNNAQGEYYLTDLIALANQDNCQVVAVQATDVMEVEGANNRLQL
ALSRLSSNNAQQELYLTDVIAILRSDGQTVHASHVDDSALVAGVNNRVQL
 *:*:..**** * ****:**: ..*.  * * :. *   * *.***:**

AALERYFQNKQASKLLLEGVMIYDPARFDLRGTLEHGKDVEIDVNVIIEG
AELASELNRRVVAAHQLAGVTVVDPATTWIDVDVTIGRDTVIHPGTQLLG
* *   ::.: .:   * ** : ***   :   :  *:*. *. .. : *
```

D.

M. tuberculosis GlmU	*H. Influenzae GlmU*
Ala236	Glu224
Gln243	Gln231
Thr142	Val131
Leu144	Leu133
Tyr150	Tyr139
Glu179	Val168
Ser232	Val220
Val235	Val223
Glu246	Ala234

Figure 7.1. Allosteric site of *H. influenzae* and its comparison with *Mtb* allosteric site: **(A)** Surface representation of $GlmU_{HI}$ wherein its allosteric residues are highlighted. The allosteric site of $GlmU_{HI}$, comprises of highly lipophilic surface and a distal depression surface **(B)** Interaction of $GlmU_{HI}$ allosteric inhibitor at the allosteric site. Hydrophobic residues are coloured in green, polar residues in blue, negatively charged residues in red. Hydrogen bond interaction of the ligand with Gln231 is shown in pink colour; Glu224 is also involved in the hydrogen bonding which is not represented here. Leu133, Tyr139, Met221, Leu235 were found to be involved in strong hydrophobic interactions with the inhibitor. Interactions were plotted with LIGPLOT. **(C)** Sequence alignment of $GlmU_{HI}$ and $GlmU_{Mtb}$ allosteric site residues. Conserved residues are highlighted in red boxes. **(D)** Table displaying allosteric residues of $GlmU_{HI}$ and $GlmU_{Mtb}$. Some of the critical residues such as Tyr150, Gln243 and Leu247 of $GlmU_{Mtb}$ are seen to be conserved.

phenylethyl)piperidin-3-yl]benzamide, was found to be interacting with Glu224 and also involved in hydrophobic interactions with Val131, Leu133, Tyr139, Val168, Val220, Val223 and Ala234 (Fig 7.1A & B). Alignment of the $GlmU_{Mtb}$ and $GlmU_{HI}$ allosteric pocket residues suggested that the interacting residues were conserved between the two proteins (Fig 7.1C & D). Shape based modelling using this inhibitor was carried out employing ROCS methodology. The model generated was able to reproduce the same features, which were seen in the crystal structure interactions. This model was used as a query and a ROCS run was performed for screening the Asinex database (ASINEX Platinum and Gold Collection) using Implicit Mills Dean force field to map all the compounds to the shape model. A total of 25,000 hits were resulted from the ROCS screening from which 10,000 hits were carried forward for molecular docking studies which were shortlisted based on the EON scoring. The molecular docking workflow operated, using Glide, included the docking of compounds in both standard precision (SP) and extra precision (XP) modes. The XP docking resulted in 126 compounds, of which 43 hits were selected based on glide score, interaction pattern and tanimoto scores and procured from to perform their inhibition studies against $GlmU_{Mtb}$.

7.2.1.2 Screening of inhibitors.

Among the 43 compounds screened, one molecule (4*Z*)-4-(2-fluorobenzylidene)-2-(naphthalen-2-yl)-1,3-oxazol-5(4*H*)-one, inhibited ~90% $GlmU_{Mtb}$ uridyltransferase activity at 100 μM (Fig 7.2). The compound was further structurally optimized by increasing the hydrophobic component over the phenyl moiety by various scaffolds thereby synthesizing a library of 53 compounds which were in turn subjected to $GlmU_{Mtb}$ enzyme inhibition studies (Fig 7.2). Among the 53 compounds, (4*Z*)-4-(4-benzyloxybenzylidene)-2-(naphthalen-2-yl)-1,3-oxazol-5(4*H*)-one (Oxa33) was found to inhibit $GlmU_{Mtb}$ efficiently with an IC_{50} of 9.96±1.1 μM (Fig 7.4A, see Fig 7.3A & 7.3B for the synthesis of Oxa33).

7.2.1.3 Isothermal Titration Calorimetry (ITC) and Differential Scanning Fluorimetry (DSF).

Binding parameters of Oxa33 to $GlmU_{Mtb}$ were carried out by ITC and DSF experiments. Binding isotherm (fitted for one site binding) suggests that Oxa33 binds to $GlmU_{Mtb}$ protein with adequately high binding affinity (K_a = 2.35×10^6 M^{-1}) and

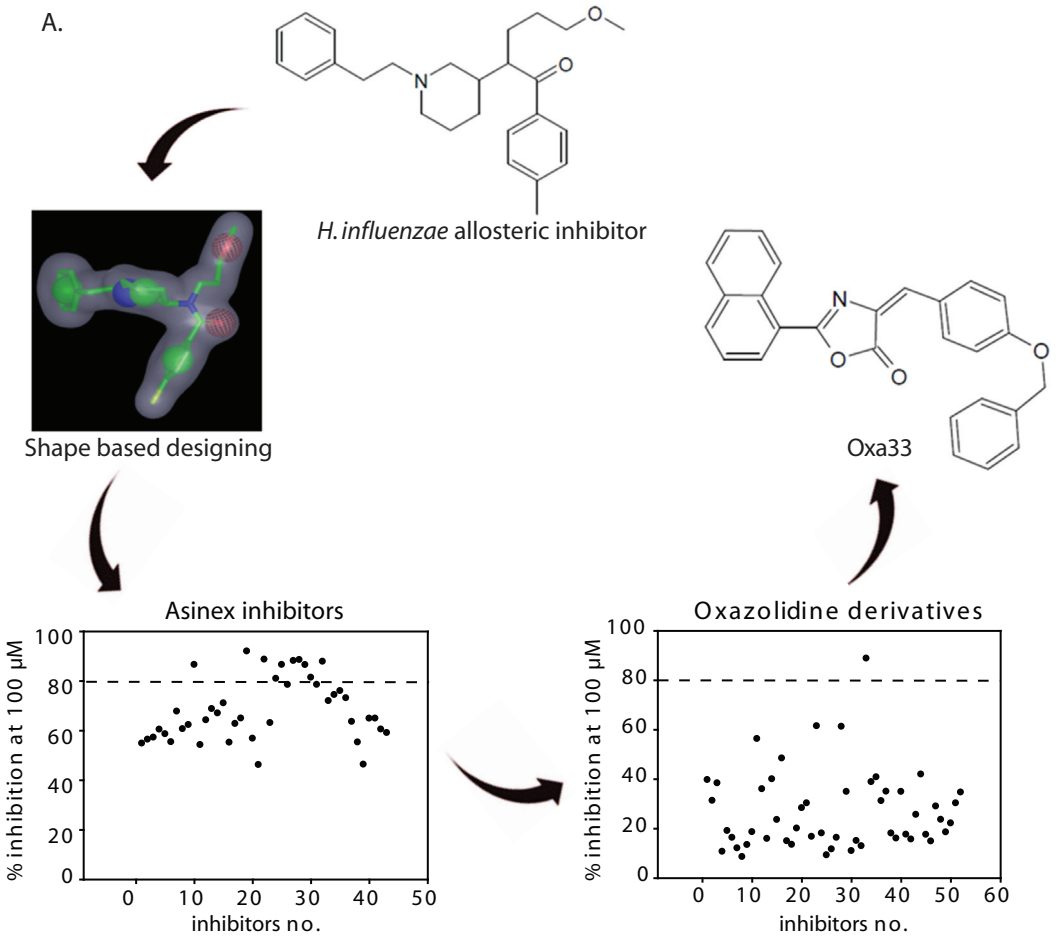

Figure 7.2. Design and development of anti-GlmU$_{Mtb}$ inhibitors: (A) Virtual screening workflow used towards the identification of allosteric inhibitors for GlmU$_{Mtb}$. Shape model of allosteric inhibitor of GlmU$_{HI}$ was generated using ROCS software. In the initial set of screening, a total of 43 compounds were identified and tested for their ability to inhibit uridyltransferase reaction. 10 among the 43 compounds showed ~90% inhibition at 100 µM. Of these, an oxozolidine derivative was identified and further chemically derivatized to a library of 52 compounds. One compound from these, Oxa33, which showed ~90% inhibition was considered for further studies.

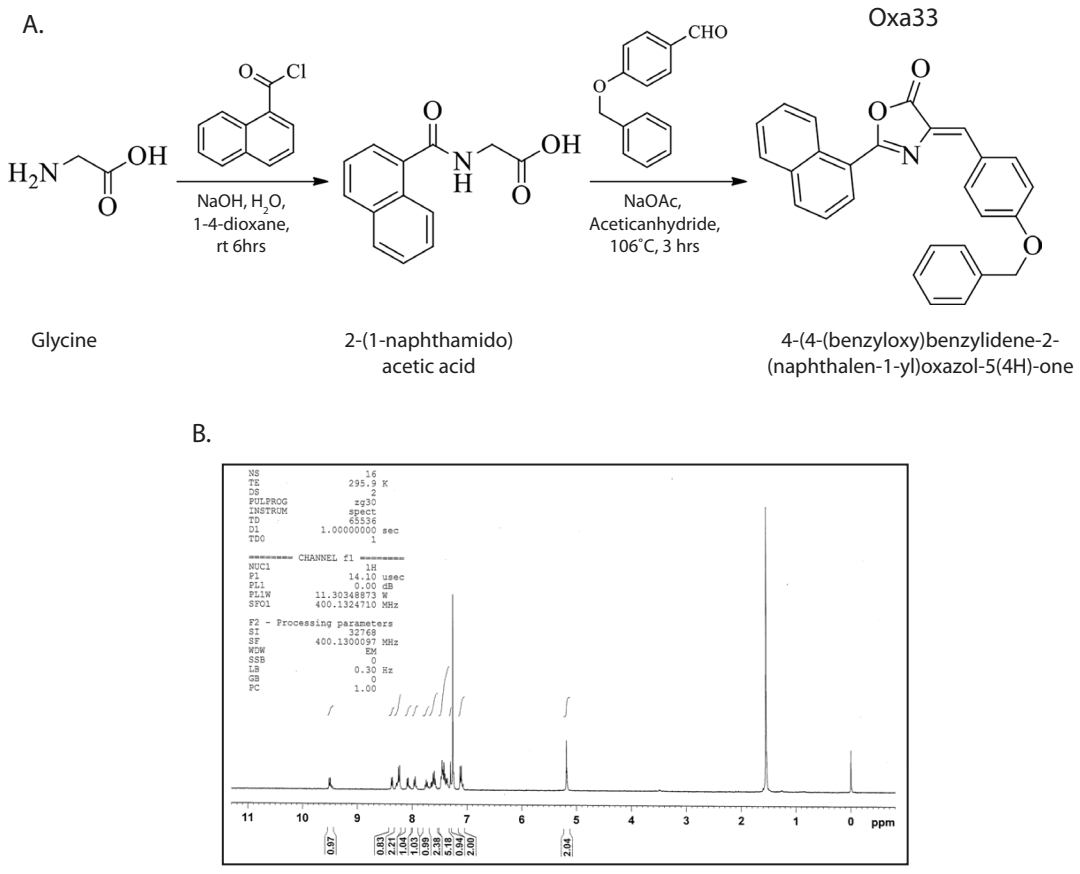

Figure 7.3. Synthesis of oxazolidine derivative series and Oxa33: (A) Synthetic scheme for the preparation of 4-(4-(benzyloxy)benzylidene)-2-(naphthalen-1-yl)oxazol-5(4H)-one (Oxa33). **(B)** Nuclear magnetic resonance spectra of purified Oxa33 (Yellow solid). 1H NMR (400 MHz, CDCl3): δ 9.51 (d, J = 8.8 Hz, 1H), 8.38 (d, J = 8.8 Hz, 1H), 8.25 (d, J = 8.4 Hz, 2H), 8.10 (d, J = 8.4 Hz, 1H), 7.93 (d, J = 8.0 Hz, 1H), 7.74 (t, J = 8.0 Hz, 1H), 7.68–7.56 (m, 2H), 7.49–7.33 (m, 5H), 7.29 (s, 1H), 7.12 (d, J = 8.4 Hz, 2H), 5.15 (s, 2H). Anal calcd for: C27H19NO3: C, 79.98; H, 4.72; N, 3.45 % Found C, 79.92; H, 4.83; N, 3.54%

binding stoichiometry was found to be n = 0.7. This binding was mainly entropy driven with $T\Delta S$ = 5.8 kcal/mol and exothermic enthalpy change ΔH = -2.8 kcal/mol (Fig 7.4B). DSF study of pure protein showed that the T_m was 47°C with 5% DMSO and 44°C with Oxa33. Decrease of T_m by 3°C and increase in initial relative fluorescence unit (RFU) of Oxa33/$GlmU_{Mtb}$ mix by ~5 times suggests possible unfolding in $GlmU_{Mtb}$ upon Oxa33 binding (Fig 7.4C).

7.2.1.4 Docking, Molecular dynamics simulations and possible mechanism of the action of Oxa33.

The docking studies of Oxa33 compound were carried out in order to identify its mode of binding at the pocket. Oxa33 was found to be interacting strongly with the active site residues at the $GlmU_{Mtb}$ allosteric site by means of polar and non-polar interactions (Fig 7.5C). The oxygen linking the phenyl group with benzyl was found to be in hydrogen bonding with Tyr150 and the carbonyl oxygen over the oxazole ring was involved in hydrogen bonding with Glu250 and Arg253 (Fig 7.5C). Also, the compound seemed to be well stabilized by strong hydrophobic interactions with Leu144, Pro147, Phe148, Tyr150, Ala233, Ala236 and Leu247 (Fig 7.5C).

Molecular dynamics simulations were carried out explicitly for $GlmU_{Mtb}$ complex with Oxa33 at its allosteric site for a period of 20 ns using OPLS_2005 force field of Desmond. The trajectory analysis was carried out so as to study the stability of the complex. The root mean square deviation for all the atoms was plotted against the time scale (Fig 7.6A). From the plot, it can be inferred that in spite of the fluctuations observed during the initial time period, which can be attributed to the relaxation of the model in the solvent system, the complex was found to be stable during the remaining time scale. This signifies the stabilization effect of the compound over $GlmU_{Mtb}$ and its better binding affinity with the protein.

Superimposition of $GlmU_{Mtb}$-Oxa33 complex before (green) and after (orange) the simulation time period (Fig 7.5B) shows that the loop regions at the uridyltransferase site undergoes major conformational changes, resulting in the decrease of uridyl site volume. The deviation in the uridyl site was observed in the range of 3-6 Å. Oxa33 was found to be binding to the allosteric site throughout the simulation proving its affinity towards $GlmU_{Mtb}$. A thorough analysis of protein-ligand complex simulation trajectory summarises the probable mechanism of action

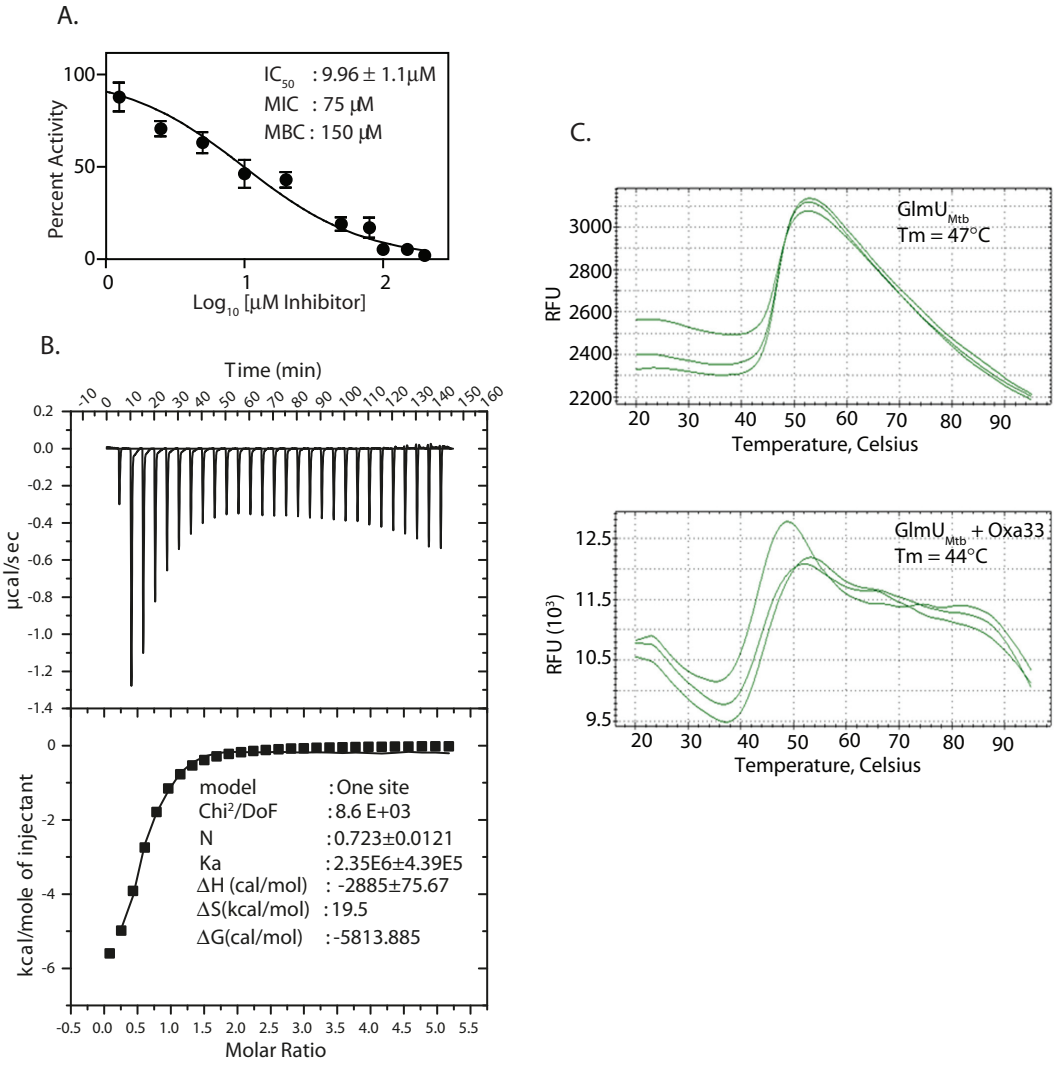

Figure 7.4. Characterization of Oxa33, a novel inhibitor against $GlmU_{Mtb}$: (A) IC_{50} values were determined by varying the concentration of Oxa33 and calculating the percent activity with respect to the uridyltransferase activity of 0.75 pM conc $GlmU_{Mtb}$ in the presence of 5% DMSO (vehicle). IC_{50} value was calculated by plotting percentage activities against different log_{10} values of inhibitor concentrations (µM). **(B)** Isothermal titration calorimetry results of Oxa33 with $GlmU_{Mtb}$. Released heat increased over the period of time (µcal/sec) is presented in upper panel while corresponding binding isotherm (fitted for one site) presented in lower panel. **(C)** Differential Scanning Fluorimetry (DSF) results of Oxa33 with $GlmU_{Mtb}$. Upper panel representing melting curve of $GlmU_{Mtb}$ in presence of 5% DMSO. While lower graph is showing -3°C T_m shift upon Oxa33 incubation with $GlmU_{Mtb}$ protein.

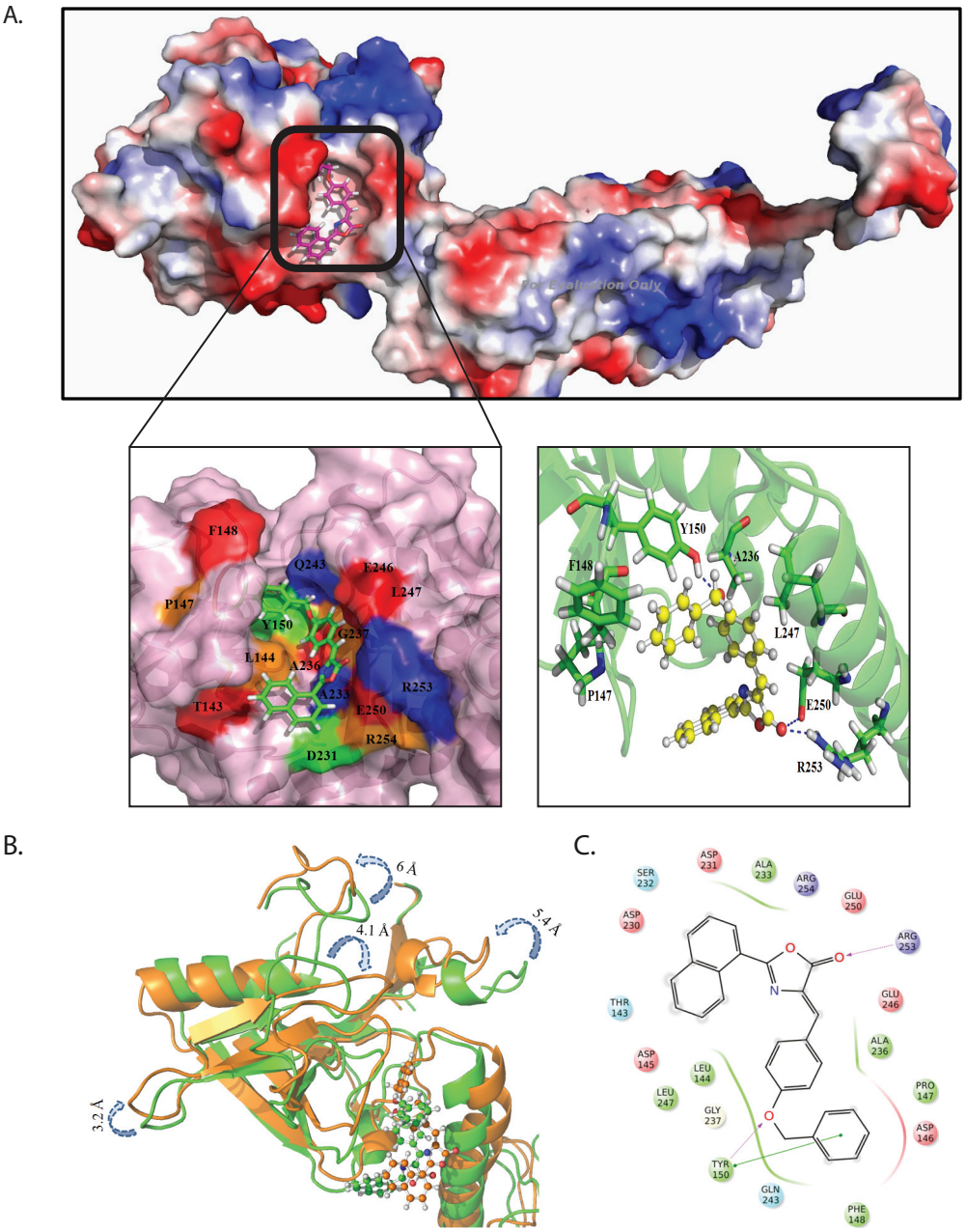

Figure 7.5. Molecular dynamics simulation study of Oxa33 with $GlmU_{Mtb}$: (A) Lower left panel depicts docking surface representation of the allosteric site on the of the $GlmU_{Mtb}$ allosteric site in complex with Oxa33. Right panel represents ribbon cartoon showing the amino acids residues of allosteric site and hinge region interacting with Oxa33 (in ball and stick model). Tyr150, Glu250 and Arg 253 were found to be in hydrogen bonding with carbonyl oxygen over the oxazole ring. While Leu144, Pro147, Phe148, Tyr150, Ala233, Ala236 and Leu247 participate in strong hydrophobic interactions with Oxa33. **(B)** Superimposed view of $GlmU_{Mtb}$-Oxa33 complex before (green) and after (orange) the simulation time period. **(C)** Two dimensional representation of binding pattern of Oxa33 at $GlmU_{Mtb}$ allosteric site. Green line represents the π-π stacking interaction of Oxa33 with Tyr150. Hydrophobic residues are coloured in green, polar residues in blue, negatively charged residues in red, positively charged in purple.

of Oxa33 against $GlmU_{Mtb}$. Oxa33 binding upon $GlmU_{Mtb}$ might result in conformational changes and structural rearrangement of the uridyltransferase site in order to accommodate Oxa33. As a result, there might be a partial closure of uridyl site (decreased volume) thereby making it unavailable for its substrates for catalysis (Fig 7.5B).

7.2.1.5 H-bond analysis.

Hydrogen bonding, being one of the crucial inter atomic interactions, helps in retaining the bound molecule at the protein active site thereby accounting for its bonding affinity towards the protein. In order to study the hydrogen bond network of $GlmU_{Mtb}$ -Oxa33 complex and its stability during simulation, hydrogen bond analysis for the trajectory was carried out, which can in turn be correlated to the $GlmU_{Mtb}$ inhibitory activity. Oxa33 was found to be in hydrogen bonding with Tyr150, Glu250 and Arg253 residues. The inter-atomic distance fluctuations between the compound and these residues were monitored during the simulation and were plotted against time (Fig 7.6B). From the plot, it can be inferred that the hydrogen bonding with Glu250 was found to be stable as there were least fluctuations observed when compared to the remaining two. The bonding with Tyr150 and Arg253 continued to be stable throughout the simulation period in spite of some minor fluctuations. These fluctuations of the residues can be well correlated with respect to their crystallographic B factor whose values are ~26, ~21 and ~31 for residues Tyr150, Glu250 and Arg253 respectively. The stability of Glu250 during simulation can be well explained by its lower B factor.

7.2.1.6. Mutational analysis of $GlmU_{Mtb}$ to determine the residues critical for interaction with Oxa33

The $GlmU_{Mtb}$ allosteric site residues interacting with Oxa33 were mutated and the mutated $GlmU_{Mtb}$ activity was studied in the absence and presence of Oxa33. Residues Tyr150 which was found to be involved in both polar and non-polar interactions with Oxa33 was mutated to phenyl alanine (aromatic amino acid) and alanine. Similarly, Gln253 was mutated to glutamine and alanine. Leu144, Gln243 and Leu247 involved in hydrophobic interactions were mutated to alanine. The conventional $GlmU_{Mtb}$ activity, in the absence of Oxa33, was found to be unaffected by these mutations with an exception of $GlmU_{L247A}$ which resulted in increase in

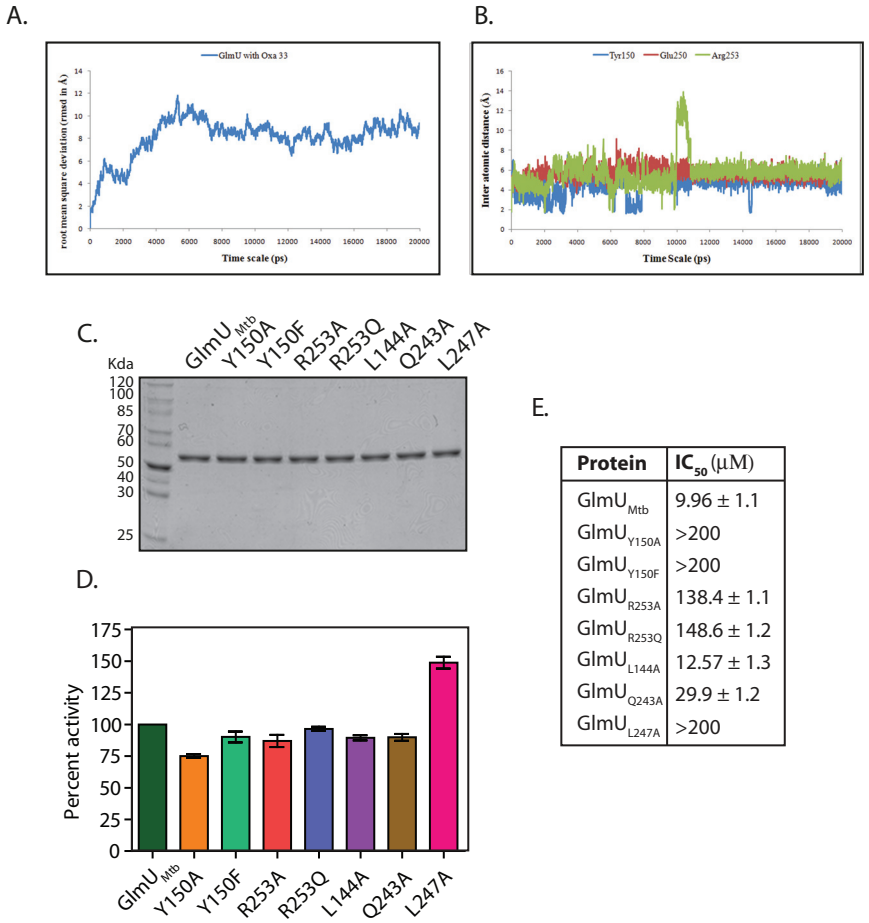

E.

Protein	IC_{50} (μM)
$GlmU_{Mtb}$	9.96 ± 1.1
$GlmU_{Y150A}$	>200
$GlmU_{Y150F}$	>200
$GlmU_{R253A}$	138.4 ± 1.1
$GlmU_{R253Q}$	148.6 ± 1.2
$GlmU_{L144A}$	12.57 ± 1.3
$GlmU_{Q243A}$	29.9 ± 1.2
$GlmU_{L247A}$	>200

Figure 7.6. RMSD plot and mutation study from MD simulations: (A) rmsd plot for $GlmU_{Mtb}$-Oxa33 complex simulated for a period of 20ns. The complex was found to be unstable during the initial time period which can be owed for its relaxation. After 8 ns, the complex was observed to be stable indicating the strong binding affinity of Oxa33 towards $GlmU_{Mtb}$ **(B)** Hydrogen bond analysis of Oxa33 analyzed during the simulation time period. **(C)** Purified $GlmU_{Mtb}$ mutants (single band) specified by the docking studies of Oxa33. **(D)** Based on the above data $GlmU_{Mtb}$ allosteric site mutants were created, proteins were purified and the uridyltransferase activity of $GlmU_{Mtb}$ mutants was determined. Wild type and mutant $GlmU_{Mtb}$ proteins show almost comparable activity. **(E)** IC_{50} values in μM were determined as described above for the wild type and the mutant GlmUMtb proteins. Tables shows the values obtained for wild type and mutant enzymes.

activity by 50% (Fig 7.6D). Interestingly while the $GlmU_{Y150A}$ mutant showed slightly reduced activity, $GlmU_{Y150F}$ activity remained unaltered, signifying the importance of an aromatic amino acid at 150th position. Determination of mutant $GlmU_{Mtb}$ uridyltransferase activity in the presence of Oxa33 resulted in quite interesting and significant result (Fig 7.6E). Mutations at Y150F, Y150A and L247A resulted in complete loss of Oxa33 mediated inhibition with IC_{50} values greater than 500 μM (compare with IC_{50} ~10 μM for the $GlmU_{Mtb}$). This loss in Oxa33 activity is most likely to due to its inability to interact with the mutant protein at the allosteric site. Mutations at R253A to glutamine or alanine resulted in ~8-9 fold decrease in IC_{50} values. Other mutations, Q253A and L144A, did not impact the IC_{50} values suggesting that they play minimal role in Oxa33 binding (Fig 7.6E).

7.2.1.6 Effect of Oxa33 on in vitro growth of M.tb.

We investigated the ability of Oxa33 to inhibit the *in vitro* growth of *M.tb. H37Rv*. Oxa33 inhibited the *in vitro* growth of *M.tb. H37Rv* with a minimum inhibitory concentration (MIC) of ~75 μM. To ascertain if this inhibitory effect was due to inhibition of $GlmU_{Mtb}$ activity we over-expressed $GlmU_{Mtb}$ (Fig 7.7A) in the cells (by addition of ATc in *Rv::glmU*) prior to drug treatment and determined the effect of this on the MIC value. Whereas the inhibition of growth in the presence of INH was similar with or without $GlmU_{Mtb}$ over expression in the cells (Fig 7.7B, middle panel), Oxa33 failed to inhibit cell growth even at concentrations as high as 150 μM (Fig 7.7B, upper panel). To check the effect in combination with INH, we have used a sub lethal dose of Oxa33 (40 μM) along with different concentrations of INH. Results depicted reduction in MIC values from 32 ng/ml to 16 ng/ml (Fig 7.7B, lower panel).

7.2.1.7 Ex vivo and in vivo efficacy of Oxa33 on infected THP1 cells or mice.

We determined the cytotoxicity of Oxa33 in THP1 cells for a period of 3 days and found it to be non-toxic up to 100 μM (Fig 7.8E). To determine the *ex vivo* efficacy, THP1 cells were infected with *Rv* or *Rv::$glmU_{tet\text{-}on}$* ($GlmU_{Mtb}$ over expressing strain) and grown in RPMI media containing 400 ng/ml ATc. 24 h post infection, the cells were provided with either Oxa33 or INH or vehicle for the next 72 h. It is apparent from the data that bacillary load of *Rv* or *Rv::$glmU_{tet\text{-}on}$* were similar at 0 and 24 h time points. While both the strains responded similarly to INH

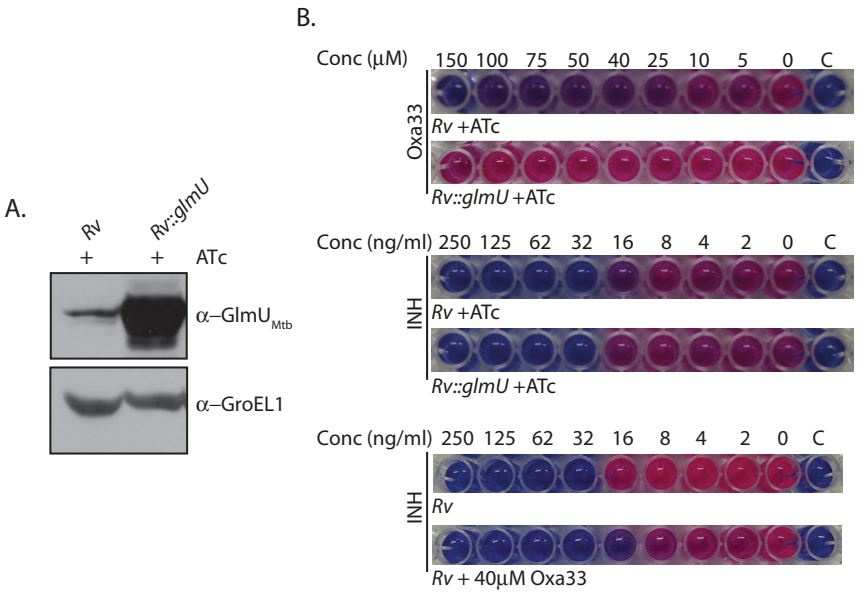

Figure 7.7. Oxa33 specifically inhibits $GlmU_{Mtb}$ inside the bacteria: (A) *Rv* and *Rv::glmU*$_{tet\text{-}on}$ strains were inoculated at an initial A_{600} of 0.1 in the presence of ATc (2 μg/ml) and grown up to 5 days. WCLs were resolved and probed with anti-GlmU and anti-GroEL1 antibodies. **(B)** *Rv* and *Rv::glmU*$_{tet\text{-}on}$ cultures were grown in presence of 1 μg/ml ATc and different concentrations of Oxa33 or INH (as indicated). 0.02% resazurin dye was added on day 7. Pink colour indicates viable bacteria while blue colour indicates dead bacteria. 'C' denotes culture media control. Lowest set of wells are showing *Rv* culture treated with sub lethal dose of Oxa33 (40 μM) and variable concentrations of INH for 6 days followed by resazurine addition. Results show decrease in MICs of INH from 32 ng/ml to 16 ng/ml.

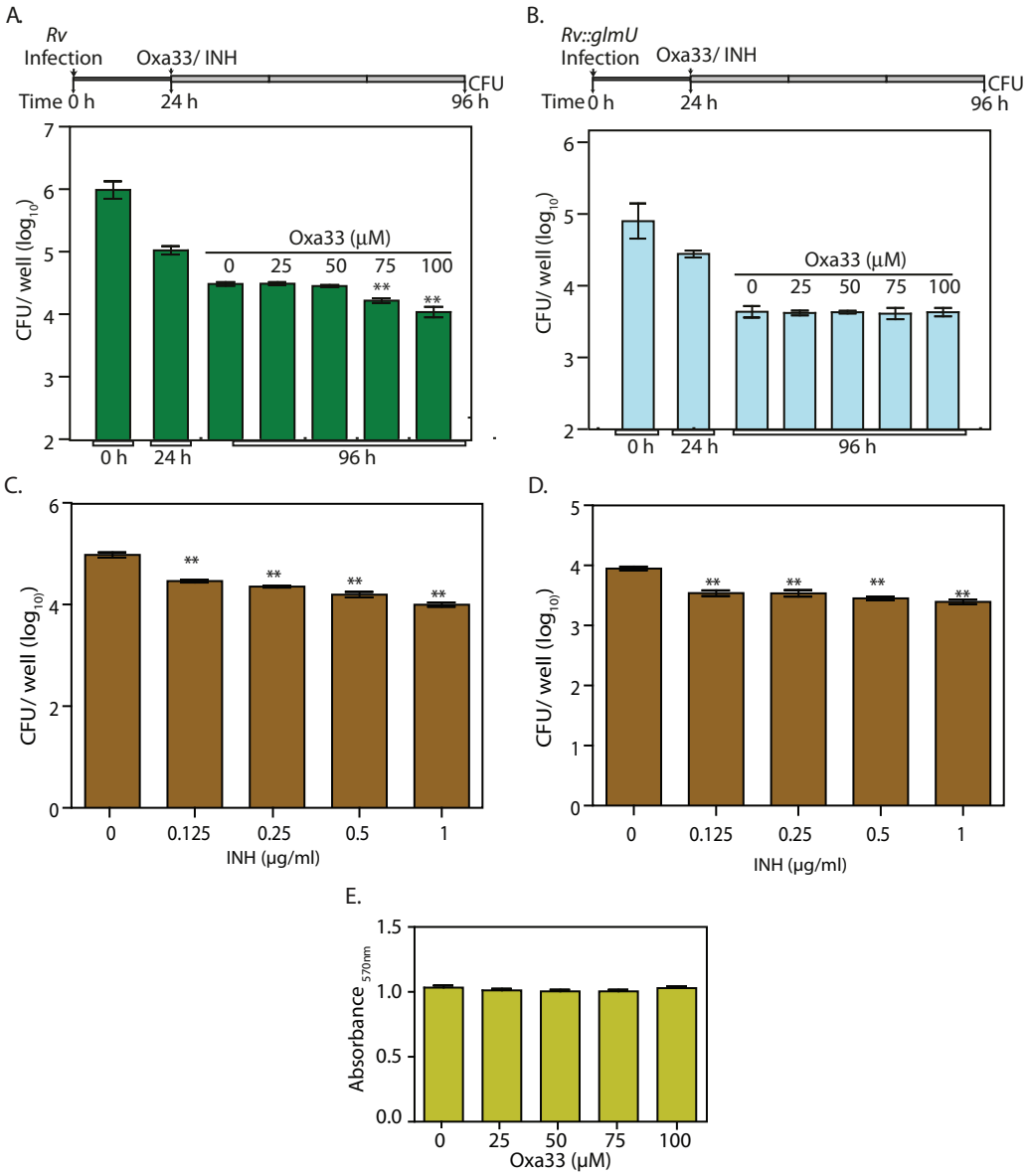

Figure 7.8. Oxa33 specifically inhibits $GlmU_{Mtb}$ in *ex vivo* conditions: (**A**) CFU results of infected THP1 cells with *Rv* strain and treated with Oxa33. Decrease in CFU counts was observed (**p<0.005, two tailed non parametric t-test, mean, s.e.m., n=3) (**B**) Bar graph showing the CFUs of *Rv::glmU*$_{tet\text{-}on}$ infected THP1 cells. No decrease in bacterial counts were observed (**p<0.005, two tailed non parametric t-test, mean, s.e.m., n=3) **(C) & (D)** CFU counts in above mentioned experiment upon INH treatment. CFU (log_{10}) per well shows gradual increase in bacterial death with increasing INH doses. Abundant $GlmU_{Mtb}$ expression in *Rv::glmU*$_{tet\text{-}on}$ infected THP1 cells (with ATc) does not affect INH efficacy on *Mtb* and gives similar results as *Rv* with increasing concentration of INH treatment for 3 days. (**p<0.005, two tailed non parametric t-test, mean, s.e.m., n=3). **(E)** Bar graph presents the cytoxicity of the Oxa33 on THP1 cells during the 3 days of treatment. Cell viability was checked with alamar blue based assay and absorbance at 570nm was plotted with increasing concentrations of Oxa33 inhibitor (n=3, mean).

treatment, treatment with Oxa33 only reduced the CFU in Rv infected THP1 cells but not in the *Rv::$glmU_{tet\text{-}on}$* infected cells (Fig 7.8A to D). These results suggest that the inhibition of mycobacterial growth by Oxa33 is specifically due to inhibition of endogenous $GlmU_{Mtb.}$

Finally, we analysed the efficacy of Oxa33 in clearing bacilli from infected lungs using a murine infection model. Oxa33 compound is highly hydrophobic in nature. After trying many solvents, we could successfully re-suspend it in 2.5% Tween-80. Prior to performing the experiments we examined the maximum dose tolerance and survival analysis to determine the toxicity (Fig 7.9A & B). Based on the data obtained we chose 50 mg / kg as the appropriate dose. Since it was difficult to predict the fate of Oxa33 during the process of digestion inside the stomach and intestine, we avoided using the oral administration route. We chose intra peritoneal route for administering the compound as the intravenous (I/V) injection of Tween80 (solvent) in the animals was known to cause hypersensitivity and anaphylactic shock [242, 243].

Next, we analysed the efficacy of Oxa33 in clearing bacilli from infected lungs using a murine infection model. Groups of mice were infected with *Rv* and we allowed the infection to establish for 28 days. 28 days post infection mice were treated with vehicle, INH, or Oxa33, for duration of 56 days. CFUs result show that compared with the vehicle-treated group where we observed a marginal increase in bacillary load, a significant reduction in the bacillary load was observed in the lungs of both, INH- and Oxa33-treated groups (~4 and 2.5 log fold, respectively) (Fig 7.10A). This was also reflected in the gross pathology and histopathology of lungs (Fig 7.10B, Table 7.1). CFUs from spleen represent almost 10 times reduction of bacillary load in spleen upon Oxa33 treatment (Fig 7.10C). Although *in vitro* MBC values of Oxa33 was ~150 µM (60 µg/ml), it seems to be a relatively more efficacious *in vivo*, which could be due to its accumulation in the lungs of infected mice. To investigate this possibility, uninfected mice were treated with 50 mg/kg Oxa33 for a period of 3 weeks or 8 weeks. In order to estimate the concentration of Oxa33 in the lung, we first determined the absorbance spectra for Oxa33, which gave a clear peak at 401 nm (data not shown). We determined the A_{401} at different concentrations of Oxa33 and the standard curve was plotted (Fig 7.11A &B). Oxa33

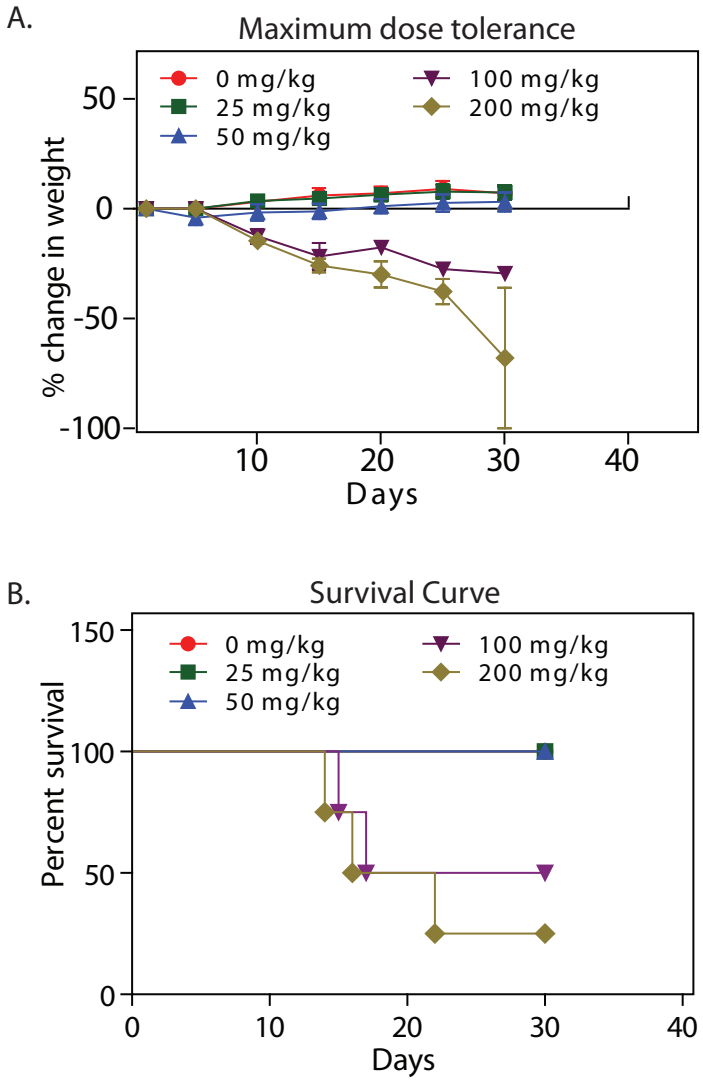

Figure 7.9 Dose tolerance and mice survival curves: (A) Maximum dose tolerance graph showing relative change in body weight of mice (4 mice / group) during the course of Oxa33 administration for 30 days. **(B)** Survival curve of mice (4 mice / group) treated with different concentrations of Oxa33 for 30 days.

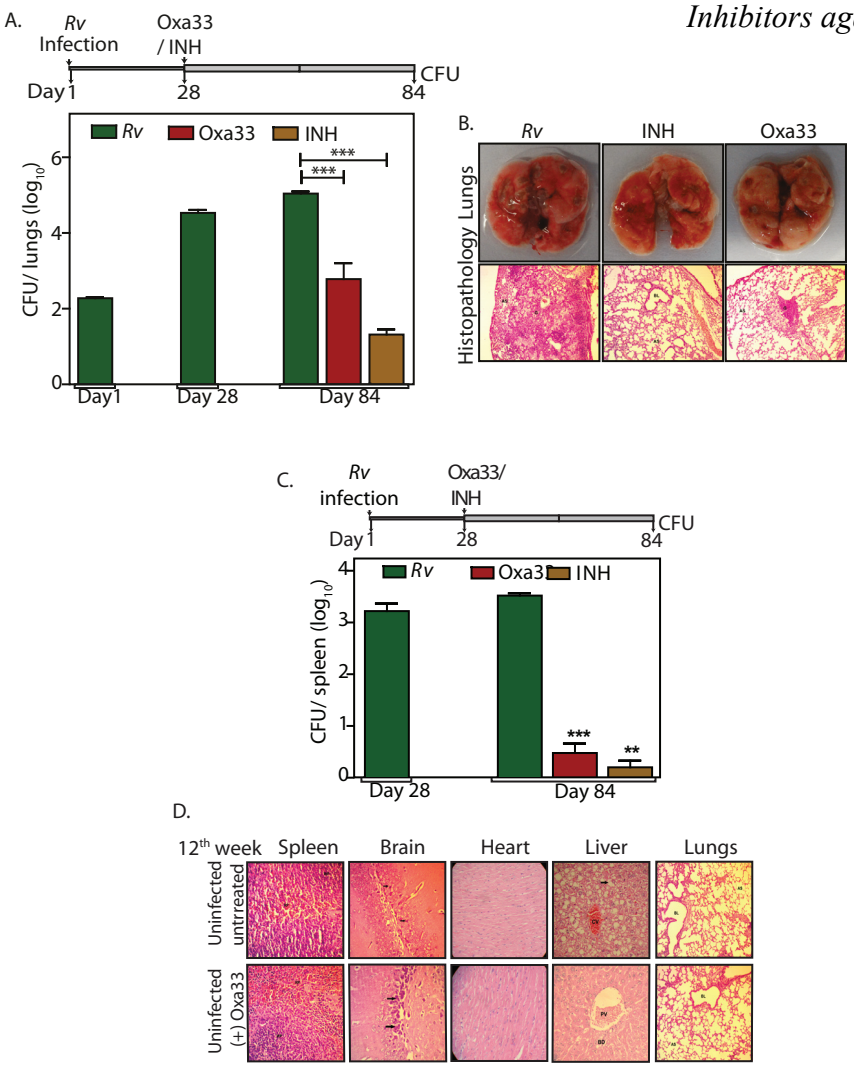

Figure 7.10. ***In vivo*** **efficacy and toxicity of Oxa33: (A)** CFUs of *Rv* infected BALB/c mice (for 28 days) were administered with Oxa33 or INH for a subsequent period of 56 days. Day 1st and day 28th CFUs show successful implantation and establishment of infection, respectively. 56 days of Oxa33 or INH treatment partially reduces the mean bacillary load to 2.78 and 1.3 on $\log_{10}$ scale. ***p<0.0005 or 0.0006, two tailed non parametric t-test, mean, s.e.m., n=6 to 11. **(B)** While the overall pathology of lungs (upper panel) illustrates robust *Mtb* infection in untreated mice, relatively smaller and fewer lesions and granuloma were observed in Oxa33 or INH treated mice. Lower panel exhibit haematoxylin and eosin stained photomicrograph of lungs from *Rv*, INH treated and Oxa33 treated mice at 100x magnification. This histopathological analysis shows large or small granuloma with lymphocytes and foamy histiocytes in *Rv* infected mice or Oxa treated mice respectively G = Granuloma, BL = Bronchial Lumen, AS = Alveolar space. **(C)** *Mtb* bacterial load in the spleen of totally infected mice (for 28 days) and treated with Oxa33 or INH for subsequently 56 days. ***p<0.0007 or **p<0.002, two tailed non parametric t-test, mean, s.e.m., n=7 to 11. **(D)** High power (400x) photomicrograph of haematoxylin and eosin stained spleen, brain, heart, liver and lungs of untreated mice or mice treated with Oxa33 for 56 days. Spleen is showing usual parenchyma. WP = White Pulp, RP = Red Pulp. While, section from hippocampus area of brain showing degenerated neurons in the neuronal layer. Section of heart is showing normal cardiac muscle fibres. Photomicrograph of liver depicts typical hepatic parenchyma. PV = Portal Vein, BD = Bile Duct. Lung section also represents usual lung parenchyma. BL = Bronchial Lumen, AS = Alveolar space.

was extracted from the lungs and its concentration was determined. The concentrations of Oxa33 in the lungs were in the range of ~200-300 µg /lungs at 3 weeks and ~800-1300 µg/lungs at 8 weeks (Fig 7.11C). The accumulation of Oxa33 in the lungs is ~13 to 18 fold higher than the MBC values, which may be the reason for higher potency of Oxa33 *in vivo* compared with *in vitro* experiments. In parallel to these experiments the lungs, spleen, liver, brain and heart of these uninfected but treated mice were subjected to histology analysis (Fig 7.10D & Table 7.2). These results indicate that Oxa33 does not have deleterious side effects on mice. Taken together, the results presented in this study establish $GlmU_{Mtb}$ to be an effective target against which new sets of inhibitors may be developed.

Table 7.1: Histological analysis of uninfected mice treated with Oxa33 for 56 days.

Group (mice)	**Bacterial strains/ treatment**	**Organs**	**No. of granuloma without necrosis, Score : 2.5**	**Total granuloma score**
4th week	*Rv*	Lungs	3	7.5
12th week	*Rv*	Lungs	4	10
	Rv + Oxa33	Lungs	1	2.5
	Rv + INH	Lungs	1	2.5
	Uninfected	Lungs	0	0
	Uninfected + Oxa33	Lungs	0	0

Table 7.2: Granuloma scores of the infected mice lungs.

Group (mice)	**Bacterial strains/ treatment**	**Organs**	**Any types of granuloma**	**Damage signs**
12th week	*Uninfected*	Spleen	0	Within normal limits
	Uninfected + Oxa33	Spleen	0	Within normal limits
	Uninfected	Brain	0	Within normal limits
	Uninfected + Oxa33	Brain	0	Degenerated neurons in dentate gyrus
	Uninfected	Heart	0	Within normal limits
	Uninfected + Oxa33	Heart	0	Within normal limits
	Uninfected	Liver	0	Within normal limits

A.

Oxa33 µg/ml	OD 401 nm			Average
	A	B	C	
2.5	0.137	0.13	0.127	0.131
5	0.253	0.247	0.254	0.251
10	0.55	0.556	0.543	0.55
20	1.006	0.946	1.021	0.991
30	1.549	1.5	1.54	1.53
40	1.94	1.98	1.92	1.95

B.

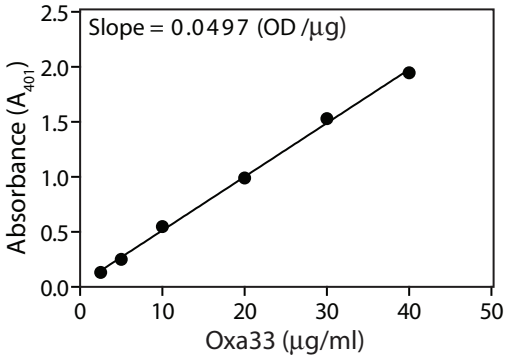

C.

Time	Lungs	Conc in µg/ lungs
3 weeks	L1	205.82
	L3	372.05
8 weeks	L2	886.60
	L3	834.53
	L4	1303.17
	L5	917.10
	L6	840.45

Figure 7.11 Standard curve for Oxa33 and its estimation in treated mice lungs: (A) We first determined the absorbance spectra for Oxa33 resuspended in tetrahydrofuran (THF). It showed a peak at 401 nm (data not shown). Absorbance readings (401 nm; performed in triplicates; A, B and C) of Oxa33 at different concentrations **(B)** Standard curve of Oxa33 showing linear regression with a slope of 0.0497 OD / µg. **(C)** Table showing Oxa33 concentrations (µg/lungs) in the lungs of mice treated with 50 mg /kg (body weight) for 3 or 8 weeks.

7.2.2 Uridyltransferase active site inhibitors.

7.2.2.1 Computational results.

The crystal structure of $GlmU_{Mtb}$ was processed for addition of hydrogen, bond order correction etc. Water molecules that interact with GlcNAc-1-P and UTP and which are present around 5 Å of these substrates were retained so as to maintain the thermodynamic stability. GlcNAc-1-P was found to be interacting with many active site residues such as Arg19, Thr89, Gly151, Glu166, Asn181 and Asn239 along with four water molecules and a co-ordinate covalent bond with Mg^{+2} 496. In case of UTP, the triphosphate tail was found to be stabilized by polar contacts with Gly17, Thr18, Arg19, one water molecule and three coordinate covalent bonds with Mg^{+2}1 and one with Mg^{+2} 496 (Fig 7.12 A**)**. The pyrimidine moiety was found to be involved in strong hydrophobic interactions with Leu12, Ala14, Val55, Pro86, Leu87 and Ala92 along with polar contacts with Ala14, Gln83 and Gly88. GlcNAc-1-P and UTP were docked to their respective sites in $GlmU_{Mtb}$ in order to validate the docking protocol followed in the present work. GlcNAc-1-P was found with XP score of 9.96 and an RMDS of 0.46 Å with respect to its crystal structure conformation. UTP docking resulted in 14.32 XP score with an RMDS of 1.06 Å with respect to its crystal conformation. The virtual screening workflow operated against Asinex database, in search of $GlmU_{Mtb}$ uridyltransferase site targeting inhibitors, resulted in many compounds, out of which 25 compounds were selected against GlcNAc-1-P site and 52 against UTP site based on the interacting behaviour of the compounds and their docking scores in comparison to the substrates (Fig 7.12B**)**. The final selected compounds were also docked using AutoDockVina and GOLD. Based on the AutoDockVina predicted binding affinity (in kcal/mol) values and GOLD score, 5 molecules were shortlisted against GlcNAc-1-P and 22 compounds were selected against UTP site which were further subjected to various docking algorithms.

The consideration of a rigid receptor, during docking calculations, does not often results in the precise binding pattern of a compound at the active site. This is because the protein often undergoes some conformational modifications upon ligand binding in reality. This can be attributed to the flexibility of the active site residues mainly corresponding to their side chains. This is considered as induced fit process,

A.

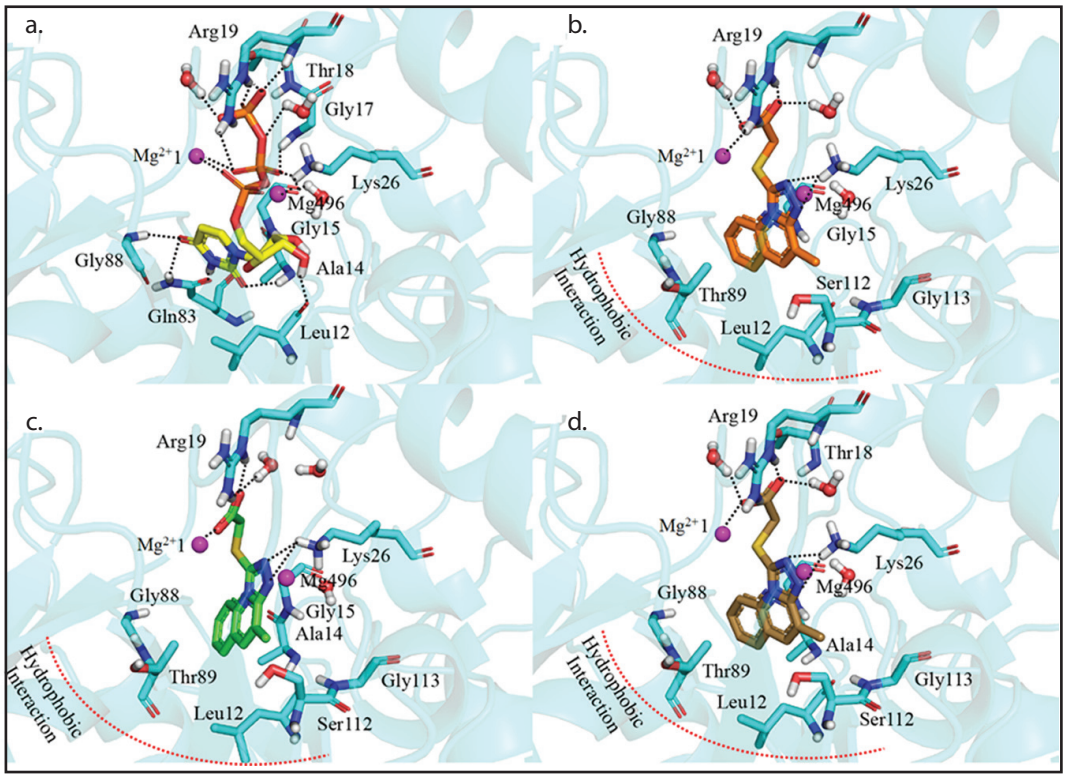

B.

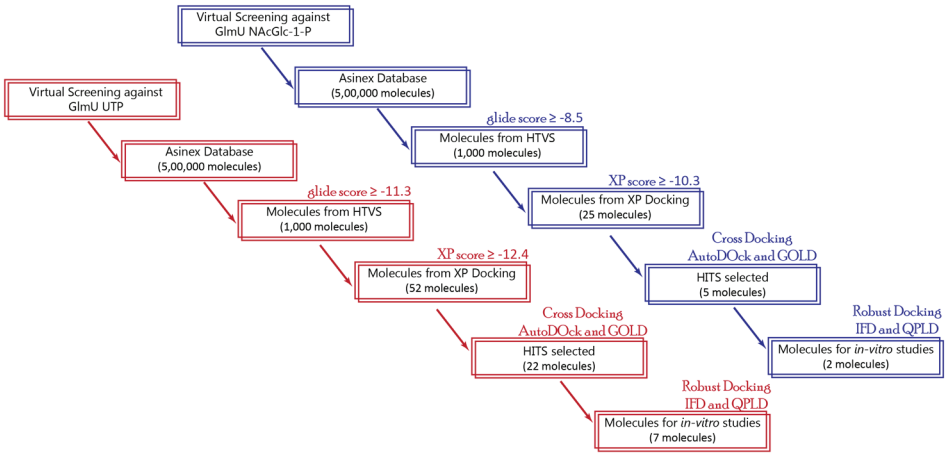

Figure 7.12. UTP binding pocket and development of uridyltransferase inhibitors against $GlmU_{Mtb}$: (A) a. UTP shown at the binding pocket of $GlmU_{Mtb}$ uridyltransferase site. Interaction pattern of compound 4 at UTP binding site using different docking protocols like **b.** Rigid docking. **c.** Induced Fit Docking (IFD) and **d.** Quantum Polarized Ligand Docking (QPLD). **(B)** Schematic representation of the *in silico* virtual screening procedure of small molecules inhibitors against $GlmU_{Mtb}$ GlcNAc-1-P and UTP binding sites.

which plays a vital role while developing inhibitors using structure based design approach. Hence in this study, the compounds were subjected to induced fit docking (IFD) so as to study their binding characteristics with protein. Visualizing the IFD results, the consideration of flexibility of active site residues of $GlmU_{Mtb}$ provide valuable insight for inhibitor design. The molecular docking of GlcNAc-1-P using a flexible protein ($GlmU_{Mtb}$) resulted in minor fluctuations in the residues position at the active site. The residues Arg19 and Tyr150 were observed to fluctuate with RMDS of 0.3-0.4 Å and the substrate binding resulted in 0.4 Å deviations with an IFD XP score of -11.88. In contrast, IFD docking of UTP at its binding site revealed the site to be flexible when compared to that of GlcNAc-1-P. The heavy atoms present around UTP up to 5Å were found to be fluctuating with RMDS of 1-1.3Å with an IFD XP score of -13.37 for UTP. These residues include Pro16, Arg19, Pro86, and His91 mainly. The most notable difference was found with $Mg^{+2}1$ ion which was found with deviation around 1.5-2.5 Å among various conformations. These deviations resulted in some additional interactions of $Mg^{+2}1$ such as a cation-π interaction with some compounds when docked.

The selected 5 compounds against GlcNAc-1-P were proceeded to induce fit docking where the results showed two compounds out of five were showing the best results and were retaining the key interactions with an RMDS of 0.4-0.8Å. The compounds 1 and 2 were found interacting with key residues like Arg19, Gly151, Asn181, Asn239 and were found to be involved in coordinate covalent bond with Mg 496. The induced fit docking of 22 compounds at the UTP site resulted in 9 best compounds, which were involved in polar contacts with Arg19, Lys26 and were found to retain interactions with Mg 1.

Current research has proved the importance of accuracy of electric charges of ligand in the protein-ligand docking, for which the quantum polarized ligand docking (QPLD) is developed. The use of quantum mechanics/molecular mechanics (QM/MM) method resulted in considerably improved insights about the electronic interactions of ligand by recalculating its partial charges in static MM charges field (protein). This includes the polarization effect of protein over the ligand. To validate QPLD docking procedure, GlcNAc-1-P and UTP were docked at their respective sites using $GlmU_{Mtb}$ crystal structure.

Table 7.3: Comparative docking scores of selected compounds calculated with GlmU$_{Mtb}$ receptor using various docking protocols.

Compounds	XP score	IFD XP score	QPLD XP score	AutoDockVina binding affinity (kcal/mol)	GOLD score
GlcNAc-1-P*	-9.96	-11.885	-11.65	-5.3	21.39
Compound 1	-10.44	-12.39	-9.42	-6.3	32.14
Compound 2	-9.02	-9.39	-8.26	-5.8	25.78
UTP*	-14.32	-13.37	-13.64	-6.3	65.61
Compound 3	-14.58	-14.14	-11.98	-5	47.09
Compound 4	-13.37	-12.92	-11.79	-8.6	43.8
Compound 5	-13.16	-11.45	-11.63	-5.9	47.12
Compound 6	12.77	-11.93	-10.74	-7.1	47.38
Compound 7	-12.49	-11.82	-11.44	-6.1	40.86
Compound 8	-12.36	-9.94	-11.25	-7.8	36.32
Compound 9	-12.20	-11.03	-10.48	-6.8	46.48

*The substrates GlcNAc-1-P and UTP were also docked for reference.

The retention of most of the polar contacts at the active site by GlcNAc-1-P, as that of crystal structure, with an RMDS of 0.59Å showed the efficiency and accuracy of QPLD algorithm. GlcNAc-1-P was found with QPLD docking score of -11.65. Similarly, UTP docking results were found to be in correlation when compared with crystal structure with RMDS of 0.94Å and QPLD XP score of -13.649. The selected compounds from HTVS and XP docking were subjected to QPLD docking and resulted in good glide score (Table 7.3).

Many compounds were found to preserve important interactions as that found in crystal structure, based on which 2 compounds from GlcNAc-1-P and 7 from UTP site directed compounds were selected for further *in vitro* assays. The selected compounds were found to be with different scaffolds like quinoline, triazoloquinoline, benzofuran, benzimidazole, tetrazole, pyrimidine etc., which are chemically acceptable for drug development. The selected compounds were procured

A.

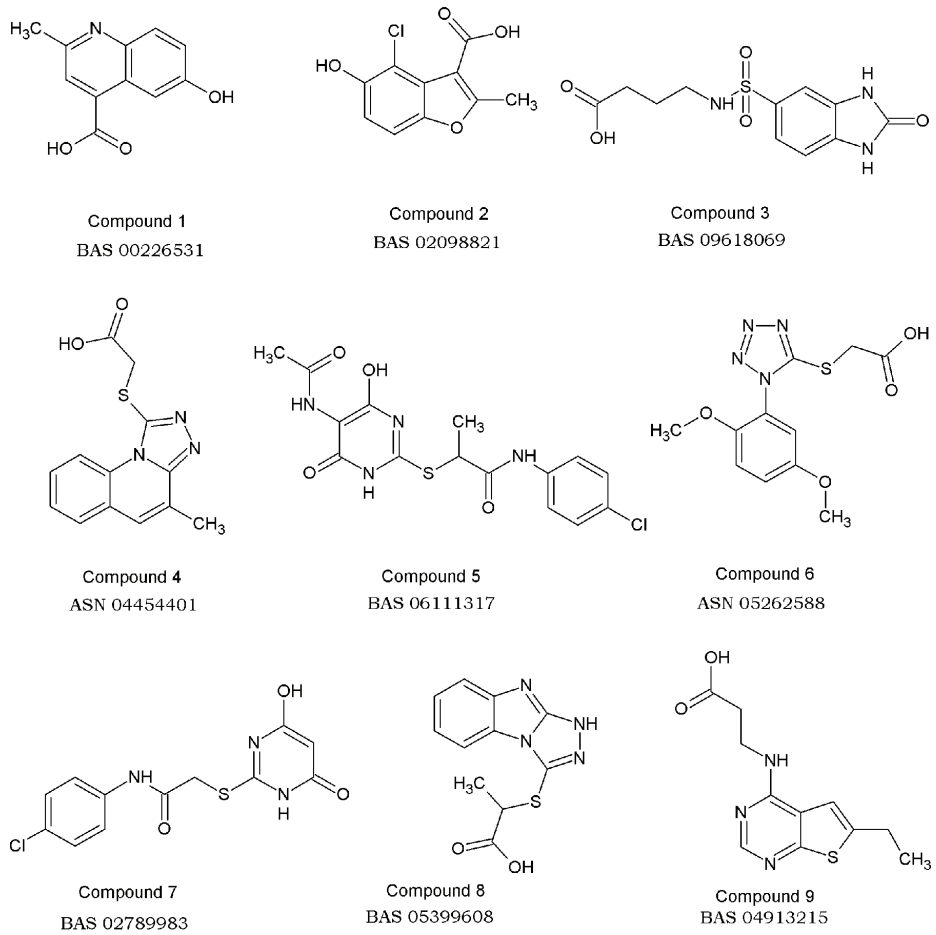

B.

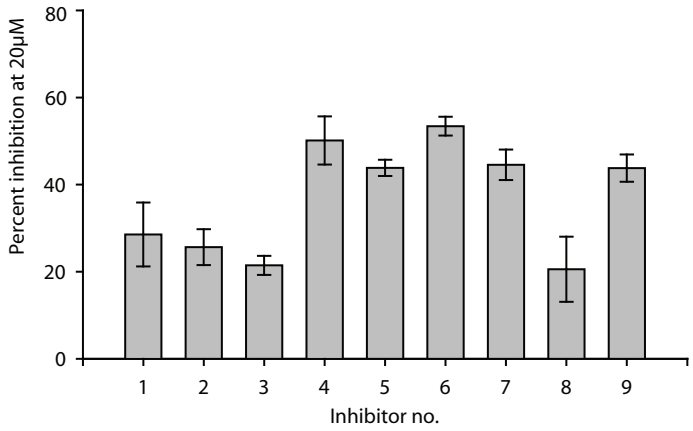

Figure 7.13. Structure of all Asinex inhibitors and their activity: (A) Structures of all nine compounds from Asinex database with their corresponding codes. **(B)** Plot showing percentage inhibition of $GlmU_{Mtb}$ when tested with the selected inhibitors. Percentage inhibition was done at 20 μM.

from Asinex database which are shown with their corresponding codes (Fig 7.13A). HPLC analysis showed that all the compounds 95% pure. These compounds were found to have good human oral absorption values as predicted by *in silico* pharmacokinetic property analyzer, QikProp. The results of same will be discussed in further sections.

7.2.2.2 Binding free energy analysis.

The binding free energies (using Prime-MMGB/SA) of all the selected compounds were carried out by using their protein-ligand complexes obtained from docking studies (Table 7.4). Considering the free energy of binding ($\Delta G_{Binding}$) values, compound **8** (-23.305 kcal/mol) and compound **4** (-25.791 kcal/mol) were found to be ligands with good binding affinity when compared to the rest. Mostly the binding ability of these two compounds can be attributed to their solvation energy due to surface area (ΔG bind Solv GB of 36 kcal/mol and 31.95 kcal/mol for compound **4** and compound **8** respectively). ΔG bind coulomb and ΔG bind vdW correspond to the non bonded binding energies due to coulomb and van der Waal interactions respectively. The van der Waals energy of binding is almost the same for both the compounds. The remaining compounds were found to possess less binding energy falling in the range from -31 kcal/mol to -52 kcal/mol. Of the selected 9 compounds, compounds 2, 5 and 9 were found to have least affinities (Table 7.4).

Table 7.4: Thermodynamics parameters computed using Prime-MMGB/SA for all the selected molecules.

Compounds	ΔG bind (kcal/mol)	ΔG bind Coulomb (kcal/mol)	ΔG bind vdW (kcal/mol)	ΔG bind Solv GB (kcal/mol)
Compound 1	-44.86	65.07	-25.09	-74.75
Compound 2	-52.66	-75.58	-15.23	52.26
Compound 3	-31.25	9.24	-43.34	15.33
Compound 4	-25.79	6.19	-45.12	36.00
Compound 5	-50.86	11.48	-52.39	19.28
Compound 6	-38.55	10.96	-46.51	17.32
Compound 7	-51.59	1.07	-42.12	11.86
Compound 8	-23.30	1.69	-41.50	31.95
Compound 9	-50.42	-2.99	-41.26	18.29

7.2.2.3 ADMET analysis.

Apart from the binding studies of the compounds and the protein, it is also important to analyze the pharmacokinetic properties of compounds. This is essential for determining their physical characteristics which are further significant in pharmaceutical studies. Hence, the selected 9 compounds were subjected to *in silico* ADMET analysis using QikProp *v*3.5. The compounds were computationally tested for many criterias such as Lipinski rule of five, percentage solubility, partition coefficient, permeability prediction of compounds through various cell lines etc. All the compounds fall in the acceptable ranges for most of the examined criteria (Table 7.5). The compounds were found to have poor permeability with MDCK cell line, which accounts for their poor blood brain barrier passage. All the compounds were found to possess adequate human oral absorption (67% - 78%).

Table 7.5: *In silico* predicted ADMET properties of the selected 9 compounds.

Compound	SASA	QPlogBB	QPlogHERG	QPPCaco	QPPMDCK	% Human Oral Absorption	QPlogKp
1	412.48	-0.92	-2.20	69.63	35.31	67.78	-3.79
2	396.97	-0.48	-1.81	147.19	148.90	76.19	-3.26
3	533.82	-2.91	-2.94	2.06	0.79	29.80	-6.54
4	496.08	-0.94	-2.86	85.49	58.10	77.89	-3.37
5	667.69	-1.80	-5.90	104.38	158.62	74.70	-4.14
6	528.28	-1.54	-2.64	31.76	18.90	62.68	-4.38
7	559.20	-1.44	-5.56	134.54	220.30	74.25	-3.89
8	440.98	-0.96	-1.95	51.87	38.56	69.16	-3.92
9	497.88	-1.05	-2.60	87.93	74.92	77.37	-3.52

Properties and Ranges: **SASA** – Predicted Solvent Accessible Surface Area in $Å^2$ (300-1000). **QPlogBB** – Predicted brain/blood partition coefficient (-3.0 to 1.2). **QPlogHERG** – Predicted IC50 value for HERG K+ channels (concern below -5). **QPPCaco** – Predicted apparent Caco-2 cell (model for gut-blood barrier) permeability in nm/s (<25 – poor, >500 – great). **QPPMDCK** - Predicted apparent MDCK cell (model for blood-brain barrier) permeability in nm/s (<25 – poor, >500 – great). **QPlogKp** – Predicted skin permeability (-8.0 to -1.0).

7.2.2.4 In vitro analysis.

In order to check the enzymatic activity of selected molecules, $GlmU_{Mtb}$ was purified with His_6 tag purification method. Malachite green based inorganic phosphate detection kit was used for inhibition studies. Substrate concentration was chosen based on K_m values of published data [3, 99]. A range finding assay was

performed to determine the enzyme concentration (limiting concentration of enzyme where it follows *Michaelis–Menten* kinetics) at which it converts only 30% to 40% substrate into product. Inhibition studies were performed at 20 μM of compound concentration and percent inhibition was calculated with reference to the activity of $GlmU_{Mtb}$ protein in the presence of buffer containing 5% DMSO only (Fig 7.13B). Results show that inhibition was ranging from 22% to 54% in the enzyme activity. The IC_{50} value for compound **4** was determined as only this compound showed better ITC results. The compound was found with an IC_{50} of 42.07 μM against $GlmU_{Mtb}$ (Fig 7.14A).

ITC experiments were performed to calculate different binding parameters of $GlmU_{Mtb}$ with lead inhibitor out of all nine selected compounds. Compound 4 showed better solubility and gave stable ITC binding isotherm. Therefore, we chose to determine various thermodynamic parameters of compound 4 interaction with $GlmU_{Mtb}$. Analysis of binding isotherm (Fig 7.14B) suggests that compound 4 is showing same two site pattern of binding as it was observed for UTP ($K_d = 5.8\times10^{-1}$ μM) (data not shown). This compound was found to bind $GlmU_{Mtb}$ with sufficiently high binding affinity with $K_a = 1.34 \times 10^7$ M^{-1} ($K_d = 7.46\times10^{-2}$ μM) and binding stoichiometry was found n = 0.876. This binding was majorly entropy driven with $T\Delta S$ = 9268 cal/mol and exothermic enthalpy change ΔH = -444.0 cal/mol. All thermodynamic parameters for compound 4 showed a better binding pattern than that of UTP. This observation was found to correlate with *in silico* binding energy data of compound **4** which was found with considerably high binding energy (-25 kcal/mol) towards uridyl site of $GlmU_{Mtb}$. This observation can be considered as one of the support for the use of computational study as a valid starting point in the drug discovery process.

7.2.2.5 Molecular Dynamics Analysis.

Based on the outcome of ITC experiments, compound **4** which showed a better binding pattern than the substrate UTP was considered for further computational elucidation using molecular dynamics simulations. The binding pattern of compound **4** using rigid docking induced fit docking and QPLD docking are shown in fig 7.12b, c and d respectively which also support the above results. A simulation of 10 ns was run for compound 4 bound $GlmU_{Mtb}$ complex in an attempt

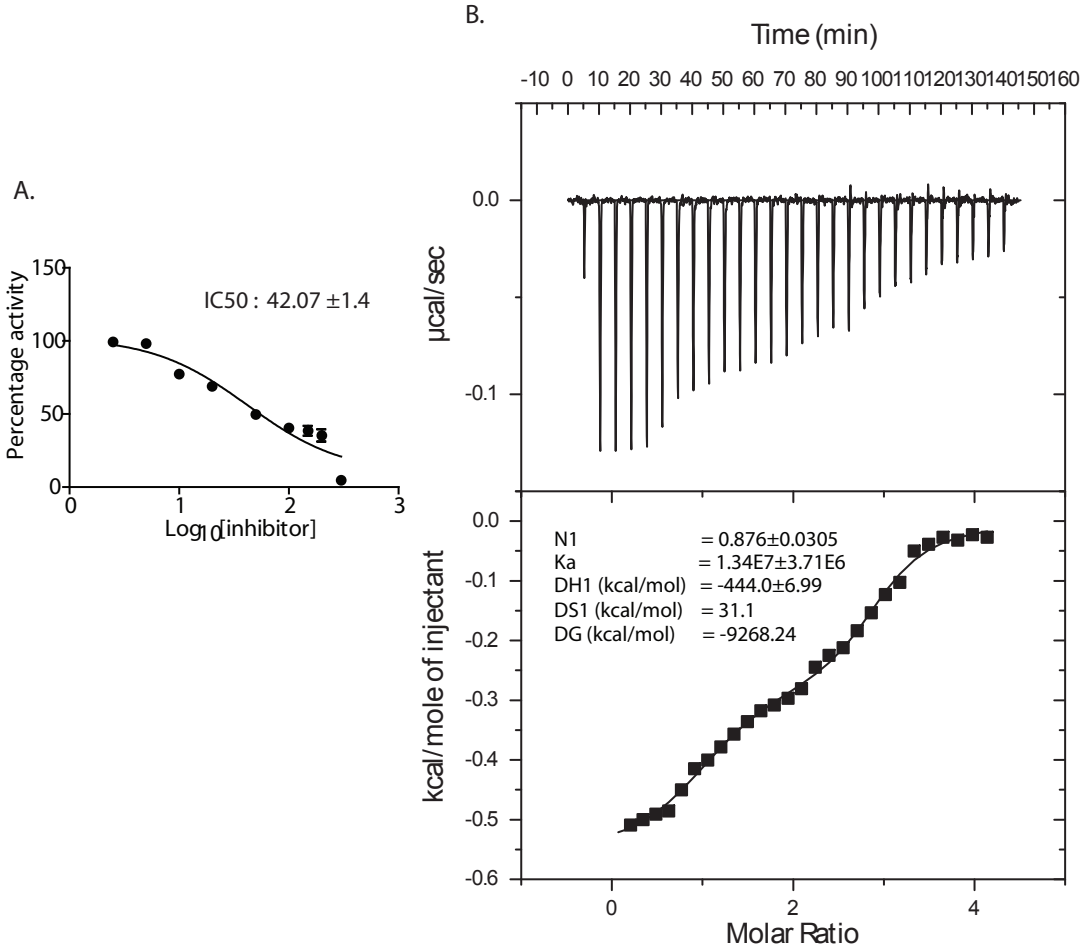

Figure 7.14. Characterization of compound no. 4 : (A) IC_{50} value determination of compound no. 4 against $GlmU_{Mtb}$. Percentage activity is plotted against $\log_{10}$ value of inhibitor concentrations. **(B)** Isothermal titration calorimetry experiment for compound 4 with $GlmU_{Mtb}$ ($K_d = 7.46\times10^{-2}$ µM). Released heats at different time points are plotted on the top and representative fitted two-site binding isotherm is depicted at the bottom.

to analyze its stability in dynamic circumstances. The crystal structure of $GlmU_{Mtb}$ with both the substrates (GlcNAc-1-P and UTP) was also run for 10 ns simulation, with the aim of comparing the active site dynamicity and fluctuations.

Fig 7.15A shows the RMDS plot of compound 4 bound $GlmU_{Mtb}$ complex in comparison with $GlmU_{Mtb}$ crystal structure with substrates considering different atoms for analysis. Root mean square deviation (RMDS) is a parameter which explains the deviation of one object to another. In compound **4**-$GlmU_{Mtb}$ complex, the side chain and backbone atoms of protein were found to comprise similar fluctuations which can be observed through their RMDS plots. The crystal structure was also found to have same behavioural pattern particularly at the uridyltransferase site, which can be depicted clearly from the plots, elucidating that the compound **4** was bound in similar fashion as that of UTP. Early jump in RMDS of both the $GlmU_{Mtb}$ complexes during the initial time scale of simulation shows the relaxation of the protein complexes. Though there were fluctuations during 2-4 ns simulation, the complex was found to be stabilized after that and remained stable till 10 ns. The protein-ligand complexes from the $GlmU_{Mtb}$ compound **4** simulation trajectories were collected at regular intervals of time so as to analyze the active site fluctuations. These protein structures when superimposed showed RMDS in the range of 1.1 - 1.7 Å (Fig 7.15B a). The active site analysis showed some positive indications which can support the compound **4** binding efficiency. In all the complexes collected, the crucial residues of uridyl site such as Arg19, Lys26 and Gln83 were found to be stable with least fluctuations. The compound was found to be consistently participating in hydrogen bonding with Arg19 and Lys26. Interestingly, another important observation found was that Mg^{2+} 1 was involved in metal ion coordination with one of the oxygen atom of carboxyl group of ligand. Also Mg^{2+} 1 was found to be involved in cation-π interaction with the triazole ring of ligand throughout the simulation time period. The position of Mg^{2+} 1 was found to be fluctuating with an RMDS of 1.1 - 1.5 Å and was seen close to the carboxyl group of ligand in all the conformations which shows the continuous binding of ion to the ligand. Tight binding of compound **4** with Mg^{2+} 1 is one of the crucial processes to make the $GlmU_{Mtb}$ protein unavailable for its biological catalysis.

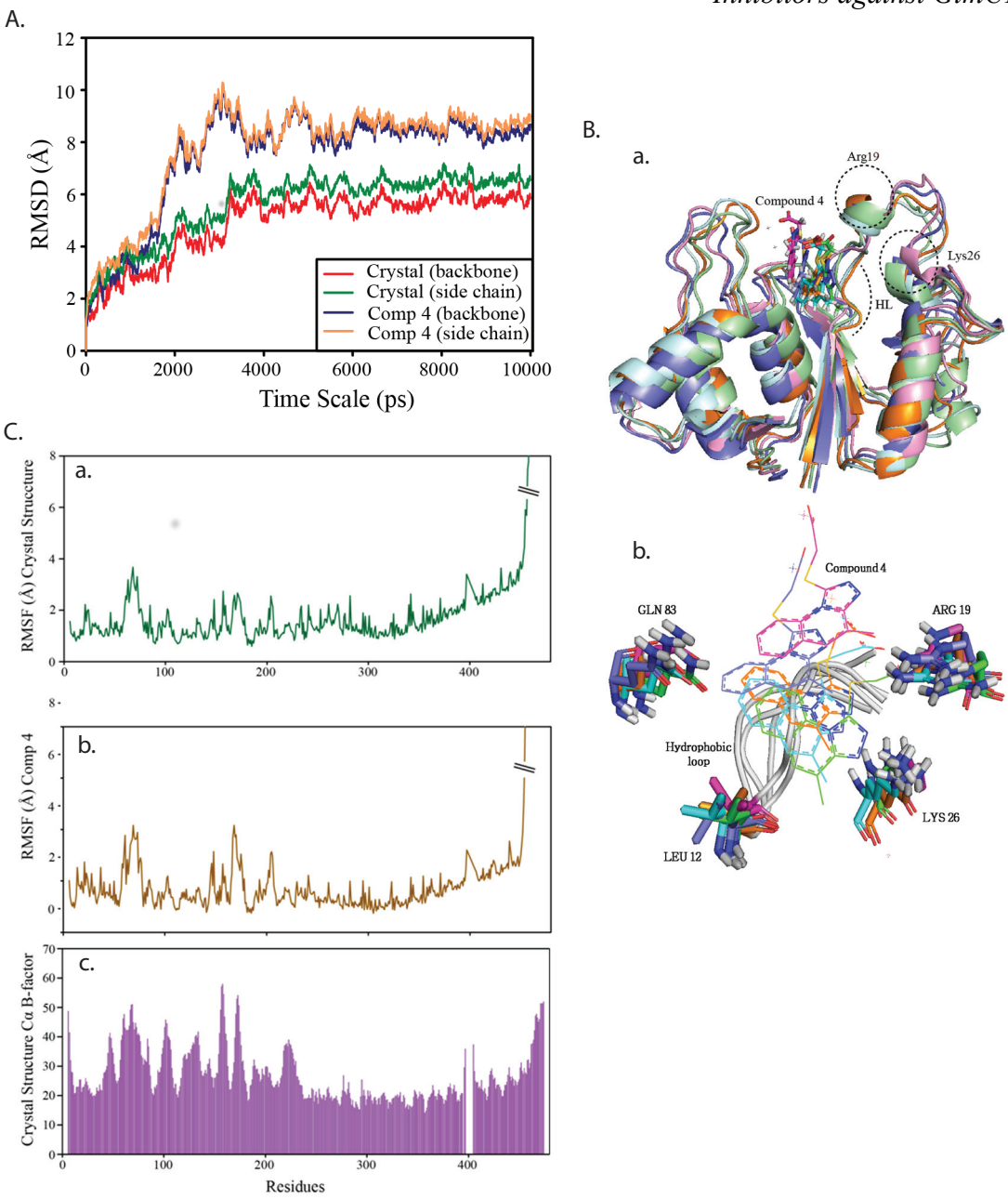

Figure 7.15. Molecular dynamic simulation study of compound 4 with $GlmU_{Mtb}$: (A) RMSD plot for $GlmU_{Mtb}$ in its bound state with substrates (GlcNAc-1-P and UTP) and with compound 4 at its uridyltransferase site. **(B) a.** Superimposition of $GlmU_{Mtb}$ compound 4 protein complex structures collected at different time intervals during simulation showing crucial active site residues of uridyltransferase active site. HL represents the hydrophobic loop at the active site. **b.** The superposition of protein structures showing the fluctuations of compound 4, active site residues, hydrophobic loop (represented in grey colour) and Mg^{2+} 1 during simulation. Different colours indicate different protein-ligand complex structures collected during simulation. **(C) a.** RMS fluctuations for each amino acid residue for a $GlmU_{Mtb}$ protein complex with substrates. **b.** $GlmU_{Mtb}$ protein bound with compound 4. **c.** Experimental B factor of $GlmU_{Mtb}$ which can be compared with the rms fluctuation of protein.

Another important force is the hydrophobic interactions of compound **4** at the active site which accounts for better binding efficiency of compound compared to UTP. The compound was observed to be binding non-polarly with the hydrophobic loop (HL) containing the residues LVLAAGPG (residue number 10 - 17), mainly Leu12, Ala14, Pro16. It was also seen interacting with Pro86 and Ala92. The loop was observed to be least fluctuating during the simulation (Fig. 7.15B b). Particularly, Leu12 was seen to be interacting consensually during the simulation. Overall analysis of RMDS data shows that the behaviour of compound **4** $GlmU_{Mtb}$ complexes was comparable to that of the $GlmU_{Mtb}$ crystal structure, accounting for the stabilization effect of compound **4** over $GlmU_{Mtb}$. This compound was also found to possess similar contacts at the active site as that of UTP.

In order to study the dynamic behaviour of protein ligand complex, the root mean square fluctuation (rmsf) analysis of protein complex with compound 4 was carried as a function of residue number (Fig 7.15C b). The rms fluctuation of $GlmU_{Mtb}$ crystal structure over 10 ns simulation was also analyzed as for comparative studies (Fig 7.15C a). The magnitude of fluctuation was found to be high at the C-terminal region of $GlmU_{Mtb}$ corresponding to terminal 20 residues.

The first 100 residues at the N-terminal region were closely analyzed as most of them form the binding pocket for UTP. This region was found to be stable except at residues ranging from 65-80, where low magnitude fluctuations were observed. This observation was found to be in correlation with the UTP bound $GlmU_{Mtb}$ complex. This shows that the compound 4 binding at the uridyl site has same properties in terms of rmsf as that of UTP binding at the active site. Most of the important residues fall under the residue range of 10 – 30 and 83. These regions were found to be stable with least fluctuations. The plot of experimental B factor of $GlmU_{Mtb}$ crystal as a function of residue number was also considered for comparison with rmsf data (Fig. 7.15C c). This data showed many similarities with the rms fluctuation during the simulation time period. The residues region with more fluctuations corresponded to the loops of the protein. These observations account for the good binding ability of compound **4**. Hence, it can be elucidated that the compound **4** serves as an initiative in the path of drug discovery against tuberculosis particularly towards the inhibition of $GlmU_{Mtb}$. It can also be considered that

computational resources can be well utilized for the drug discovery and optimization purposes as most of the results obtained from *in silico* studies were in correlation with the *in vitro* data in the present study.

7.3 Discussion.

In this chapter we demonstrated GlmU$_{Mtb}$ is a promising drug target for therapeutic intervention against TB. Having core function in *M.tb.* cell wall synthesis, GlmU$_{Mtb}$ is crucial both in normoxic and hypoxic growth stages (chapter 6). Both first line and second line of drugs from current tuberculosis regimen are recognized to target some cell wall synthesis enzymes. These include Isoniazid (targeting enoyl-[acyl-carrier-protein] reductase and inhibiting mycolic acid synthesis, Ethambutol (targeting arabinosyl transferase, inhibiting arabinogalactan biosynthesis), Ethionamide (targeting enoyl-[acyl-carrier-protein] reductase, inhibits mycolic acid synthesis) and Cycloserine (targets D- alanine recemase and ligase, inhibits peptidoglycan synthesis). But most of these drugs are unable to act against dormant or latent bacterial stages of tuberculosis. A long time treatment is required to eradicate the persistent form of the pathogen. Hence targeting GlmU$_{Mtb}$ (non-differentially regulated at any stage of growth) would be central to the next generation of therapeutic interventions against TB.

As described earlier, uridyltransferase site of GlmU$_{Mtb}$ was thought to be a good target site due to feedback inhibition by the product UDP-GlcNAc [171]. Earlier competitive, non-competitive and allosteric inhibitors targeting either activity of GlmU were reported in various organisms including *E.coli*, *H. influenza, S. pneumonia, X. oryzae* [162, 163, 170, 179, 180, 239-241]. UAP protein (final protein in UDP-GlcNAC synthesis) of *Trypanosoma brucei* was also targeted by allosteric site inhibitors [239]. But the specificity and the efficacy of these inhibitors, both in *ex vivo* or *in vivo* systems has never have been established. Here we have developed two different categories of inhibitors, one against the allosteric site and the other against substrate binding active site, impacting the uridyltransferase activity of GlmU$_{Mtb}$.

Allosteric inhibitors were designed and developed based on allosteric site inhibitor of *H. influenzae* GlmU [162]. Initially shape based inhibitor designing was used to procure 43 molecules from Asinex database and further one lead inhibitor

was selected to generate 53 different derivatives. From these, Oxa33 was used as final inhibitor to study in advance. We have confirmed its binding site on $GlmU_{Mtb}$ by MD simulations followed by mutational studies (Fig 7.5 & 7.6) and showed that Oxa33 is perturbing the conformation of the uridyltransferase active site by binding at the allosteric site and inhibiting it (Fig 7.6B & 7.4C). In order to demonstrate the specificity, $GlmU_{Mtb}$ was over-expressed in *Rv* (to generate *Rv::glmU*$_{tet\text{-}on}$) and MIC values for Oxa33 were determined both *in vitro* and *ex vivo* (Fig 7.7 & 7.8). Increased MICs in *Rv::glmU*$_{tet\text{-}on}$ strain compared with *Rv* suggests that Oxa33 specifically interacts and inhibits $GlmU_{Mtb}$. Administrating the Oxa33 to fully infected (28 days) mice resulted in partial ablation of pathogen load in the lungs. Most interestingly it was found that amount of Oxa33 accumulating in lungs is much higher (12 to 18 fold) as compared to MBC (150 µM i.e. equal to 60.75 µg/ml) of Oxa33 and this could be the reason behind efficacy of Oxa33.

Substrates of uridyltransferase domains have better affinity for the active site (chapter 5). Apo and product bound structures of $GlmU_{Mtb}$ have been described [161]. Considering these two aspects we sought to target the uridyltransferase domain. We have performed *in silico* studies and validated it with the help of different methodologies of docking like induced fit docking (IFD), quantum polarized ligand docking (QPLD), taking into account the flexibility of the active site residues and their partial charges. Various small molecules were characterized and confirmed the binding parameters with the help of ITC. Different thermodynamic factors were also determined with computational based methodology. Compound **4**, [(4-methyl[1,2,4]triazolo[4,3-*a*]quinolin-1 yl)sulfanyl]acetic acid was found to be one of such kind which showed a better binding affinity at UTP site over the substrate. This can serve as a valid starting point in development of novel $GlmU_{Mtb}$ inhibitors. Taken together we have identified lead compounds that would inhibit uridyltransferase activity of $GlmU_{Mtb}$ at different sites (active and allosteric sites). We have demonstrated the *in vitro* and *ex vivo* specificity of allosteric site inhibitor Oxa33 and identified the possible binding site. *In vivo* efficacy authenticates $GlmU_{Mtb}$ as a promising target for future therapeutic interventions against *M.tb*.

7.4 Conclusion.

In addition to the acetyltransferase and uridyltransferase active site pockets, $GlmU_{Mtb}$ also contains an allosteric site. Binding of any suitable molecule/inhibitor to the allosteric site would prevent the conformational change essential for $GlmU_{Mtb}$ uridyltransferase catalytic activity. To target the allosteric site on $GlmU_{Mtb}$ we drew on crystal structure data of *H. influenza* GlmU ($GlmU_{HI}$) bound to its allosteric small molecule inhibitor. The Asinex database was screened against shape as described and the resulting 43 hits were biochemically characterized for their ability to inhibit $GlmU_{Mtb}$ uridyltransferase activity. One of the promising molecules was used for further structural optimization. Of the 53 structurally optimized compounds one molecule, namely (4*Z*)-4-(4-benzyloxybenzylidene)-2-(naphthalen-2-yl)-1,3-oxazol-5(4*H*)-one (Oxa33), was found to be an efficient inhibitor of $GlmU_{Mtb}$ activity with an IC_{50} of 9.96 ± 1.1 μM. Docking and MD simulation studies revealed polar, non-polar and hydrophobic interactions between Oxa33 and the allosteric site residues. Oxa33 inhibited the *in vitro* growth of *M.tb. H37Rv* with a minimum inhibitory concentration (MIC) of ~75 μM (~30 μg / ml). To ascertain if this inhibitory effect was due to inhibition of $GlmU_{Mtb}$ activity we overexpressed $GlmU_{Mtb}$ in the cells prior to drug treatment and determined the effect of this on the MIC value. In concurrence with the *in vitro* growth data, overexpression of $GlmU_{Mtb}$ alleviated Oxa33-mediated clearance of *M.tb.* from THP-1 cells. Finally, we analysed the efficacy of Oxa33 in clearing bacilli from infected lungs using a murine infection model. The administration of Oxa33, a novel oxazolidine derivative that specifically inhibits $GlmU_{Mtb}$, to infected mice resulted in significant decrease in the bacillary load.

Inhibitors were also developed based on the substrates of uridyltransferase activity of $GlmU_{Mtb}$. Crystal structure information was used to design 9 compounds against UTP and GlcNAc-1-P. Extensive computational analysis and docking were performed to determine the various parameters of these compounds. Out of these 9 inhibitors, compound no 4 was showing IC_{50} of 42.02 μM with a better K_a value (1.34×10^7). Compound no. 4 can be pursued as a lead molecule which needs to be developed further to improve its efficacy.

Chapter 8.

Recapitulation and future perspectives

Chapter 8.

Recapitulation and future perspectives

Constant increase in occurrence of tuberculosis cases alarms us to start identification of new generation of inhibitors, drug targets and therapeutic approaches. Currently running DOTs therapy is not able to cure MDR and XDR strains of TB. The relative rate of increasing incidences of tuberculosis and discovery of new inhibitors; are on the flip side of the coin. Considering the crucial role of cell wall in bacterial pathogenesis and survival, targeting it would be effective for remedial approaches against tuberculosis. Therefore, the cell wall of mycobacteria is targeted by various drugs.

In this work we have validated the biochemical and biological importance of *M.tb.* GlmU and established it as a potential drug target. We have solved the crystal structure of *M.tb.* GlmU and determined its different biochemical and biophysical parameters. For biological studies, conditional gene mutant of GlmU in *M.tb.* was generated and its essentiality was checked by depleting it at various phases of growth and infection. Our study also established that both reactions of $GlmU_{Mtb}$ are essential and UDP-GlcNAc is required to maintain the dormancy. Next a new allosteric inhibitor, Oxa33, targeting *M.tb.* GlmU was also generated and the possible allosteric sites of binding were determined by MD simulation and mutational studies. Specificity of the Oxa33 towards $GlmU_{Mtb}$ was also confirmed followed by its efficacy in mice TB infection model.

Interestingly, possibility of any other salvage pathways assimilating GlcNAc from host or from cell wall recycling is an important question to address (Fig 8.1). After comparison with other bacterial salvage pathways we found that *M.tb.* also contains some important genes for GlcNAc reutilization and these can be mutated by genetic recombineering to further study their role (Fig 8.1). The exact mechanism of feedback inhibition of $GlmU_{Mtb}$, role of T156 and T418 phosphorylations in mycobacterial metabolism are important details to explore (Fig 8.1). Further, detailed QSAR study is also required to improve Oxa33 as a potential drug candidate.

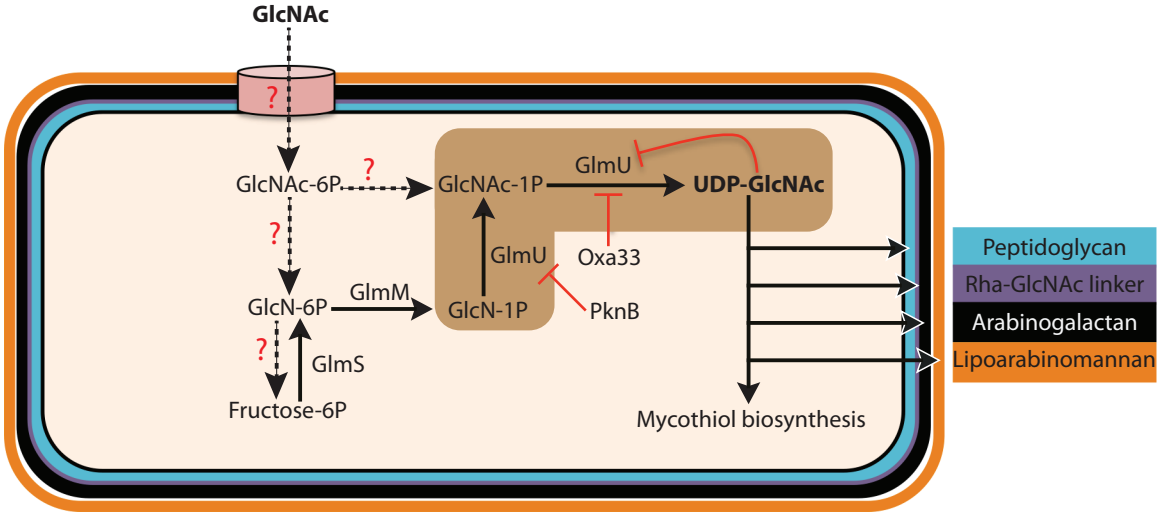

Figure 8.1. Model for the UDP-GlcNAc synthesis pathways in *Mtb*. Model shows *de novo* pathway for UDP-GlcNAc synthesis is mediate by GlmS, GlmM and GlmU enzymes. Shaded pathway is conserved in *Mtb*. UPD-GlcNAc can inhibit uridyltransferase activity by feedback inhibition mechanism. Also GlcNAc from host resources or from cell wall recycling can be transported inside the bacteria and further metabolized and feeded into the de novo pathways through GlmS/ GlmU mediated reactions. Question marks show that these pathways are still not characterized in *Mtb*. Dashed lines shows possible input of substrates or unknown pathway while complete lines shows established and known pathways for UDP-GlcNAc synthesis.

Bibliography.

Bibliography

1. Wirth, T., Hildebrand, F., Allix-Beguec, C., Wolbeling, F., Kubica, T., Kremer, K., van Soolingen, D., Rusch-Gerdes, S., Locht, C., Brisse, S., et al. (2008). Origin, spread and demography of the Mycobacterium tuberculosis complex. PLoS pathogens *4*, e1000160.
2. Gagneux, S. (2012). Host-pathogen coevolution in human tuberculosis. Philos Trans R Soc Lond B Biol Sci *367*, 850-859.
3. Jagtap, P.K., Soni, V., Vithani, N., Jhingan, G.D., Bais, V.S., Nandicoori, V.K., and Prakash, B. (2012). Substrate-bound crystal structures reveal features unique to Mycobacterium tuberculosis N-acetyl-glucosamine 1-phosphate uridyltransferase and a catalytic mechanism for acetyl transfer. J Biol Chem *287*, 39524-39537.
4. Verma, S.K., Jaiswal, M., Kumar, N., Parikh, A., Nandicoori, V.K., and Prakash, B. (2009). Structure of N-acetylglucosamine-1-phosphate uridyltransferase (GlmU) from Mycobacterium tuberculosis in a cubic space group. Acta Crystallogr Sect F Struct Biol Cryst Commun *65*, 435-439.
5. Sakamoto, K. (2012). The pathology of Mycobacterium tuberculosis infection. Vet Pathol *49*, 423-439.
6. Cardona, P.J. (2009). A dynamic reinfection hypothesis of latent tuberculosis infection. Infection *37*, 80-86.
7. Rodrigue, S., Provvedi, R., Jacques, P.E., Gaudreau, L., and Manganelli, R. (2006). The sigma factors of Mycobacterium tuberculosis. FEMS Microbiol Rev *30*, 926-941.
8. Honer Zu Bentrup, K., Miczak, A., Swenson, D.L., and Russell, D.G. (1999). Characterization of activity and expression of isocitrate lyase in Mycobacterium avium and Mycobacterium tuberculosis. J Bacteriol *181*, 7161-7167.
9. Glickman, M.S., Cox, J.S., and Jacobs, W.R., Jr. (2000). A novel mycolic acid cyclopropane synthetase is required for cording, persistence, and virulence of Mycobacterium tuberculosis. Mol Cell *5*, 717-727.
10. Ramakrishnan, L., Federspiel, N.A., and Falkow, S. (2000). Granuloma-specific expression of Mycobacterium virulence proteins from the glycine-rich PE-PGRS family. Science *288*, 1436-1439.
11. Gengenbacher, M., and Kaufmann, S.H. (2012). Mycobacterium tuberculosis: success through dormancy. FEMS Microbiol Rev *36*, 514-532.
12. Murphy, D.J., and Brown, J.R. (2007). Identification of gene targets against dormant phase Mycobacterium tuberculosis infections. BMC Infect Dis *7*, 84.
13. Mohan, V.P., Scanga, C.A., Yu, K., Scott, H.M., Tanaka, K.E., Tsang, E., Tsai, M.M., Flynn, J.L., and Chan, J. (2001). Effects of tumor necrosis factor alpha on host immune response in chronic persistent tuberculosis: possible role for limiting pathology. Infect Immun *69*, 1847-1855.
14. Flynn, J.L., and Chan, J. (2001). Tuberculosis: latency and reactivation. Infect Immun *69*, 4195-4201.

15. Nunes-Alves, C., Booty, M.G., Carpenter, S.M., Jayaraman, P., Rothchild, A.C., and Behar, S.M. (2014). In search of a new paradigm for protective immunity to TB. Nat Rev Microbiol *12*, 289-299.
16. Sharma, S.K., and Mohan, A. (2004). Extrapulmonary tuberculosis. Indian J Med Res *120*, 316-353.
17. Heifets, L.B., and Cangelosi, G.A. (1999). Drug susceptibility testing of Mycobacterium tuberculosis: a neglected problem at the turn of the century. Int J Tuberc Lung Dis *3*, 564-581.
18. David, H.L. (1970). Probability distribution of drug-resistant mutants in unselected populations of Mycobacterium tuberculosis. Appl Microbiol *20*, 810-814.
19. Zhang, Y., Heym, B., Allen, B., Young, D., and Cole, S. (1992). The catalase-peroxidase gene and isoniazid resistance of Mycobacterium tuberculosis. Nature *358*, 591-593.
20. Banerjee, A., Dubnau, E., Quemard, A., Balasubramanian, V., Um, K.S., Wilson, T., Collins, D., de Lisle, G., and Jacobs, W.R., Jr. (1994). inhA, a gene encoding a target for isoniazid and ethionamide in Mycobacterium tuberculosis. Science *263*, 227-230.
21. Mdluli, K., Slayden, R.A., Zhu, Y., Ramaswamy, S., Pan, X., Mead, D., Crane, D.D., Musser, J.M., and Barry, C.E., 3rd (1998). Inhibition of a Mycobacterium tuberculosis beta-ketoacyl ACP synthase by isoniazid. Science *280*, 1607-1610.
22. Wilson, T.M., and Collins, D.M. (1996). ahpC, a gene involved in isoniazid resistance of the Mycobacterium tuberculosis complex. Mol Microbiol *19*, 1025-1034.
23. Telenti, A., Imboden, P., Marchesi, F., Lowrie, D., Cole, S., Colston, M.J., Matter, L., Schopfer, K., and Bodmer, T. (1993). Detection of rifampicin-resistance mutations in Mycobacterium tuberculosis. Lancet *341*, 647-650.
24. Roy, A., Eisenhut, M., Harris, R.J., Rodrigues, L.C., Sridhar, S., Habermann, S., Snell, L., Mangtani, P., Adetifa, I., Lalvani, A., et al. (2014). Effect of BCG vaccination against Mycobacterium tuberculosis infection in children: systematic review and meta-analysis. BMJ *349*, g4643.
25. Andersen, P., and Doherty, T.M. (2005). The success and failure of BCG - implications for a novel tuberculosis vaccine. Nat Rev Microbiol *3*, 656-662.
26. Skeiky, Y.A., and Sadoff, J.C. (2006). Advances in tuberculosis vaccine strategies. Nat Rev Microbiol *4*, 469-476.
27. Horwitz, M.A., and Harth, G. (2003). A new vaccine against tuberculosis affords greater survival after challenge than the current vaccine in the guinea pig model of pulmonary tuberculosis. Infect Immun *71*, 1672-1679.
28. Conradt, P., Hess, J., and Kaufmann, S.H. (1999). Cytolytic T-cell responses to human dendritic cells and macrophages infected with Mycobacterium bovis BCG and recombinant BCG secreting listeriolysin. Microbes Infect *1*, 753-764.
29. Grode, L., Kursar, M., Fensterle, J., Kaufmann, S.H., and Hess, J. (2002). Cell-mediated immunity induced by recombinant Mycobacterium bovis Bacille Calmette-Guerin strains against an intracellular bacterial pathogen: importance of antigen secretion or membrane-targeted antigen display as lipoprotein for vaccine efficacy. J Immunol *168*, 1869-1876.

30. Skeiky, Y.A., Alderson, M.R., Ovendale, P.J., Guderian, J.A., Brandt, L., Dillon, D.C., Campos-Neto, A., Lobet, Y., Dalemans, W., Orme, I.M., et al. (2004). Differential immune responses and protective efficacy induced by components of a tuberculosis polyprotein vaccine, Mtb72F, delivered as naked DNA or recombinant protein. J Immunol *172*, 7618-7628.
31. Brandt, L., Skeiky, Y.A., Alderson, M.R., Lobet, Y., Dalemans, W., Turner, O.C., Basaraba, R.J., Izzo, A.A., Lasco, T.M., Chapman, P.L., et al. (2004). The protective effect of the Mycobacterium bovis BCG vaccine is increased by coadministration with the Mycobacterium tuberculosis 72-kilodalton fusion polyprotein Mtb72F in M. tuberculosis-infected guinea pigs. Infect Immun *72*, 6622-6632.
32. Doherty, T.M., Olsen, A.W., Weischenfeldt, J., Huygen, K., D'Souza, S., Kondratieva, T.K., Yeremeev, V.V., Apt, A.S., Raupach, B., Grode, L., et al. (2004). Comparative analysis of different vaccine constructs expressing defined antigens from Mycobacterium tuberculosis. J Infect Dis *190*, 2146-2153.
33. Weinrich Olsen, A., van Pinxteren, L.A., Meng Okkels, L., Birk Rasmussen, P., and Andersen, P. (2001). Protection of mice with a tuberculosis subunit vaccine based on a fusion protein of antigen 85b and esat-6. Infect Immun *69*, 2773-2778.
34. Lingnau, K., Egyed, A., Schellack, C., Mattner, F., Buschle, M., and Schmidt, W. (2002). Poly-L-arginine synergizes with oligodeoxynucleotides containing CpG-motifs (CpG-ODN) for enhanced and prolonged immune responses and prevents the CpG-ODN-induced systemic release of pro-inflammatory cytokines. Vaccine *20*, 3498-3508.
35. McShane, H., Pathan, A.A., Sander, C.R., Keating, S.M., Gilbert, S.C., Huygen, K., Fletcher, H.A., and Hill, A.V. (2004). Recombinant modified vaccinia virus Ankara expressing antigen 85A boosts BCG-primed and naturally acquired antimycobacterial immunity in humans. Nat Med *10*, 1240-1244.
36. Goonetilleke, N.P., McShane, H., Hannan, C.M., Anderson, R.J., Brookes, R.H., and Hill, A.V. (2003). Enhanced immunogenicity and protective efficacy against Mycobacterium tuberculosis of bacille Calmette-Guerin vaccine using mucosal administration and boosting with a recombinant modified vaccinia virus Ankara. J Immunol *171*, 1602-1609.
37. Rodrigues, L.C., Diwan, V.K., and Wheeler, J.G. (1993). Protective effect of BCG against tuberculous meningitis and miliary tuberculosis: a meta-analysis. Int J Epidemiol *22*, 1154-1158.
38. Zumla, A., Nahid, P., and Cole, S.T. (2013). Advances in the development of new tuberculosis drugs and treatment regimens. Nat Rev Drug Discov *12*, 388-404.
39. Cole, S.T., and Riccardi, G. (2011). New tuberculosis drugs on the horizon. Curr Opin Microbiol *14*, 570-576.
40. Koul, A., Arnoult, E., Lounis, N., Guillemont, J., and Andries, K. (2011). The challenge of new drug discovery for tuberculosis. Nature *469*, 483-490.
41. Barry, C.E., 3rd, Boshoff, H.I., Dartois, V., Dick, T., Ehrt, S., Flynn, J., Schnappinger, D., Wilkinson, R.J., and Young, D. (2009). The spectrum of

latent tuberculosis: rethinking the biology and intervention strategies. Nat Rev Microbiol *7*, 845-855.

42. Smith, I. (2003). Mycobacterium tuberculosis pathogenesis and molecular determinants of virulence. Clin Microbiol Rev *16*, 463-496.
43. Cole, S.T., Brosch, R., Parkhill, J., Garnier, T., Churcher, C., Harris, D., Gordon, S.V., Eiglmeier, K., Gas, S., Barry, C.E., 3rd, et al. (1998). Deciphering the biology of Mycobacterium tuberculosis from the complete genome sequence. Nature *393*, 537-544.
44. Blouin, Y., Hauck, Y., Soler, C., Fabre, M., Vong, R., Dehan, C., Cazajous, G., Massoure, P.L., Kraemer, P., Jenkins, A., et al. (2012). Significance of the identification in the Horn of Africa of an exceptionally deep branching Mycobacterium tuberculosis clade. PLoS One *7*, e52841.
45. Comas, I., Coscolla, M., Luo, T., Borrell, S., Holt, K.E., Kato-Maeda, M., Parkhill, J., Malla, B., Berg, S., Thwaites, G., et al. (2013). Out-of-Africa migration and Neolithic coexpansion of Mycobacterium tuberculosis with modern humans. Nat Genet *45*, 1176-1182.
46. Warner, D.F., and Mizrahi, V. (2013). Complex genetics of drug resistance in Mycobacterium tuberculosis. Nat Genet *45*, 1107-1108.
47. Reed, M.B., Pichler, V.K., McIntosh, F., Mattia, A., Fallow, A., Masala, S., Domenech, P., Zwerling, A., Thibert, L., Menzies, D., et al. (2009). Major Mycobacterium tuberculosis lineages associate with patient country of origin. J Clin Microbiol *47*, 1119-1128.
48. Cooper, A.M. (2009). Cell-mediated immune responses in tuberculosis. Annu Rev Immunol *27*, 393-422.
49. Flynn, J.L., and Chan, J. (2001). Immunology of tuberculosis. Annu Rev Immunol *19*, 93-129.
50. North, R.J., and Jung, Y.J. (2004). Immunity to tuberculosis. Annu Rev Immunol *22*, 599-623.
51. Alcais, A., Fieschi, C., Abel, L., and Casanova, J.L. (2005). Tuberculosis in children and adults: two distinct genetic diseases. J Exp Med *202*, 1617-1621.
52. Alcais, A., Quintana-Murci, L., Thaler, D.S., Schurr, E., Abel, L., and Casanova, J.L. (2010). Life-threatening infectious diseases of childhood: single-gene inborn errors of immunity? Ann N Y Acad Sci *1214*, 18-33.
53. Flynn, J.L., Goldstein, M.M., Chan, J., Triebold, K.J., Pfeffer, K., Lowenstein, C.J., Schreiber, R., Mak, T.W., and Bloom, B.R. (1995). Tumor necrosis factor-alpha is required in the protective immune response against Mycobacterium tuberculosis in mice. Immunity *2*, 561-572.
54. Keane, J., Gershon, S., Wise, R.P., Mirabile-Levens, E., Kasznica, J., Schwieterman, W.D., Siegel, J.N., and Braun, M.M. (2001). Tuberculosis associated with infliximab, a tumor necrosis factor alpha-neutralizing agent. N Engl J Med *345*, 1098-1104.
55. O'Garra, A., Redford, P.S., McNab, F.W., Bloom, C.I., Wilkinson, R.J., and Berry, M.P. (2013). The immune response in tuberculosis. Annu Rev Immunol *31*, 475-527.
56. Brandli, O. (1998). The clinical presentation of tuberculosis. Respiration *65*, 97-105.
57. Milburn, H.J. (2001). Primary tuberculosis. Curr Opin Pulm Med *7*, 133-141.

58. Schlesinger, L.S. (1996). Entry of Mycobacterium tuberculosis into mononuclear phagocytes. Curr Top Microbiol Immunol *215*, 71-96.
59. Eruslanov, E.B., Lyadova, I.V., Kondratieva, T.K., Majorov, K.B., Scheglov, I.V., Orlova, M.O., and Apt, A.S. (2005). Neutrophil responses to Mycobacterium tuberculosis infection in genetically susceptible and resistant mice. Infect Immun *73*, 1744-1753.
60. Eum, S.Y., Kong, J.H., Hong, M.S., Lee, Y.J., Kim, J.H., Hwang, S.H., Cho, S.N., Via, L.E., and Barry, C.E., 3rd (2010). Neutrophils are the predominant infected phagocytic cells in the airways of patients with active pulmonary TB. Chest *137*, 122-128.
61. Wolf, A.J., Linas, B., Trevejo-Nunez, G.J., Kincaid, E., Tamura, T., Takatsu, K., and Ernst, J.D. (2007). Mycobacterium tuberculosis infects dendritic cells with high frequency and impairs their function in vivo. J Immunol *179*, 2509-2519.
62. Behar, S.M., Martin, C.J., Booty, M.G., Nishimura, T., Zhao, X., Gan, H.X., Divangahi, M., and Remold, H.G. (2011). Apoptosis is an innate defense function of macrophages against Mycobacterium tuberculosis. Mucosal Immunol *4*, 279-287.
63. Chen, M., Divangahi, M., Gan, H., Shin, D.S., Hong, S., Lee, D.M., Serhan, C.N., Behar, S.M., and Remold, H.G. (2008). Lipid mediators in innate immunity against tuberculosis: opposing roles of PGE2 and LXA4 in the induction of macrophage death. J Exp Med *205*, 2791-2801.
64. Bafica, A., Scanga, C.A., Serhan, C., Machado, F., White, S., Sher, A., and Aliberti, J. (2005). Host control of Mycobacterium tuberculosis is regulated by 5-lipoxygenase-dependent lipoxin production. J Clin Invest *115*, 1601-1606.
65. Divangahi, M., Desjardins, D., Nunes-Alves, C., Remold, H.G., and Behar, S.M. (2010). Eicosanoid pathways regulate adaptive immunity to Mycobacterium tuberculosis. Nat Immunol *11*, 751-758.
66. Martin, C.J., Booty, M.G., Rosebrock, T.R., Nunes-Alves, C., Desjardins, D.M., Keren, I., Fortune, S.M., Remold, H.G., and Behar, S.M. (2012). Efferocytosis is an innate antibacterial mechanism. Cell Host Microbe *12*, 289-300.
67. Blomgran, R., and Ernst, J.D. (2011). Lung neutrophils facilitate activation of naive antigen-specific CD4+ T cells during Mycobacterium tuberculosis infection. J Immunol *186*, 7110-7119.
68. Meroueh, S.O., Bencze, K.Z., Hesek, D., Lee, M., Fisher, J.F., Stemmler, T.L., and Mobashery, S. (2006). Three-dimensional structure of the bacterial cell wall peptidoglycan. Proc Natl Acad Sci U S A *103*, 4404-4409.
69. Chatterjee, D., Lowell, K., Rivoire, B., McNeil, M.R., and Brennan, P.J. (1992). Lipoarabinomannan of Mycobacterium tuberculosis. Capping with mannosyl residues in some strains. J Biol Chem *267*, 6234-6239.
70. Kaur, D., Obregon-Henao, A., Pham, H., Chatterjee, D., Brennan, P.J., and Jackson, M. (2008). Lipoarabinomannan of Mycobacterium: mannose capping by a multifunctional terminal mannosyltransferase. Proc Natl Acad Sci U S A *105*, 17973-17977.

71. Benson, T.E., Walsh, C.T., and Hogle, J.M. (1996). The structure of the substrate-free form of MurB, an essential enzyme for the synthesis of bacterial cell walls. Structure *4*, 47-54.
72. Schleifer, K.H., and Kandler, O. (1972). Peptidoglycan types of bacterial cell walls and their taxonomic implications. Bacteriol Rev *36*, 407-477.
73. Petit, J.F., Adam, A., Wietzerbin-Falszpan, J., Lederer, E., and Ghuysen, J.M. (1969). Chemical structure of the cell wall of Mycobacterium smegmatis. I. Isolation and partial characterization of the peptidoglycan. Biochem Biophys Res Commun *35*, 478-485.
74. Takayama, K., David, H.L., Wang, L., and Goldman, D.S. (1970). Isolation and characterization of uridine diphosphate-N-glycolylmuramyl-L-alanyl-gamma-D-glutamyl-meso-alpha,alpha'-diamino pimelic acid from Mycobacterium tuberculosis. Biochem Biophys Res Commun *39*, 7-12.
75. Mahapatra, S., Yagi, T., Belisle, J.T., Espinosa, B.J., Hill, P.J., McNeil, M.R., Brennan, P.J., and Crick, D.C. (2005). Mycobacterial lipid II is composed of a complex mixture of modified muramyl and peptide moieties linked to decaprenyl phosphate. J Bacteriol *187*, 2747-2757.
76. Wietzerbin, J., Das, B.C., Petit, J.F., Lederer, E., Leyh-Bouille, M., and Ghuysen, J.M. (1974). Occurrence of D-alanyl-(D)-meso-diaminopimelic acid and meso-diaminopimelyl-meso-diaminopimelic acid interpeptide linkages in the peptidoglycan of Mycobacteria. Biochemistry *13*, 3471-3476.
77. De Smet, K.A., Kempsell, K.E., Gallagher, A., Duncan, K., and Young, D.B. (1999). Alteration of a single amino acid residue reverses fosfomycin resistance of recombinant MurA from Mycobacterium tuberculosis. Microbiology *145 (Pt 11)*, 3177-3184.
78. Raymond, J.B., Mahapatra, S., Crick, D.C., and Pavelka, M.S., Jr. (2005). Identification of the namH gene, encoding the hydroxylase responsible for the N-glycolylation of the mycobacterial peptidoglycan. J Biol Chem *280*, 326-333.
79. de Pedro, M.A., Donachie, W.D., Holtje, J.V., and Schwarz, H. (2001). Constitutive septal murein synthesis in Escherichia coli with impaired activity of the morphogenetic proteins RodA and penicillin-binding protein 2. J Bacteriol *183*, 4115-4126.
80. Ikeda, M., Sato, T., Wachi, M., Jung, H.K., Ishino, F., Kobayashi, Y., and Matsuhashi, M. (1989). Structural similarity among Escherichia coli FtsW and RodA proteins and Bacillus subtilis SpoVE protein, which function in cell division, cell elongation, and spore formation, respectively. J Bacteriol *171*, 6375-6378.
81. Khattar, M.M., Addinall, S.G., Stedul, K.H., Boyle, D.S., Lutkenhaus, J., and Donachie, W.D. (1997). Two polypeptide products of the Escherichia coli cell division gene ftsW and a possible role for FtsW in FtsZ function. J Bacteriol *179*, 784-793.
82. Yuan, Y., Barrett, D., Zhang, Y., Kahne, D., Sliz, P., and Walker, S. (2007). Crystal structure of a peptidoglycan glycosyltransferase suggests a model for processive glycan chain synthesis. Proc Natl Acad Sci U S A *104*, 5348-5353.
83. Goffin, C., and Ghuysen, J.M. (1998). Multimodular penicillin-binding proteins: an enigmatic family of orthologs and paralogs. Microbiol Mol Biol Rev *62*, 1079-1093.

84. Magnet, S., Arbeloa, A., Mainardi, J.L., Hugonnet, J.E., Fourgeaud, M., Dubost, L., Marie, A., Delfosse, V., Mayer, C., Rice, L.B., et al. (2007). Specificity of L,D-transpeptidases from gram-positive bacteria producing different peptidoglycan chemotypes. J Biol Chem *282*, 13151-13159.
85. Lederer, E., Adam, A., Ciorbaru, R., Petit, J.F., and Wietzerbin, J. (1975). Cell walls of Mycobacteria and related organisms; chemistry and immunostimulant properties. Mol Cell Biochem *7*, 87-104.
86. McNeil, M., Wallner, S.J., Hunter, S.W., and Brennan, P.J. (1987). Demonstration that the galactosyl and arabinosyl residues in the cell-wall arabinogalactan of Mycobacterium leprae and Mycobacterium tuberculosis are furanoid. Carbohydr Res *166*, 299-308.
87. Daffe, M., Brennan, P.J., and McNeil, M. (1990). Predominant structural features of the cell wall arabinogalactan of Mycobacterium tuberculosis as revealed through characterization of oligoglycosyl alditol fragments by gas chromatography/mass spectrometry and by 1H and 13C NMR analyses. J Biol Chem *265*, 6734-6743.
88. Crick, D.C., Mahapatra, S., and Brennan, P.J. (2001). Biosynthesis of the arabinogalactan-peptidoglycan complex of Mycobacterium tuberculosis. Glycobiology *11*, 107R-118R.
89. McNeil, M., Daffe, M., and Brennan, P.J. (1990). Evidence for the nature of the link between the arabinogalactan and peptidoglycan of mycobacterial cell walls. J Biol Chem *265*, 18200-18206.
90. Mikusova, K., Mikus, M., Besra, G.S., Hancock, I., and Brennan, P.J. (1996). Biosynthesis of the linkage region of the mycobacterial cell wall. J Biol Chem *271*, 7820-7828.
91. Weston, A., Stern, R.J., Lee, R.E., Nassau, P.M., Monsey, D., Martin, S.L., Scherman, M.S., Besra, G.S., Duncan, K., and McNeil, M.R. (1997). Biosynthetic origin of mycobacterial cell wall galactofuranosyl residues. Tuber Lung Dis *78*, 123-131.
92. Scherman, M., Weston, A., Duncan, K., Whittington, A., Upton, R., Deng, L., Comber, R., Friedrich, J.D., and McNeil, M. (1995). Biosynthetic origin of mycobacterial cell wall arabinosyl residues. J Bacteriol *177*, 7125-7130.
93. Scherman, M.S., Kalbe-Bournonville, L., Bush, D., Xin, Y., Deng, L., and McNeil, M. (1996). Polyprenylphosphate-pentoses in mycobacteria are synthesized from 5-phosphoribose pyrophosphate. J Biol Chem *271*, 29652-29658.
94. Mikusova, K., Yagi, T., Stern, R., McNeil, M.R., Besra, G.S., Crick, D.C., and Brennan, P.J. (2000). Biosynthesis of the galactan component of the mycobacterial cell wall. J Biol Chem *275*, 33890-33897.
95. Belanger, A.E., Besra, G.S., Ford, M.E., Mikusova, K., Belisle, J.T., Brennan, P.J., and Inamine, J.M. (1996). The embAB genes of Mycobacterium avium encode an arabinosyl transferase involved in cell wall arabinan biosynthesis that is the target for the antimycobacterial drug ethambutol. Proc Natl Acad Sci U S A *93*, 11919-11924.
96. Besra, G.S., and Brennan, P.J. (1997). The mycobacterial cell wall: biosynthesis of arabinogalactan and lipoarabinomannan. Biochem Soc Trans *25*, 845-850.

97. Chatterjee, D. (1997). The mycobacterial cell wall: structure, biosynthesis and sites of drug action. Curr Opin Chem Biol *1*, 579-588.
98. Takayama, K., Wang, C., and Besra, G.S. (2005). Pathway to synthesis and processing of mycolic acids in Mycobacterium tuberculosis. Clin Microbiol Rev *18*, 81-101.
99. Parikh, A., Verma, S.K., Khan, S., Prakash, B., and Nandicoori, V.K. (2009). PknB-mediated phosphorylation of a novel substrate, N-acetylglucosamine-1-phosphate uridyltransferase, modulates its acetyltransferase activity. J Mol Biol *386*, 451-464.
100. Gupta, M., Sajid, A., Arora, G., Tandon, V., and Singh, Y. (2009). Forkhead-associated domain-containing protein Rv0019c and polyketide-associated protein PapA5, from substrates of serine/threonine protein kinase PknB to interacting proteins of Mycobacterium tuberculosis. J Biol Chem *284*, 34723-34734.
101. Prisic, S., Dankwa, S., Schwartz, D., Chou, M.F., Locasale, J.W., Kang, C.M., Bemis, G., Church, G.M., Steen, H., and Husson, R.N. (2010). Extensive phosphorylation with overlapping specificity by Mycobacterium tuberculosis serine/threonine protein kinases. Proc Natl Acad Sci U S A *107*, 7521-7526.
102. Boitel, B., Ortiz-Lombardia, M., Duran, R., Pompeo, F., Cole, S.T., Cervenansky, C., and Alzari, P.M. (2003). PknB kinase activity is regulated by phosphorylation in two Thr residues and dephosphorylation by PstP, the cognate phospho-Ser/Thr phosphatase, in Mycobacterium tuberculosis. Mol Microbiol *49*, 1493-1508.
103. Sureka, K., Hossain, T., Mukherjee, P., Chatterjee, P., Datta, P., Kundu, M., and Basu, J. (2010). Novel role of phosphorylation-dependent interaction between FtsZ and FipA in mycobacterial cell division. PLoS One *5*, e8590.
104. Hamasha, K., Sahana, M.B., Jani, C., Nyayapathy, S., Kang, C.M., and Rehse, S.J. (2010). The effect of Wag31 phosphorylation on the cells and the cell envelope fraction of wild-type and conditional mutants of Mycobacterium smegmatis studied by visible-wavelength Raman spectroscopy. Biochem Biophys Res Commun *391*, 664-668.
105. Molle, V., Brown, A.K., Besra, G.S., Cozzone, A.J., and Kremer, L. (2006). The condensing activities of the Mycobacterium tuberculosis type II fatty acid synthase are differentially regulated by phosphorylation. J Biol Chem *281*, 30094-30103.
106. Vilcheze, C., Molle, V., Carrere-Kremer, S., Leiba, J., Mourey, L., Shenai, S., Baronian, G., Tufariello, J., Hartman, T., Veyron-Churlet, R., et al. (2014). Phosphorylation of KasB regulates virulence and acid-fastness in Mycobacterium tuberculosis. PLoS pathogens *10*, e1004115.
107. Veyron-Churlet, R., Zanella-Cleon, I., Cohen-Gonsaud, M., Molle, V., and Kremer, L. (2010). Phosphorylation of the Mycobacterium tuberculosis beta-ketoacyl-acyl carrier protein reductase MabA regulates mycolic acid biosynthesis. J Biol Chem *285*, 12714-12725.
108. Molle, V., Gulten, G., Vilcheze, C., Veyron-Churlet, R., Zanella-Cleon, I., Sacchettini, J.C., Jacobs, W.R., Jr., and Kremer, L. (2010). Phosphorylation of InhA inhibits mycolic acid biosynthesis and growth of Mycobacterium tuberculosis. Mol Microbiol *78*, 1591-1605.

109. Slama, N., Leiba, J., Eynard, N., Daffe, M., Kremer, L., Quemard, A., and Molle, V. (2011). Negative regulation by Ser/Thr phosphorylation of HadAB and HadBC dehydratases from Mycobacterium tuberculosis type II fatty acid synthase system. Biochem Biophys Res Commun *412*, 401-406.
110. Khan, S., Nagarajan, S.N., Parikh, A., Samantaray, S., Singh, A., Kumar, D., Roy, R.P., Bhatt, A., and Nandicoori, V.K. (2010). Phosphorylation of enoyl-acyl carrier protein reductase InhA impacts mycobacterial growth and survival. J Biol Chem *285*, 37860-37871.
111. LeMagueres, P., Im, H., Ebalunode, J., Strych, U., Benedik, M.J., Briggs, J.M., Kohn, H., and Krause, K.L. (2005). The 1.9 A crystal structure of alanine racemase from Mycobacterium tuberculosis contains a conserved entryway into the active site. Biochemistry *44*, 1471-1481.
112. Bruning, J.B., Murillo, A.C., Chacon, O., Barletta, R.G., and Sacchettini, J.C. (2011). Structure of the Mycobacterium tuberculosis D-alanine:D-alanine ligase, a target of the antituberculosis drug D-cycloserine. Antimicrob Agents Chemother *55*, 291-301.
113. Li, Y., Zhou, Y., Ma, Y., and Li, X. (2011). Design and synthesis of novel cell wall inhibitors of Mycobacterium tuberculosis GlmM and GlmU. Carbohydr Res *346*, 1714-1720.
114. Li, S., Kang, J., Yu, W., Zhou, Y., Zhang, W., Xin, Y., and Ma, Y. (2012). Identification of M. tuberculosis Rv3441c and M. smegmatis MSMEG_1556 and essentiality of M. smegmatis MSMEG_1556. PLoS One *7*, e42769.
115. Zhang, W., Jones, V.C., Scherman, M.S., Mahapatra, S., Crick, D., Bhamidi, S., Xin, Y., McNeil, M.R., and Ma, Y. (2008). Expression, essentiality, and a microtiter plate assay for mycobacterial GlmU, the bifunctional glucosamine-1-phosphate acetyltransferase and N-acetylglucosamine-1-phosphate uridyltransferase. Int J Biochem Cell Biol *40*, 2560-2571.
116. Escuyer, V.E., Lety, M.A., Torrelles, J.B., Khoo, K.H., Tang, J.B., Rithner, C.D., Frehel, C., McNeil, M.R., Brennan, P.J., and Chatterjee, D. (2001). The role of the embA and embB gene products in the biosynthesis of the terminal hexaarabinofuranosyl motif of Mycobacterium smegmatis arabinogalactan. J Biol Chem *276*, 48854-48862.
117. Seidel, M., Alderwick, L.J., Birch, H.L., Sahm, H., Eggeling, L., and Besra, G.S. (2007). Identification of a novel arabinofuranosyltransferase AftB involved in a terminal step of cell wall arabinan biosynthesis in Corynebacterianeae, such as Corynebacterium glutamicum and Mycobacterium tuberculosis. J Biol Chem *282*, 14729-14740.
118. Huang, H., Scherman, M.S., D'Haeze, W., Vereecke, D., Holsters, M., Crick, D.C., and McNeil, M.R. (2005). Identification and active expression of the Mycobacterium tuberculosis gene encoding 5-phospho-{alpha}-d-ribose-1-diphosphate: decaprenyl-phosphate 5-phosphoribosyltransferase, the first enzyme committed to decaprenylphosphoryl-d-arabinose synthesis. J Biol Chem *280*, 24539-24543.
119. Pan, F., Jackson, M., Ma, Y., and McNeil, M. (2001). Cell wall core galactofuran synthesis is essential for growth of mycobacteria. J Bacteriol *183*, 3991-3998.

120. Li, W., Xin, Y., McNeil, M.R., and Ma, Y. (2006). rmlB and rmlC genes are essential for growth of mycobacteria. Biochem Biophys Res Commun *342*, 170-178.
121. Quemard, A., Sacchettini, J.C., Dessen, A., Vilcheze, C., Bittman, R., Jacobs, W.R., Jr., and Blanchard, J.S. (1995). Enzymatic characterization of the target for isoniazid in Mycobacterium tuberculosis. Biochemistry *34*, 8235-8241.
122. Rozwarski, D.A., Vilcheze, C., Sugantino, M., Bittman, R., and Sacchettini, J.C. (1999). Crystal structure of the Mycobacterium tuberculosis enoyl-ACP reductase, InhA, in complex with NAD+ and a C16 fatty acyl substrate. J Biol Chem *274*, 15582-15589.
123. Kremer, L., Nampoothiri, K.M., Lesjean, S., Dover, L.G., Graham, S., Betts, J., Brennan, P.J., Minnikin, D.E., Locht, C., and Besra, G.S. (2001). Biochemical characterization of acyl carrier protein (AcpM) and malonyl-CoA:AcpM transacylase (mtFabD), two major components of Mycobacterium tuberculosis fatty acid synthase II. J Biol Chem *276*, 27967-27974.
124. Choi, K.H., Kremer, L., Besra, G.S., and Rock, C.O. (2000). Identification and substrate specificity of beta -ketoacyl (acyl carrier protein) synthase III (mtFabH) from Mycobacterium tuberculosis. J Biol Chem *275*, 28201-28207.
125. Musayev, F., Sachdeva, S., Scarsdale, J.N., Reynolds, K.A., and Wright, H.T. (2005). Crystal structure of a substrate complex of Mycobacterium tuberculosis beta-ketoacyl-acyl carrier protein synthase III (FabH) with lauroyl-coenzyme A. J Mol Biol *346*, 1313-1321.
126. Marrakchi, H., Ducasse, S., Labesse, G., Montrozier, H., Margeat, E., Emorine, L., Charpentier, X., Daffe, M., and Quemard, A. (2002). MabA (FabG1), a Mycobacterium tuberculosis protein involved in the long-chain fatty acid elongation system FAS-II. Microbiology *148*, 951-960.
127. Cohen-Gonsaud, M., Ducasse, S., Hoh, F., Zerbib, D., Labesse, G., and Quemard, A. (2002). Crystal structure of MabA from Mycobacterium tuberculosis, a reductase involved in long-chain fatty acid biosynthesis. J Mol Biol *320*, 249-261.
128. Kremer, L., Douglas, J.D., Baulard, A.R., Morehouse, C., Guy, M.R., Alland, D., Dover, L.G., Lakey, J.H., Jacobs, W.R., Jr., Brennan, P.J., et al. (2000). Thiolactomycin and related analogues as novel anti-mycobacterial agents targeting KasA and KasB condensing enzymes in Mycobacterium tuberculosis. J Biol Chem *275*, 16857-16864.
129. Boissier, F., Bardou, F., Guillet, V., Uttenweiler-Joseph, S., Daffe, M., Quemard, A., and Mourey, L. (2006). Further insight into S-adenosylmethionine-dependent methyltransferases: structural characterization of Hma, an enzyme essential for the biosynthesis of oxygenated mycolic acids in Mycobacterium tuberculosis. J Biol Chem *281*, 4434-4445.
130. Portevin, D., De Sousa-D'Auria, C., Houssin, C., Grimaldi, C., Chami, M., Daffe, M., and Guilhot, C. (2004). A polyketide synthase catalyzes the last condensation step of mycolic acid biosynthesis in mycobacteria and related organisms. Proc Natl Acad Sci U S A *101*, 314-319.
131. Portevin, D., de Sousa-D'Auria, C., Montrozier, H., Houssin, C., Stella, A., Laneelle, M.A., Bardou, F., Guilhot, C., and Daffe, M. (2005). The acyl-AMP ligase FadD32 and AccD4-containing acyl-CoA carboxylase are

required for the synthesis of mycolic acids and essential for mycobacterial growth: identification of the carboxylation product and determination of the acyl-CoA carboxylase components. J Biol Chem *280*, 8862-8874.

132. Gago, G., Kurth, D., Diacovich, L., Tsai, S.C., and Gramajo, H. (2006). Biochemical and structural characterization of an essential acyl coenzyme A carboxylase from Mycobacterium tuberculosis. J Bacteriol *188*, 477-486.
133. Kumar, P., Arora, K., Lloyd, J.R., Lee, I.Y., Nair, V., Fischer, E., Boshoff, H.I., and Barry, C.E., 3rd (2012). Meropenem inhibits D,D-carboxypeptidase activity in Mycobacterium tuberculosis. Mol Microbiol *86*, 367-381.
134. Mahapatra, S., Scherman, H., Brennan, P.J., and Crick, D.C. (2005). N Glycolylation of the nucleotide precursors of peptidoglycan biosynthesis of Mycobacterium spp. is altered by drug treatment. J Bacteriol *187*, 2341-2347.
135. Skovierova, H., Larrouy-Maumus, G., Pham, H., Belanova, M., Barilone, N., Dasgupta, A., Mikusova, K., Gicquel, B., Gilleron, M., Brennan, P.J., et al. (2010). Biosynthetic origin of the galactosamine substituent of Arabinogalactan in Mycobacterium tuberculosis. J Biol Chem *285*, 41348-41355.
136. Seiler, P., Ulrichs, T., Bandermann, S., Pradl, L., Jorg, S., Krenn, V., Morawietz, L., Kaufmann, S.H., and Aichele, P. (2003). Cell-wall alterations as an attribute of Mycobacterium tuberculosis in latent infection. J Infect Dis *188*, 1326-1331.
137. Bhamidi, S., Shi, L., Chatterjee, D., Belisle, J.T., Crick, D.C., and McNeil, M.R. (2012). A bioanalytical method to determine the cell wall composition of Mycobacterium tuberculosis grown in vivo. Anal Biochem *421*, 240-249.
138. Rachman, H., Strong, M., Ulrichs, T., Grode, L., Schuchhardt, J., Mollenkopf, H., Kosmiadi, G.A., Eisenberg, D., and Kaufmann, S.H. (2006). Unique transcriptome signature of Mycobacterium tuberculosis in pulmonary tuberculosis. Infect Immun *74*, 1233-1242.
139. Flores, A.R., Parsons, L.M., and Pavelka, M.S., Jr. (2005). Characterization of novel Mycobacterium tuberculosis and Mycobacterium smegmatis mutants hypersusceptible to beta-lactam antibiotics. J Bacteriol *187*, 1892-1900.
140. Flores, A.R., Parsons, L.M., and Pavelka, M.S., Jr. (2005). Genetic analysis of the beta-lactamases of Mycobacterium tuberculosis and Mycobacterium smegmatis and susceptibility to beta-lactam antibiotics. Microbiology *151*, 521-532.
141. McDonough, J.A., Hacker, K.E., Flores, A.R., Pavelka, M.S., Jr., and Braunstein, M. (2005). The twin-arginine translocation pathway of Mycobacterium smegmatis is functional and required for the export of mycobacterial beta-lactamases. J Bacteriol *187*, 7667-7679.
142. Wang, F., Cassidy, C., and Sacchettini, J.C. (2006). Crystal structure and activity studies of the Mycobacterium tuberculosis beta-lactamase reveal its critical role in resistance to beta-lactam antibiotics. Antimicrob Agents Chemother *50*, 2762-2771.
143. Milewski, S., Gabriel, I., and Olchowy, J. (2006). Enzymes of UDP-GlcNAc biosynthesis in yeast. Yeast *23*, 1-14.
144. Krzeslak, A. (2007). [Role of O-GlcNAc modification of cellular proteins in signal transduction]. Postepy Biochem *53*, 389-399.

145. Hart, G.W., Slawson, C., Ramirez-Correa, G., and Lagerlof, O. (2011). Cross talk between O-GlcNAcylation and phosphorylation: roles in signaling, transcription, and chronic disease. Annu Rev Biochem *80*, 825-858.
146. Itano, N., and Kimata, K. (2002). Mammalian hyaluronan synthases. IUBMB Life *54*, 195-199.
147. Tanner, M.E. (2005). The enzymes of sialic acid biosynthesis. Bioorg Chem *33*, 216-228.
148. Narasimhan, S. (1982). Control of glycoprotein synthesis. UDP-GlcNAc:glycopeptide beta 4-N-acetylglucosaminyltransferase III, an enzyme in hen oviduct which adds GlcNAc in beta 1-4 linkage to the beta-linked mannose of the trimannosyl core of N-glycosyl oligosaccharides. J Biol Chem *257*, 10235-10242.
149. Vimr, E.R., Kalivoda, K.A., Deszo, E.L., and Steenbergen, S.M. (2004). Diversity of microbial sialic acid metabolism. Microbiol Mol Biol Rev *68*, 132-153.
150. Prehm, P. (2006). Biosynthesis of hyaluronan: direction of chain elongation. Biochem J *398*, 469-473.
151. Wang, X., and Quinn, P.J. (2010). Lipopolysaccharide: Biosynthetic pathway and structure modification. Prog Lipid Res *49*, 97-107.
152. Swoboda, J.G., Campbell, J., Meredith, T.C., and Walker, S. (2010). Wall teichoic acid function, biosynthesis, and inhibition. Chembiochem *11*, 35-45.
153. Shen, A., Kamp, H.D., Grundling, A., and Higgins, D.E. (2006). A bifunctional O-GlcNAc transferase governs flagellar motility through anti-repression. Genes Dev *20*, 3283-3295.
154. Hett, E.C., and Rubin, E.J. (2008). Bacterial growth and cell division: a mycobacterial perspective. Microbiol Mol Biol Rev *72*, 126-156, table of contents.
155. Vilcheze, C., Av-Gay, Y., Attarian, R., Liu, Z., Hazbon, M.H., Colangeli, R., Chen, B., Liu, W., Alland, D., Sacchettini, J.C., et al. (2008). Mycothiol biosynthesis is essential for ethionamide susceptibility in Mycobacterium tuberculosis. Mol Microbiol *69*, 1316-1329.
156. Brennan, P.J. (2003). Structure, function, and biogenesis of the cell wall of Mycobacterium tuberculosis. Tuberculosis (Edinb) *83*, 91-97.
157. Sonnenburg, J.L., Xu, J., Leip, D.D., Chen, C.H., Westover, B.P., Weatherford, J., Buhler, J.D., and Gordon, J.I. (2005). Glycan foraging in vivo by an intestine-adapted bacterial symbiont. Science *307*, 1955-1959.
158. Tailford, L.E., Crost, E.H., Kavanaugh, D., and Juge, N. (2015). Mucin glycan foraging in the human gut microbiome. Front Genet *6*, 81.
159. Martens, E.C., Chiang, H.C., and Gordon, J.I. (2008). Mucosal glycan foraging enhances fitness and transmission of a saccharolytic human gut bacterial symbiont. Cell Host Microbe *4*, 447-457.
160. Vithani, N., Bais, V., and Prakash, B. (2014). GlmU (N-acetylglucosamine-1-phosphate uridyltransferase) bound to three magnesium ions and ATP at the active site. Acta Crystallogr F Struct Biol Commun *70*, 703-708.
161. Jagtap, P.K., Verma, S.K., Vithani, N., Bais, V.S., and Prakash, B. (2013). Crystal structures identify an atypical two-metal-ion mechanism for uridyltransfer in GlmU: its significance to sugar nucleotidyl transferases. J Mol Biol *425*, 1745-1759.

162. Mochalkin, I., Lightle, S., Narasimhan, L., Bornemeier, D., Melnick, M., Vanderroest, S., and McDowell, L. (2008). Structure of a small-molecule inhibitor complexed with GlmU from Haemophilus influenzae reveals an allosteric binding site. Protein Sci *17*, 577-582.
163. Larsen, N.A., Nash, T.J., Morningstar, M., Shapiro, A.B., Joubran, C., Blackett, C.J., Patten, A.D., Boriack-Sjodin, P.A., and Doig, P. (2012). An aminoquinazoline inhibitor of the essential bacterial cell wall synthetic enzyme GlmU has a unique non-protein-kinase-like binding mode. Biochem J *446*, 405-413.
164. Green, O.M., McKenzie, A.R., Shapiro, A.B., Otterbein, L., Ni, H., Patten, A., Stokes, S., Albert, R., Kawatkar, S., and Breed, J. (2012). Inhibitors of acetyltransferase domain of N-acetylglucosamine-1-phosphate-uridyltransferase/glucosamine-1-phosphate-acetylt ransferase (GlmU). Part 1: Hit to lead evaluation of a novel arylsulfonamide series. Bioorg Med Chem Lett *22*, 1510-1519.
165. Sulzenbacher, G., Gal, L., Peneff, C., Fassy, F., and Bourne, Y. (2001). Crystal structure of Streptococcus pneumoniae N-acetylglucosamine-1-phosphate uridyltransferase bound to acetyl-coenzyme A reveals a novel active site architecture. J Biol Chem *276*, 11844-11851.
166. Kostrewa, D., D'Arcy, A., Takacs, B., and Kamber, M. (2001). Crystal structures of Streptococcus pneumoniae N-acetylglucosamine-1-phosphate uridyltransferase, GlmU, in apo form at 2.33 A resolution and in complex with UDP-N-acetylglucosamine and Mg(2+) at 1.96 A resolution. J Mol Biol *305*, 279-289.
167. Brown, K., Pompeo, F., Dixon, S., Mengin-Lecreulx, D., Cambillau, C., and Bourne, Y. (1999). Crystal structure of the bifunctional N-acetylglucosamine 1-phosphate uridyltransferase from Escherichia coli: a paradigm for the related pyrophosphorylase superfamily. EMBO J *18*, 4096-4107.
168. Olsen, L.R., and Roderick, S.L. (2001). Structure of the Escherichia coli GlmU pyrophosphorylase and acetyltransferase active sites. Biochemistry *40*, 1913-1921.
169. Olsen, L.R., Vetting, M.W., and Roderick, S.L. (2007). Structure of the E. coli bifunctional GlmU acetyltransferase active site with substrates and products. Protein Sci *16*, 1230-1235.
170. Buurman, E.T., Andrews, B., Gao, N., Hu, J., Keating, T.A., Lahiri, S., Otterbein, L.R., Patten, A.D., Stokes, S.S., and Shapiro, A.B. (2011). In vitro validation of acetyltransferase activity of GlmU as an antibacterial target in Haemophilus influenzae. J Biol Chem *286*, 40734-40742.
171. Singh, V.K., Das, K., and Seshadri, K. (2012). Kinetic modelling of GlmU reactions - prioritization of reaction for therapeutic application. PLoS One *7*, e43969.
172. Pompeo, F., van Heijenoort, J., and Mengin-Lecreulx, D. (1998). Probing the role of cysteine residues in glucosamine-1-phosphate acetyltransferase activity of the bifunctional GlmU protein from Escherichia coli: site-directed mutagenesis and characterization of the mutant enzymes. J Bacteriol *180*, 4799-4803.

173. Mengin-Lecreulx, D., and van Heijenoort, J. (1993). Identification of the glmU gene encoding N-acetylglucosamine-1-phosphate uridyltransferase in Escherichia coli. J Bacteriol *175*, 6150-6157.
174. Plumbridge, J. (1995). Co-ordinated regulation of amino sugar biosynthesis and degradation: the NagC repressor acts as both an activator and a repressor for the transcription of the glmUS operon and requires two separated NagC binding sites. EMBO J *14*, 3958-3965.
175. Gehring, A.M., Lees, W.J., Mindiola, D.J., Walsh, C.T., and Brown, E.D. (1996). Acetyltransfer precedes uridylyltransfer in the formation of UDP-N-acetylglucosamine in separable active sites of the bifunctional GlmU protein of Escherichia coli. Biochemistry *35*, 579-585.
176. Pompeo, F., Bourne, Y., van Heijenoort, J., Fassy, F., and Mengin-Lecreulx, D. (2001). Dissection of the bifunctional Escherichia coli N-acetylglucosamine-1-phosphate uridyltransferase enzyme into autonomously functional domains and evidence that trimerization is absolutely required for glucosamine-1-phosphate acetyltransferase activity and cell growth. J Biol Chem *276*, 3833-3839.
177. Sassetti, C.M., Boyd, D.H., and Rubin, E.J. (2003). Genes required for mycobacterial growth defined by high density mutagenesis. Mol Microbiol *48*, 77-84.
178. Qi, X., Deng, W., Gao, M., Mao, B., Xu, S., Chen, C., and Zhang, Q. (2015). Novel lead compound optimization and synthesized based on the target structure of Xanthomonas oryzae pv. oryzae GlmU. Pestic Biochem Physiol *122*, 22-28.
179. Pereira, M.P., Blanchard, J.E., Murphy, C., Roderick, S.L., and Brown, E.D. (2009). High-throughput screening identifies novel inhibitors of the acetyltransferase activity of Escherichia coli GlmU. Antimicrob Agents Chemother *53*, 2306-2311.
180. Min, J., Lin, D., Zhang, Q., Zhang, J., and Yu, Z. (2012). Structure-based virtual screening of novel inhibitors of the uridyltransferase activity of Xanthomonas oryzae pv. oryzae GlmU. Eur J Med Chem *53*, 150-158.
181. Stokes, S.S., Albert, R., Buurman, E.T., Andrews, B., Shapiro, A.B., Green, O.M., McKenzie, A.R., and Otterbein, L.R. (2012). Inhibitors of the acetyltransferase domain of N-acetylglucosamine-1-phosphate-uridylyltransferase/glucosamine-1-phosphate-acety ltransferase (GlmU). Part 2: Optimization of physical properties leading to antibacterial aryl sulfonamides. Bioorg Med Chem Lett *22*, 7019-7023.
182. Tran, A.T., Wen, D., West, N.P., Baker, E.N., Britton, W.J., and Payne, R.J. (2013). Inhibition studies on Mycobacterium tuberculosis N-acetylglucosamine-1-phosphate uridyltransferase (GlmU). Org Biomol Chem *11*, 8113-8126.
183. Singla, D., Anurag, M., Dash, D., and Raghava, G.P. (2011). A web server for predicting inhibitors against bacterial target GlmU protein. BMC Pharmacol *11*, 5.
184. Mehra, R., Sharma, R., Khan, I.A., and Nargotra, A. (2015). Identification and optimization of Escherichia coli GlmU inhibitors: an in silico approach with validation thereof. Eur J Med Chem *92*, 78-90.

185. Philips, J.A., and Ernst, J.D. (2012). Tuberculosis pathogenesis and immunity. Annu Rev Pathol *7*, 353-384.
186. McNeil, M.R., and Brennan, P.J. (1991). Structure, function and biogenesis of the cell envelope of mycobacteria in relation to bacterial physiology, pathogenesis and drug resistance; some thoughts and possibilities arising from recent structural information. Res Microbiol *142*, 451-463.
187. Brennan, P.J., and Nikaido, H. (1995). The envelope of mycobacteria. Annu Rev Biochem *64*, 29-63.
188. Lee, A., Wu, S.W., Scherman, M.S., Torrelles, J.B., Chatterjee, D., McNeil, M.R., and Khoo, K.H. (2006). Sequencing of oligoarabinosyl units released from mycobacterial arabinogalactan by endogenous arabinanase: identification of distinctive and novel structural motifs. Biochemistry *45*, 15817-15828.
189. Mengin-Lecreulx, D., and van Heijenoort, J. (1994). Copurification of glucosamine-1-phosphate acetyltransferase and N-acetylglucosamine-1-phosphate uridyltransferase activities of Escherichia coli: characterization of the glmU gene product as a bifunctional enzyme catalyzing two subsequent steps in the pathway for UDP-N-acetylglucosamine synthesis. J Bacteriol *176*, 5788-5795.
190. Alderwick, L.J., Birch, H.L., Mishra, A.K., Eggeling, L., and Besra, G.S. (2007). Structure, function and biosynthesis of the Mycobacterium tuberculosis cell wall: arabinogalactan and lipoarabinomannan assembly with a view to discovering new drug targets. Biochem Soc Trans *35*, 1325-1328.
191. Barreteau, H., Kovac, A., Boniface, A., Sova, M., Gobec, S., and Blanot, D. (2008). Cytoplasmic steps of peptidoglycan biosynthesis. FEMS Microbiol Rev *32*, 168-207.
192. Birch, H.L., Alderwick, L.J., Bhatt, A., Rittmann, D., Krumbach, K., Singh, A., Bai, Y., Lowary, T.L., Eggeling, L., and Besra, G.S. (2008). Biosynthesis of mycobacterial arabinogalactan: identification of a novel alpha(1-->3) arabinofuranosyltransferase. Mol Microbiol *69*, 1191-1206.
193. Mills, J.A., Motichka, K., Jucker, M., Wu, H.P., Uhlik, B.C., Stern, R.J., Scherman, M.S., Vissa, V.D., Pan, F., Kundu, M., et al. (2004). Inactivation of the mycobacterial rhamnosyltransferase, which is needed for the formation of the arabinogalactan-peptidoglycan linker, leads to irreversible loss of viability. J Biol Chem *279*, 43540-43546.
194. Dover, L.G., Cerdeno-Tarraga, A.M., Pallen, M.J., Parkhill, J., and Besra, G.S. (2004). Comparative cell wall core biosynthesis in the mycolated pathogens, Mycobacterium tuberculosis and Corynebacterium diphtheriae. FEMS Microbiol Rev *28*, 225-250.
195. Mio, T., Yabe, T., Arisawa, M., and Yamada-Okabe, H. (1998). The eukaryotic UDP-N-acetylglucosamine pyrophosphorylases. Gene cloning, protein expression, and catalytic mechanism. J Biol Chem *273*, 14392-14397.
196. Jackson, M., McNeil, M.R., and Brennan, P.J. (2013). Progress in targeting cell envelope biogenesis in Mycobacterium tuberculosis. Future Microbiol *8*, 855-875.
197. Renzi, F., Manfredi, P., Dol, M., Fu, J., Vincent, S., and Cornelis, G.R. (2015). Glycan-foraging systems reveal the adaptation of Capnocytophaga canimorsus to the dog mouth. MBio *6*, e02507.

198. Renzi, F., Manfredi, P., Mally, M., Moes, S., Jeno, P., and Cornelis, G.R. (2011). The N-glycan glycoprotein deglycosylation complex (Gpd) from Capnocytophaga canimorsus deglycosylates human IgG. PLoS pathogens *7*, e1002118.
199. Ryckaert JP, C.G., Berendsen (1977). Numerical integration of the cartesian equations of motion of a system with constraints: molecular dynamics of n-alkanes. J Comp Phys *23*, 327-341.
200. Chawla, Y., Upadhyay, S., Khan, S., Nagarajan, S.N., Forti, F., and Nandicoori, V.K. (2014). Protein kinase B (PknB) of Mycobacterium tuberculosis is essential for growth of the pathogen in vitro as well as for survival within the host. J Biol Chem *289*, 13858-13875.
201. Blokpoel, M.C., Murphy, H.N., O'Toole, R., Wiles, S., Runn, E.S., Stewart, G.R., Young, D.B., and Robertson, B.D. (2005). Tetracycline-inducible gene regulation in mycobacteria. Nucleic Acids Res *33*, e22.
202. Jain, P., Hsu, T., Arai, M., Biermann, K., Thaler, D.S., Nguyen, A., Gonzalez, P.A., Tufariello, J.M., Kriakov, J., Chen, B., et al. (2014). Specialized transduction designed for precise high-throughput unmarked deletions in Mycobacterium tuberculosis. MBio *5*, e01245-01214.
203. Bardarov, S., Bardarov Jr, S., Jr., Pavelka Jr, M.S., Jr., Sambandamurthy, V., Larsen, M., Tufariello, J., Chan, J., Hatfull, G., and Jacobs Jr, W.R., Jr. (2002). Specialized transduction: an efficient method for generating marked and unmarked targeted gene disruptions in Mycobacterium tuberculosis, M. bovis BCG and M. smegmatis. Microbiology *148*, 3007-3017.
204. Wayne, L.G., and Hayes, L.G. (1996). An in vitro model for sequential study of shiftdown of Mycobacterium tuberculosis through two stages of nonreplicating persistence. Infect Immun *64*, 2062-2069.
205. Lasco, T.M., Cassone, L., Kamohara, H., Yoshimura, T., and McMurray, D.N. (2005). Evaluating the role of tumor necrosis factor-alpha in experimental pulmonary tuberculosis in the guinea pig. Tuberculosis (Edinb) *85*, 245-258.
206. Boyle, W.J., van der Geer, P., and Hunter, T. (1991). Phosphopeptide mapping and phosphoamino acid analysis by two-dimensional separation on thin-layer cellulose plates. Methods in enzymology *201*, 110-149.
207. Kirchmair, J., Distinto, S., Markt, P., Schuster, D., Spitzer, G.M., Liedl, K.R., and Wolber, G. (2009). How to optimize shape-based virtual screening: choosing the right query and including chemical information. J Chem Inf Model *49*, 678-692.
208. Hawkins, P.C., Skillman, A.G., and Nicholls, A. (2007). Comparison of shape-matching and docking as virtual screening tools. J Med Chem *50*, 74-82.
209. György Kóczána, G.C.k., Antal Csámpaic, Erika Balogb, Szilvia Bőszea, Pál Sohárc, Ferenc Hudecza (2001). Synthesis and characterization of 4-ethoxymethylene-2-[1]-naphthyl-5(4H)-oxazolone and its fluorescent amino acid derivatives Tetrahedron *57*, 4589–4598.
210. William L. Jorgensen, D.S.M., and Julian Tirado-Rives (1996). Development and Testing of the OPLS All-Atom Force Field on Conformational Energetics and Properties of Organic Liquids. Journal of the American Chemical Society *118*, 11225-11236.

211. William L. Jorgensen, J.C., Jeffry D. Madura, Roger W. Impey and Michael L. Klein (1983). Comparison of simple potential functions for simulating liquid water. The Journal of Chemical Physics *79*, 926-935.
212. Vincent Kräutler, W.F.v.G.a.H.H. (2001). A fast SHAKE algorithm to solve distance constraint equations for small molecules in molecular dynamics simulations. Journal of Computational Chemistry *22*, 501–508.
213. Olsson MHM, S.C., Rostkowski M, Jensen JH (2011). PROPKA3: consistent treatment of internal and surface residues in empirical p K a predictions. J. Chem. Theor. Comput *7*, 525–537.
214. Trott, O., and Olson, A.J. (2010). AutoDock Vina: improving the speed and accuracy of docking with a new scoring function, efficient optimization, and multithreading. J Comput Chem *31*, 455-461.
215. Verdonk, M.L., Cole, J.C., Hartshorn, M.J., Murray, C.W., and Taylor, R.D. (2003). Improved protein-ligand docking using GOLD. Proteins *52*, 609-623.
216. Beard, H., Cholleti, A., Pearlman, D., Sherman, W., and Loving, K.A. (2013). Applying physics-based scoring to calculate free energies of binding for single amino acid mutations in protein-protein complexes. PLoS One *8*, e82849.
217. Lyne, P.D., Lamb, M.L., and Saeh, J.C. (2006). Accurate prediction of the relative potencies of members of a series of kinase inhibitors using molecular docking and MM-GBSA scoring. J Med Chem *49*, 4805-4808.
218. Anderson, M.S., and Raetz, C.R. (1987). Biosynthesis of lipid A precursors in Escherichia coli. A cytoplasmic acyltransferase that converts UDP-N-acetylglucosamine to UDP-3-O-(R-3-hydroxymyristoyl)-N-acetylglucosamine. J Biol Chem *262*, 5159-5169.
219. Zhang, Z., Bulloch, E.M., Bunker, R.D., Baker, E.N., and Squire, C.J. (2009). Structure and function of GlmU from Mycobacterium tuberculosis. Acta Crystallogr D Biol Crystallogr *65*, 275-283.
220. Zhou, Y., Yu, W., Zheng, Q., Xin, Y., and Ma, Y. (2012). Identification of amino acids involved in catalytic process of M. tuberculosis GlmU acetyltransferase. Glycoconj J *29*, 297-303.
221. Nicklaus, M.C., Wang, S., Driscoll, J.S., and Milne, G.W. (1995). Conformational changes of small molecules binding to proteins. Bioorg Med Chem *3*, 411-428.
222. Wang-Gillam, A., Pastuszak, I., and Elbein, A.D. (1998). A 17-amino acid insert changes UDP-N-acetylhexosamine pyrophosphorylase specificity from UDP-GalNAc to UDP-GlcNAc. J Biol Chem *273*, 27055-27057.
223. Wang-Gillam, A., Pastuszak, I., Stewart, M., Drake, R.R., and Elbein, A.D. (2000). Identification and modification of the uridine-binding site of the UDP-GalNAc (GlcNAc) pyrophosphorylase. J Biol Chem *275*, 1433-1438.
224. Parikh, A., Kumar, D., Chawla, Y., Kurthkoti, K., Khan, S., Varshney, U., and Nandicoori, V.K. (2013). Development of a new generation of vectors for gene expression, gene replacement, and protein-protein interaction studies in mycobacteria. Appl Environ Microbiol *79*, 1718-1729.
225. Zhang, Y.J., Ioerger, T.R., Huttenhower, C., Long, J.E., Sassetti, C.M., Sacchettini, J.C., and Rubin, E.J. (2012). Global assessment of genomic regions required for growth in Mycobacterium tuberculosis. PLoS pathogens *8*, e1002946.

226. Moraes, G.L., Gomes, G.C., Monteiro de Sousa, P.R., Alves, C.N., Govender, T., Kruger, H.G., Maguire, G.E., Lamichhane, G., and Lameira, J. (2015). Structural and functional features of enzymes of Mycobacterium tuberculosis peptidoglycan biosynthesis as targets for drug development. Tuberculosis (Edinb) *95*, 95-111.
227. Chao, M.C., and Rubin, E.J. (2010). Letting sleeping dos lie: does dormancy play a role in tuberculosis? Annu Rev Microbiol *64*, 293-311.
228. Karakousis, P.C., Williams, E.P., and Bishai, W.R. (2008). Altered expression of isoniazid-regulated genes in drug-treated dormant Mycobacterium tuberculosis. J Antimicrob Chemother *61*, 323-331.
229. Alavi, H.A., and Moscovic, E.A. (1996). Immunolocalization of cell-wall-deficient forms of Mycobacterium tuberculosis complex in sarcoidosis and in sinus histiocytosis of lymph nodes draining carcinoma. Histol Histopathol *11*, 683-694.
230. V. BERAN, M.H., J. KAUSTOVA, L. DVORSKA, I. PAVLIK (2006). Cell wall deficient forms of mycobacteria: a review. Veterinarni Medicina *51*, 365–389.
231. Gisin, J., Schneider, A., Nagele, B., Borisova, M., and Mayer, C. (2013). A cell wall recycling shortcut that bypasses peptidoglycan de novo biosynthesis. Nat Chem Biol *9*, 491-493.
232. Lovering, A.L., Safadi, S.S., and Strynadka, N.C. (2012). Structural perspective of peptidoglycan biosynthesis and assembly. Annu Rev Biochem *81*, 451-478.
233. Gill, W.P., Harik, N.S., Whiddon, M.R., Liao, R.P., Mittler, J.E., and Sherman, D.R. (2009). A replication clock for Mycobacterium tuberculosis. Nat Med *15*, 211-214.
234. Naseem, S., Parrino, S.M., Buenten, D.M., and Konopka, J.B. (2012). Novel roles for GlcNAc in cell signaling. Commun Integr Biol *5*, 156-159.
235. Handford, M., Rodriguez-Furlan, C., and Orellana, A. (2006). Nucleotide-sugar transporters: structure, function and roles in vivo. Braz J Med Biol Res *39*, 1149-1158.
236. Konopka, J.B. (2012). N-acetylglucosamine (GlcNAc) functions in cell signaling. Scientifica (Cairo) *2012*.
237. Ormerod, L.P. (2005). Multidrug-resistant tuberculosis (MDR-TB): epidemiology, prevention and treatment. Br Med Bull *73-74*, 17-24.
238. Mio, T., Yamada-Okabe, T., Arisawa, M., and Yamada-Okabe, H. (1999). Saccharomyces cerevisiae GNA1, an essential gene encoding a novel acetyltransferase involved in UDP-N-acetylglucosamine synthesis. J Biol Chem *274*, 424-429.
239. Urbaniak, M.D., Collie, I.T., Fang, W., Aristotelous, T., Eskilsson, S., Raimi, O.G., Harrison, J., Navratilova, I.H., Frearson, J.A., van Aalten, D.M., et al. (2013). A novel allosteric inhibitor of the uridine diphosphate N-acetylglucosamine pyrophosphorylase from Trypanosoma brucei. ACS Chem Biol *8*, 1981-1987.
240. Moir, D.T., Di, M., Moore, R.A., Schweizer, H.P., and Woods, D.E. (2008). Cellular reporter screens for inhibitors of Burkholderia pseudomallei targets in Pseudomonas aeruginosa. Trans R Soc Trop Med Hyg *102 Suppl 1*, S152-162.

241. Doig, P., Boriack-Sjodin, P.A., Dumas, J., Hu, J., Itoh, K., Johnson, K., Kazmirski, S., Kinoshita, T., Kuroda, S., Sato, T.O., et al. (2014). Rational design of inhibitors of the bacterial cell wall synthetic enzyme GlmU using virtual screening and lead-hopping. Bioorg Med Chem *22*, 6256-6269.
242. Engels, F.K., Mathot, R.A., and Verweij, J. (2007). Alternative drug formulations of docetaxel: a review. Anticancer Drugs *18*, 95-103.
243. Coors, E.A., Seybold, H., Merk, H.F., and Mahler, V. (2005). Polysorbate 80 in medical products and nonimmunologic anaphylactoid reactions. Ann Allergy Asthma Immunol *95*, 593-599.

Appendix.

Appendix

Table A1: List of bacterial strains, plasmids and phages used in the study.

Plasmid constructs	Description	Source
pQE2	*E. coli* expression vector, T5 promoter, Amp^R	Qiagen
pQE2-His_6-*glmU*$_{Mtb}$	His_6 tag *glmU*$_{Mtb}$ cloned into *NdeI*/*HindIII* sites of MCS	This study
pQE2-His_6-*glmU*$_{1-352}$	His_6 tag *glmU*$_{1-352}$ cloned into *NdeI*/*HindIII* sites of MCS	This study
pQE2-His_6-*glmU*$_{150-495}$	His_6 tag *glmU*$_{150-495}$ cloned into *NdeI*/*HindIII* sites of MCS	This study
pQE2-His_6-*glmU*$_{K26A}$	His_6 tag *glmU*$_{K26A}$ cloned into *NdeI*/*HindIII* sites of MCS	This study
pQE2-His_6-*glmU*$_{H374A}$	His_6 tag *glmU*$_{H374A}$ cloned into *NdeI*/*HindIII* sites of MCS	This study
pQE2-His_6-*glmU*$_{DM}$	His_6 tag *glmU*$_{DM}$ cloned into *NdeI*/*HindIII* sites of MCS	This study
pQE2-His_6-*glmU*$_{1-480(\Delta 15)}$	His_6 tag *glmU*$_{1-480}$ cloned into *NdeI*/*HindIII* sites of MCS	This study
pQE2-His_6-*glmU*$_{1-470\ (\Delta 25)}$	His_6 tag *glmU*$_{1-470}$ cloned into *NdeI*/*HindIII* sites of MCS	This study
pQE2-His_6-*glmU*$_{1-465(\Delta 30)}$	His_6 tag *glmU*$_{1-465}$ cloned into *NdeI*/*HindIII* sites of MCS	This study
pQE2-His_6-*glmU*$_{1-458(\Delta 37)}$	His_6 tag *glmU*$_{1-458}$ cloned into *NdeI*/*HindIII* sites of MCS	This study
pQE2-His_6-*glmU*$_{Mt\ (A434)-Ec(G424)Chimera}$	His_6 tag *glmU*$_{Mt\ (A434)-Ec(G424)Chimera}$ cloned into *NdeI*/*HindIII* sites of MCS	This study
pQE2-His_6-*glmU*$_{Ec(A423)-Mt(G435)Chimera}$	His_6 tag *glmU*$_{Ec(A423)-Mt(G435)Chimera}$ cloned into *NdeI*/*HindIII* sites of MCS	This study
pQE2-His_6-*glmU*$_{R439T}$	His_6 tag *glmU*$_{R439T}$ cloned into *NdeI*/*HindIII* sites of MCS	This study
pQE2-His_6-*glmU*$_{A451R}$	His_6 tag *glmU*$_{A451R}$ cloned into *NdeI*/*HindIII* sites of MCS	This study
pQE2-His_6-*glmU*$_{W460A}$	His_6 tag *glmU*$_{W460A}$ cloned into *NdeI*/*HindIII* sites of MCS	This study
pQE2-His_6-*glmU*$_{K464A}$	His_6 tag *glmU*$_{K464A}$ cloned into *NdeI*/*HindIII* sites of MCS	This study
pQE2-His_6-*glmU*$_{S416A}$	His_6 tag *glmU*$_{S416A}$ cloned into *NdeI*/*HindIII* sites of MCS	This study
pQE2-His_6-*glmU*$_{N397A}$	His_6 tag *glmU*$_{N397A}$ cloned into *NdeI*/*HindIII* sites of MCS	This study
pQE2-His_6-*glmU*$_{T418A}$	His_6 tag *glmU*$_{T418A}$ cloned into *NdeI*/*HindIII* sites of MCS	This study
pQE2-His_6-*glmU*$_{T418E}$	His_6 tag *glmU*$_{T418E}$ cloned into *NdeI*/*HindIII* sites of MCS	This study
pQE2-His_6-*glmU*$_{T418S}$	His_6 tag *glmU*$_{T418S}$ cloned into *NdeI*/*HindIII* sites of MCS	This study
pQE2-His_6-*glmU*$_{R455T+I457K}$	His_6 tag *glmU*$_{R455T+I457K}$ cloned into *NdeI*/*HindIII* sites of MCS	This study
pQE2-His_6-*glmU*$_{W449A}$	His_6 tag *glmU*$_{W449A}$ cloned into *NdeI*/*HindIII* sites of MCS	This study

pQE2-His_6-$glmU_{SP}$ *(S. pneumoniae)*	His_6 tag $glmU_{SP}$ cloned into *NdeI*/*HindIII* sites of MCS	This study
pQE2-His_6-$glmU_{CG}$ *(C. glutamicum)*	His_6 tag $glmU_{CG}$ cloned into *NdeI*/*HindIII* sites of MCS	This study
pQE2-His_6-$glmU_{EC}$ *(E.coli)*	His_6 tag $glmU_{EC}$ cloned into *NdeI*/*HindIII* sites of MCS	This study
pQE2-His_6-$glmU_{MS}$ *(M. smegmatis)*	His_6 tag $glmU_{MS}$ cloned into *NdeI*/*HindIII* sites of MCS	This study
pQE2-His_6-$glmU_{R19A}$	His_6 tag $glmU_{R19A}$ cloned into *NdeI*/*HindIII* sites of MCS	This study
pQE2-His_6-$glmU_{Q83S}$	His_6 tag $glmU_{Q83S}$ cloned into *NdeI*/*HindIII* sites of MCS	This study
pQE2-His_6-$glmU_{Q83A}$	His_6 tag $glmU_{Q83A}$ cloned into *NdeI*/*HindIII* sites of MCS	This study
pQE2-His_6-$glmU_{N239A}$	His_6 tag $glmU_{N239A}$ cloned into *NdeI*/*HindIII* sites of MCS	This study
pQE2-His_6-$glmU_{Mt\ (I389)\text{-}Ec(G379)Chimera}$	His_6 tag $glmU_{Mt\ (I389)\text{-}Ec(G379)Chimera}$ cloned into *NdeI*/*HindIII* sites of MCS	This study
pQE2-His_6-$glmU_{Ec(I378)\text{-}Mt(G390)Chimera}$	His_6 tag $glmU_{Ec(I378)\text{-}Mt(G390)Chimera}$ cloned into *NdeI*/*HindIII* sites of MCS	This study
pQE2-His_6-$glmU_{Y150A}$	His_6 tag $glmU_{Y150A}$ cloned into *NdeI*/*HindIII* sites of MCS	This study
pQE2-His_6-$glmU_{Y150F}$	His_6 tag $glmU_{Y150F}$ cloned into *NdeI*/*HindIII* sites of MCS	This study
pQE2-His_6-$glmU_{L247A}$	His_6 tag $glmU_{L247A}$ cloned into *NdeI*/*HindIII* sites of MCS	This study
pQE2-His_6-$glmU_{R253A}$	His_6 tag $glmU_{R253A}$ cloned into *NdeI*/*HindIII* sites of MCS	This study
pQE2-His_6- $glmU_{R253Q}$	His_6 tag $glmU_{R253Q}$ cloned into *NdeI*/*HindIII* sites of MCS	This study
pQE2-His_6-$glmU_{Q242A}$	His_6 tag $glmU_{Q242A}$ cloned into *NdeI*/*HindIII* sites of MCS	This study
pQE2-His_6-$glmU_{L144A}$	His_6 tag $glmU_{L144A}$ cloned into *NdeI*/*HindIII* sites of MCS	This study
pQE2-His_6-*garA*	His_6 tag *garA* cloned into *NdeI*/*HindIII* sites of MCS	This study
pET28b-His_6-$pknB_{1\text{-}330}$ (KD2)	His_6 tag $pknB_{1\text{-}330}$ cloned into *NdeI*/*HindIII* sites of MCS	[200]
pTC28S15-OX	Contains reverse tetracycline repressor.	Addgene
pST-KirT	Integrative (for *attB* site) *M.tb.* expression vector with N-terminal FLAG tag and reverse tetracycline repressor gene (r*tetR)*.	This study
pST-KirT-$glmU_{Mtb}$	$GlmU_{Mtb}$ cloned into *NdeI*/*HindIII* sites of MCS of pST-KirT under P_{myc1}*tetO* promotor.	This study
pSTKT-$glmU_{tet\text{-}on}$	FLAG tag *glmU* cloned into *NdeI*/*HindIII* sites of MCS under P_{myc1}*tetO* promotor.	This study
pYUB1474	Containing the hyg^R antibiotic marker cassette and *oriE* + *cosλ*	[202]
pNIT	*M.tb.* expression vector, *nitA* promoter, Chl^R, IVN inducible	[162]
pNIT-$glmU_{Mtb}$	$glmU_{Mtb}$ cloned into *NdeI*/*HindIII* sites of pNIT vector.	This study

pNIT-glmU$_{1-352}$	*glmU*$_{1-352}$ cloned into *NdeI*/*HindIII* sites of pNIT vector.	This study
pNIT-*glmU*$_{150-495}$	*glmU*$_{150-495}$ cloned into *NdeI*/*HindIII* sites of pNIT vector.	This study
pNIT-*glmU*$_{K26A}$	*glmU*$_{K26A}$ cloned into *NdeI*/*HindIII* sites of pNIT vector.	This study
pNIT-*glmU*$_{H374A}$	*glmU*$_{H374A}$ cloned into *NdeI*/*HindIII* sites of pNIT vector.	This study
pNIT-*glmU*$_{DM}$	*glmU*$_{DM}$ cloned into *NdeI*/*HindIII* sites of pNIT vector.	This study
pNIT-*glmU*$_{1-480(\Delta 15)}$	*glmU*$_{1-480(\Delta 15)}$ cloned into *NdeI*/*HindIII* sites of pNIT vector.	This study
pNIT-*glmU*$_{1-470\ (\Delta 25)}$	*glmU*$_{1-470\ (\Delta 25)}$ cloned into *NdeI*/*HindIII* sites of pNIT vector.	This study
pNIT-*glmU*$_{1-465(\Delta 30)}$	*glmU*$_{1-465(\Delta 30)}$ cloned into *NdeI*/*HindIII* sites of pNIT vector.	This study
pNIT-*glmU*$_{1-458(\Delta 37)}$	*glmU*$_{1-458(\Delta 37)}$ cloned into *NdeI*/*HindIII* sites of pNIT vector.	This study
pNIT-*glmU*$_{W460A}$	*glmU*$_{W460A}$ cloned into *NdeI*/*HindIII* sites of pNIT vector.	This study
pNIT-*glmU*$_{SP}$ *(S. pneumoniae)*	*glmU*$_{SP}$ cloned into *NdeI*/*HindIII* sites of pNIT vector.	This study
pNIT-*glmU*$_{CG}$ *(C. glutamicum)*	*glmU*$_{CG}$ cloned into *NdeI*/*HindIII* sites of pNIT vector.	This study
pNIT-*glmU*$_{EC}$ *(E.coli)*	*glmU*$_{EC}$ cloned into *NdeI*/*HindIII* sites of pNIT vector.	This study
pNIT-*glmU*$_{MS}$ *(M. smegmatis)*	*glmU*$_{MS}$ cloned into *NdeI*/*HindIII* sites of pNIT vector.	This study
pNIT-*glmU*$_{T418A}$	*glmU*$_{T418A}$ cloned into *NdeI*/*HindIII* sites of pNIT vector.	This study
pNIT-*glmU*$_{T418E}$	*glmU*$_{T418E}$ cloned into *NdeI*/*HindIII* sites of pNIT vector.	This study
pNIT-*glmU*$_{T418S}$	*glmU*$_{T418S}$ cloned into *NdeI*/*HindIII* sites of pNIT vector.	This study
Bacterial strains		
DH5α	*E. coli* strain, for cloning experiments	Invitrogen
BL21 (DE3) codon plus	*E. coli* strain, for protein expression	Stratagene
mc^2*155* or *Ms*	Wild type *M, smegmatis* strain	ATCC, 700084
H37Rv or *Rv*	Wild type *M. tuberculosis* strain	ATCC
Rv::*glmU* (merodiploid strain)	*H37Rv* electroporated with integrative construct pST-KirT-glmU.	This study
Ms::*glmU* (merodiploid strain)	*mc*^{2}*155* electroporated with integrative construct pST-KirT-glmU.	This study
Rv::*glmU*$_{tet\text{-}on}$	H37Rv electroporated with episomal pSTKT-*glmU*$_{tet\text{-}on}$, containing ATc inducible GlmU$_{Mtb}$, Kan^R.	This study
RvΔglmU	H37Rv *glmU* conditional mutant. *glmU*$_{Mtb}$ gene expression is under the regulation of ATc inducible Tet promoter, Kan^R.	This study
MsΔglmU	*mc*^{2}*155 glmU* conditional mutant. *glmU*$_{Ms}$ gene expression is under the regulation of ATc inducible Tet promoter, Kan^R.	This study

*Rv*Δ*glmU*::pNIT$_{chl}$	H37Rv *glmU* conditional mutant strain complimented with pNIT vector only, Chl^R.	This study
*Rv*Δ*glmU*::*glmU*$_{WT}$	H37Rv *glmU* conditional mutant strain complimented with pNIT-*glmU*$_{Mtb}$, Chl^R.	This study
*Rv*Δ*glmU*::*glmU*$_{1-352}$	H37Rv *glmU* conditional mutant strain complimented with pNIT-*glmU*$_{1-352}$, Chl^R.	This study
Rv Δ*glmU*:: *glmU*$_{150-495}$	H37Rv *glmU* conditional mutant strain complimented with pNIT-*glmU*$_{150-495}$, Chl^R.	This study
Rv Δ*glmU*:: *glmU*$_{K26A}$	H37Rv *glmU* conditional mutant strain complimented with pNIT-*glmU*$_{K26A}$, Chl^R.	This study
Rv Δ*glmU*:: *glmU*$_{H374A}$	H37Rv *glmU* conditional mutant strain complimented with pNIT-*glmU*$_{H374A}$, Chl^R.	This study
Rv Δ*glmU*::*glmU*$_{DM}$	H37Rv *glmU* conditional mutant strain complimented with pNIT-*glmU*$_{DM}$, Chl^R.	This study
Rv Δ*glmU*::*glmU*$_{1-480(Δ15)}$	H37Rv *glmU* conditional mutant strain complimented with pNIT-*glmU*$_{1-480(Δ15)}$, Chl^R.	This study
Rv Δ*glmU*::*glmU*$_{1-470\ (Δ25)}$	H37Rv *glmU* conditional mutant strain complimented with pNIT-*glmU*$_{1-470\ (Δ25)}$, Chl^R.	This study
Rv Δ*glmU*::*glmU*$_{1-465(Δ30)}$	H37Rv *glmU* conditional mutant strain complimented with pNIT-*glmU*$_{1-465(Δ30)}$, Chl^R.	This study
Rv Δ*glmU*::*glmU*$_{1-458(Δ37)}$	H37Rv *glmU* conditional mutant strain complimented with pNIT-*glmU*$_{1-458(Δ37)}$, Chl^R.	This study
Rv Δ*glmU*::*glmU*$_{W460A}$	H37Rv *glmU* conditional mutant strain complimented with pNIT-*glmU*$_{W460A}$, Chl^R.	This study
Rv Δ*glmU*::*glmU*$_{SP}$	H37Rv *glmU* conditional mutant strain complimented with pNIT-*glmU*$_{SP}$, Chl^R.	This study
Rv Δ*glmU*::*glmU*$_{CG}$	H37Rv *glmU* conditional mutant strain complimented with pNIT-*glmU*$_{CG}$, Chl^R.	This study
Rv Δ*glmU*::*glmU*$_{EC}$	H37Rv *glmU* conditional mutant strain complimented with pNIT-*glmU*$_{EC}$, Chl^R.	This study
Rv Δ*glmU*::*glmU*$_{MS}$	H37Rv *glmU* conditional mutant strain complimented with pNIT-*glmU*$_{MS}$, Chl^R.	This study
Rv Δ*glmU*::*glmU*$_{T418A}$	H37Rv *glmU* conditional mutant strain complimented with pNIT-*glmU*$_{T418A}$, Chl^R.	This study
Rv Δ*glmU*::*glmU*$_{T418E}$	H37Rv *glmU* conditional mutant strain complimented with pNIT-*glmU*$_{T418E}$, Chl^R.	This study
Rv Δ*glmU*::*glmU*$_{T418S}$	H37Rv *glmU* conditional mutant strain complimented with pNIT-*glmU*$_{T418S}$, Chl^R.	This study
Phages		
pHAE159	Temperature sensitive shuttle phagemid	[203]
pHAE159:: *glmU*$_{Mtb}$ AES	GlmU$_{Mtb}$ AES constructs were cloned into *PacI* site and used for specialized transduction to replace *glmU*$_{Mtb}$ with hygromycin resistance gene in *M.tb.*	This study

His$_6$: 6 Histidine tag; MCS: Multiple cloning site; AES allelic exchange substrate; DM: Double mutant (K26A + H374A); IVN: Iso valeronitrile; ATc: anhydrotratracycline.

Table A2: Primers used in the study		
Primer code	**Name**	**Sequence**
VK643	$GlmU_{Mtb}$ F	5'CACCGAATTCCATATGACGTTTCCTGGTGACACC3'
VK413	$GlmU_{Mtb}$ R	5'GGAAGCTTATCTAGATGGTGTCTGATCAGCGTCGGG3'
VK924	*E.coli* GlmU F	5'CACCCATATGTTGAATAATGCTATGAGC3'
VK925	*E.coli* GlmU R	5'GCGCCCAAGCTTTCACTTTTTCTTTACCGG3'
VK596	$GlmU_{Mtb}$:1-352 R	5'GGAAGCTTATCTAGAGTCGGCACCCAACGCGGTTC3'
VK597	$GlmU_{Mtb}$: 150-495 R	5'CACCCATATGTACGGCCGTATCCTGCGCACC3'
VK964	$GlmU_{Mtb}$:1-480 R	5'GGGAAGCTTCATTTCGGAGGCTCTTTTTGAGGC3'
VK963	$GlmU_{Mtb}$:1-470 R	5'GGGAAGCTTCGCGGGGCTGCCGGGGCGTTTGCG3'
VK505	$GlmU_{Mtb}$:1-465 R	5'TCTAGAAGCTTACTCGATGTTGCGTTGCGGACC3'
VK962	$GlmU_{Mtb}$:1-458 R	5'CCCAAGCTTGCGTTTGCGTTGCACCCAGTTCTC3'
VKN215	$GlmU_{Mt\ (A434)-Ec(G424)}$ F	5'CGGCGCGTATACCGGGGCCGGTACAACTGTGACGCGT AAT3'
VKN216	$GlmU_{\ Mt\ (A434)-Ec(G424)}$ R (*Mtb-Ec* Chimera)	5'ATTACGCGTCACAGTTGTACCGGCCCCGGTATACGCG CCGT3'
VKN217	$GlmU_{Ec(A423)-Mt(G435)}$ F	5'AAAGGCGCGACCATTGCTGCGGGCACAGTGGTGCGGG AGGAT3'
VKN218	$GlmU_{Ec(A423)-Mt(G435)}$ R Chimera *Ec-Mtb*	5'ATCCTCCCGCACCACTGTGCCCGCAGCAATGGTCGCG CCTTT3'
VKN207	$GlmU_{Mtb}$:R439T F	5'CCGGCACAGTGGTGACCGAGGATGTCCCGCC3'
VKN208	$GlmU_{Mtb}$:R439T R	5'GGCGGGACATCCTCGGTCACCACTGTGCCGG3'
VKN209	$GlmU_{Mtb}$:A451R F	5'CGCTGGCAGTGTCGCGGGGTCCGCAACGCAAC3'
VKN210	$GlmU_{Mtb}$:A451 R	5'GTTGCGTTGCGGACCCCGCGACACTGCCAGCG3'
VKN211	$GlmU_{Mtb}$:W460A F	5'CGCAACATCGAGAACGCGGTGCAGCGC3'
VKN212	$GlmU_{Mtb}$:W460A R	5'GCGCTGCACCGCGTTCTCGATGTTGCG3'
VKN213	$GlmU_{Mtb}$: K464A F	5'GGTGCAGCGCGCACGCCCCGGCAGCCCAGC3'
VKN214	$GlmU_{Mtb}$: K464A R	5'GCTGGGCTGCCGGGGCGTGCGCGCTGCACC3'
From IITK	$GlmU_{Mtb}$:S416A F	5'CACGTACGGACCGGGGCCGACACCATGTTCGTG3'
	$GlmU_{Mtb}$:S416A R	5'CACGAACATGGTGTCGGCCCCGGTCCGTACGTG3'
From IITK	$GlmU_{Mtb}$:N397A F	5'TCC AGCGTGTTCGTCGCCTACGACGGTACGTCCAAA3'
	$GlmU_{Mtb}$:N397A R	5'TTTGGACGTACCGTCGTAGGCGACGAACACGCTGGA3'
From IITK	$GlmU_{Mtb}$:H374A F	5'GGCACCAAGGTGCCGGCCCTGACCTACGTCGGCGAC3'
	$GlmU_{Mtb}$:H374A R	5'GTCGCCGACGTAGGTCAGGGCCGGCACCTTGGTGCC3'
VK601	$GlmU_{Mtb}$:T418A F	5'ACCGGGTCCGACGCTATGTTCGTGGCC3'
VK602	$GlmU_{Mtb}$: T418A R	5'GGCCACGAACATAGCGTCGGACCCGGT3'
VK828	$GlmU_{Mtb}$: T418E F	5'ACCGGGTCCGACGAAATGTTCGTGGCC3'
VK829	$GlmU_{Mtb}$: T418E R	5'GGCCACGAACATTTCGTCGGACCCGGT3'
VK960	$GlmU_{Mtb}$: T418S F	5'ACCGGGTCCGACTCCATGTTCGTGGCC3'
VK961	$GlmU_{Mtb}$: T418S R	5'GGCCACGAACATGGAGTCGGACCCGGT3'
VKN428	$GlmU_{Mtb}$:R455T+I457F	5'CCGCAAACCAACAAGGAGAACTGG3'
VKN429	$GlmU_{Mtb}$:R455T+I457R	5'CCAGTTCTCCTTGTTGGTTTGCGG 3'
VKN422	$GlmU_{Ec}$: W449A F	5'CTCAGAAAGAAGGCGCGCGTCGTCCGGTAAAG3'
VKN423	$GlmU_{Ec}$: W449A R	5'CTTTACCGGACGACGCGCGCCTTCTTTCTGAG3'
VK890	*S. pneumoniae* GlmU F	5'CACCGAATTCCATATGTCAAATTTTGCCATTAT3'
VK891	*S. pneumoniae* GlmU R	5GATATCCTACTGCAGCTGGTTCTTAGGATGATGAGG3'
VK892	*C. glutamicum* GlmU F	5'CACCGAATTCCATATGAGCGCAAGCGATTTCTCG3'
VK893	*C. glutamicum* GlmU R	5'GATATCTTAAAGCTTGCCTTCCTGGTTGTGGACGTT3'
VK894	*E.coli* GlmU F	5'CACCGAATTCCATATGTTGAATAATGCTATGAGC3'
VK895	*E.coli* GlmU R	5'GATATCTCAAAGCTTTTTCTTTACCGGACGACG3'
VK896	*M. smegmatis* GlmU F	5'CACCGAATTCCATATGACCGCATCAACCGAGGCC3'
VK897	*M. smegmatis* GlmU R	5'GATATCTCAAAGCTTGCTCTCGTCGCCCAACGCCTT3'
VK990	$GlmU_{Mtb}$:R19A F	5'GGGCCCGGGACCGCGATGCGTTCGGACACC3'
VK991	$GlmU_{Mtb}$:R19A R	5'GGTGTCCGAACGCATCGCGGTCCCGGGCCC3'

VK992 VK993	$GlmU_{Mtb}$:K26A F $GlmU_{Mtb}$:K26A R	5'GTTCGGACACCCCCGCGGTGCTGCACACAC3' 5'GTGTGTGCAGCACCGCGGGGGTGTCCGAAC3'
VK994 VK995	$GlmU_{Mtb}$:Q83S F $GlmU_{Mtb}$:Q83S R	5'CGACGTCGCCCTGTCGGATCGACCGCTAGG3' 5'CCTAGCGGTCGATCCGACAGGGCGACGTCG3'
VK996 VK997	$GlmU_{Mtb}$:Q83A F $GlmU_{Mtb}$:Q83A R	5'CGACGTCGCCCTGGCGGATCGACCGCTAGG3' 5'CCTAGCGGTCGATCCGCCAGGGCGACGTC3'
VK998 VK999	$GlmU_{Mtb}$:N239A F $GlmU_{Mtb}$:N239A R	5'GGTGGCCGGCGTCGCCAATCGCGTCCAGC3' 5'GCTGGACGCGATTGGCGACGCCGGCCACC3'
VKN87 VKN88	$GlmU_{Mtb}$ KO AES Product 1 F $GlmU_{Mtb}$ KO AES Product 1 R	5'TTTTTTTTCCATAAATTGGATCGGCCTCCAGGTGGGTCAG3' 5'TTTTTTTTCCATTTCTTGGACCGACTAGCGGCGCGATGCG3'
VKN89 VKN90	$GlmU_{Mtb}$ KO AES Product 2 F $GlmU_{Mtb}$ KO AES Product 2 R	5'TTTTTTTTCCATAGATTGGGTGGCCCCAGTAACCATCGGC3' 5'TTTTTTTTCCATCTTTTGGACGCGGTTGGACACCACTTGG3'
VKN160 VKN161	$GlmU_{MS}$ KO AES Product 1 F $GlmU_{MS}$ KO AES Product 1 R	5'TTTTTTTTCACAAAGTGGTACAACGGCGCGAGATCGGG3' 5'TTTTTTTTCACTTCGTGTCCTGCACGGCGACGTCGATC3'
VKN162 VKN163	$GlmU_{MS}$ KO AES Product 2 F $GlmU_{MS}$ KO AES Product 2 R	5'TTTTTTTTCACAGAGTGTGTCTTCGTCAACTACGACGG3' 5'TTTTTTTTCACCTTGTGGGCGATGATGACGTCCTTGGC3'
VKN424 VKN425	$GlmU_{Mt\ (I389)\text{-}Ec(G379)}$ F $GlmU_{\ Mt\ (I389)\text{-}Ec(G379)}$ R Chimera *Ec-Mtb*	5'ATCGGCGAGTACAGCAACATCGGTGCGAATAAATTTAAGACCA3' 5'TGGTCTTAAATTTATTCGCACCGATGTTGCTGTACTCGCCGAT3'
VKN426 VKN427	$GlmU_{Ec(I378)\text{-}Mt(G390)}$ F $GlmU_{Ec(I378)\text{-}Mt(G390)}$ R Chimera *Ec-Mtb*	5'ATTGGCGATAACGTTAACATCGGCGCCTCCAGCGTGTTCGT3' 5'GACGAACACGCTGGAGGCGCCGATGTTAACGTTATCGCCAAT3'
VKN1195 VKN1196	$GlmU_{Mtb}$: L144A F $GlmU_{Mtb}$: L144A R	5'GACCACGACGGCGGATGATCCCT3' 5'AGGGATCATCCGCCGTCGTGGTC3'
VKN1197 VKN1198	$GlmU_{Mtb}$: Y150F F $GlmU_{Mtb}$: Y150F R	5'TCCCTTCGGCTTCGGCCGCATCC3' 5'GGATGCGGCCGAAGCCGAAGGGA3'
VKN1199 VKN1200	$GlmU_{Mtb}$: Y150A F $GlmU_{Mtb}$: Y150A R	5'TCCCTTCGGCGCCGGCCGCATCC3' 5'GGATGCGGCCGGCGCCGAAGGGA3'
VKN1201 VKN1202	$GlmU_{Mtb}$: Y156A F $GlmU_{Mtb}$: Y156A R	5'CATCCTGCGCGCCCAGGATCACG3' 5'CGTGATCCTGGGCGCGCAGGATG3'
VKN1203 VKN1204	$GlmU_{Mtb}$: Y156E F $GlmU_{Mtb}$: Y156E R	5'CATCCTGCGCGAACAGGATCACG3' 5'CGTGATCCTGTTCGCGCAGGATG3'
VKN1205 VKN1206	$GlmU_{Mtb}$: Y156S F $GlmU_{Mtb}$: Y156S R	5'CATCCTGCGCTCCCAGGATCACG3' 5'CGTGATCCTGGGAGCGCAGGATG3'
VKN1207 VKN1208	$GlmU_{Mtb}$: Q243A F $GlmU_{Mtb}$: Q243A R	5'CAATCGCGTCGCGCTGGCCGAGC3' 5'GCTCGGCCAGCGCGACGCGATTG3'
VKN1209 VKN1210	$GlmU_{Mtb}$: L247A F $GlmU_{Mtb}$: L247A R	5'GCTGGCCGAGGCGGCCTCCGAAC3' 5'GTTCGGAGGCCGCCTCGGCCAGC3'
VKN1211 VKN1212	$GlmU_{Mtb}$: R253A F $GlmU_{Mtb}$: R253A R	5'CGAACTCAACGCGCGGGTGGTGG3' 5'CCACCACCCGCGCGTTGAGTTCG3'
VKN1213 VKN1214	$GlmU_{Mtb}$: R253Q F $GlmU_{Mtb}$: R253Q R	5'CGAACTCAACCAGCGGGTGGTGG3' 5'CCACCACCCGCTGGTTGAGTTCG3'
VK17	pQE2 forward sequencing primer binds 139 bpsbefore the promoter	5'TCATTGTGAGCGGATAACAATTTC3'

VK459	pQE2 reverse sequencing primer binds 543 bps after *HindIII* site	5'GAAACTGCCGGAAATCGTCGTGG3'
VK309	pQE2 reverse sequencing primer binds 75 bps after *HindIII* site	5'GGCGGCAACCGAGCGTTCTG3'
VKN104	Forward sequencing primer (OL) of pYUB1474	5'CGGCCGCATAATACGACTCA3'
VKN105	Reverse sequencing primer (HL) of pYUB1474	5'AGGATACAGGACCTGCCAAT3'
VKN106	Forward sequencing primer (HR) of pYUB1474	5'CTTCACCGATCCGGAGGAAC3'
VKN107	Reverse sequencing primer (OR) of pYUB1474	5'CTGACGCTCAGTCGAACGAA3'
VK307	M13 forward primer and pENTR forward primer	5'GTA AAACGACGGCCAG3'
VK308	M13 reverse primer	5'CAGGAAACAGCTATGAC3'

Vectro Map:

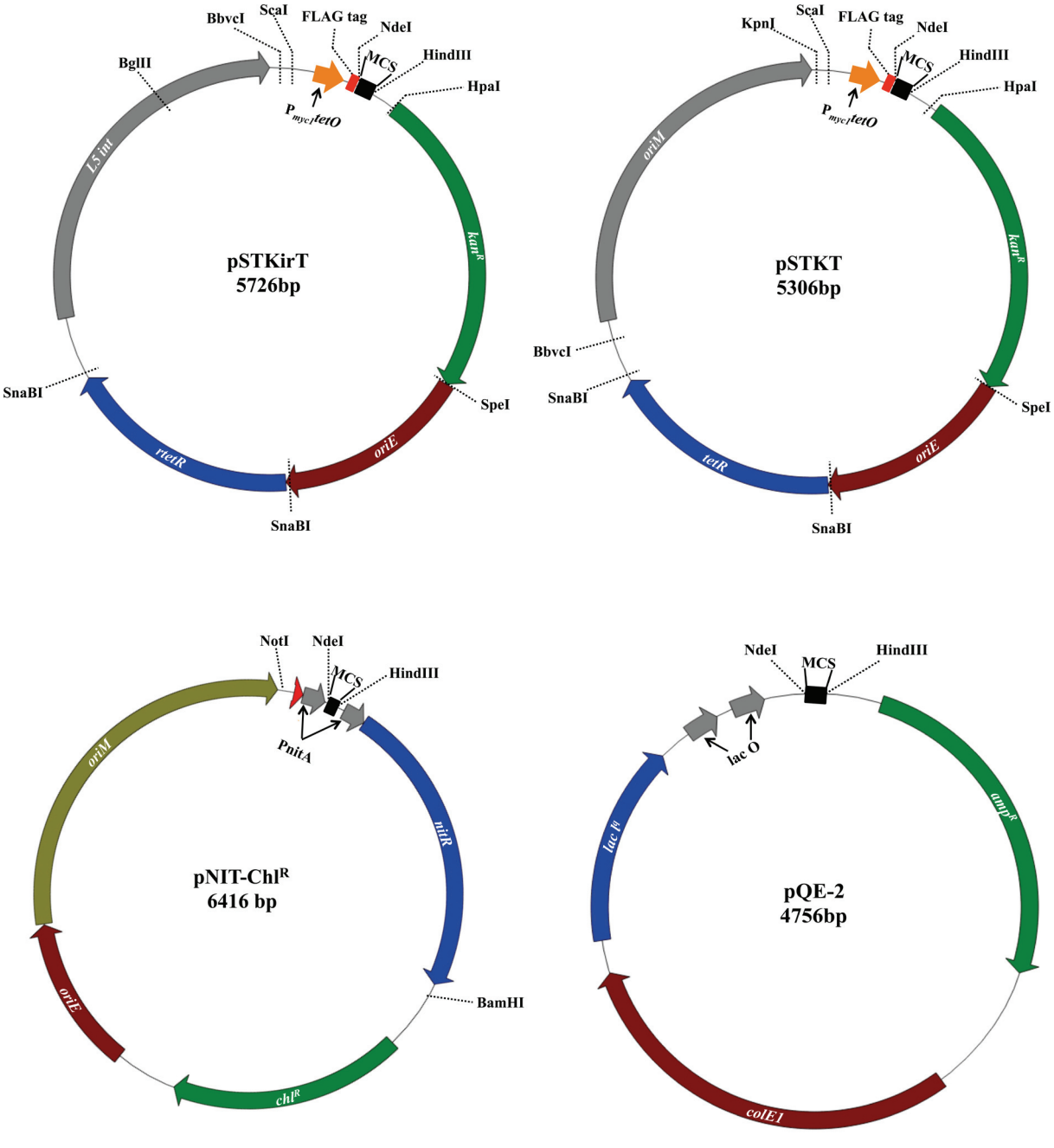
BbvcI
ScaI
FLAG tag
NdeI
BglII
MCS
HindIII
HpaI
$P_{myc1tetO}$
L5 int
kan^R
pSTKirT
5726bp
SnaBI
SpeI
rtetR
oriE
SnaBI
KpnI
ScaI
FLAG tag
NdeI
MCS
HindIII
HpaI
$P_{myc1tetO}$
oriM
kan^R
pSTKT
5306bp
BbvcI
SnaBI
SpeI
tetR
oriE
SnaBI
NotI
NdeI
MCS
HindIII
PnitA
oriM
nirR
pNIT-Chl^R
6416 bp
BamHI
oriE
chl^R
NdeI
MCS
HindIII
lac O
lac I^q
amp^R
pQE-2
4756bp
colE1

List of publications

From thesis work

1. **Vijay Soni**, Sandeep Upadhayay, Priyanka Suryadevara, Ganesh Samla, Archana Singh, Perumal Yogeeswari, Dharmarajan Sriram, Vinay Kumar Nandicoori, Depletion of *M. tuberculosis* GlmU from infected murine lungs effects the clearence of the pathogen (Under review).
2. **Soni V****, Suryadevara P, Sriram D; OSDD Consortium, Ku mar S, Nandicoori VK, Yogeeswari P. Structure-based design of diverse inhibitors of *Mycobacterium tuberculosis* N-acetylglucosamine-1-phosphate uridyltransferase: combined molecular docking, dynamic simulation, and biological activity. ***J Mol Model.*** 2015 Jul;21(7):2704. **** First Co-author.***
3. Jagtap PK, **Soni V****, Vithani N, Jhingan GD, Bais VS, Nandicoori VK, Prakash B. Substrate-bound crystal structures reveal features unique to *Mycobacterium tuberculosis* N-acetyl-glucosamine 1-phosphate uridyltransferase and a catalytic mechanism for acetyl transfer. ***J Biol Chem.*** 2012 Nov 16;287(47):39524-37. **** First Co-author.***

Other Publications

4. Suryadevara P, Yogeeswari P, **Soni V**, Devi PB, Nandicoori VK, Sriram D. Computational Sampling and Simulation Based Assessment of Novel *Mycobacterium tuberculosis* Glutamine Synthetase Inhibitors: Study involving Structure Based Drug Design and Free Energy Perturbation. ***Curr Top Med Chem.*** 2015 Aug 25.
5. Devi PB, Sridevi JP, Kakan SS, Saxena S, Jeankumar VU, **Soni V**, Anantaraju HS, Yogeeswari P, Sriram D. Discovery of novel lysine ε-aminotransferase inhibitors: An intriguing potential target for latent tuberculosis. ***Tuberculosis*** (Edinb). 2015 Aug 8.
6. Petersen GO, Saxena S, Renuka J, **Soni V**, Yogeeswari P, Santos DS, Bizarro CV, Sriram D. Structure-based virtual screening as a tool for the identification of novel inhibitors against *Mycobacterium tuberculosis* 3-dehydroquinate dehydratase. ***J Mol Graph Model.*** 2015 May 11.

7. Pulla VK, Sriram DS, **Soni V**, Viswanadha S, Sriram D, Yogeeswari P. Targeting NAMPT for Therapeutic Intervention in Cancer and Inflammation: Structure-Based Drug Design and Biological Screening. ***Chem Biol Drug Des.*** 2015 Apr 7.
8. Sridevi JP, Suryadevara P, Janupally R, Sridhar J, **Soni V**, Anantaraju HS, Yogeeswari P, Sriram D. Identification of potential *Mycobacterium tuberculosis* topoisomerase I inhibitors: a study against active, dormant and resistant tuberculosis. ***Eur J Pharm Sci.*** 2015 May 25;72:81-92.
9. Janupally R, Jeankumar VU, Bobesh KA, **Soni V**, Devi PB, Pulla VK, Suryadevara P, Chennubhotla KS, Kulkarni P, Yogeeswari P, Sriram D. Structure-guided design and development of novel benzimidazole class of compounds targeting DNA gyraseB enzyme of *Staphylococcus aureus*. ***Bioorg Med Chem.*** 2014 Nov 1;22(21):5970-87.
10. Jeankumar VU, Renuka J, Pulla VK, **Soni V**, Sridevi JP, Suryadevara P, Shravan M, Medishetti R, Kulkarni P, Yogeeswari P, Sriram D. Development of novel N-linked aminopiperidine-based mycobacterial DNA gyrase B inhibitors: scaffold hopping from known antibacterial leads. ***Int J Antimicrob Agents***. 2014 Mar;43(3):269-78.
11. Saxena S, Devi PB, **Soni V**, Yogeeswari P, Sriram D. Identification of novel inhibitors against *Mycobacterium tuberculosis* L-alanine dehydrogenase (MTB-AlaDH) through structure-based virtual screening. ***J Mol Graph Model.*** 2014 Feb;47:37-43.
12. Jeankumar VU, Renuka J, Santosh P, **Soni V**, Sridevi JP, Suryadevara P, Yogeeswari P, Sriram D. Thiazole-aminopiperidine hybrid analogues: design and synthesis of novel *Mycobacterium tuberculosis* GyrB inhibitors. ***Eur J Med Chem.*** 2013;70:143-53.

List of conference presentations

1. **Vijay Soni**, Sandeep Upadhayay, Priyanka Suryadevara, Ganesh Samla, Archana Singh, Perumal Yogeeswari, Dharmarajan Sriram, Vinay Kumar Nandicoori, *Mycobacterium tuberculosis* N-acetyl-glucosamine-1-phosphate uridyltransferase (*glmU*) is critical for survival both in early and late phase of infection, Oral presentation at Gordon Research Seminar (GRS) on Tuberculosis Drug Discovery & Development, July 11th-12th, 2015, Girona, Spain.
2. **Vijay Soni**, Sandeep Upadhayay, Priyanka Suryadevara, Ganesh Samla, Archana Singh, Perumal Yogeeswari, Dharmarajan Sriram, Vinay Kumar Nandicoori, *Mycobacterium tuberculosis* N-acetyl-glucosamine-1-phosphate uridyltransferase (*glmU*) is critical for survival both in early and late phase of infection, Poster presentation at Gordon Research Conferences (GRC) on Tuberculosis Drug Discovery & Development, July 12th-17th, 2015, Girona, Spain.

Biography of Professor D. Sriram

Prof. D. Sriram is presently working in the capacity of Chair Professor at Pharmacy Group, Birla Institute of Technology and Science, Pilani, Hyderabad campus. He received his Ph. D. in 2000 from Banaras Hindu University, Varanasi. He has been involved in teaching and research for last 15 years. He has 285 peer-reviewed research publications to his credit. He has collaborations with various national and international organizations such as Karolinska institute, Sweden; the Indian Institute of Science, Bangalore; National Institute of Immunology, New Delhi; AstraZeneca, India. He was awarded the Young Pharmacy Teacher of the year award of 2006 by the Association of Pharmacy Teachers of India. He received ICMR Centenary year award in 2011. He has guided 13 Ph.D. students and 11 students are pursuing Ph.D currently. His research is funded by agencies like the UGC, CSIR, ICMR, DBT and DST.

Biography of Dr. Vinay K Nandicoori

Dr. Vinay K Nandicoori is currently working as Scientist VI at National Institute of Immunology, New Delhi. He received his Ph.D. in 1997 from Indian Institute of Science, Bangalore and M.Sc. from Indian Institute of Technology, Mumbai in Biotechnology. He has worked as post-doctoral fellow from 1997 to 2000 at Texas A & M University Texas, USA followed by 2000 to 2004 at University of Virginia Charlottesville, USA. He is working as staff scientist at National Institute of Immunology since 2004 till date. He has 40 peer-reviewed research publications in his credit. In 2009 he was awarded with NASI-Scopus Young Scientist Award and with National Bioscience Award for Career Development in 2010. He is also fellow of National Academy of Sciences (India), Allahabad, (2014), Guha Research Conference, India (2009), Society of Biological Chemists (India), Bangalore, India and Member of American Society for Biochemistry and Molecular Biology, USA. He has guided 6 Ph.D students 7 studens are pursuing Ph.D. currently. His research is funded by various agencies like the DBT, CSIR, OSDD and DST.

Biography of Vijay Soni

Mr. Vijay Soni completed his Bachelore in Science (B.Sc.) in Biology and Master of Science (M.Sc.) in Biotechnology from Mohan Lal Sukhadia Univerysity, Udaipur, Rajasthan, India. He has worked as junior research fellow in OSDD-CSIR funded project at National Institute of Immunology, New Delhi from April, 2010 to December 2012 under the supervision of Dr. Vinay K Nandicoori. Then he has been appointed in another OSDD-CSIR funded project as senior research fellow at pharmacy department of Birla Institute of Technology and Science, Pilani, Hyderabad campus from January, 2012- August 2015 under the supervision of Prof. D. Sriram. He has published 12 scientific publications in well-renowned international journals and presented papers in various national and international conferences.